



**MANIPAL**  
ACADEMY of HIGHER EDUCATION  
*(Deemed to be University under Section 3 of the UGC Act, 1956)*

---

# Designing novel catalysts for conversion of biomass derivatives furfuryl alcohol and levulinic acid into value-added chemicals

---

A THESIS SUBMITTED TO  
MANIPAL ACADEMY OF HIGHER EDUCATION

FOR FULFILLMENT OF THE REQUIREMENT FOR THE  
AWARD OF THE DEGREE  
OF  
DOCTOR OF PHILOSOPHY  
BY

**VAISHNAVI B J**

UNDER THE GUIDANCE OF

**DR. GANAPATI V. SHANBHAG**  
DEAN (ACADEMICS), HOD AND ASSOCIATE PROFESSOR  
MATERIALS SCIENCE AND CATALYSIS DIVISION



**POORNAPRAJNA INSTITUTE OF SCIENTIFIC  
RESEARCH, BENGALURU**





**MANIPAL**  
ACADEMY of HIGHER EDUCATION  
*(Institution of Eminence Deemed to be University)*

## **DECLARATION BY THE CANDIDATE**

I declare that this thesis titled “**Designing novel catalysts for conversion of biomass derivatives furfuryl alcohol and levulinic acid into value-added chemicals**”, submitted for the degree of Doctor of Philosophy to Manipal Academy of Higher Education, is my original work, conducted under the supervision of my guide **Dr. Ganapati V. Shanbhag**, Dean (Academics), HOD and Associate professor, Materials Science and Catalysis Division, Poornaprajna Institute of Scientific Research. I also wish to inform that no part of the research has been submitted for a degree or examination at any university. References, help and material obtained from other sources have been duly acknowledged.

### **Candidate**

**Vaishnavi B. J.**

Senior Research Fellow (CSIR)

Poornaprajna Institute of Scientific Research

Bengaluru-562164

Registration Number: **189001063**

July 2023





**MANIPAL**  
ACADEMY of HIGHER EDUCATION  
*(Institution of Eminence Deemed to be University)*

## **CERTIFICATE**

This is to certify that the work incorporated in this thesis “**Designing novel catalysts for conversion of biomass derivatives furfuryl alcohol and levulinic acid into value-added chemicals**” submitted by **Vaishnavi B J**, Senior Research Fellow (CSIR), Materials Science and Catalysis Division, Poornaprajna Institute of Scientific Research was carried out under my supervision. No part of this thesis has been submitted for a degree or examination at any university. References, help, and materials obtained from other sources have been duly acknowledged.

### **Research Guide**

**Dr. Ganapati V. Shanbhag**

Dean (Academics),

HOD and Associate Professor

Materials Science and Catalysis Division

Poornaprajna Institute of Scientific Research

Bengaluru-562164

July 2023



## **Acknowledgements**

The successful completion of this thesis is possible because of the contribution and support of several people. I would like to express my heartfelt gratitude to all the people who have supported me during my Ph.D. journey.

First and foremost, I wish to express my sincere gratitude to my research guide **Dr. Ganapati V. Shanbhag**, Dean (academics), Associate Professor & HOD, Materials Science and Catalysis Division, Poornaprajna Institute of Scientific Research for his valuable guidance, constant support, and encouragement throughout my research journey. I am forever indebted for his patience, motivation, and also for teaching valuable life lessons.

I would like to thank our Director **Dr. Anand B. Halgeri** for all the opportunities, support for my research, and valuable feedback on my performance.

I am grateful to **Dr. R. Vetrivel** (Emeritus Professor, Center for Quantum and Computational Studies, PPISR) for his complete support, guidance, and collaboration in computational chemistry and also for his suggestions given as a subject expert during Doctoral Advisory Committee meetings.

I place my profound sense of gratitude and pranamas to Parama Pujya Swamijis, **Late. H. H. Shree Vibudhesha Theertha Swamiji** (Founder, Chairman of PPISR), the former Chairman **H. H. Shree Vishwapriya Theertha Swamiji**, and present Chairman **H.H. Shree Eeshapriya Theertha Swamiji** for their blessings and support.

I take this opportunity to thank external subject experts in my Doctoral Advisory Committee (DAC), **Dr. N. Nagaraju**, (Former Professor and HoD, Chemistry Dept., St. Joseph's College, Bengaluru) and **Late. Dr. Y. S. Bhat** (Former Professor and HoD, Chemistry, Dept., BIT, Bengaluru) for their active participation during DAC meetings and imparting their knowledge through valuable comments which helped in improving the quality of my work. I thank **Dr. Ananda K**, Associate Professor, Ph.D. co-ordinator, PPISR, for constant monitoring of my research documents according to MAHE norms.

---

I am deeply grateful to **Prof. B. Viswanathan** (NCCR, IITM) for the guidance I received throughout my research journey.

I acknowledge my professors from my master studies, **Prof. B Narayana** (Mangalore University), **Prof. B.K. Sarojini** (Mangalore University) for their guidance and support to take up research.

I express my sincere gratitude to **Dr. U. Ramagopal**, former Dean Academics, and all the former and current faculties of PPISR, **Dr. Sanjeev P Maradur**, **Dr. Suresh Babu Kalidindi**, **Dr. Nalini G Sundaram**, **Dr. D. H. K. Murthy**, **Dr. Srikanth**, **Dr. Sujit Sarkar** for providing guidance and suggestions throughout my Ph.D.

I thank my research collaborator and friend **Mr. Sujith S.** (PPISR) for the constant discussions, support, and help throughout my research. I thank my labmate **Mr. R. Vaibhav** for the collaboration.

I wish to thank my senior doctoral students **Dr. Janardhan H. L**, **Dr. Manjunathan Pandian**, **Dr. Nagendra Kulal**, and **Dr. Marilyn Dmello** for their feedback and support.

I thank my colleagues, **Dr. Chethana A**, **Mr. Saikiran**, **Mr. Harsha**, **Ms. Meghana Hubli**, **Ms. Jyothi**, **Ms. Meghana K**, **Ms. Chaitra**, **Mr. Rahul**, **Mr. Neehar**, **Ms. Varsha**, **Mr. Sujay**, and **Mr. Vidhwath** for all their help during my Ph.D.

My sincere thanks to people from other departments, **Dr. Rahul**, **Mr. Ranjith**, **Dr. Kartik**, **Dr. Shrilakshmi**, **Dr. Shankar Kundapura**, **Mr. Vinod**, **Dr. Shrikant**, **Dr. Raghuram Hegde**, **Dr. Swetha Lankipalli**.

My sincere thanks to **Dr. Ramya Prabhu** (CENS), **Dr. Mayur** (ICT-M) and **Mr. Akhil Chandran P** (BITS Hyderabad), **Mr. Vineet Mishra** (IITM) for their help in various characterizations.

I thank friends and research scholars from other universities, **Dr. Ariharan**, **Ms. Shanmughapriya**, and **Mr. Himanshu** for their help during my research

---



I extend my sincere thanks to **Sri. P. Sreenivasa Rao**, Financial Advisor, AMEF, and **Dr. K. Srihari**, Hon. Secretary, AMEF, for all their support during the course of my research.

I would like to acknowledge administrative staff members **Mr. Nagarajan R. and Mrs. Latha Srinivasan, Mrs. Nandini, and Mr. Kishore Gaikwad, Mr. Praveen** for their timely help and support.

I am grateful to **Admar Mutt Education Foundation (AMEF)** for providing research fellowship and facilities to carry out research work.

I would like to thank the **Council of Scientific & Industrial Research (CSIR)**, New Delhi for awarding the **Senior Research Fellowship (09/1052(0011)2020-EMR-I)** for the period of two years from November 2020 to October 2022.

I thank the **Manipal Academy of Higher Education (MAHE)** for enrolling me for the Ph.D. and smoothly conducting official procedures throughout my Ph.D. program.

I would like to express my heartfelt gratitude to my family (**Appa, Amma, Subbu, Sindu, Mami, and Doddappa**), all my teachers in various classes, and all my well-wishers and friends.

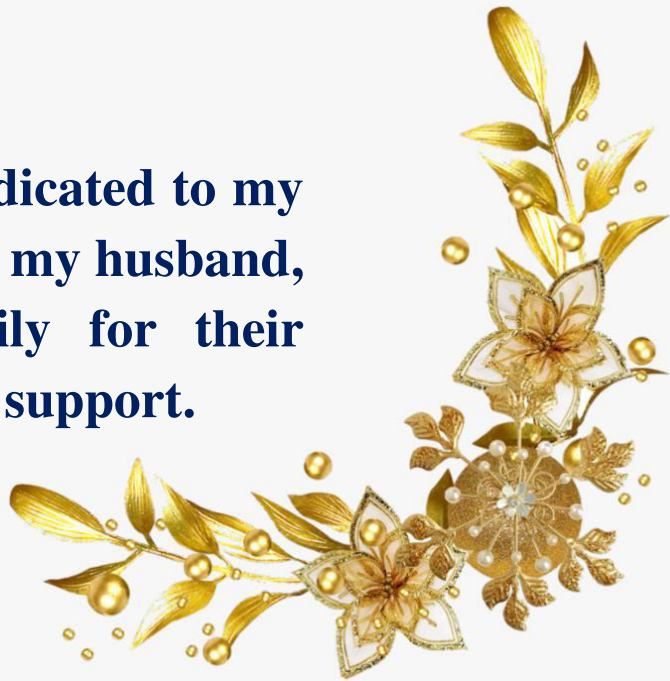
My sense of gratitude to one and all, who directly or indirectly, have lent their hand in this venture.

**-Vaishnavi**

---



**This thesis is dedicated to my  
beloved parents, my husband,  
sister and family for their  
endless love and support.**





---

## Table of Contents

	Page No.
<b>Abbreviations</b>	i
<b>Abstract</b>	iii
<b>1. Chapter–1: Introduction</b>	1
1.1 Biomass and its advantages	1
1.2 Biomass as a feedstock for the production of speciality chemicals	1
1.3 Furfuryl alcohol	3
1.4 Levulinic acid	4
1.5 Catalysis	4
1.5.1 Heterogeneous catalysis	6
1.5.2 Solid acid catalysts	7
1.5.3 Zeolites	8
1.5.3.1 Properties of zeolites that help in solid acid catalysis	10
1.5.3.2 Synthesis of zeolites	11
1.5.3.3 Zeolite modifications	12
1.5.4 Silicoaluminophosphate / Zeotype materials	14
1.5.5 Mesoporous materials	14
1.5.5.1 Ordered mesoporous materials (OMMs)	15
1.5.5.2 Synthesis of mesoporous materials	16
1.5.6 Functionalized zirconia	18
1.5.6.1 Active sites of sulfated zirconia	19
1.5.6.2 Synthesis of sulfated zirconia	19
1.5.7 Metal–Organic Framework Materials	20
1.5.7.1 Properties of MOFs for catalysis	20
1.5.7.2 Synthesis of MOFs	22
1.6 Literatures survey	22
1.6.1 Butanolysis of furfuryl alcohol to produce butyl levulinate.	22
1.6.2 Furfuryl acetate synthesis from furfuryl alcohol via esterification	23
1.6.3 Hydrolysis of furfuryl alcohol to produce Levulinic acid	24
1.6.4 Ethyl levulinate synthesis from furfuryl alcohol and levulinic acid	25
1.7 Gaps found in the literature	28
1.7.1 Butanolysis of furfuryl alcohol to produce butyl levulinate.	28
1.7.2 Furfuryl acetate synthesis from furfuryl alcohol via esterification	29
1.7.3 Hydrolysis of furfuryl alcohol to produce Levulinic acid	29
1.7.4 Ethyl levulinate synthesis from furfuryl alcohol and levulinic acid	29
1.8 Objectives of the proposed work	30
1.9 Bibliography	30
<b>2. Chapter–2: Catalyst preparation and Characterization Techniques</b>	
2.1 Introduction	51
2.2 Synthesis of heterogeneous solid acid catalysts	52
2.2.1 Preparation of ZSM–5	52
2.2.2 Modification of ZSM–5	52

---

---

2.2.3 SAPO-34	53
2.2.4 SAPO-11	53
2.2.5 Al-SBA-15	54
2.2.6 Sulfated zirconia	54
2.2.7 BUT-8-Cr-SO <sub>3</sub> H	55
2.3 Characterization Techniques	55
2.3.1 X-ray diffraction	55
2.3.2 X-ray fluorescence spectroscopy	56
2.3.3 Inductively coupled plasma optical emission spectroscopy	57
2.3.4 Fourier transform infrared spectroscopy	57
2.3.5 Nitrogen sorption	58
2.3.6 Acid-base titration	58
2.3.7 NH <sub>3</sub> -Temperature programmed desorption	59
2.3.8 Pyridine-FTIR	59
2.3.9 Thermogravimetric analysis	60
2.3.10 Scanning electron microscopy	60
2.3.11 Transmission electron microscopy	60
2.4 Bibliography	61
<b>3. Chapter-3:</b>	
3.1 Introduction	67
3.2 Chemicals and reagents	70
3.3 Catalyst synthesis	70
3.4 Catalytic activity study	71
3.5 Catalyst characterization	71
3.5.1 X-ray fluorescence analysis	71
3.5.2 Powder X-ray diffraction	71
3.5.3 Nitrogen sorption studies	74
3.5.4 Temperature programmed desorption and Pyridine-FTIR	76
3.5.5 Scanning electron microscopy	80
3.6 Catalytic activity studies	81
3.6.1 Catalyst screening and comparison	81
3.6.2 Effect of SAR	83
3.6.3 Catalytic activity studies for post synthetically modified HZSM-5	85
3.6.4 Influence of reaction conditions	87
3.6.5 Catalyst recyclability study	90
3.6.6 Time resolved study	91
3.7 Plausible reaction mechanism	92
3.8 Substrate scope study	93
3.9 Comparison with literature results	94
3.10 Conclusions	95
3.11 Bibliography	95
<b>4. Chapter-4:</b>	
4.1 Introduction	103

---

---

4.2 Chemicals and reagents	104
4.3 Catalyst synthesis	105
4.4 Catalytic activity study	106
4.5 DFT Method	106
4.6 Catalyst characterization	107
4.6.1 Powder X–ray diffraction	107
4.6.2 Nitrogen sorption studies	108
4.6.3 Temperature programmed desorption and Pyridine–FTIR	111
4.6.4 FTIR spectroscopy	113
4.6.5 Scanning electron microscopy	113
4.7 Catalytic activity studies	114
4.7.1 Catalyst screening and comparison	114
4.7.2 Optimization of sulfation on zirconia support	116
4.7.3 Influence of reaction conditions	118
4.7.4 Catalyst recyclability study	120
4.7.5 Time resolved study	121
4.8 Plausible reaction mechanism	122
4.9 DFT approach	123
4.9.1 Model	123
4.9.2 Calculation of adsorption energy	124
4.9.3 Hydrogen removal energy	125
4.10 Comparison with literature result	126
4.11 Conclusions	127
4.12 Bibliography	128
<b>5. Chapter–5:</b>	
5.1 Introduction	135
5.2 Chemicals and reagents	138
5.3 Catalyst synthesis	138
5.4 Catalytic activity study	138
5.5 Catalyst characterization	139
5.5.1 Powder X–ray diffraction	139
5.5.2 FTIR spectroscopy	140
5.5.3 Thermogravimetric analysis	141
5.5.4 Temperature programmed desorption	141
5.5.5 Microscopic techniques	142
5.6 Catalytic activity studies	142
5.6.1 Catalyst screening and comparison	142
5.6.2 Influence of reaction conditions	144
5.6.3 Catalyst recyclability study	147
5.6.5 Time resolved study	148
5.7 Plausible reaction mechanism	149
5.8 Comparison with literature results	150
5.9 Conclusions	151
5.10 Bibliography	151

---

---

<b>6. Chapter–6:</b>	
6.1 Introduction	157
6.2 Chemicals and reagents	160
6.3 Catalyst synthesis	160
6.4 Catalytic activity study	161
6.5 Catalyst characterization	162
6.5.1 Powder X–ray diffraction	162
6.5.2 FTIR spectroscopy	163
6.5.3 Thermogravimetric analysis	164
6.5.4 Temperature programmed desorption	164
6.5.5 Microscopic techniques	165
6.6 Catalytic activity studies	166
6.6.1 Catalyst screening and comparison	166
6.6.2 Influence of reaction conditions	169
6.6.2.1 Pathway (I) Alcoholysis of furfuryl alcohol	169
6.6.2.2 Pathway (II) Esterification of levulinic acid	171
6.6.3 Catalyst recyclability study	173
6.6.4 Time resolved study	175
6.6.5 Leaching studies	176
6.7 Plausible reaction mechanism	176
6.8 Substrate scope study	177
6.9 Comparison with literature results	179
6.10 Conclusions	182
6.11 Bibliography	183
<b>7. Chapter–7: Summary and conclusions</b>	<b>195</b>
<b>Annexure</b>	
Annexure–1: List of publications	203
Annexure–2: Conferences attended	205
Annexure–3: Awards/Achievements	207

---



---

## Abbreviations

AMF	Alkoxy methyl furan
BET	Brunner–Emmett–Teller
BJH	Barrett–Joyner–Halenda
BL	Butyl levulinate
BMF	Butoxy methyl furan
DFT	Density functional theory
DMF	Dimethylformamide
E <sub>a</sub>	Activation energy
EL	Ethyl levulinate
EMF	Ethoxy methyl furan
FA	Furfuryl alcohol
FAc	Furfuryl acetate
FTIR	Fourier transform infrared spectroscopy
GC	Gas chromatography
GCMS	Gas chromatography mass spectroscopy
HMF	Hydroxy methyl furan
ICP–OES	Inductively coupled plasma optical emission spectroscopy
LA	Levulinic acid
LCB	Lignocellulosic biomass
ML	Methyl levulinate
MMF	Methoxy methyl furan
MOF	Metal organic framework
OMMs	Ordered mesoporous materials
PL	Propyl levulinate
PMF	Propoxy methyl furan
POMs	Polyoxometallates
SAPO	Silicoaluminophosphate
SAR	Silica to alumina ratio

---

SBA-15	Santa Barbara amorphous type15
SBU	Secondary building units
SEM	Scanning electron microscopy
TDA	Thermal conductivity detector
TEM	Transmission electron microscopy
TGA	Thermogravimetric analysis
TON	Turn over number
TPD	Temperature programmed desorption
XRD	X-ray powder diffraction
XRF	X-ray fluorescence

---

## Abstract

This thesis entitled “**Designing novel catalysts for conversion of biomass derivatives furfuryl alcohol and levulinic acid into value-added chemicals**” is focused on exploring the potential solid acid catalysts for furfuryl alcohol and levulinic acid valorization. The contents of this thesis are divided into seven chapters. The summary of each thesis chapter is described below in detail

**Chapter 1:** Introduction and literature survey of the various furfuryl alcohol transformations.

Chapter 1 provides a general introduction to biomass, the advantages of biomass, and furfuryl alcohol and levulinic acid as biomass feedstock for the production of speciality chemicals. Further, the topic of catalysis, heterogeneous catalysis, and details regarding important types of solid acid catalysts (zeolites, zeotype catalysts, mesoporous materials, functionalized metal oxides, MOFs) are covered. The advantages and valorization of furfuryl alcohol to butyl levulinate, ethyl levulinate, furfuryl acetate, and levulinic acid with the thorough literature study, respective gaps in the reports and objectives of the proposed work are highlighted.

**Chapter 2:** Catalyst synthesis and characterization techniques employed

This chapter describes important catalyst synthesis procedures such as the precipitation method, hydrothermal/ solvothermal method, and impregnation/ ion exchange method employed. Also, the characterization techniques incorporated to understand the various physicochemical properties of catalysts such as zeolites, zeotype materials, MOFs, mesoporous compounds, ion-exchanged resin, etc. The theory and the analysis procedures of each synthesis procedure and characterization technique are briefly described.

**Chapter 3:** Butanolysis of furfuryl alcohol to produce butyl levulinate

In this chapter, an investigation on the synthesis of butyl levulinate from furfuryl alcohol via butanolysis with the aid of various solid acid catalysts was performed. A detailed study on various zeolites, ZSM-5 with different SAR, and post-synthetic modification of

---

ZSM-5 revealed the exclusive requirement of the optimal number of acid sites and strong Brønsted acidity. Additionally, the presence of uniform medium-size micropore structure, high surface area, and good thermal stability of the unmodified ZSM-5 helped in achieving better butyl levulinate yield. The catalyst recyclability and the plausible mechanistic pathway were explored. The best catalyst HZSM-5 exhibited enhanced catalytic performance at moderate experimental conditions, low catalyst concentration, and reactants mole ratio, and good reusability abiding by the green chemistry principles.

#### **Chapter 4:** Esterification of furfuryl alcohol to produce furfuryl acetate

This chapter reports an exclusive investigation of the nature of acid sites for the furfuryl acetate production from furfuryl alcohol esterification. Catalysts with different physicochemical properties were screened and the experimental outcome was integrated with DFT studies to understand the nature of acid sites of the top-performing catalysts. The catalysts were well characterized by PXRD, FTIR spectroscopy, ICP-OES, NH<sub>3</sub>-TPD, BET, and SEM measurement. Sulfated zirconia outperformed the well known conventional solid acid catalysts (H-Beta, Ferrierite, Y-zeolite, Al-SBA-15, amberlyst-15, SAPO-11) and the reaction parameter optimization was performed.

#### **Chapter 5:** Hydrolysis of furfuryl alcohol to yield levulinic acid

This chapter describes the synthesis of an important speciality chemical levulinic acid via hydrolysis of furfuryl alcohol. A high-density sulfonic acid functionalized MOF, BUT-8(Cr)-SO<sub>3</sub>H was screened along with the conventional catalysts (HZSM-5 and amberlyst-15). The physicochemical properties of the catalyst were obtained by employing various characterization methods such as PXRD, FTIR spectroscopy, ICP-OES, acid-base titration, NH<sub>3</sub>-TPD, TGA, SEM, and TEM. The reaction optimization, solvent study, leaching, and recyclability study were performed using BUT-8(Cr)-SO<sub>3</sub>H to get the best levulinic acid yield.

#### **Chapter 6:** Ethanolysis and esterification of furfuryl alcohol and levulinic acid respectively for the synthesis of ethyl levulinate

In this chapter, a Brønsted acidic BUT-8(Cr)-SO<sub>3</sub>H metal organic framework, prepared by the solvothermal method was used for the synthesis of ethyl levulinate from two

---

different biomass-derived platform chemicals *viz.* furfuryl alcohol and levulinic acid. The catalyst was well characterized using various methods such as PXRD, ICP-OES, FTIR spectroscopy, acid-base titration, NH<sub>3</sub>-TPD, TGA, SEM, and TEM. The catalytic performance of BUT-8(Cr)-SO<sub>3</sub>H was compared with conventional solid acid catalysts such as HZSM-5, H-Beta, and amberlyst-15. The reaction optimization, recyclability, leaching study, and plausible reaction mechanism for both pathways using BUT-8(Cr)-SO<sub>3</sub>H were obtained.

### **Chapter 7:**

This chapter summarizes the conclusions arrived at this thesis.



# **Chapter 1**

## **Introduction and Literature Survey**

---





## **1.1 Biomass and its advantages**

Biomass is a renewable source obtained from nonedible agricultural waste, municipal and forest residue rich with carbon, hydrogen, and oxygen. Biomass for centuries was used as a solid fuel for cooking or heating purposes by employing wood, cow dung, and crop residues. Along with the fossil fuels dangerously contributing to greenhouse gas emissions, burning biomass by unscientific methods does harm our ecosystem. As biomass is carbon neutral, organic, and abundant, one can choose it as a source for the production of various value-added chemicals that substitute the petrochemicals obtained from fossil fuels. Apart from CO/CO<sub>2</sub> valorization, biomass stands as the only other source for the synthesis of building block chemicals in the renewable source sector. These chemicals can be upgraded to secondary chemicals, intermediates that would either supplement or substitute the manufacture of commodity chemicals, fuels, and fuel additives obtained from the fossil fuel chain. Additionally, these building blocks have applications in industries, transportation, textiles, health & hygiene, safe food supply, and environmental health<sup>1</sup>. Biomass when systematically collected, and segregated with the knowledge of its periodic availability can be used as a potential replacement for nonrenewable resources<sup>2</sup>. Biomass also reduces the burden of dependency on fossil fuels, improves waste management, delivers global peace as one can be liberated from foreign political policies, and enables us to choose the indigenous source to valorize.

## **1.2 Biomass as a feedstock for the production of speciality chemicals**

Biomass can be classified into six major components such as cellulose, hemicellulose, lignin, starch, oil, and protein which yield syngas and sugars upon valorization using catalyst-aided chemical and biological routes<sup>1,3</sup>. Lignocellulosic biomass (LCB) constituting cellulose, hemicellulose, and lignin can be digested and used to obtain various platform chemicals, secondary chemicals, and intermediates (figure 1.1)<sup>4,5</sup>. Cellulose is a carbohydrate present in the form of long microfibrils and hemicellulose consists of branched and single-chained polysaccharides cross-linked with the fibrils of cellulose. Lignin, on the other hand, provides strength to the cell wall due to its composition of complex cross-linked macromolecules.

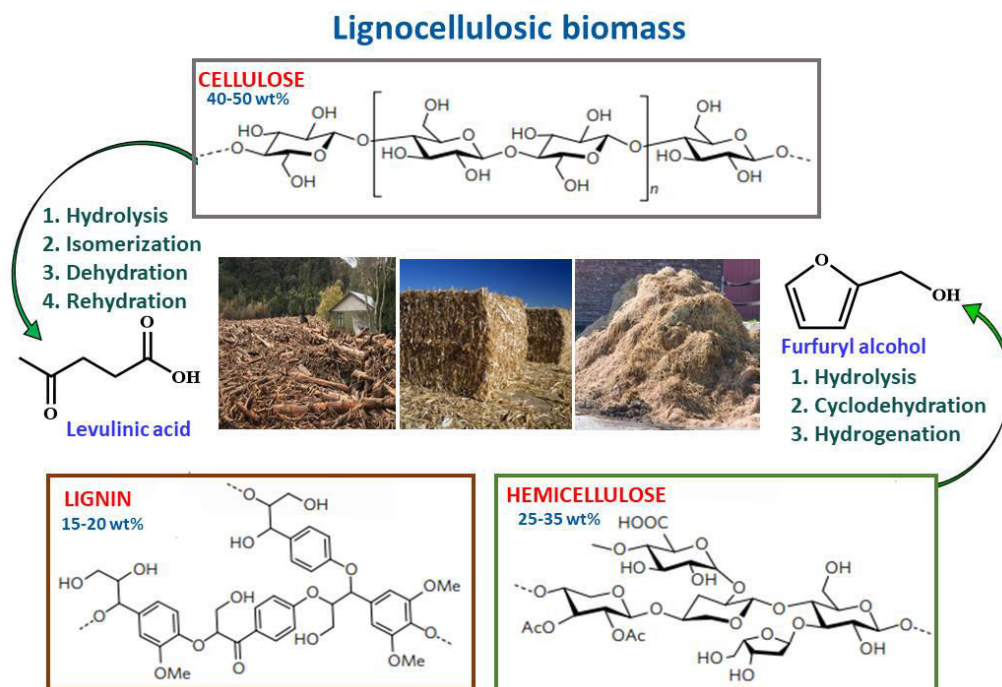


**Figure 1.1.** Major feedstock fraction of biomass

The flowchart of obtaining biobased products for final applications from biomass feedstocks is presented in figure 1.2. In this valorization, the process undergoes various stages of transformations such as the formation of intermediates, building blocks, and secondary chemicals. One such promising building block is a furan derivative and an aromatic aldehyde called furfural that can be used to produce various speciality chemicals such as furfuryl alcohol, glycerol acetals, furfuryl amine, pentanediols, tetrahydro furfuryl alcohol, furfuryl acetate, furoic acid, 2-methyl furan, etc <sup>6,7</sup>.

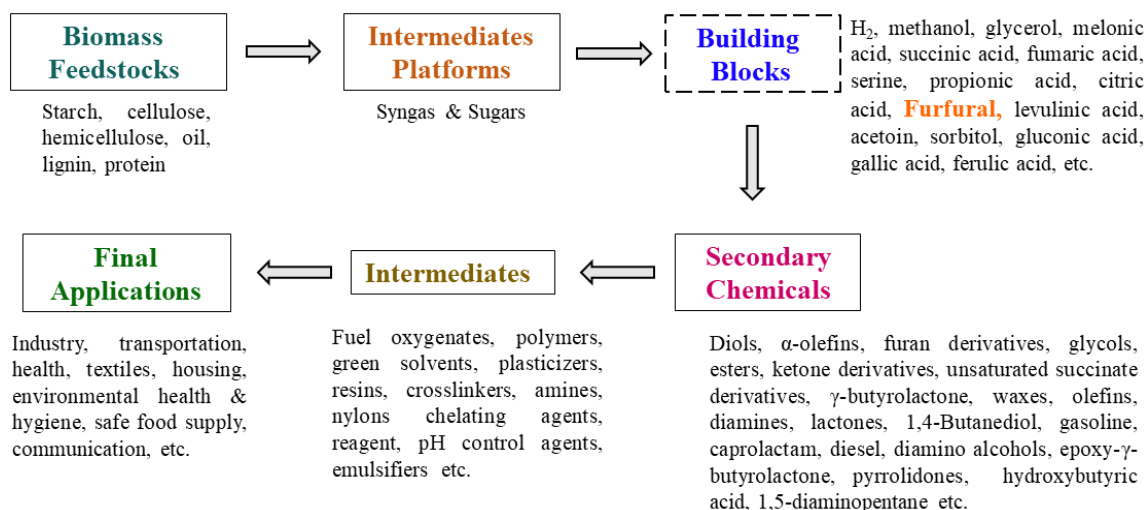


**Figure 1.2.** Flowchart of biomass feedstock conversion to biobased final products

Furfural is obtained from multiple-step transformations where the hemicellulose is converted to pentose sugar (xylose and arabinose) via acid-catalyzed digestion and further, the sugar undergoes cyclodehydration to yield furfural.

### 1.3 Furfuryl alcohol

Furfural upon hydrogenation via chemo selective catalytic route produces furfuryl alcohol (FA) that has similar applications as furfural and acts as a platform chemical as well. Worldwide around 62% of the furfural is converted into FA due to the potential applications and accelerated demand for FA. Importantly, there are many acid-catalyzed reactions reported for one-pot synthesis starting from furfural where FA acts as an intermediate. Instead of obtaining competing side products/intermediates with the desired product, and using a hydrogenating agent and metal catalysts (mostly noble metal), we can choose FA itself over furfural as a feedstock of our interest. Furfuryl alcohol is a C-5 sustainable platform chemical that can be used to produce corrosion inhibitors, foundry, pharmaceuticals, biofuels, foams, polymer concrete, solvents, lubricants, wood adhesives, resins, plasticizers, and fragrances <sup>8,9</sup>. Figure 1.3 presents the important chemicals obtained by furfuryl alcohol valorization such as alkyl levulinate, levulinic acid,  $\gamma$ -valerolactone, pentanediols, cyclopentanone, furfuryl acetate, etc.

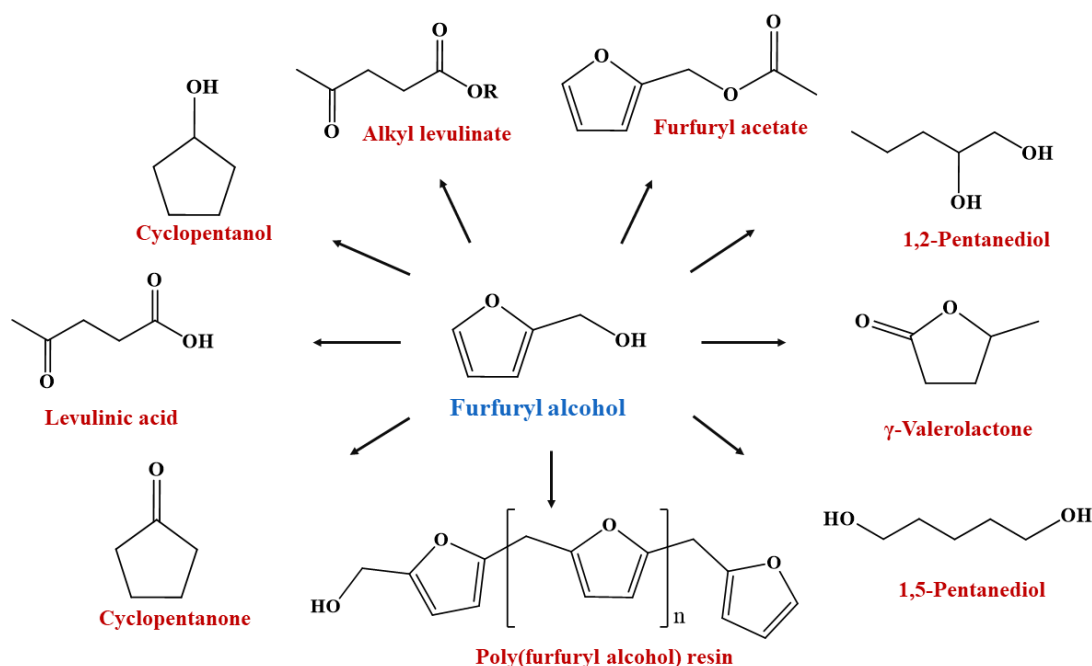


**Figure 1.3.** FA transformation to value-added chemicals

## 1.4 Levulinic acid

Levulinic acid, also called 4-oxopentanoic acid, is obtained from multistep transformations from biomass-derived cellulose which upon acid-catalyzed hydrolysis gets converted to glucose (a hexose sugar). Glucose gets further converted to fructose via an isomerization reaction to yield hydroxy methyl furan (HMF) that upon hydration produces levulinic acid (LA)<sup>10</sup>. Levulinic acid is a platform chemical whose valorization produces various important chemicals such as 5-bromolevulinic acid, 5-nonanone, 2-methyl tetrahydrofuran, levulinate esters, diphenolic acid,  $\gamma$ -valerolactone,  $\alpha$ -angelicalactone,  $\delta$ -amino levulinic acid as depicted in figure 1.4<sup>11</sup>. These chemicals find applications as/in fuels, detergents, pharmaceuticals, polymer industries, plasticizers, herbicides, solvents, resins, food, flavoring and fragrance industries.

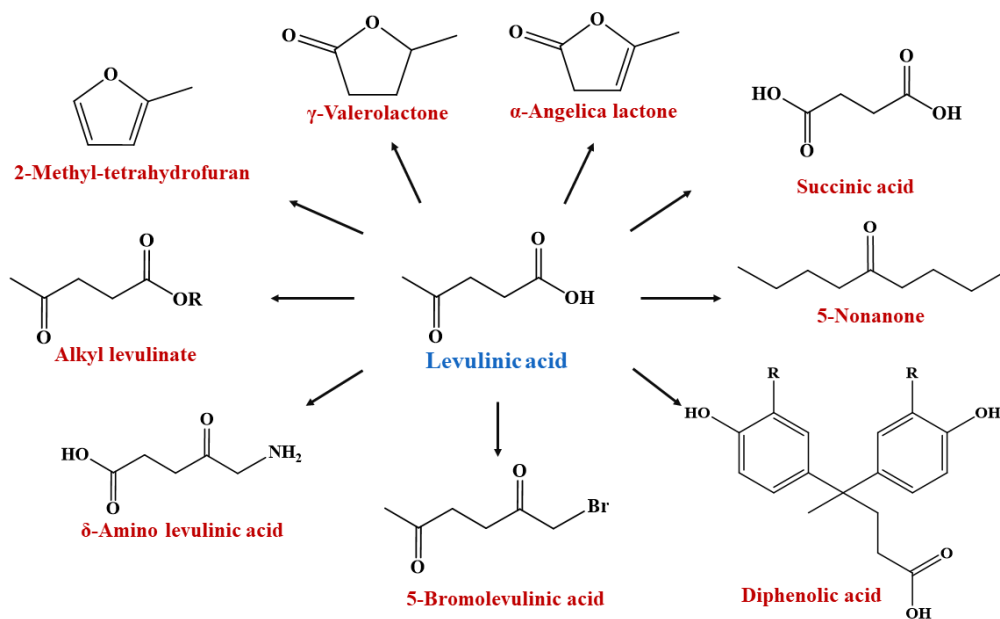


**Figure 1.4.** LA transformation to value-added chemicals

## 1.5 Catalysis

Catalysis is an interdisciplinary science that has played a significant part in establishing its territory right from fine chemical synthesis in industries to the upgradation of crude oil in large-scale operations for centuries. It has a vital role in boosting the efficiency of the existing technologies towards sustainability as it is crucial for our survival. Importantly, catalysis is one of the postulates of the green chemistry principles which itself shows its impact on our day-to-day lives. Catalysis has a huge impact on the economy and it is

confirmed that it contributes more than one-third of the global GDP<sup>12</sup>. Around 90% of the chemicals synthesized and 20% of the products obtained commercially depend on catalysis<sup>13</sup>. By definition, a catalyst is a substance present in a small proportion, that increases the rate of the chemical reaction temporarily being consumed in the reaction without modifying the thermodynamic factors. The activation energy ( $E_a$ ) of a reaction is lowered in the presence of a catalyst thus accelerating the reaction. Table 1.1 presents the list of Noble prizes received in homogeneous, heterogeneous, and enzymatic catalysis. There are numerous benchmark catalyst systems apart from the catalysts mentioned in Table 1.1 that have revolutionized the industrial sectors, saved lives and billions of dollars, as well as helped in resolving environmental issues. In general, the scope of catalysts is in the valorization of feedstocks to value-added chemicals, elimination of pollutants, and production of clean and green energy<sup>14</sup>.

**Table 1.1.** List of Noble prizes awarded for work related to catalysis<sup>15</sup>

Sn	Year	Laureate	Achievement
1.	1909	Wilhelm Ostwald	Pioneer work on catalysis, chemical equilibrium, and reaction velocities
		Victor Grignard	Discovery of the Grignard reagents
2.	1912	Paul Sabatier	Method of hydrogenating organic compounds
3.	1918	Fritz Haber	Synthesis of ammonia
4.	1929	Sir Arthur Harden	Investigations on the fermentation of sugar and fermentative enzyme
		Hans von Euler-Chelpin	
5.	1931	Carl Bosch	Invention and development of chemical high-pressure methods
		Friedrich Bergius	
6.	1956	Sir Cyril Norman Hinshelwood	Work on the kinetics of chemical reactions
		Nikolay Nikolayevich Semyonov	
7.	1963	Giulio Natta	Structure and synthesis of polymers in the field of plastics
		Karl Ziegler	
8.	1973	Ernst Otto Fischer	Organometallic chemistry
		Sir Geoffrey Wilkinson	
9.	1989	Sidney Altman	Catalytic properties of RNA
		Thomas Cech	

---

10.	1990	Elias James Corey	Development of retrosynthetic analysis for the synthesis of complex molecules
11.	1997	Paul D. Boyer John E. Walker	Elucidation of enzymatic mechanism
12.	2001	William S. Knowles Ryoji Noyori K. Barry Sharpless Yves Chauvin	Chirally catalyzed hydrogenation reactions Chirally catalyzed oxidation reactions
13.	2005	Robert H. Grubbs Richard R. Schrock	Development of the metathesis method in organic synthesis
14.	2007	Gerhard Ertl Richard F. Heck	Chemical processes on solid surfaces
15.	2010	Ei-ichi Negishi Akira Suzuki	Palladium-catalyzed cross coupling in complex carbon molecules
16.	2021	Benjamin List David W.C. MacMillan	Development of asymmetric organocatalysis
17.	2022	Morten Meldal K. Barry Sharpless	Development of click chemistry

---

### 1.5.1 Heterogeneous catalysis

Among the three types of catalyst systems present (homogeneous, heterogeneous, and biocatalysts), although each system has its own advantages, heterogeneous catalysts have been placed top due to its flexible and multifaceted properties. Importantly, the ease of separating the catalyst for regeneration, flexibility in operation at elevated temperatures, materials being less corrosive, and applications in continuous production systems that benefit industrial use are the major advantages of heterogeneous catalyst systems<sup>16</sup>. Heterogeneous catalysts are materials that differ in phase with the reactants or products. There are a lot of prospects and challenges in chemical industries and scientists believe that a heterogeneous catalytic system would be one of the solutions that would additionally help in building cleaner and greener processes. Catalyst scientists have a huge responsibility in designing environmentally benign catalysts as their applications are one of the important elements that help in developing sustainable cities.

### 1.5.2 Solid acid catalysts

The heterogeneous catalysts can be designed for three types of reactions which are acid-catalyzed, base-catalyzed, and redox reactions. The majority of the furfuryl alcohol transformations to value-added chemicals are dominated by acid-promoted processes typically requiring a solid acid catalyst system. Table 1.2 presents various types of solid acid catalysts studied for acid-catalyzed reactions.

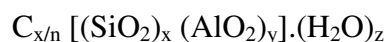
**Table 1.2.** Important types of solid acid catalysts

Sn	Class	Important Examples	Ref
1.	Zeolites	HZSM-5, H-Beta, Y-zeolite, H-mordenite, H-ferrierite, MCM-22, silicalite-1, HZSM-11	17 18
2.	Zeotype	Silicoaluminophosphates (SAPO-11 and SAPO-34), titanosilicates, gallosilicate	19
3.	Clays	Saponite, montmorillonite, kaolinite	20
4.	Ordered mesoporous materials	KIT-6, SBA-16, TUD-1, SBA-15, KCC-1, MCM-41, CMK-3	21 18
5.	Metal oxides and mixed metal oxides	SiO <sub>2</sub> , Al <sub>2</sub> O <sub>3</sub> , WO <sub>3</sub> , TiO <sub>2</sub> , Nb <sub>2</sub> O <sub>5</sub> , α-Fe <sub>2</sub> O <sub>3</sub> , SiO <sub>2</sub> -MgO, SiO <sub>2</sub> -Al <sub>2</sub> O <sub>3</sub> , WO <sub>3</sub> -ZrO <sub>2</sub> , TiO <sub>2</sub> -SiO <sub>2</sub> , WO <sub>3</sub> -Al <sub>2</sub> O <sub>3</sub> , WO <sub>3</sub> -SnO <sub>2</sub> , Nb <sub>2</sub> O <sub>5</sub> -Al <sub>2</sub> O <sub>3</sub>	21
6.	Functionalized or modified metal oxides	SO <sub>4</sub> /ZrO <sub>2</sub> , zirconium phosphate, SO <sub>4</sub> /TiO <sub>2</sub> , SO <sub>4</sub> /SnO <sub>2</sub> , H <sub>3</sub> PW <sub>12</sub> /ZrO <sub>2</sub> -Si(Ph)Si	21
7.	Cation exchange resin	Amberlyst-15, purolite C275, purolite D5081, nafion, aquivion mP98, dowex 50Wx2	22
8.	Heteropoly compounds	Cs <sub>3</sub> PW <sub>12</sub> O <sub>40</sub> , FePW <sub>12</sub> O <sub>40</sub> , Sn <sub>1</sub> -TPA/K-10, H <sub>4</sub> SiW <sub>12</sub> O <sub>40</sub> /SiO <sub>2</sub> , H <sub>2</sub> Zr <sub>1</sub> PW <sub>12</sub> O <sub>40</sub> / Sn-β, TPA/SBA-16, Zn <sub>1</sub> TPA/Nb <sub>2</sub> O <sub>5</sub>	23
9.	Ionic liquids and modified ionic liquids	[MBsIm][CF <sub>3</sub> SO <sub>3</sub> ], [(HSO <sub>3</sub> -p) <sub>2</sub> im][HSO <sub>4</sub> ], H <sub>2</sub> SO <sub>4</sub> /[BMIm]Cl, [BmimSO <sub>3</sub> H] <sub>3</sub> PW <sub>12</sub> O <sub>40</sub> , [MIMBS] <sub>5</sub> [AlW <sub>12</sub> O <sub>40</sub> ], [MIM][HSO <sub>4</sub> ]	24
10.	Metal organic framework (MOF) and modified MOF	UiO-66, MIL-101(Cr), HKUST-1, Cu-BTC, MOF-808, NU-1000, reo-MOF-1, PCN-222-SO <sub>3</sub> H, Hf-NU-1000, POMsC-MIL-101, MOF-808-SO <sub>4</sub>	25 26

Solid acid catalysts are alternatives to mineral acids due to their disadvantages such as toxicity, separation issues, disposal of the waste generated due to mineral acids, and environmental pollution <sup>21</sup>. Typically, properties such as Brönsted or/and Lewis acidity, type & nature of acidic sites, number & strength of the active sites, surface area, porosity, accessibility, morphology, topology, chemical, mechanical & thermal stability influence the catalytic performance.

### 1.5.3 Zeolites

Zeolites are a class of crystalline inorganic materials with microporosity built from tetrahedral units of silica (SiO<sub>2</sub>) and alumina (Al<sub>2</sub>O<sub>3</sub>) that are linked by oxygen atoms <sup>17</sup>. These are microporous (<2 nm) structures that own a high surface area obtained due to the cages and channels present in the framework. The composition of the zeolites (hydrated) can be represented using the following empirical formula.

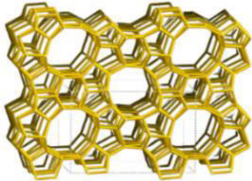
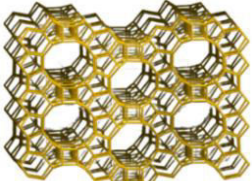
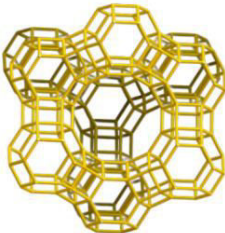
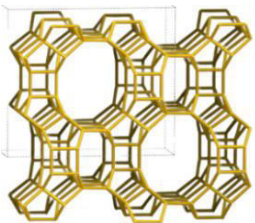
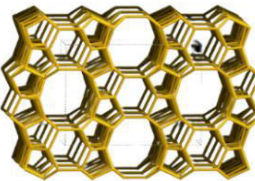
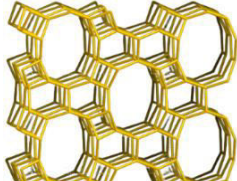
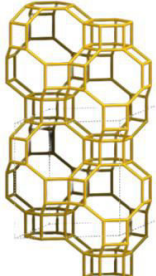


Where C is the charge compensating cation with n being its valency. The moles of Si, Al, and H<sub>2</sub>O are respectively x, y, and z.

Zeolites find applications as catalysts (majorly in petrochemical industries), molecular sieves, radioactive contaminant removal materials, adsorbents, gas treatments, medicines, detergents, water softeners, concrete additives, etc <sup>27</sup>. Unlike zeolites which are aluminosilicates, there is another class of material termed as zeotype in which atoms such as P, B, Ge, Fe, Ga, etc. are introduced in the silicate or aluminosilicate framework <sup>28</sup>. Table 1.3 presents some industrially important zeolites and zeotype materials along with their structural features.



**Table 1.3.** Zeolite and zeotype frameworks and their structural features <sup>29</sup>

Zeolite material	No of rings	Pore size (Å)	Channel dimension	Framework type	Framework structure
ZSM-5	10, 10	5.1 × 5.5 5.3 × 5.6	3	MFI	
Beta	12, 12	5.6 × 5.6 6.6 × 6.7	3	BEA	
Y-Zeolite	12	7.4 × 7.4	3	FAU	
Mordenite	12, 8, 8	6.5 × 7.0 2.6 × 5.7 3.4 × 4.8	1	MOR	
Ferrierite	10, 8	4.2 × 5.4 3.5 × 4.8	2	FER	
SAPO-11	10	6.5 × 4.0	1	AEL	
SAPO-34	8	3.8 × 3.8	3	CHA	

### 1.5.3.1 Properties of zeolites that help in solid acid catalysis<sup>5,16,30</sup>

- Zeolites are the green alternatives for mineral acids as catalysts due to their non-toxic, and non-corrosive nature. Importantly, they have high thermal and hydrothermal stability which makes the high temperature reaction and oxidative regeneration at high temperatures using steam feasible.
- The amount of acid sites is dictated by the concentration of aluminium present in the zeolite framework and the acidity can be altered by modifying the aluminium content or silica to alumina ratio (SAR). As the  $\text{Si}^{4+}$  is replaced by  $\text{Al}^{3+}$  in zeolites, the imbalance developed in the charge neutrality in the framework is compensated by the cations which are typically alkali metals or alkaline earth metals. Brønsted acidic bridging hydroxyl groups are generated by ammonium ion exchange of metal ions and subsequent calcination (figure 1.5)<sup>31</sup>. Modifications using metals by ion exchange, impregnation, substitution, or encapsulation result in the production of Lewis acidity. The Al can be isomorphically substituted by elements such as B, Ti, Ga, or Fe that alter the acidic and redox properties of zeolite. Post-synthetic modification by removing silicon or aluminium atoms produces hierarchical zeolites that change the number and strength of the acid sites as well as the pore structure along with the size of the framework.

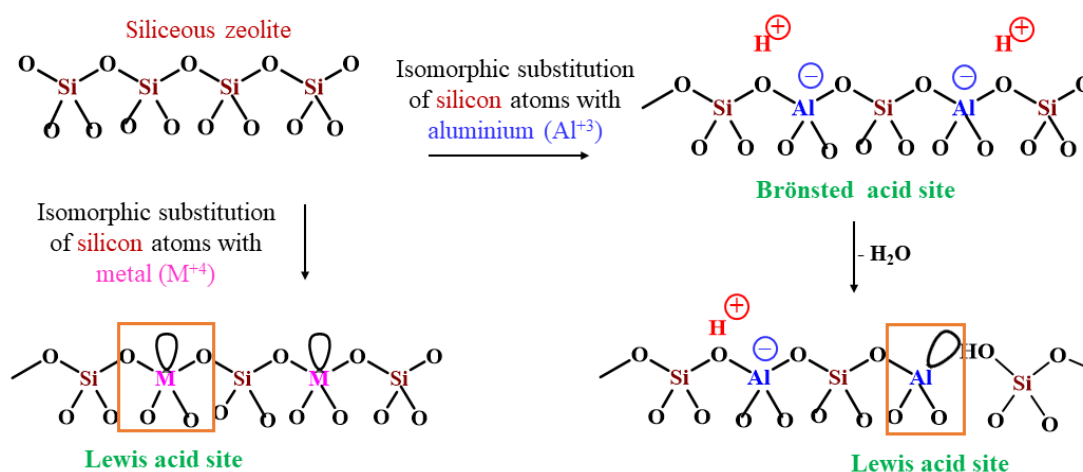


**Figure 1.5.** Structure of acidic sites in zeolites

- The pores/channels in the zeolites act as cages having active centers and provide the reactant molecules a restricted path length to interact and produce products inside the

channels. Also, zeolites are known for their applications in shape-selective catalysis due to the close pore sizes to the molecular sizes of the reactants/products.

### 1.5.3.2 Synthesis of zeolites

Though there are naturally occurring zeolites, these are also synthesized in the laboratory by a template-assisted hydrothermal method<sup>32</sup>. Zeolite preparation occurs in two stages when the hydrothermal synthesis procedure is adapted<sup>33</sup> and the schematic representation of zeolite synthesis is shown in figure 1.6.

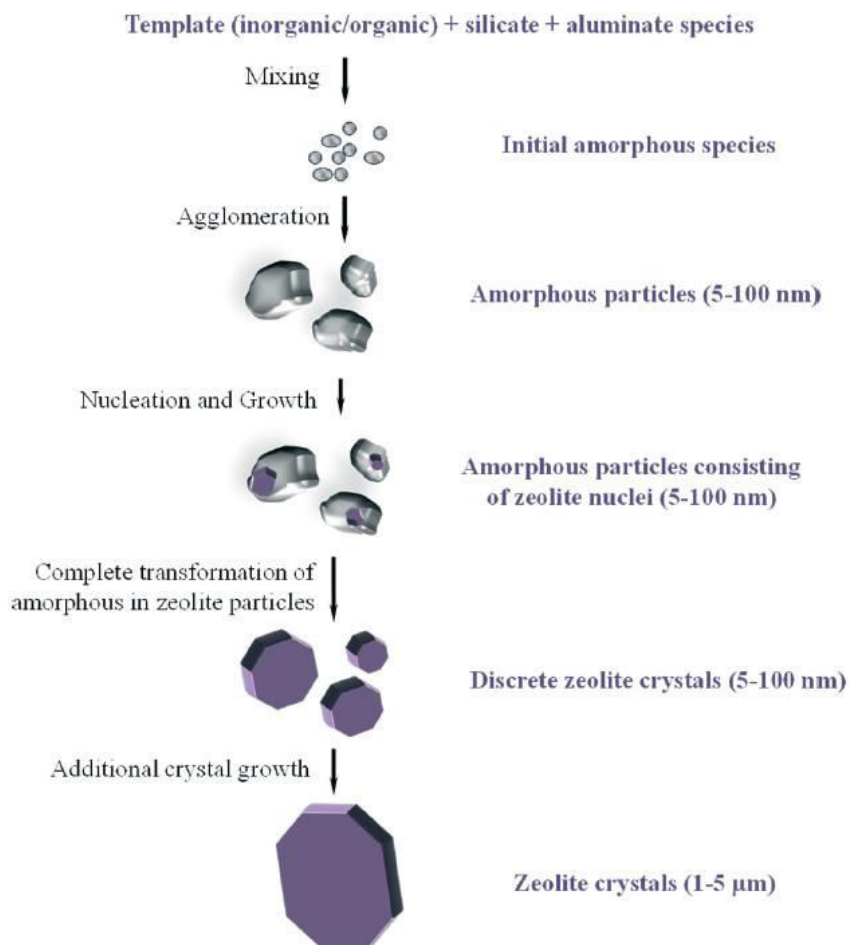


**Figure 1.6.** Schematic representation of the general steps in zeolite synthesis<sup>34</sup>

Initially, in stage I, the aluminium and the silicon precursors are transformed into hydrated aluminosilicate gel with the aid of an alkali solution to which a structure-directing agent is added. The mixture is transferred into a teflon-lined stainless steel autoclave and placed in a preheated oven for a certain time to achieve stage II of the

synthesis called the crystallization stage. The crystallization stage consists of substages for the formation of zeolites which are as follows.

- i. Condensation of silicate and aluminate species to form –Si–O–Al– linkages
- ii. Nucleation and growth of nuclei of the zeolite
- iii. Growth of the crystal to yield zeolite

Once the autoclave is cooled to room temperature, the product is filtered, washed, dried, and calcined to yield a zeolite. The proton exchange by ammonium salt is performed for an alkali form of zeolite if required and finally, the catalyst is calcined to get a protonic form of the zeolite<sup>35</sup>. Factors that affect the synthesis of zeolites are the type of silica and alumina precursors used, the SAR, the concentration of water, the aging period, the templates (structure directing agents) used, the synthesis temperature, and the pH of the solution.

### 1.5.3.3 Zeolite modifications

Post-synthetic modification methods such as desilication, dealumination, phosphate modification, and metal ion exchange have a significant impact on the physicochemical properties of zeolites<sup>36,37,38,39</sup>. These methods offer flexibility in altering the nature/type of active sites, strength/amount of acidity, pore size, texture, morphology, etc.

- Desilication and dealumination are the methods used to etch Si and Al atoms respectively without causing significant destruction to the zeolite framework as presented in figure 1.7<sup>40,41,42</sup>.
- Desilication is achieved by treating the optimized molar concentration of a basic solution (usually NaOH) with the zeolite followed by ion exchange of Na<sup>+</sup> by ammonium ion to generate Brönsted acidic sites<sup>43,44</sup>. The acidity of the desilicated zeolite changes due to the variation that occurred in the SAR. Additionally, due to the generation of extra framework aluminium and also the reincorporation of leached Al species, the Lewis acidity increases. Also, the treatment has an impact on the surface area and porosity of the material.
- Dealumination is performed by hydrothermal (steam) or chemical acid treatment resulting in the selective removal of framework or extra framework aluminium<sup>39,45</sup>. Similar to desilication, the amount and strength of acidity, B/L (Brönsted to Lewis acid sites) ratio, surface area, and porosity are altered.

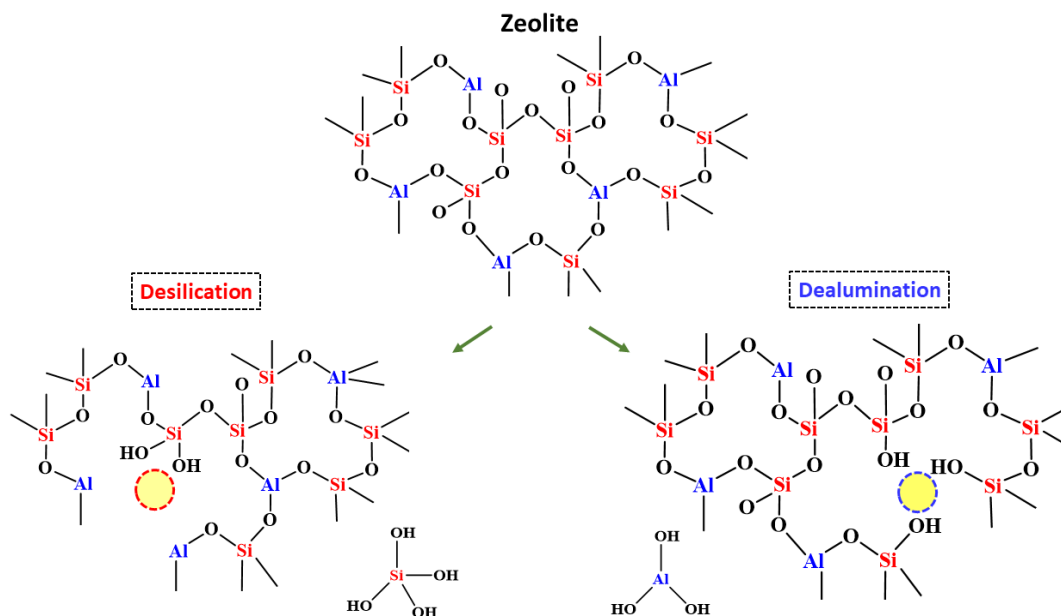


**Figure 1.7.** Representation of desilication and dealumination of zeolite

- Phosphate modification on zeolites results in the generation of a new kind of low-strength phosphate type (P–OH) of acid sites as presented in figure 1.8<sup>38</sup>.

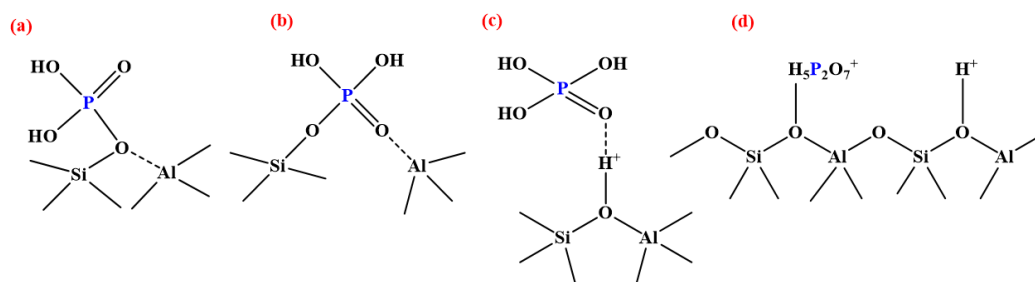


**Figure 1.8.** Types of phosphate acid site species in phosphate-modified zeolites

Upon phosphate addition, the pore size is narrowed and volume gets decreased, whereas Brönsted acidic sites in the framework are altered. The SAR of the zeolites directs the formation of different types of phosphate active sites. At higher SAR, the acidity would increase and the density of the phosphate acid sites decreases resulting in better acid site spacing and offering more number of acid sites. Similarly, for lower SAR, the acidity can either increase or slightly decrease depending on the treatment and conditions.

- Metal ion exchange, metal loading by impregnation, encapsulation, or isomorphous substitution generates Lewis acidic sites. Such catalysts owing to their bifunctional acidic nature (Brönsted and Lewis acidic sites) can help in exploring reactions that demand both Brönsted and Lewis acidity.

### 1.5.4 Silicoaluminophosphate / Zeotype materials

Silicoaluminophosphates (SAPO) are zeotype (zeolite-like) materials formed by the substitution of Si by P or Al–P pair and these materials are made up of well-defined channels that specifically help in shape selective heterogeneous catalysis<sup>46</sup>. They are also called molecular sieves due to the arrangements present in the channels that accommodate molecules with respect to their shape and size. SAPO–11 and SAPO–34 are important examples of the class of silicoaluminophosphate materials that find industrial applications for their shape-selective catalytic nature. SAPO–11 due to the unidimensional medium tubular-elliptical pore channel system (6.5×4.0) and mild acid strength has an excellent application in hydroisomerization processes<sup>16</sup>. SAPO–34 is an exceptional catalyst for methanol to olefin (MTO) reaction as it offers restriction for the diffusion of branched and heavy hydrocarbons thereby enhancing the linear olefins (ethylene and propylene) selectivity<sup>47</sup>. The acidity in SAPO materials is due to the charge imbalance generated by the substitution of Si by an aluminophosphate type of species which results in the formation of bridging hydroxyl groups yielding Brønsted acidity (figure 1.9)<sup>48</sup>.

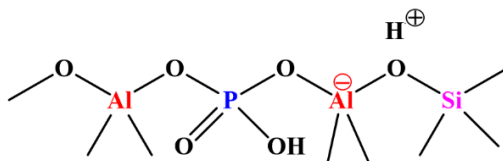


**Figure 1.9.** Structure of acid site in silicoaluminophosphate material

SAPO–11 and SAPO–34 are synthesized by template-assisted hydrothermal method, in which the precursors (silica, alumina, and phosphate source) are homogenized in distilled water. The mixture is then transferred to a teflon lined stainless steel autoclave and placed in a preheated oven at the required temperature and time for the formation of the framework. Once the reactor is cooled, the material is filtered, washed, dried, and calcined at high temperatures yielding SAPO catalyst.

### 1.5.4 Mesoporous materials

Porous materials can be basically classified into three major categories considering their pore size. The pore diameter of the mesoporous materials is in the range of 2 to 50 nm, whereas the micropore and macroporous range is <2 nm and >50 nm respectively. The

examples for mesoporous materials are silica–alumina, IRMOF–16, NU–100, KIT–5, KIT–6, MCM–48, pillared clay, FDU–12, starbon, metal oxides, sulfated zirconia, SBA–15 etc <sup>49</sup>. The mesoporous materials have advantages such as the availability of a varied range of pore sizes (2 to 50 nm) that helps in efficient mass transport and better interface reaction sites compared to microporous materials. Additionally, materials with different morphologies such as nanosheets, nanofibers, nanospheres, and core shells can be obtained <sup>50</sup>.

#### 1.5.4.1 Ordered mesoporous materials (OMMs)

These are a class of porous materials with ordered mesoporosity that are mostly determined by low–angle XRD diffractograms and the walls of the materials are amorphous in nature <sup>51</sup>. Some examples for OMMs are MCM–41, SBA–15, SBA–16, IITM–56, FDU–15, CMK–1, CMK–3, MOF–180, MOF–200 <sup>51,52</sup> etc. Among these materials, SBA–15 (Santa Barbara Amorphous type15), an ordered mesoporous silica has remarkable applications in the field of heterogeneous catalysis <sup>53</sup> due to its high surface area, good thermal stability, fairly high acidity upon suitable modification, and uniform mesoporosity. SBA–15 as such is used as a support material for various catalytic transformations. It is made up of a two–dimensional hexagonal array of mesopores distributed uniformly that ease the diffusion of reactive species during the reaction. As such SBA–15 is inert towards catalysis and functionalizing it by dispersion with the specific active site species is easily feasible due to the availability of a large surface area ( $>600 \text{ m}^2 \text{ g}^{-1}$ ). Functionalization or modification of SBA–15 to produce different catalysts by active site addition or modification such as Ti–SBA–15, Co–SBA–15, Pd/SBA–15, ZrO<sub>2</sub>/SBA–15, WO<sub>3</sub>/SBA–15, MOF–5/SBA–15, Rh complex/SBA–15 has been reported <sup>53</sup>. These catalyst systems were applied for various catalytic reactions such as ethylene polymerization, epoxidation of styrene using O<sub>2</sub> hydrodeoxygenation reaction of phenol, synthesis of GVL, oxidative removal of 4,6–dimethyldibenzothiophene (DMDBT), Friedel–Crafts alkylation reaction, C–Heteroatom bond formation for the addition of alkynes <sup>53</sup>. Similar to zeolites, when the Si in SBA–15 is isomorphically substituted by Al, acidic sites (B/L ratio  $>1$ ) are generated as shown in figure 1.10.

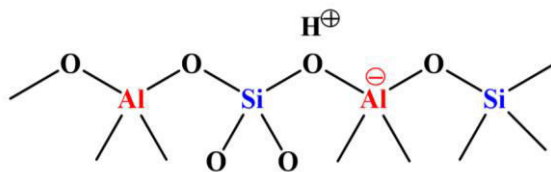


**Figure 1.10.** Nature of acid site in Al-SBA-15

#### 1.5.4.2 Synthesis of mesoporous materials

Mesoporous materials are synthesized by several methods namely soft-templating method, hard-templating method, In-situ templating pathway, template-free packing method, multiple-templating method, and reticular chemistry guiding approach as shown in figure 1.11<sup>54</sup>. Details of each method are presented below.

- a. In the soft-templating method (or endotemplating), initially, the precursors and templates (structure directing agents) are assembled to get mesoporous structure and upon further removal of the template, OMM is obtained. Examples of the catalysts synthesized using the soft-templating method are MCM-41, and SBA-15<sup>55,56</sup>.
- b. In the hard-templating (nano casting or exotemplating) method of synthesis, there is direct mixing of the preformed templates and precursors and upon removal of the template, OMM is produced. Examples of the materials synthesized using hard-templating method are KIT-6, CMK-1, mesoporous graphene nanoball<sup>56,57</sup>.
- c. Multiple-templating method is a synthesis procedure where both hard and soft-templating routes are employed that produces a hierarchical form of porous materials. Some of the materials synthesized using multiple-templating method are mesoporous  $\text{Co}_3\text{O}_4$ ,  $\alpha\text{-MnO}_2$ , 3D-porous graphitic carbon composites containing sulfur nanoparticles, multi-layered mesoporous  $\text{TiO}_2$  thin films<sup>58,59,60</sup>.
- d. In-situ templating pathway is a synthesis method in which a template is obtained in situ during the material synthesis itself without the need for a presynthesized template. Examples of the materials obtained via in-situ templating pathway are mesoporous  $\text{TiO}_2$  mesocrystals, mesoporous  $\text{Cu}_3(\text{BTC})_2$ <sup>61,62</sup>.
- e. In the template-free packing method, self-aggregation of the precursors occurs in the absence of a template in which the precursor undergoes nucleation, growth, and



- aggregation to yield a mesoporous structure. Materials obtained via template-free packing method are organo-lead trihalide perovskite,  $\text{Fe}_3\text{O}_4$ @titanate<sup>63,64</sup>.
- f. The reticular chemistry guiding approach uses building blocks (typically organic linkers, inorganic complexes, or clusters) that transform into the backbone of the material during the synthesis process itself. Mesoporous metal organic frameworks and covalent organic frameworks are synthesized using this method<sup>65</sup>.

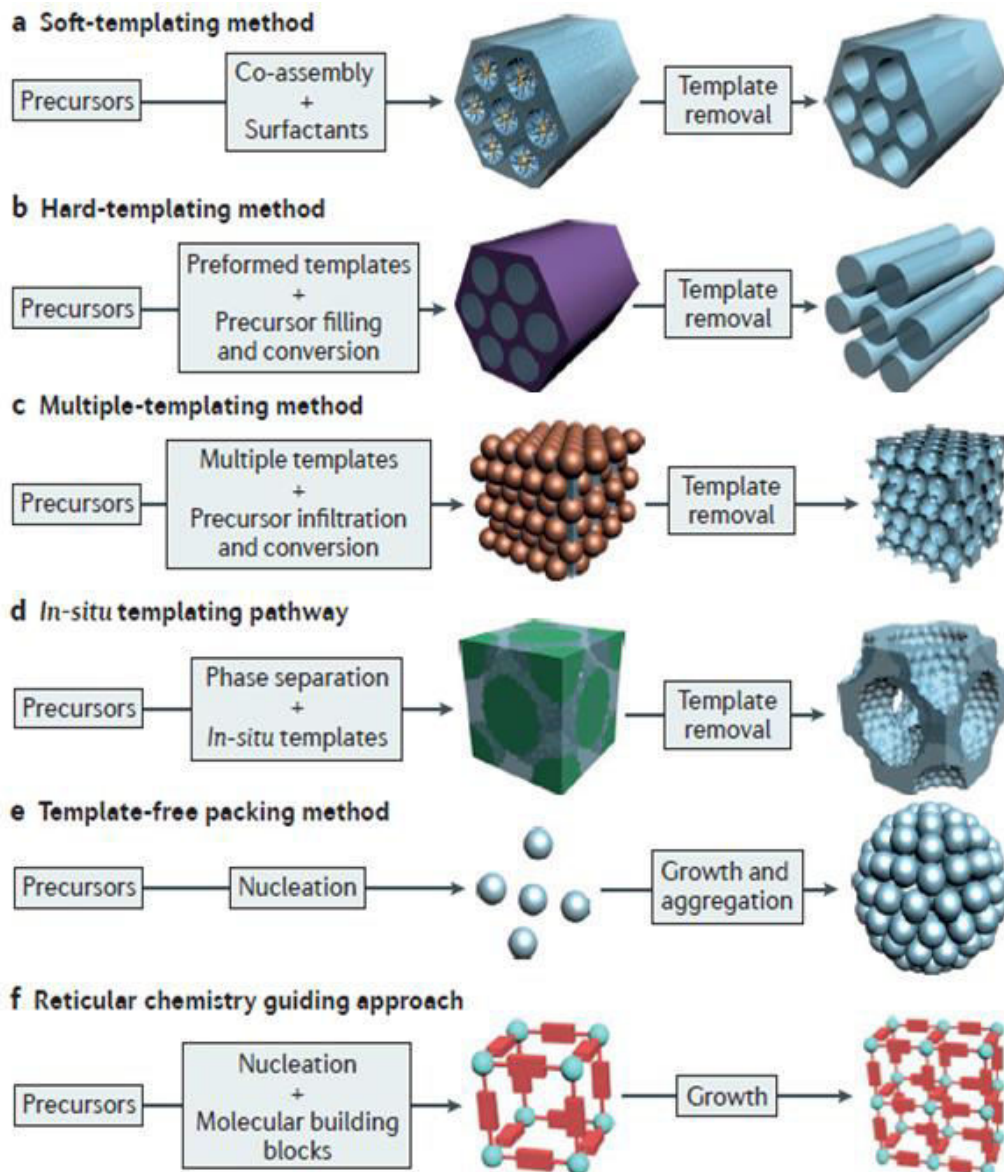


**Figure 1.11.** Various methods for mesoporous material synthesis<sup>54</sup>. (a) Soft-templating method, (b) Hard-templating method (c) Multiple-templating method, (d) In-situ templating pathway, (e) Template-free packing method, (f) Reticular chemistry guiding approach

### 1.5.5 Functionalized zirconia

Metal oxides are one of the important types of catalysts for industrial heterogeneous catalysis. Various metal oxides such as  $\text{Al}_2\text{O}_3$ ,  $\text{TiO}_2$ ,  $\text{SiO}_2$ ,  $\text{ZrO}_2$ ,  $\text{CeO}_2$ ,  $\text{ZnO}$ , clays, zeolites, silica–alumina, mesoporous oxides, polyoxometallates (POMs), perovskites have made their ways for different industrial processes <sup>66,67</sup>. Metal oxides find applications in acid–base catalysis, oxidation and hydrogenation reactions, photocatalysis, pollution control, etc due to their properties such as redox property, acidity, and basicity. The Brønsted acidity is generated by functionalizing the metal oxides by various modifications and examples for such materials are  $\text{H}_4\text{SiW}_{12}\text{O}_{40}/\text{ZrO}_2$ ,  $\text{WO}_3/\text{Al}_2\text{O}_3$ ,  $\text{WO}_3\text{–SnO}_2$ ,  $\text{SO}_4^{2-}\text{–ZrO}_2$ .

Sulfation of metal oxides is one such functionalization technique that results in the generation of super acidity due to which such materials can efficiently catalyze various catalytic reactions by successfully competing with the strong mineral acids <sup>68</sup>. The super acidity of various solid materials can be compared with the mineral acid using a Hammett acidity function ( $H_0$ ) as presented in table 1.4.

**Table 1.4.** Hammett acidity values of solid acid catalysts

Sn	Catalysts	$H_0$ value	Ref
1.	$\text{SO}_4^{2-}\text{–ZrO}_2$	-16.1	68
2.	$\text{SO}_4^{2-}\text{–HfO}_2$	-16.0	68
3.	$\text{SO}_4^{2-}\text{–TiO}_2$	-14.6	68
4.	$\text{WO}_3\text{–SnO}_2$	-14.6	68
5.	$\text{H}_2\text{SO}_4$	-11.9	16
6.	Y–Zeolite (SAR 5.1)	-10.4 <sup>(a)</sup>	69
7.	Ferrierite (SAR20)	-8.4 <sup>(a)</sup>	69
8.	Al–SBA–15 (SAR35)	-8.3 <sup>(a)</sup>	69
9.	H–Beta (SAR25)	-8.1 <sup>(a)</sup>	69

(a) Experimentally determined using the formula  $H_0 = a+b (1/T_m)$  where a and b are empirical constants specific for aluminosilicate catalysts <sup>70,71</sup> and  $T_m$  is the temperature peak maximum from  $\text{NH}_3\text{–TPD}$  profile.

As it is evident, the sulfated zirconia, a super acid has the  $H_0$  value of -16.1 higher than 100%  $\text{H}_2\text{SO}_4$  ( $H_0 = -11.9$ ). The high thermal stability, super acidity, and heterogeneity make sulfated zirconia one of the most desirable catalysts to work for many organic transformations such as cyclization, ethanol dehydration, benzene acylation, naphthalene,

alkane isomerization, anthracene, ring–opening of aziridines, ring–opening of epoxides, aromatic gem–dihalides production, chlorobenzene nitration, production of diaryl sulfoxides and many more<sup>72,73, 74</sup>.

### 1.5.6.1 Active sites of sulfated zirconia

Extensive studies on the active site structure of sulfated zirconia have been done to arrive at the nature of the active site offered by the material for reactions. Figure 1.12 summarizes the elucidation of various active site species of sulfated zirconia structures (a to l) predicted by various subject experts in literature<sup>75,76,77,78,79,80,81,82</sup>.

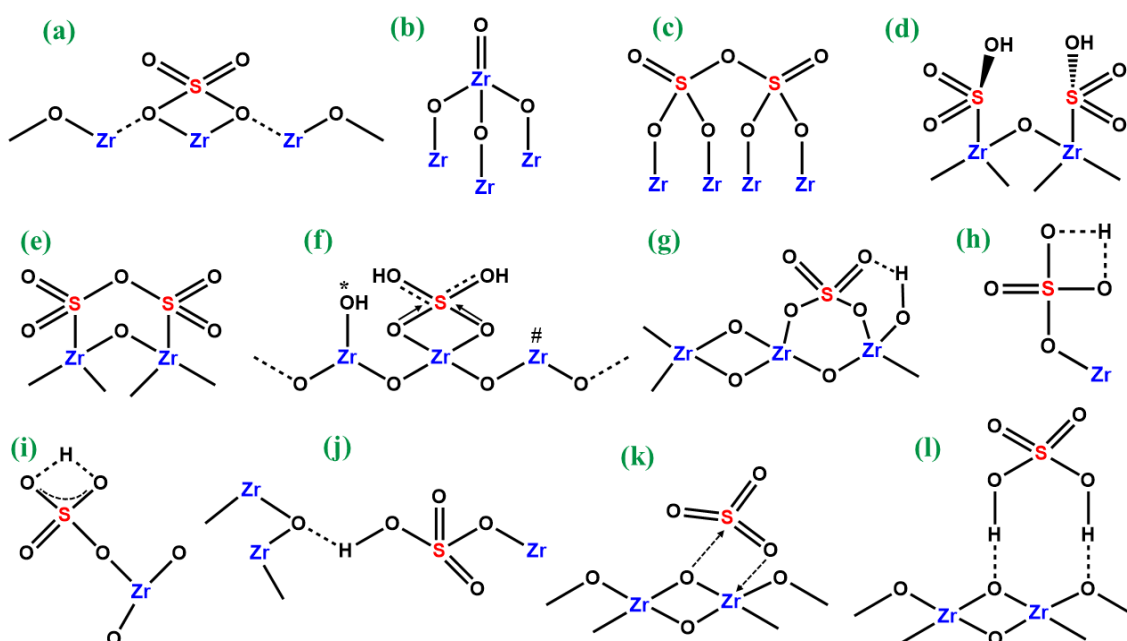


**Figure 1.12.** Proposed structure of the active site species in sulfated zirconia

### 1.5.6.2 Synthesis of sulfated zirconia.

Sulfated zirconia is synthesized by a precipitation process where zirconium precursor is precipitated to  $Zr(OH)_4$  by the addition of a basic solution. The intermediate  $Zr(OH)_4$  is thoroughly washed using distilled water to remove the halides adsorbed on the material and dried well before subjecting it to sulfation. A certain molar solution of sulfuric acid is treated with the material in order to generate Brönsted acidity. The catalyst was calcined and then the physisorbed leachable sulfate species were removed by water wash to yield sulfated zirconia.

### 1.5.7 Metal–Organic Framework Materials

MOFs are a class of porous, synthetic materials made up of organic linkers which are the backbone of the framework interacting with metal clusters leading to the formation of networks<sup>83</sup>. The metal clusters are the secondary building units (SBU) of the material which represent the nodes of the MOFs that are stitched with multifunctional, branched organic linkers generating a framework for the material (figure 1.13)<sup>84</sup>. MOFs have major applications in the field of catalysis (heterogeneous, photocatalysis, electrocatalysis)<sup>25,85,86,87</sup>, bioremediation<sup>88</sup>, drug storage and delivery<sup>89,90</sup>, gas storage and separation<sup>91</sup>, hydrogen economy<sup>92</sup>, and sensing<sup>93</sup>.

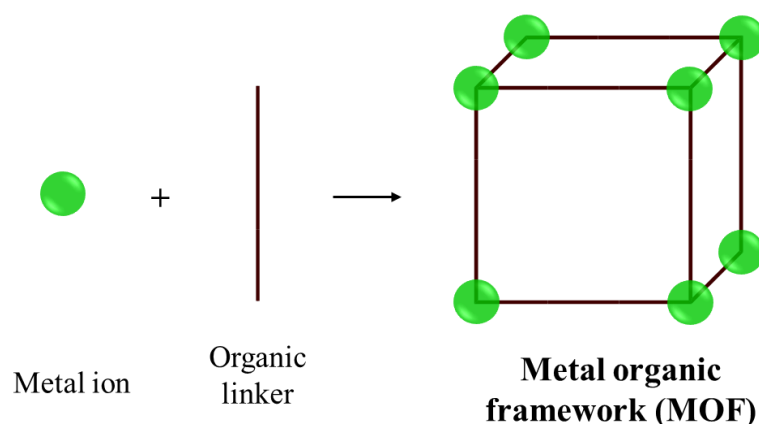


**Figure 1.13.** The basic structure of metal–organic framework (MOF)

#### 1.5.7.1 Properties of MOFs for catalysis<sup>94,95</sup>

- The base MOFs without functionalization contain metal centers and linkers as active centers and may have a large surface area, topology, chemical and thermal stability, and porosity which can have a significant impact on their catalytic applications.
- Easy functionalization and generation of heterogeneity in the material: This can be done by mixing different organic linkers within a MOF, mixing more than one metal cluster in the MOF, mixing both organic linkers and the metal clusters within the same MOF, introducing different functional groups and defects in the framework, the addition of nanoparticles or single atoms within the pores. The design and architecture of the MOFs can be modified flexibly for any given application achieved by substituting, functionalizing, or encapsulating new species into the framework. Through this process, specific active sites as required by the catalytic reaction can be incorporated into the framework.

- Acidity in MOFs for catalysis: The acidity (Lewis and Brønsted acid sites) in MOF can be obtained from the metal clusters, linkers, functionalization of both, or the guest species bound to the metal clusters, linker, or pores<sup>96,97,98,99,100</sup>. Possible types of Brønsted and Lewis acid sites in MOFs are shown in figure 1.14. The Lewis acidity is generated due to the metal clusters, coordinatively unsaturated metal sites, missing linker, missing metal clusters, isolated metal clusters, or the presence of electron-withdrawing moieties. Some examples of Lewis acidic MOFs are UiO-66, MIL-101, MOF-808, MOF-5, Fe(BTC), MIL-100(Fe), Dy-MOF, Tb-MOF, ZrOTf-BTC, MOF-545-TFA. On the other hand, the Brønsted acidity can be generated by the presence of strongly acidic proton, inorganic moieties with protonic sites covalently bound to the clusters or Brønsted acidic molecules encapsulated in the pores of the MOFs. Some examples for the Brønsted acidic MOFs are MIL-101-SO<sub>3</sub>H, UiO-SO<sub>3</sub>H (Zr/Hf), MOF-808-SO<sub>4</sub>, POM@HKUST-1, NU-601, defective UiO-66, reo-MOF-1, BUT-8(Cr)-SO<sub>3</sub>H, spiro-1/2, Cu-MOF-HCl, In-MOF-PO<sub>2</sub>H.

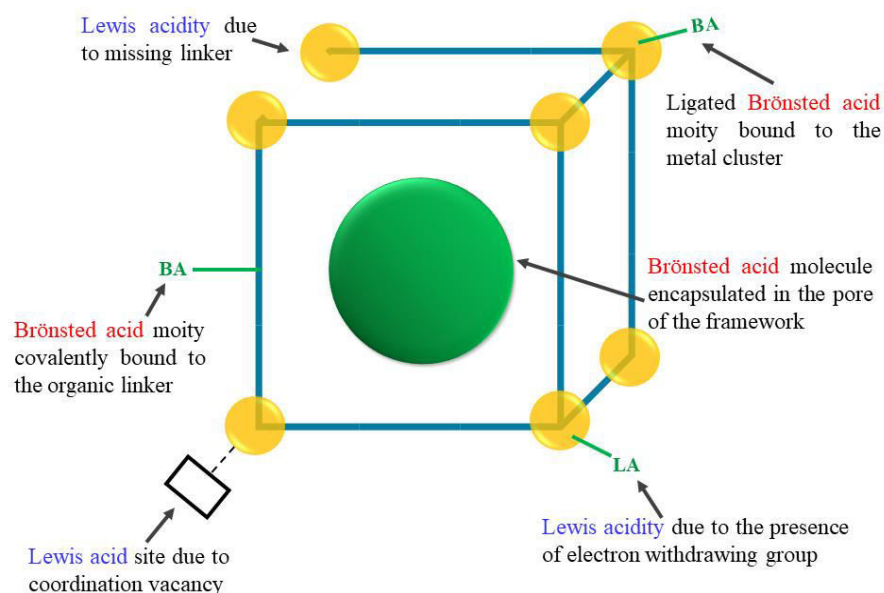


**Figure 1.14.** Types of acid sites in metal-organic framework

- Tunable porosity: The pore size of a MOF can be tailor-made by switching the existing linkers with the linkers containing bigger or lengthier ring structures. The materials thus obtained are referred to as isorecticular MOFs. UiO-66, UiO-67 and UiO-68 MOFs fall under the category of isorecticular MOFs.

- Encapsulation of species: The incorporation of various active species such as metal nanoparticles, polyoxometalate compounds, heteropoly compounds, metal clusters, etc. can be successfully done inside the pores of the MOFs

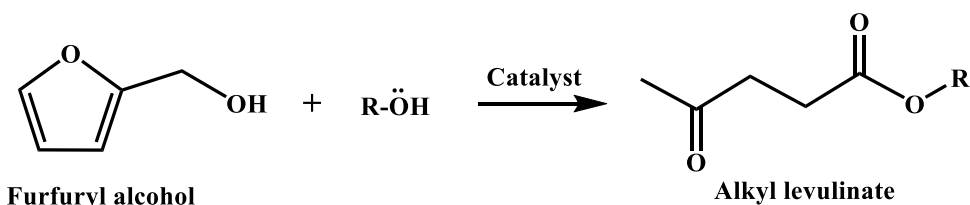
### 1.5.7.2 Synthesis of MOFs

Various procedures such as hydrothermal, solvothermal, microwave, sonochemical, electrochemical, and mechanochemical methods can be employed to synthesize MOFs. The majority of the catalyst is synthesized by a solvothermal method in the presence of a basic solvent (in general DMF) that helps in the deprotonation of the organic linker thus helping it bind with the metal cluster. In a typical synthesis, the precursor (metal clusters, organic linker, modulator) are homogenized in the presence of solvent and then transferred to the teflon lined stainless steel autoclave which is then placed in the preheated oven for a certain time. Once the autoclave is cooled to room temperature, the material is thoroughly washed with required solvents to remove unreacted precursors and finally activated to remove the guest molecules.

## 1.6 Literatures survey

### 1.6.1 Butanolysis of furfuryl alcohol to produce butyl levulinate.

Alkyl levulinates are the versatile building blocks for the synthesis of various chemicals owing to the presence of two functional groups *viz.* a ketone, and an ester <sup>101</sup>. They have shown great potential for bio-renewable fuels like bio-lubricants and blending components in biodiesel. Also, it has additional applications in chemical synthesis, polymer or resin precursors, green solvents, plasticizers, food-flavor agents, and pharmaceuticals <sup>102,103,104</sup>. The major application of butyl levulinate (BL) and ethyl levulinate (EL) is their use as a fuel additive due to their distinguishing properties present for blending applications (nontoxic, solubility, flow, and lubricity) <sup>105</sup>. Alcoholysis of furfuryl alcohol driven by solid acid catalyst yields alkyl levulinate (Scheme 1.1).



**Scheme 1.1.** Alkyl levulinate synthesis from furfuryl alcohol and alkyl alcohol

An intermediate called alkoxy methyl furan (AMF) is easily formed from FA whose further transformation to alkyl levulinate is challenging due to the ring opening step. There are several solid catalysts such as zeolites, mesoporous materials, functionalized metal oxides, ionic liquids, heteropolycompounds, etc reported for the butanolysis of FA to produce BL, and a thorough literature survey with the reaction conditions, recyclability data is presented in table 1.5.

**Table 1.5.** The Literature survey of furfuryl alcohol butanolysis to produce butyl levulinate

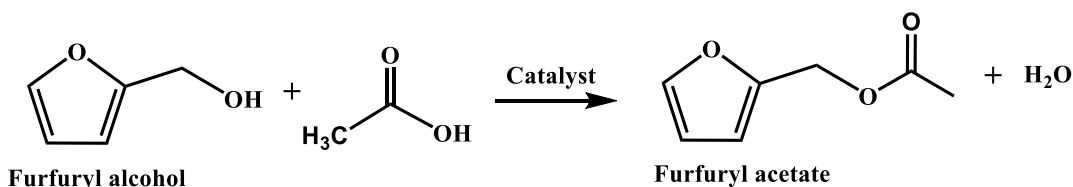
Sn	Catalysts	Catalyst (wt. %) wrt FA	T (°C)	Mole ratio	BL Yield (%)	Reusability	Ref
1.	Reduced graphite oxide	4	110	1:25	99	NR	106
2.	Sn <sub>1</sub> TPA/K-10	160	120	1:10	98	3	107
3.	TPA/SBA-16	300	110	1:65	97	84%-4 C	108
4.	Sulfated SBA-15	25	110	1:35	96	NR	109
5.	Lignin-based carbonaceous acid	75	110	1:53	95	84%-3C	110
6.	Ti-KIT-6	300	110	1:60	94	4	111
7.	Al-SBA-15	400	110	1:65	94	82%-4C	112
8.	HPAs and POM-based IL- H <sub>5</sub> AlW <sub>12</sub> O <sub>40</sub> & [MIMBS] <sub>5</sub> [AlW <sub>12</sub> O <sub>40</sub> ]	5% mmol	120	1:55	94	80%-4C	113
9.	Zn <sub>x</sub> TPA/Nb <sub>2</sub> O <sub>5</sub>	300	110	1:65	94	4	101
10.	SnPO-P123	100	160	1:10	94	3	114
11.	[(HSO <sub>3</sub> -p) <sub>2</sub> im] [HSO <sub>4</sub> ]	13	120	1:22	93	8	115
12.	[BmimSO <sub>3</sub> H] <sub>3</sub> PW <sub>12</sub> O <sub>40</sub>	180	120	1:48	93	1	116
13.	α- Fe <sub>2</sub> O <sub>3</sub>	5200	250	1:500	86	38%-1C	117
14.	KCC-1/Pr-SO <sub>3</sub> H	98	120	1:10	81	70%-4C	118
15.	TNTs-SO <sub>3</sub> H	300	120	1:55	80	67%-4C	119

NR-not reported

### 1.6.2 Esterification of furfuryl alcohol to produce furfuryl acetate

Esterification of furfuryl alcohol with acetic acid yielding furfuryl acetate (FAC) is a typical acid-catalyzed reaction as shown in Scheme 1.2. FAC has applications in the food

and flavor industries and as a potential fuel additive. The report on this transformation is limited to one <sup>120</sup> although one-pot synthesis of FAc from furfural (hydrogenation and esterification) has a few reports <sup>121,122,123</sup>. Table 1.6 presents the literature of the reported catalyst, the metal exchanged heteropoly acid encapsulated in MOF.



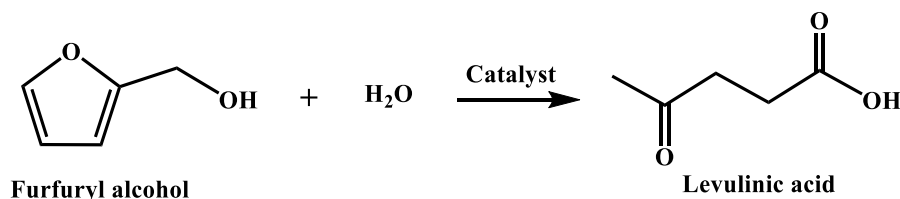
**Scheme 1.2.** Furfuryl acetate synthesis from furfuryl alcohol and acetic acid via esterification.

**Table 1.6.** The Literature survey of furfuryl alcohol esterification to produce furfuryl acetate

Sn	Catalyst	Reaction conditions	FAc Yield (%)	Reusability	Ref
1.	Fe-DTP@ZIF-8	T=100 °C, time =6h, mole ratio = 1:6	78	73%–5 runs	<sup>120</sup>

### 1.6.3 Hydrolysis of furfuryl alcohol to produce Levulinic acid

The furfuryl alcohol hydrolysis yields levulinic acid which itself is another important platform chemical used to obtain various speciality chemicals such as GVL, angelica lactone, alkyl levulinates, amino levulinic acid, succinic acid, etc (Scheme 1.3).



**Scheme 1.3.** Furfuryl alcohol hydrolysis to produce levulinic acid

Levulinic acid can be produced from the hexose route starting from cellulose which transforms into LA via various intermediates (glycerol, fructose, HMF). HMF is a commercially important compound and more expensive than FA and hence, its direct hydration to produce LA is not a viable route. There are a few acid catalyst systems reported for the FA hydrolysis to produce LA as presented in table 1.7 with details of the reaction conditions employed <sup>124,125,126,127,128</sup>. The reported catalysts are majorly Brønsted acidic in nature with hydroxy or sulfonic acid moieties as active sites.



**Table 1.7.** The Literature survey of furfuryl alcohol hydrolysis to produce levulinic acid

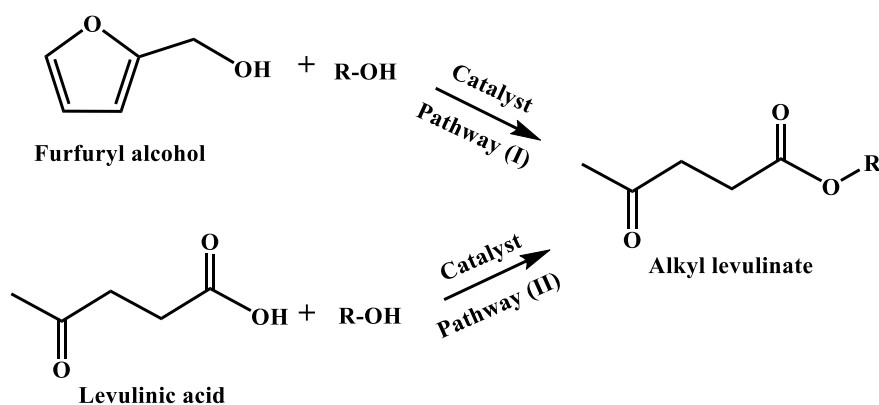
Sn	Catalyst	Temp, catalyst conc, time	FA: H <sub>2</sub> O: solvent mole ratio	Reactor system	LA Yield (%)	Reusability cycles	Ref
1.	SiNFeSO <sub>3</sub> H	120 °C, 99wt %, 2.5h,	1: 55: 95 (GVL)	30 bar N <sub>2</sub> in HPA <sup>a</sup>	90	3C (decreased)	124
2.	ArSO <sub>3</sub> H–Et –HNS	120°C, 2h	1: 15: 15 (Acetone)	HPA <sup>a</sup>	83	3C (decreased)	125
3.	Dealuminate d HZSM–5 (SAR 23)	120 °C, 39 wt %, 0.5h	1: 18: 40 (Acetone)	Seal tube	76	3 C (decreased)	128
4.	HZSM–5 (SAR 23)	120 °C, 62 wt %, 0.5h	1: 9.3: 9.3 (THF)	Seal tube	74	2 C (Good)	126
5.	HZSM–5 (SAR 50)	140 °C, 9.8 wt %, 23 h	1: 5.6: 4.2 (MEK)	10 bar H <sub>2</sub> in HPA <sup>a</sup>	77	2 C (decreased)	127

<sup>a</sup>High pressure autoclave

#### 1.6.4 Ethyl levulinate synthesis from furfuryl alcohol/levulinic acid and ethanol

Ethyl levulinate, a product obtained from ethanolyis of furfuryl alcohol or esterification of levulinic acid ( Scheme 1.4 ) is used as an oxygenate and additive for petrodiesel <sup>129</sup>. Its fuel additive application is due to its properties such as lubricity, solubility, and nontoxic nature <sup>105</sup>. Alkyl levulinates as such have applications in various fields *viz.* food–flavor agents, polymer or resin precursors, green solvents, etc <sup>102,104</sup>. Ethyl levulinate (EL) synthesized from two different pathways *i.e.* furfuryl alcohol/ levulinic acid and EtOH is an acid–catalyzed reaction and various catalyst systems such as zeolites, modified zeolites, heteropolycompounds, metal–organic frameworks, organic–inorganic hybrid materials, functionalized mesoporous materials, supported metal catalysts, etc have been reported for both the pathway separately. There are common catalyst systems reported for both pathways too <sup>130,131,132,133</sup>. The overall literature of the reported catalysts with the reaction conditions and EL yield are presented separately for

both the pathways in Table 1.8 [pathway (I): Ethanolysis of furfuryl alcohol] and Table 1.9 [pathway (II): Esterification of levulinic acid].



**Scheme 1.4.** Ethyl levulinate synthesis from furfuryl alcohol and levulinic acid

Pathway (I): Furfuryl alcohol ethanolysis to produce ethyl levulinate

**Table 1.8.** The Literature survey of furfuryl alcohol ethanolysis to produce ethyl levulinate

Sn	Catalysts	T (°C)	Time (h)	Mole ratio	EL yield (%)	Reusability	Ref
1.	Modified zirconium phosphate	200	2	1:50	97	94%–4C	134
2.	TiHTPA	120	0.5	1:43	97	95%–5C	135
3.	ZrTPA/ $\beta$ -zeolite	130	5	1:85	96	4C	136
4.	Zr-DBS	150	2	1:170	95	4C	137
5.	[(HSO <sub>3</sub> -p) <sub>2</sub> im][HSO <sub>4</sub> ]	110	3	1:27	95	4C	115
6.	Polystyrene microspheres PS-SO <sub>3</sub> H	120	1.5	1:170	95	4C	138
7.	p-TSA-PFD	78	6	1:30	94	6C	139
8.	SBA-15/H-ZSM-5	110	5	1:35	89	48%–4C	140
9.	UiO-66 (Hf)-SO <sub>3</sub> H	120	4	1:350	88	73%–4C	130
10.	Meso-MIL-101(Cr)	160	2	1:60	84	66%–5C	141
11.	ArSO <sub>3</sub> H-Si(Et)Si-Ph-NTs	120	2	1:60	83	59%–5C	133
12.	ArSO <sub>3</sub> H-HMCS	120	–	1:69	82	–	131
13.	Al-TUD-1	140	1	1:56	80	–	142
14.	P doped carbon	140	6	1:54	80	56%–6 C	143
15.	MIL-101(Cr)-SO <sub>3</sub> H	140	2	1:60	79	71%–5C	144
16.	$\alpha$ -Fe <sub>2</sub> O <sub>3</sub>	250	1	1:20	73	38%	117

17.	Nano H-ZSM-5	120	6	1:8	69	5C decreased	145
18.	PW <sub>12</sub> /ZrO <sub>2</sub> -Si(Et)Si	120	2	1:60	64	53%-3 C	146
19.	Phosphomolybdic acid/ activated charcoal	140	3	1:168	63	-	132
20.	ZSM-5 (30)	125	-	1:2.7	65 *		
21.	H-Beta	125	-	1:2.7	15 *	-	147
22.	Mordenite	225	-	1:2.7	37 *		
23.	Si(Et)Si-PrSO <sub>3</sub> H-Et-H NS	120	2	1:60	59	56%-3C	148

\*Semi batch mode,  $WHSV=7 \text{ g}_{\text{Falc}}\text{g}_{\text{cat}}^{-1}\text{h}^{-1}$

Pathway (II): Levulinic acid esterification to produce ethyl levulinate

**Table 1.9.** The Literature survey of levulinic acid esterification to produce ethyl levulinate

Sn	Catalyst	T (°C)	Time (h)	Mole ratio	EL yield (%)	Reusability	Ref
1.	ArSO <sub>3</sub> H-HMCS	78	4	1:7	100	10C	131
2.	UDCaT-5	160	3	-	100	-	149
3.	MOF supported polyoxometalates Cu BTC	120	4	-	100	3C	150
4.	SO <sub>3</sub> H- benzimidazolium based polyionic liquid	70	9	1:10	99	5-C	151
5.	HClO <sub>4</sub> /SiO <sub>2</sub>	100	5	1:86	99	90%-5C	152
6.	UiO-66- (COOH) <sub>2</sub>	78	24	1:20	97	93%-5C	153
7.	PWA/ZrO <sub>2</sub>	150	3	1:17	97	81%-5C	154
8.	Micro/meso-HZSM-5	120	5	1:8	95	-	155
9.	Desilicated HZSM-5	120	5	1:8	95	6C	156
10.	EPTN (phosphotungstic acid/TiO <sub>2</sub> )	120	2	1:42	95	5C	157
11.	Sulfonated hydrothermal carbon glucose	60	3	1:5	94	-	158
12.	DodecaTPA/desilicated H-ZSM-5	84	4	1:8	94	4C	159
13.	ArSO <sub>3</sub> H-Si(Et)Si-Ph-NTs	78	3	1:7	94	3C	133
14.	Loofah sponge derived carbon	80	10	1:5	91	4C	160

15.	H <sub>3</sub> PW <sub>12</sub> /ZrO <sub>2</sub> -Si(Ph)Si	Reflux	3	1:7	91	75%-3C	161
16.	H <sub>4</sub> SiW <sub>12</sub> O <sub>40</sub>	25	8	1:18	90	-	162
17.	Sulphated TiO <sub>2</sub> /ZrO <sub>2</sub> nano-composites	105	3	-	90	60%-5C	163
18.	Sulfonated carbon	120	9	1:5	88	76%-2C	164
19.	Silicotungstic acid/AlSBA-15	75	5	1:10	87	41%-4C	165
20.	UiO66-SO <sub>3</sub> H	80	6	1:10	87	84%-5C	166
21.	Carboncryogel crystal	150	4	1:15	87	-	167
22.	Sulfated zirconia NP	70	8	1:10	86	81%-3C	168
23.	UiO-66(Hf) -SO <sub>3</sub> H	120	2	1:330	86	82%-5C	130
24.	Phosphomolybdic acid /activated charcoal	80	15	1:100	80	3C-decreased	132
25.	Sulfated ZrSBA-15	70	24	1:10	79	55%-5C	169
26.	Hierarchical ZSM-12 nanolayers	100	24	1:1	77	-	170
27.	Nanosized tin oxide	70	7.5	1:5	77	-	171
28.	Amberlyst-15	78	5	1:20	71	-	172
29.	Sulfated Si-doped ZrO <sub>2</sub>	70	10	1:10	65	5	173
30.	Carboncryogel crystal	78	10	1:19	61	-	167
31.	Sulphonated MWCNT	70	5	1:5	54	-	174
32.	Micro-meso H/BEA zeolite	78	5	1:6	40	4	175
33.	Powder Sulfated zirconia	70	7	1:3	40	39%-5C	167

## 1.7. Gaps found in the literature

Following research gaps have been identified based on the literature survey for all four schemes.

### 1.7.1 Butanolysis of furfuryl alcohol to produce butyl levulinate

- Usage of a higher amount of catalyst and higher FA to alcohol ratio which doesn't meet the requirements of green chemistry
- Many reports involve difficult catalyst synthesis procedures
- The major pitfall observed is the saturation of the active sites of the catalyst due to the humin deposition. This affects recyclability which is not addressed in most of the reported literature

### **1.7.2 Furfuryl acetate synthesis from furfuryl alcohol via esterification**

- It is a less explored reaction where the literature is limited to one report. The catalyst studied involved a tedious synthesis procedure and the best furfuryl acetate yield reported so far from furfuryl alcohol is 78%. Therefore, there is room for improvement in enhancing the furfuryl acetate yield using new catalyst systems
- The nature of active sites required for this reaction remains unexplored as a thorough catalyst study is not conducted so far

### **1.7.3 Hydrolysis of furfuryl alcohol to produce levulinic acid**

- There are only a few literatures available which motivated us to investigate more with newer materials.
- In a few reported literatures, reactions are operated in pressurized reaction conditions using a high–pressure autoclave reactor system.
- Some reports employ a high amount of catalyst and also the catalysts have failed to retain their catalytic activity upon recycling.
- As the use of solvent is important in the reaction, the reported solvents are mostly lower boiling compounds that sometimes raise the question of the resinification of furfuryl alcohol due to the lack of homogeneity in the reaction mixture. Therefore, investigation of an appropriate solvent system that would help in the reduction of the humin formation is necessary.

### **1.7.4 Ethyl levulinate synthesis from furfuryl alcohol/levulinic acid and ethanol**

- There are very few studies reported on designing a common catalyst system for both ethanolysis and esterification reactions
- Most of the reports with the higher ethyl levulinate yield used a high amount of catalyst or reactants (ethanol) or used a longer reaction time. In some cases, the reaction temperatures operated were unusually higher than the other reported conditions
- Many catalysts failed to give competitive results during the recyclability study

## 1.8. Objectives of the proposed work

- To synthesize eco–friendly, novel solid acid catalysts for furfuryl alcohol valorization to produce butyl levulinate, ethyl levulinate, furfuryl acetate, and levulinic acid via various routes
- To understand and get deep insights into the synthesized catalysts assisted by the advanced characterization techniques and to correlate the physicochemical properties with its catalytic performance
- To achieve better catalytic performance and/or address the drawbacks of the reported catalysts without compromising on catalytic activity
- To study the influence of reaction parameters, catalyst reusability and address the issue of leaching of active sites.
- To obtain computational insights using DFT for a better understanding of the catalyst and the reactions for selected studies

## 1.9 Bibliography

- (1) Werpy, T.; Petersen, G. *Top value added chemicals from biomass: volume I--results of screening for potential candidates from sugars and synthesis gas*; National Renewable Energy Lab., Golden, CO (US), 2004.
- (2) Sharma, S.; Ghoshal, S. K. Hydrogen the future transportation fuel: From production to applications. *Renewable and sustainable energy reviews* **2015**, *43*, 1151-1158.
- (3) Šivec, R.; Grilc, M.; Huš, M.; Likozar, B. Multiscale modeling of (hemi) cellulose hydrolysis and cascade hydrotreatment of 5-hydroxymethylfurfural, furfural, and levulinic acid. *Industrial & Engineering Chemistry Research* **2019**, *58* (35), 16018-16032.
- (4) Wang, F.; Ouyang, D.; Zhou, Z.; Page, S. J.; Liu, D.; Zhao, X. Lignocellulosic biomass as sustainable feedstock and materials for power generation and energy storage. *Journal of Energy Chemistry* **2021**, *57*, 247-280.
- (5) Ennaert, T.; Van Aelst, J.; Dijkmans, J.; De Clercq, R.; Schutyser, W.; Dusselier, M.; Verboekend, D.; Sels, B. F. Potential and challenges of zeolite chemistry in the catalytic conversion of biomass. *Chemical Society Reviews* **2016**, *45* (3), 584-611.

- (6) Mariscal López, R.; Maireles-Torres, P.; Ojeda Pineda, M.; Sádaba Zubiri, I.; López Granados, M. Furfural: A renewable and versatile platform molecule for the synthesis of chemicals and fuels. **2016**.
- (7) Wang, Y.; Zhao, D.; Rodríguez-Padrón, D.; Len, C. Recent advances in catalytic hydrogenation of furfural. *Catalysts* **2019**, 9 (10), 796.
- (8) Iroegbu, A. O.; Hlangothi, S. P. Furfuryl alcohol a versatile, eco-sustainable compound in perspective. *Chemistry Africa* **2019**, 2 (2), 223-239.
- (9) Tukacs, J. M.; Bohus, M.; Dibó, G.; Mika, L. T. Ruthenium-catalyzed solvent-free conversion of furfural to furfuryl alcohol. *RSC advances* **2017**, 7 (6), 3331-3335.
- (10) Signoretto, M.; Taghavi, S.; Ghedini, E.; Menegazzo, F. Catalytic production of levulinic acid (LA) from actual biomass. *Molecules* **2019**, 24 (15), 2760.
- (11) Hayes, G. C.; Becer, C. R. Levulinic acid: A sustainable platform chemical for novel polymer architectures. *Polymer Chemistry* **2020**, 11 (25), 4068-4077.
- (12) Zaera, F. Molecular approaches to heterogeneous catalysis. *Coordination Chemistry Reviews* **2021**, 448, 214179.
- (13) Narayanan, S.; Tamizhdurai, P.; Mangesh, V.; Ragupathi, C.; Ramesh, A. Recent advances in the synthesis and applications of mordenite zeolite—review. *RSC advances* **2021**, 11 (1), 250-267.
- (14) Cesário, M. R.; Barros, B.; Aouad, S.; Gennequin, C.; Abi-Aad, E.; Macedo, D. A. Understanding heterogeneous catalysis: A brief study on performance parameters. In *Heterogeneous Catalysis*, Elsevier, 2022; pp 1-18.
- (15) *Nobel Prizes in Chemistry*. <https://www.nobelprize.org/prizes/lists/all-nobel-prizes-in-chemistry/> (accessed).
- (16) Hattori, H.; Ono, Y. *Solid acid catalysis: from fundamentals to applications*; CRC Press, 2015.
- (17) Li, Y.; Yu, J. Emerging applications of zeolites in catalysis, separation and host–guest assembly. *Nature Reviews Materials* **2021**, 6 (12), 1156-1174.
- (18) Liang, J.; Liang, Z.; Zou, R.; Zhao, Y. Heterogeneous catalysis in zeolites, mesoporous silica, and metal–organic frameworks. *Advanced Materials* **2017**, 29 (30), 1701139.

- (19) Martens, J. A.; Grobet, P. J.; Jacobs, P. A. Catalytic activity and Si, Al, P ordering in microporous silicoaluminophosphates of the SAPO-5, SAPO-11, and SAPO-37 type. *Journal of catalysis* **1990**, *126* (1), 299-305.
- (20) Nagendrappa, G. Organic synthesis using clay catalysts. *Resonance* **2002**, *7* (1), 64-77.
- (21) Gupta, P.; Paul, S. Solid acids: Green alternatives for acid catalysis. *Catalysis Today* **2014**, *236*, 153-170.
- (22) Trombettoni, V.; Lanari, D.; Prinsen, P.; Luque, R.; Marrocchi, A.; Vaccaro, L. Recent advances in sulfonated resin catalysts for efficient biodiesel and bio-derived additives production. *Progress in Energy and Combustion Science* **2018**, *65*, 136-162.
- (23) da Silva, M. J.; de Oliveira, C. M. Catalysis by Keggin heteropolyacid salts. *Current Catalysis* **2018**, *7* (1), 26-34.
- (24) Pârvulescu, V. I.; Hardacre, C. Catalysis in ionic liquids. *Chemical Reviews* **2007**, *107* (6), 2615-2665.
- (25) Gong, W.; Liu, Y.; Li, H.; Cui, Y. Metal-organic frameworks as solid Brønsted acid catalysts for advanced organic transformations. *Coordination Chemistry Reviews* **2020**, *420*, 213400.
- (26) Li, B.; Wen, H. M.; Cui, Y.; Zhou, W.; Qian, G.; Chen, B. Emerging multifunctional metal-organic framework materials. *Advanced Materials* **2016**, *28* (40), 8819-8860.
- (27) Bacakova, L.; Vandrovcova, M.; Kopova, I.; Jirka, I. Applications of zeolites in biotechnology and medicine—a review. *Biomaterials science* **2018**, *6* (5), 974-989.
- (28) Corma, A.; Martinez, A. Zeolites and zeotypes as catalysts. *Advanced Materials* **1995**, *7* (2), 137-144.
- (29) *Database of Zeolite Structures*. [https://asia.iza-structure.org/IZA-SC/ftc\\_table.php](https://asia.iza-structure.org/IZA-SC/ftc_table.php) (accessed).
- (30) Shamzhy, M.; Opanasenko, M.; Concepción, P.; Martínez, A. New trends in tailoring active sites in zeolite-based catalysts. *Chemical Society Reviews* **2019**, *48* (4), 1095-1149.
- (31) Schulman, E.; Wu, W.; Liu, D. Two-dimensional zeolite materials: structural and acidity properties. *Materials* **2020**, *13* (8), 1822.



- (32) Cundy, C. S.; Cox, P. A. The hydrothermal synthesis of zeolites: history and development from the earliest days to the present time. *Chemical reviews* **2003**, *103* (3), 663-702.
- (33) Derbe, T.; Temesgen, S.; Bitew, M. A Short Review on Synthesis, Characterization, and Applications of Zeolites. *Advances in Materials Science & Engineering* **2021**.
- (34) Grand, J.; Awala, H.; Mintova, S. Mechanism of zeolites crystal growth: new findings and open questions. *CrystEngComm* **2016**, *18* (5), 650-664.
- (35) Jia, C.-J.; Liu, Y.; Schmidt, W.; Lu, A.-H.; Schüth, F. Small-sized HZSM-5 zeolite as highly active catalyst for gas phase dehydration of glycerol to acrolein. *Journal of Catalysis* **2010**, *269* (1), 71-79.
- (36) Feliczak-Guzik, A. Hierarchical zeolites: Synthesis and catalytic properties. *Microporous and Mesoporous Materials* **2018**, *259*, 33-45.
- (37) Janardhan, H.; Shanbhag, G.; Halgeri, A. Shape-selective catalysis by phosphate modified ZSM-5: Generation of new acid sites with pore narrowing. *Applied Catalysis A: General* **2014**, *471*, 12-18.
- (38) Blasco, T.; Corma, A.; Martínez-Triguero, J. Hydrothermal stabilization of ZSM-5 catalytic-cracking additives by phosphorus addition. *Journal of catalysis* **2006**, *237* (2), 267-277.
- (39) Manjunathan, P.; Maradur, S. P.; Halgeri, A.; Shanbhag, G. V. Room temperature synthesis of solketal from acetalization of glycerol with acetone: Effect of crystallite size and the role of acidity of beta zeolite. *Journal of Molecular Catalysis A: Chemical* **2015**, *396*, 47-54.
- (40) Feng, R.; Yan, X.; Hu, X.; Wang, Y.; Li, Z.; Hou, K.; Lin, J. Hierarchical ZSM-5 zeolite designed by combining desilication and dealumination with related study of n-heptane cracking performance. *Journal of Porous Materials* **2018**, *25* (6), 1743-1756.
- (41) Groen, J.; Peffer, L. A.; Moulijn, J.; Pérez-Ramirez, J. On the introduction of intracrystalline mesoporosity in zeolites upon desilication in alkaline medium. *Microporous and Mesoporous Materials* **2004**, *69* (1-2), 29-34.
- (42) Ma, Q.; Fu, T.; Li, H.; Cui, L.; Li, Z. Insight into the Selection of the Post-Treatment Strategy for ZSM-5 Zeolites for the Improvement of Catalytic Stability in the Conversion

of Methanol to Hydrocarbons. *Industrial & Engineering Chemistry Research* **2020**, *59* (24), 11125-11138.

(43) Gil, B.; Mokrzycki, Ł.; Sulikowski, B.; Olejniczak, Z.; Walas, S. Desilication of ZSM-5 and ZSM-12 zeolites: Impact on textural, acidic and catalytic properties. *Catalysis Today* **2010**, *152* (1-4), 24-32.

(44) Aloise, A.; Marino, A.; Dalena, F.; Giorgianni, G.; Migliori, M.; Frusteri, L.; Cannilla, C.; Bonura, G.; Frusteri, F.; Giordano, G. Desilicated ZSM-5 zeolite: Catalytic performances assessment in methanol to DME dehydration. *Microporous and Mesoporous Materials* **2020**, *302*, 110198.

(45) Fan, Y.; Bao, X.; Lin, X.; Shi, G.; Liu, H. Acidity adjustment of HZSM-5 zeolites by dealumination and realumination with steaming and citric acid treatments. *The Journal of Physical Chemistry B* **2006**, *110* (31), 15411-15416.

(46) Jin, D.; Li, L.; Ye, G.; Ding, H.; Zhao, X.; Zhu, K.; Coppens, M.-O.; Zhou, X. Manipulating the mesostructure of silicoaluminophosphate SAPO-11 via tumbling-assisted, oriented assembly crystallization: a pathway to enhance selectivity in hydroisomerization. *Catalysis Science & Technology* **2018**, *8* (19), 5044-5061.

(47) Najafi, N.; Askari, S.; Halladj, R. Hydrothermal synthesis of nanosized SAPO-34 molecular sieves by different combinations of multi templates. *Powder technology* **2014**, *254*, 324-330.

(48) Jin, D.; Liu, Z.; Zheng, J.; Hua, W.; Chen, J.; Zhu, K.; Zhou, X. Nonclassical from-shell-to-core growth of hierarchically organized SAPO-11 with enhanced catalytic performance in hydroisomerization of n-heptane. *RSC advances* **2016**, *6* (39), 32523-32533.

(49) Linares, N.; Silvestre-Albero, A. M.; Serrano, E.; Silvestre-Albero, J.; García-Martínez, J. Mesoporous materials for clean energy technologies. *Chemical Society Reviews* **2014**, *43* (22), 7681-7717.

(50) Zu, L.; Zhang, W.; Qu, L.; Liu, L.; Li, W.; Yu, A.; Zhao, D. Mesoporous materials for electrochemical energy storage and conversion. *Advanced Energy Materials* **2020**, *10* (38), 2002152.

(51) Szczęśniak, B.; Choma, J.; Jaroniec, M. Major advances in the development of ordered mesoporous materials. *Chemical Communications* **2020**, *56* (57), 7836-7848.

- (52) Krishna, N.; Selvam, P. Physico-Chemical Characteristics of Novel Ordered Mesoporous Silicate, IITM-56: The Effect of Synthesis Parameters. *Advanced Porous Materials* **2014**, 2 (2), 106-112.
- (53) Verma, P.; Kuwahara, Y.; Mori, K.; Raja, R.; Yamashita, H. Functionalized mesoporous SBA-15 silica: recent trends and catalytic applications. *Nanoscale* **2020**, 12 (21), 11333-11363.
- (54) Li, W.; Liu, J.; Zhao, D. Mesoporous materials for energy conversion and storage devices. *Nature Reviews Materials* **2016**, 1 (6), 1-17.
- (55) Kresge, a. C.; Leonowicz, M.; Roth, W. J.; Vartuli, J.; Beck, J. Ordered mesoporous molecular sieves synthesized by a liquid-crystal template mechanism. *nature* **1992**, 359 (6397), 710-712.
- (56) Li, W.; Zhao, D. An overview of the synthesis of ordered mesoporous materials. *Chemical Communications* **2013**, 49 (10), 943-946.
- (57) Lee, J.-S.; Kim, S.-I.; Yoon, J.-C.; Jang, J.-H. Chemical vapor deposition of mesoporous graphene nanoballs for supercapacitor. *ACS nano* **2013**, 7 (7), 6047-6055.
- (58) Petkovich, N. D.; Stein, A. Controlling macro-and mesostructures with hierarchical porosity through combined hard and soft templating. *Chemical Society Reviews* **2013**, 42 (9), 3721-3739.
- (59) Feng, D.; Luo, W.; Zhang, J.; Xu, M.; Zhang, R.; Wu, H.; Lv, Y.; Asiri, A. M.; Khan, S. B.; Rahman, M. M. Multi-layered mesoporous TiO<sub>2</sub> thin films with large pores and highly crystalline frameworks for efficient photoelectrochemical conversion. *Journal of Materials Chemistry A* **2013**, 1 (5), 1591-1599.
- (60) Li, G.; Sun, J.; Hou, W.; Jiang, S.; Huang, Y.; Geng, J. Three-dimensional porous carbon composites containing high sulfur nanoparticle content for high-performance lithium-sulfur batteries. *Nature communications* **2016**, 7 (1), 1-10.
- (61) Liu, Y.; Luo, Y.; Elzatahry, A. A.; Luo, W.; Che, R.; Fan, J.; Lan, K.; Al-Enizi, A. M.; Sun, Z.; Li, B. Mesoporous TiO<sub>2</sub> mesocrystals: remarkable defects-induced crystallite-interface reactivity and their in situ conversion to single crystals. *ACS central science* **2015**, 1 (7), 400-408.

- (62) Peng, L.; Zhang, J.; Xue, Z.; Han, B.; Sang, X.; Liu, C.; Yang, G. Highly mesoporous metal–organic framework assembled in a switchable solvent. *Nature communications* **2014**, *5* (1), 1-7.
- (63) Jeon, N. J.; Noh, J. H.; Kim, Y. C.; Yang, W. S.; Ryu, S.; Seok, S. I. Solvent engineering for high-performance inorganic–organic hybrid perovskite solar cells. *Nature materials* **2014**, *13* (9), 897-903.
- (64) Li, W.; Deng, Y.; Wu, Z.; Qian, X.; Yang, J.; Wang, Y.; Gu, D.; Zhang, F.; Tu, B.; Zhao, D. Hydrothermal etching assisted crystallization: a facile route to functional yolk-shell titanate microspheres with ultrathin nanosheets-assembled double shells. *Journal of the American Chemical Society* **2011**, *133* (40), 15830-15833.
- (65) Xuan, W.; Zhu, C.; Liu, Y.; Cui, Y. Mesoporous metal–organic framework materials. *Chemical Society Reviews* **2012**, *41* (5), 1677-1695.
- (66) Védrine, J. C. Importance, features and uses of metal oxide catalysts in heterogeneous catalysis. *Chinese Journal of Catalysis* **2019**, *40* (11), 1627-1636.
- (67) Védrine, J. C. Heterogeneous catalysis on metal oxides. *Catalysts* **2017**, *7* (11), 341.
- (68) Arata, K. Organic syntheses catalyzed by superacidic metal oxides: sulfated zirconia and related compounds. *Green Chemistry* **2009**, *11* (11), 1719-1728.
- (69) Vaishnavi, B.; Sujith, S.; Vaibhava, K. R.; Bhat, P. J.; Vetrivel, R.; Shanbhag, G. V. Selective synthesis of furfuryl acetate over solid acid catalysts and active site exploration using density functional theory. *Catalysis Science & Technology* **2022**.
- (70) Yori, J.; Krasnogor, L.; Castro, A. Correlation between acid strength (H<sub>0</sub>) and ammonia desorption temperature for aluminas and silica-aluminas. *Reaction Kinetics and Catalysis Letters* **1986**, *32* (1), 27-32.
- (71) Corma, A. Inorganic solid acids and their use in acid-catalyzed hydrocarbon reactions. *Chemical Reviews* **1995**, *95* (3), 559-614.
- (72) Wang, P.; Yue, Y.; Wang, T.; Bao, X. Alkane isomerization over sulfated zirconia solid acid system. *International Journal of Energy Research* **2020**, *44* (5), 3270-3294.
- (73) Reddy, B. M.; Patil, M. K. Organic syntheses and transformations catalyzed by sulfated zirconia. *Chemical reviews* **2009**, *109* (6), 2185-2208.

- (74) Marakatti, V. S.; Shanbhag, G. V.; Halgeri, A. Sulfated zirconia; an efficient and reusable acid catalyst for the selective synthesis of 4-phenyl-1, 3-dioxane by Prins cyclization of styrene. *Applied Catalysis A: General* **2013**, *451*, 71-78.
- (75) Rosenberg, D. J.; Anderson, J. A. On determination of acid site densities on sulfated oxides. *Catalysis letters* **2002**, *83* (1), 59-63.
- (76) Saur, O.; Bensitel, M.; Saad, A. M.; Lavalley, J.; Tripp, C. P.; Morrow, B. The structure and stability of sulfated alumina and titania. *Journal of Catalysis* **1986**, *99* (1), 104-110.
- (77) Jin, T.; Yamaguchi, T.; Tanabe, K. Mechanism of acidity generation on sulfur-promoted metal oxides. *The Journal of Physical Chemistry* **1986**, *90* (20), 4794-4796.
- (78) Babou, F.; Bigot, B.; Coudurier, G.; Sautet, P.; Vedrine, J. 4.23 Sulfated Zirconia for n-Butane Isomerization Experimental and Theoretical Approaches. In *Studies in Surface Science and Catalysis*, Vol. 90; Elsevier, 1994; pp 519-529.
- (79) Kustov, L.; Kazansky, V.; Figueras, F.; Tichit, D. Investigation of the acidic properties of ZrO<sub>2</sub> modified by SO<sub>2</sub>-4 anions. *Journal of Catalysis* **1994**, *150* (1), 143-149.
- (80) White, R. L.; Sikabwe, E. C.; Coelho, M. A.; Resasco, D. E. Potential role of penta-coordinated sulfur in the acid site structure of sulfated zirconia. *Journal of Catalysis* **1995**, *157* (2), 755-758.
- (81) Ward, D. A.; Ko, E. I. One-step synthesis and characterization of zirconia-sulfate aerogels as solid superacids. *Journal of Catalysis* **1994**, *150* (1), 18-33.
- (82) Hino, M.; Kurashige, M.; Matsushashi, H.; Arata, K. The surface structure of sulfated zirconia: Studies of XPS and thermal analysis. *Thermochimica acta* **2006**, *441* (1), 35-41.
- (83) Zhou, H.-C.; Long, J. R.; Yaghi, O. M. Introduction to metal-organic frameworks. ACS Publications: 2012; Vol. 112, pp 673-674.
- (84) Schoedel, A.; Rajeh, S. Why design matters: From decorated metal-oxide clusters to functional metal-organic frameworks. *Metal-Organic Framework* **2020**, 1-55.
- (85) Bavykina, A.; Kolobov, N.; Khan, I. S.; Bau, J. A.; Ramirez, A.; Gascon, J. Metal-organic frameworks in heterogeneous catalysis: recent progress, new trends, and future perspectives. *Chemical reviews* **2020**, *120* (16), 8468-8535.

- (86) Daliran, S.; Oveisi, A. R.; Peng, Y.; López-Magano, A.; Khajeh, M.; Mas-Ballesté, R.; Alemán, J.; Luque, R.; Garcia, H. Metal–organic framework (MOF)-, covalent-organic framework (COF)-, and porous-organic polymers (POP)-catalyzed selective C–H bond activation and functionalization reactions. *Chemical Society Reviews* **2022**.
- (87) Yang, D.; Gates, B. C. Catalysis by metal organic frameworks: perspective and suggestions for future research. *Acs Catalysis* **2019**, *9* (3), 1779-1798.
- (88) Ladole, M. R.; Pokale, P. B.; Patil, S. S.; Belokar, P. G.; Pandit, A. B. Laccase immobilized peroxidase mimicking magnetic metal organic frameworks for industrial dye degradation. *Bioresource Technology* **2020**, *317*, 124035.
- (89) Mallakpour, S.; Nikkhoo, E.; Hussain, C. M. Application of MOF materials as drug delivery systems for cancer therapy and dermal treatment. *Coordination Chemistry Reviews* **2022**, *451*, 214262.
- (90) He, S.; Wu, L.; Li, X.; Sun, H.; Xiong, T.; Liu, J.; Huang, C.; Xu, H.; Sun, H.; Chen, W. Metal-organic frameworks for advanced drug delivery. *Acta Pharmaceutica Sinica B* **2021**, *11* (8), 2362-2395.
- (91) Li, H.; Wang, K.; Sun, Y.; Lollar, C. T.; Li, J.; Zhou, H.-C. Recent advances in gas storage and separation using metal–organic frameworks. *Materials Today* **2018**, *21* (2), 108-121.
- (92) Bakuru, V. R.; DMello, M. E.; Kalidindi, S. B. Metal-organic frameworks for hydrogen energy applications: advances and challenges. *ChemPhysChem* **2019**, *20* (10), 1177-1215.
- (93) DMello, M. E.; Sundaram, N. G.; Singh, A.; Singh, A. K.; Kalidindi, S. B. An amine functionalized zirconium metal–organic framework as an effective chemiresistive sensor for acidic gases. *Chemical communications* **2019**, *55* (3), 349-352.
- (94) Mashhadzadeh, A. H.; Taghizadeh, A.; Taghizadeh, M.; Munir, M. T.; Habibzadeh, S.; Salmankhani, A.; Stadler, F. J.; Saeb, M. R. Metal–Organic Framework (MOF) through the lens of molecular dynamics simulation: current status and future perspective. *Journal of Composites Science* **2020**, *4* (2), 75.
- (95) Furukawa, H.; Müller, U.; Yaghi, O. M. “Heterogeneity within order” in metal–organic frameworks. *Angewandte Chemie International Edition* **2015**, *54* (11), 3417-3430.

- (96) Jiang, J.; Yaghi, O. M. Brønsted acidity in metal–organic frameworks. *Chemical reviews* **2015**, *115* (14), 6966-6997.
- (97) Hu, Z.; Zhao, D. Metal–organic frameworks with Lewis acidity: synthesis, characterization, and catalytic applications. *CrystEngComm* **2017**, *19* (29), 4066-4081.
- (98) Ji, P.; Feng, X.; Oliveres, P.; Li, Z.; Murakami, A.; Wang, C.; Lin, W. Strongly lewis acidic metal–organic frameworks for continuous flow catalysis. *Journal of the American Chemical Society* **2019**, *141* (37), 14878-14888.
- (99) Wang, W.; Liu, H.; Yang, C.; Fan, T.; Cui, C.; Lu, X.; Tang, Z.; Li, G. Coordinating Zirconium Nodes in Metal-Organic Framework with Trifluoroacetic Acid for Enhanced Lewis Acid Catalysis. *Chemical Research in Chinese Universities* **2022**, 1-7.
- (100) Trickett, C. A.; Osborn Popp, T. M.; Su, J.; Yan, C.; Weisberg, J.; Huq, A.; Urban, P.; Jiang, J.; Kalmutzki, M. J.; Liu, Q. Identification of the strong Brønsted acid site in a metal–organic framework solid acid catalyst. *Nature chemistry* **2019**, *11* (2), 170-176.
- (101) Rao, B. S.; Kumari, P. K.; Dhanalakshmi, D.; Lingaiah, N. Selective conversion of furfuryl alcohol into butyl levulinate over zinc exchanged heteropoly tungstate supported on niobia catalysts. *Molecular Catalysis* **2017**, *427*, 80-86.
- (102) Démolis, A.; Essayem, N.; Rataboul, F. Synthesis and applications of alkyl levulinates. *ACS Sustainable Chemistry & Engineering* **2014**, *2* (6), 1338-1352.
- (103) Rao, S.; Lingaiah, N. One pot selective transformation of biomass derived chemicals towards alkyl levulinates over titanium exchanged heteropoly tungstate catalysts. *Catalysis Today* **2018**, *309*, 269-275.
- (104) Badgujar, K. C.; Badgujar, V. C.; Bhanage, B. M. A review on catalytic synthesis of energy rich fuel additive levulinate compounds from biomass derived levulinic acid. *Fuel Processing Technology* **2020**, *197*, 106213.
- (105) Di Bucchianico, D. D. M.; Wang, Y.; Buvat, J.-C.; Pan, Y.; Moreno, V. C.; Leveneur, S. Production of levulinic acid and alkyl levulinates: a process insight. *Green Chemistry* **2022**, *24* (2), 614-646.
- (106) Gitis, V.; Chung, S.-H.; Shiju, N. R. Conversion of furfuryl alcohol into butyl levulinate with graphite oxide and reduced graphite oxide. *FlatChem* **2018**, *10*, 39-44.

- (107) Tiwari, M. S.; Dicks, J. S.; Keogh, J.; Ranade, V. V.; Manyar, H. G. J. M. C. Direct conversion of furfuryl alcohol to butyl levulinate using tin exchanged tungstophosphoric acid catalysts. **2020**, *488*, 110918.
- (108) Sankar, E. S.; Reddy, K. S.; Jyothi, Y.; Raju, B. D.; Rao, K. S. R. Alcoholysis of furfuryl alcohol into n-butyl levulinate over SBA-16 supported heteropoly acid catalyst. *Catalysis Letters* **2017**, *147* (11), 2807-2816.
- (109) Demma Carà, P.; Ciriminna, R.; Shiju, N.; Rothenberg, G.; Pagliaro, M. Enhanced heterogeneous catalytic conversion of furfuryl alcohol into butyl levulinate. *ChemSusChem* **2014**, *7* (3), 835-840.
- (110) Yu, X.; Peng, L.; Pu, Q.; Tao, R.; Gao, X.; He, L.; Zhang, J. J. R. o. C. I. Efficient valorization of biomass-derived furfuryl alcohol to butyl levulinate using a facile lignin-based carbonaceous acid. **2020**, *46* (2), 1469-1485.
- (111) Appaturi, J. N.; Johan, M. R.; Ramalingam, R. J.; Al-Lohedan, H. A.; Vijaya, J. J. Efficient synthesis of butyl levulinate from furfuryl alcohol over ordered mesoporous Ti-KIT-6 catalysts for green chemistry applications. *RSC advances* **2017**, *7* (87), 55206-55214.
- (112) Enumula, S. S.; Koppadi, K. S.; Gurram, V. R. B.; Burri, D. R.; Kamaraju, S. R. R. Conversion of furfuryl alcohol to alkyl levulinate fuel additives over Al<sub>2</sub>O<sub>3</sub>/SBA-15 catalyst. *Sustainable Energy & Fuels* **2017**, *1* (3), 644-651.
- (113) Hao, R.; He, J.; Zhao, L.; Zhang, Y. HPAs and POM-based ILs Catalyzed Effective Conversion of Furfuryl Alcohol to Alkyl Levulinate. *ChemistrySelect* **2017**, *2* (26), 7918-7924.
- (114) Manjunathan, P.; Shanbhag, D. Y.; Vinu, A.; Shanbhag, G. V. Recognizing soft templates as stimulators in multivariate modulation of tin phosphate and its application in catalysis for alkyl levulinate synthesis. *Catalysis Science & Technology* **2021**, *11* (1), 272-282.
- (115) Wang, G.; Zhang, Z.; Song, L. Efficient and selective alcoholysis of furfuryl alcohol to alkyl levulinates catalyzed by double SO<sub>3</sub>H-functionalized ionic liquids. *Green Chemistry* **2014**, *16* (3), 1436-1443.



- (116) Zhang, Z.; Dong, K.; Zhao, Z. K. Efficient conversion of furfuryl alcohol into alkyl levulinates catalyzed by an organic–inorganic hybrid solid acid catalyst. *ChemSusChem* **2011**, *4* (1), 112-118.
- (117) Ren, D.; Fu, J.; Li, L.; Liu, Y.; Jin, F.; Huo, Z. Efficient conversion of biomass-derived furfuryl alcohol to levulinate esters over commercial  $\alpha$ -Fe<sub>2</sub>O<sub>3</sub>. *RSC advances* **2016**, *6* (26), 22174-22178.
- (118) Mohammadbagheri, Z.; Chermahini, A. N. KCC-1/Pr-SO<sub>3</sub>H as an efficient heterogeneous catalyst for production of n-butyl levulinate from furfuryl alcohol. *Journal of industrial and engineering chemistry* **2018**, *62*, 401-408.
- (119) Zhou, S.; Lai, J.; Liu, X.; Huang, G.; You, G.; Xu, Q.; Yin, D. J. G. E.; Environment. Selective conversion of biomass-derived furfuryl alcohol into n-butyl levulinate over sulfonic acid functionalized TiO<sub>2</sub> nanotubes. **2020**.
- (120) Malkar, R. S.; Daly, H.; Hardacre, C.; Yadav, G. D. Novelty of iron-exchanged heteropolyacid encapsulated inside ZIF-8 as an active and superior catalyst in the esterification of furfuryl alcohol and acetic acid. *Reaction Chemistry & Engineering* **2019**, *4* (10), 1790-1802.
- (121) Yu, W.; Tang, Y.; Mo, L.; Chen, P.; Lou, H.; Zheng, X. One-step hydrogenation–esterification of furfural and acetic acid over bifunctional Pd catalysts for bio-oil upgrading. *Bioresource technology* **2011**, *102* (17), 8241-8246.
- (122) Hashim, L. H.; Halilu, A.; Sudarsanam, P.; Umar, Y. B.; Johan, M. R. B.; Bhargava, S. K. Bifunctional rice husk-derived SiO<sub>2</sub>-Cu-Al-Mg nanohybrid catalyst for one-pot conversion of biomass-derived furfural to furfuryl acetate. *Fuel* **2020**, *275*, 117953.
- (123) Yu, W.; Tang, Y.; Mo, L.; Chen, P.; Lou, H.; Zheng, X. Bifunctional Pd/Al-SBA-15 catalyzed one-step hydrogenation–esterification of furfural and acetic acid: A model reaction for catalytic upgrading of bio-oil. *Catalysis Communications* **2011**, *13* (1), 35-39.
- (124) Wang, R.; Shen, F.; Tang, Y.; Guo, H.; Smith Jr, R. L.; Qi, X. Selective conversion of furfuryl alcohol to levulinic acid by SO<sub>3</sub>H-containing silica nanoflower in GVL/H<sub>2</sub>O system. *Renewable Energy* **2021**, *171*, 124-132.

- (125) An, S.; Song, D.; Sun, Y.; Zhang, Q.; Zhang, P.; Guo, Y. Conversion of furfuryl alcohol to levulinic acid in aqueous solution catalyzed by shell thickness-controlled arenesulfonic acid-functionalized ethyl-bridged organosilica hollow nanospheres. *ACS Sustainable Chemistry & Engineering* **2018**, *6* (3), 3113-3123.
- (126) Mellmer, M. A.; Gallo, J. M. R.; Martin Alonso, D.; Dumesic, J. A. Selective production of levulinic acid from furfuryl alcohol in THF solvent systems over H-ZSM-5. *ACS Catalysis* **2015**, *5* (6), 3354-3359.
- (127) Guzmán, I.; Heras, A.; Guemez, M.; Iriondo, A.; Cambra, J. F.; Requies, J. s. Levulinic acid production using solid-acid catalysis. *Industrial & Engineering Chemistry Research* **2016**, *55* (18), 5139-5144.
- (128) Yan, P.; Wang, H.; Liao, Y.; Sun, P.; Wang, C. Introducing mesopore and regulating Al distribution for improving catalytic performances of ZSM-5 in furfuryl alcohol to levulinic acid. *Fuel* **2022**, *329*, 125213.
- (129) Joshi, H.; Moser, B. R.; Toler, J.; Smith, W. F.; Walker, T. Ethyl levulinate: A potential bio-based diluent for biodiesel which improves cold flow properties. *Biomass and bioenergy* **2011**, *35* (7), 3262-3266.
- (130) Gupta, S. S. R.; Kantam, M. L. Catalytic conversion of furfuryl alcohol or levulinic acid into alkyl levulinates using a sulfonic acid-functionalized hafnium-based MOF. *Catalysis Communications* **2019**, *124*, 62-66.
- (131) Song, D.; An, S.; Lu, B.; Guo, Y.; Leng, J. Arylsulfonic acid functionalized hollow mesoporous carbon spheres for efficient conversion of levulinic acid or furfuryl alcohol to ethyl levulinate. *Applied Catalysis B: Environmental* **2015**, *179*, 445-457.
- (132) Chhabra, T.; Rohilla, J.; Krishnan, V. Nanoarchitectonics of phosphomolybdic acid supported on activated charcoal for selective conversion of furfuryl alcohol and levulinic acid to alkyl levulinates. *Molecular Catalysis* **2022**, *519*, 112135.
- (133) Song, D.; An, S.; Sun, Y.; Zhang, P.; Guo, Y.; Zhou, D. Ethane-Bridged Organosilica Nanotubes Functionalized with Arenesulfonic Acid and Phenyl Groups for the Efficient Conversion of Levulinic Acid or Furfuryl Alcohol to Ethyl Levulinate. *ChemCatChem* **2016**, *8* (12), 2037-2048.

- (134) Zhai, P.; Lv, G.; Cai, Z.; Zhu, Y.; Li, H.; Zhang, X.; Wang, F. Efficient production of ethyl levulinate from furfuryl alcohol catalyzed by modified zirconium phosphate. *ChemistrySelect* **2019**, *4* (13), 3940-3947.
- (135) Lingaiah, N. One pot selective transformation of biomass derived chemicals towards alkyl levulinates over titanium exchanged heteropoly tungstate catalysts. *Catalysis Today* **2018**, *309*, 269-275.
- (136) Rao, B. S.; Subrahmanyam, C.; Lingaiah, N. The selective conversion of furfuryl alcohol to ethyl levulinate over Zr-modified tungstophosphoric acid supported on  $\beta$ -zeolites. *New Journal of Chemistry* **2021**, *45* (6), 3224-3233.
- (137) Li, X.; Li, Y.; Wang, X.; Peng, Q.; Hui, W.; Wang, H. Zr-DBS with sulfonic group: A green and highly efficient catalyst for alcoholysis of furfuryl alcohol to ethyl levulinate. *Catalysis Letters* **2021**, *151* (9), 2622-2630.
- (138) Hu, A.; Wang, H.; Ding, J. Novel Sulfonic Acid Polystyrene Microspheres for Alcoholysis of Furfuryl Alcohol to Ethyl Levulinate. *Catalysis Letters* **2022**, 1-10.
- (139) Patil, C. R.; Kamble, S. P.; Rode, C. V. Single-Pot Alcoholysis of Furfuryl Alcohol to Alkyl Levulinates Using Heterogenized p-TSA Catalyst. *ChemistrySelect* **2021**, *6* (26), 6636-6643.
- (140) Prajapati, R.; Srivastava, S.; Jadeja, G.; Parikh, J. A Novel SBA-15/H-ZSM-5 Composite Catalyst for Conversion of Furfuryl Alcohol to Ethyl Levulinate. *Waste and Biomass Valorization* **2022**, 1-10.
- (141) Liu, X.; Pan, H.; Zhang, H.; Li, H.; Yang, S. Efficient catalytic upgradation of bio-based furfuryl alcohol to ethyl levulinate using mesoporous acidic MIL-101 (Cr). *ACS omega* **2019**, *4* (5), 8390-8399.
- (142) Neves, P.; Antunes, M. M.; Russo, P. A.; Abrantes, J. P.; Lima, S.; Fernandes, A.; Pillinger, M.; Rocha, S. M.; Ribeiro, M. F.; Valente, A. A. Production of biomass-derived furanic ethers and levulinate esters using heterogeneous acid catalysts. *Green Chemistry* **2013**, *15* (12), 3367-3376.
- (143) Zhang, H.; Wang, S.; Zhang, H.; Cui, L.; Cao, F. P-doped carbon as an efficient metal-free catalyst for alcoholysis of furfural alcohol to ethyl levulinate. *Fuel* **2022**, *324*, 124024.

- (144) Liu, X.-F.; Li, H.; Zhang, H.; Pan, H.; Huang, S.; Yang, K.-L.; Yang, S. Efficient conversion of furfuryl alcohol to ethyl levulinate with sulfonic acid-functionalized MIL-101 (Cr). *RSC advances* **2016**, *6* (93), 90232-90238.
- (145) Li, Y.; Wang, S.; Fan, S.; Ali, B.; Lan, X.; Wang, T. Nano-H-ZSM-5 with Short b-Axis Channels as a Highly Efficient Catalyst for the Synthesis of Ethyl Levulinate from Furfuryl Alcohol. *ACS Sustainable Chemistry & Engineering* **2022**, *10* (12), 3808-3816.
- (146) Song, D.; An, S.; Sun, Y.; Guo, Y. Efficient conversion of levulinic acid or furfuryl alcohol into alkyl levulinates catalyzed by heteropoly acid and ZrO<sub>2</sub> bifunctionalized organosilica nanotubes. *Journal of Catalysis* **2016**, *333*, 184-199.
- (147) Lange, J. P.; van de Graaf, W. D.; Haan, R. J. Conversion of furfuryl alcohol into ethyl levulinate using solid acid catalysts. *ChemSusChem: Chemistry & Sustainability Energy & Materials* **2009**, *2* (5), 437-441.
- (148) An, S.; Song, D.; Lu, B.; Yang, X.; Guo, Y. H. Morphology Tailoring of Sulfonic Acid Functionalized Organosilica Nanohybrids for the Synthesis of Biomass-Derived Alkyl Levulinates. *Chemistry—A European Journal* **2015**, *21* (30), 10786-10798.
- (149) Yadav, G. D.; Yadav, A. R. Synthesis of ethyl levulinate as fuel additives using heterogeneous solid superacidic catalysts: Efficacy and kinetic modeling. *Chemical Engineering Journal* **2014**, *243*, 556-563.
- (150) Guo, T.; Qiu, M.; Qi, X. Selective conversion of biomass-derived levulinic acid to ethyl levulinate catalyzed by metal organic framework (MOF)-supported polyoxometalates. *Applied Catalysis A: General* **2019**, *572*, 168-175.
- (151) Khiratkar, A. G.; Balinge, K. R.; Krishnamurthy, M.; Cheralathan, K.; Patle, D. S.; Singh, V.; Arora, S.; Bhagat, P. R. Sulphonic acid-functionalized benzimidazolium based poly ionic liquid catalyzed esterification of levulinic acid. *Catalysis Letters* **2018**, *148* (2), 680-690.
- (152) Yang, F.; Tang, J. Catalytic upgrading of renewable levulinic acid to levulinate esters using perchloric acid decorated nanoporous silica gels. *ChemistrySelect* **2019**, *4* (4), 1403-1409.
- (153) Wang, F.; Chen, Z.; Chen, H.; Goetjen, T. A.; Li, P.; Wang, X.; Alayoglu, S.; Ma, K.; Chen, Y.; Wang, T. Interplay of Lewis and Brønsted acid sites in Zr-based metal-

organic frameworks for efficient esterification of biomass-derived levulinic acid. *ACS applied materials & interfaces* **2019**, *11* (35), 32090-32096.

(154) Ramli, N. A. S.; Sivasubramaniam, D.; Amin, N. A. S. Esterification of levulinic acid using ZrO<sub>2</sub>-supported phosphotungstic acid catalyst for ethyl levulinate production. *BioEnergy Research* **2017**, *10* (4), 1105-1116.

(155) Nandiwale, K. Y.; Bokade, V. V. Environmentally benign catalytic process for esterification of renewable levulinic acid to various alkyl levulinates biodiesel. *Environmental Progress & Sustainable Energy* **2015**, *34* (3), 795-801.

(156) Nandiwale, K. Y.; Niphadkar, P. S.; Deshpande, S. S.; Bokade, V. V. Esterification of renewable levulinic acid to ethyl levulinate biodiesel catalyzed by highly active and reusable desilicated H-ZSM-5. *Journal of Chemical Technology & Biotechnology* **2014**, *89* (10), 1507-1515.

(157) Ahmad, E.; Pant, K. K.; Haider, M. A. Synthesis and application of TiO<sub>2</sub>-supported phosphotungstic acid for ethyl levulinate production. *Materials Science for Energy Technologies* **2022**, *5*, 189-196.

(158) Pileidis, F. D.; Tabassum, M.; Coutts, S.; Titirici, M.-M. Esterification of levulinic acid into ethyl levulinate catalysed by sulfonated hydrothermal carbons. *Chinese Journal of Catalysis* **2014**, *35* (6), 929-936.

(159) Nandiwale, K. Y.; Sonar, S. K.; Niphadkar, P. S.; Joshi, P. N.; Deshpande, S. S.; Patil, V. S.; Bokade, V. V. Catalytic upgrading of renewable levulinic acid to ethyl levulinate biodiesel using dodecatungstophosphoric acid supported on desilicated H-ZSM-5 as catalyst. *Applied Catalysis A: General* **2013**, *460*, 90-98.

(160) Li, N.; Jiang, S.; Liu, Z.-Y.; Guan, X.-X.; Zheng, X.-C. Preparation and catalytic performance of loofah sponge-derived carbon sulfonic acid for the conversion of levulinic acid to ethyl levulinate. *Catalysis Communications* **2019**, *121*, 11-14.

(161) Su, F.; Wu, Q.; Song, D.; Zhang, X.; Wang, M.; Guo, Y. Pore morphology-controlled preparation of ZrO<sub>2</sub>-based hybrid catalysts functionalized by both organosilica moieties and Keggin-type heteropoly acid for the synthesis of levulinate esters. **2013**.

(162) Vilanculo, C. B.; de Andrade Leles, L. C.; da Silva, M. J. H<sub>4</sub>SiW<sub>12</sub>O<sub>40</sub>-catalyzed levulinic acid esterification at room temperature for production of fuel bioadditives. *Waste and Biomass Valorization* **2020**, *11* (5), 1895-1904.

- (163) Li, Z.; Wnetrzak, R.; Kwapinski, W.; Leahy, J. J. Synthesis and characterization of sulfated TiO<sub>2</sub> nanorods and ZrO<sub>2</sub>/TiO<sub>2</sub> nanocomposites for the esterification of biobased organic acid. *ACS applied materials & interfaces* **2012**, *4* (9), 4499-4505.
- (164) Liu, C.; Zhang, K.; Liu, Y.; Wu, S. Esterification of levulinic acid into ethyl levulinate catalyzed by sulfonated bagasse-carbonized solid acid. *BioResources* **2019**, *14* (1), 2186-2196.
- (165) Lucas, N.; Gurralla, L.; Athawale, A. Heteropolyacids supported on mesoporous AISBA-15 as efficient catalysts for esterification of levulinic acid. *Journal of Porous Materials* **2019**, *26* (5), 1335-1343.
- (166) Desidery, L.; Yusubov, M. S.; Zhuiykov, S.; Verpoort, F. Fully-sulfonated hydrated UiO66 as efficient catalyst for ethyl levulinate production by esterification. *Catalysis Communications* **2018**, *117*, 33-37.
- (167) Zainol, M. M.; Amin, N. A. S.; Asmadi, M. Effects of thermal treatment on carbon cryogel preparation for catalytic esterification of levulinic acid to ethyl levulinate. *Fuel Processing Technology* **2017**, *167*, 431-441.
- (168) Popova, M.; Szegedi, Á.; Lazarova, H.; Dimitrov, M.; Kalvachev, Y.; Atanasova, G.; Ristić, A.; Wilde, N.; Gläser, R. Influence of the preparation method of sulfated zirconia nanoparticles for levulinic acid esterification. *Reaction Kinetics, Mechanisms and Catalysis* **2017**, *120* (1), 55-67.
- (169) Kuwahara, Y.; Fujitani, T.; Yamashita, H. Esterification of levulinic acid with ethanol over sulfated mesoporous zirconsilicates: Influences of the preparation conditions on the structural properties and catalytic performances. *Catalysis Today* **2014**, *237*, 18-28.
- (170) Dugkhuntod, P.; Imyen, T.; Wannapakdee, W.; Yuthalekha, T.; Salakhum, S.; Wattanakit, C. Synthesis of hierarchical ZSM-12 nanolayers for levulinic acid esterification with ethanol to ethyl levulinate. *RSC advances* **2019**, *9* (32), 18087-18097.
- (171) Popova, M.; Shestakova, P.; Lazarova, H.; Dimitrov, M.; Kovacheva, D.; Szegedi, A.; Mali, G.; Dasireddy, V.; Likozar, B.; Wilde, N. Efficient solid acid catalysts based on sulfated tin oxides for liquid phase esterification of levulinic acid with ethanol. *Applied Catalysis A: General* **2018**, *560*, 119-131.

(172) Ramli, N. A. S.; Hisham, N. I.; Amin, N. A. S. Esterification of levulinic acid to levulinate esters in the presence of sulfated silica catalyst. *Sains Malaysiana* **2018**, *47* (6), 1131-1138.

(173) Kuwahara, Y.; Kaburagi, W.; Nemoto, K.; Fujitani, T. Esterification of levulinic acid with ethanol over sulfated Si-doped ZrO<sub>2</sub> solid acid catalyst: study of the structure–activity relationships. *Applied Catalysis A: General* **2014**, *476*, 186-196.

(174) Oliveira, B. L.; da Silva, V. T. Sulfonated carbon nanotubes as catalysts for the conversion of levulinic acid into ethyl levulinate. *Catalysis Today* **2014**, *234*, 257-263.

(175) Patil, C.; Niphadkar, P.; Bokade, V.; Joshi, P. Esterification of levulinic acid to ethyl levulinate over bimodal micro–mesoporous H/BEA zeolite derivatives. *Catalysis Communications* **2014**, *43*, 188-191.





# **Chapter 2**

## **Catalyst Preparation and Characterization Techniques**



## 2.1 Introduction

Designing solid acid catalysts for the transformation of biomass derivatives is of great interest to catalysis researchers due to the recent developments in the utilization of renewable sources for making fuels and chemicals. There is a challenge to achieve high conversion in addition to a high selectivity for the desired products in case of biomass transformations, especially for furanic biomass derivative owing to its tendency of resinification leading to humin formation. This results in the formation of undesired products called humins that saturate the active sites thereby decreasing the catalytic performance. There are several reasons for this phenomenon to occur where some are elevated reaction temperatures, employing immiscible reactants (eg. furfuryl alcohol and water), the presence of a highly acidic environment, a catalyst with a high amount/concentration of acidic sites, very narrow pore channel, etc. This phenomenon can be avoided or minimized with the addition of solvents and/or by employing catalysts with a lesser amount of acidic sites. Sometimes resinification occurs in a negligible quantity which can be addressed by burning the humins off at high temperatures provided the catalyst used has good thermal stability. Also, in some cases, the removal of such species can be successively done by subjecting the spent catalyst to successive solvent washing. Overall, the material chosen for catalysis to valorize furfuryl alcohol and levulinic acid should possess appropriate active sites to produce a high yield towards the desired product, good chemical stability against humins, good thermal stability, and recyclability for successive cycles. Hence, a suitable synthesis procedure that generates all the essential properties required for catalysis and appropriate characterization techniques to understand and correlate the catalytic performance with its properties is employed. This investigation unravels new ideas and provides better insights for improving the catalytic activity and enhancing the efficiency of the catalyst as well.

Considering all the above aspects of the chosen reactions and catalyst requirements, various catalysts with targeted physicochemical properties were synthesized using the precipitation method, hydrothermal/ solvothermal method, and impregnation/ion exchange method. The synthesized heterogeneous catalyst was examined by several characterization techniques such as powder X-ray diffraction, X-ray fluorescence spectroscopy, ICP-OES, FTIR, pyridine-FTIR, nitrogen sorption, acid-base titration,

---

NH<sub>3</sub>-Temperature programmed desorption, thermogravimetric analysis, scanning electron microscopy, and transmission electron microscopy.

The theory and experimental procedure for material synthesis and the characterization techniques employed are illustrated in brief in this chapter.

## **2.2. Synthesis of heterogeneous solid acid catalysts**

### **2.2.1 Synthesis of ZSM-5**

HZSM-5 catalyst was synthesized by hydrothermal synthesis procedure in accordance with the reported procedure <sup>1</sup>. In a typical synthesis, the required quantity of Al(NO<sub>3</sub>)<sub>3</sub> (aluminium source), ludox (silicon source) tetra propyl ammonium bromide (TPABr), and NaOH were added to the distilled water and stirred well. The molar composition of the reaction gel was: 4 TPABr: nSiO<sub>2</sub>: Al(NO<sub>3</sub>)<sub>3</sub>: 16.5NaOH, 1420 H<sub>2</sub>O, with n=80 (as determined from XRF). The gel was transferred to an autoclave (teflon-lined stainless steel) and placed in a preheated oven (24 h, 180 °C). The crystallized material was collected upon cooling and was washed (distilled water), filtered, dried (120 °C, 12 h), and calcined at 550 °C to yield Na-ZSM-5. The proton exchange by ammonium acetate (0.5 M) at 80 °C for 4 h was performed three times to the Na-ZSM-5. The NH<sub>4</sub> form of ZSM-5 was calcined (550 °C, 5 h with 5 °C min<sup>-1</sup> ramp) to produce HZSM-5.

### **2.2.2 Modification of ZSM-5**

#### **2.2.2.1 Desilication of ZSM-5**

Desilication of HZSM-5 (3 g) was performed by stirring the catalyst with 30 mL 0.1M/0.2M NaOH at 85 °C for 1 h <sup>2</sup>. The catalysts were filtered, washed (distilled water), dried (120 °C, 12 h), and calcined for 5 h at 550 °C (ramp: 5 °C min<sup>-1</sup>). The catalysts were transformed into ammonium form by treating it with 0.5M ammonium acetate solution for 4 h at 80 °C. The solution was filtered and dried. The Na form of HZSM-5 was converted to a protonic form by the ammonium exchange process followed by subsequent calcination (550 °C, 5 h).

### 2.2.2.2 Dealumination of ZSM-5

Dealumination was performed by magnetically stirring 30 mL of 0.2M of citric acid/ HCl with HZSM-5 (3 g) at 80 °C for 24 h in oil bath <sup>3</sup>. The dealuminated catalysts were filtered, washed (distilled water), dried (12 h, 120 °C), and calcined (550 °C, 5 h).

### 2.2.2.3 Phosphate modification of ZSM-5

Varying concentrations (1, 2, and 5 % P) of ammonium dihydrogen phosphate were dissolved in distilled water, and HZSM-5 (3 g) was added and stirred well and further subjected to evaporation <sup>4</sup>. The phosphate-modified ZSM-5 was dried and calcined (stepwise: 330 °C, 3 h and 560 °C, 10 h) and the physisorbed phosphate was removed by washing with distilled water (80 °C, 12 h).

### 2.2.3.4 Metal ion exchange of ZSM-5

HZSM-5 (3g) was stirred with 0.1M aqueous solution of  $\text{Cu}(\text{NO}_3)_2 \cdot 3\text{H}_2\text{O}$  or 0.1M aqueous  $\text{Zn}(\text{NO}_3)_2 \cdot 6\text{H}_2\text{O}$  at 80 °C for 12 h <sup>3</sup>. The catalysts (Cu-ZSM-5 and Zn-ZSM-5) were washed (distilled water), filtered, and dried (120 °C, 12 h). The metal ion exchange was performed twice and finally, the catalysts were calcined (550 °C, 5 h).

### 2.2.3 SAPO-34

SAPO-34 was synthesized by hydrothermal synthesis method as per the reported literature in which an aluminium precursor, pseudoboehmite (9 g),  $\text{H}_3\text{PO}_4$  (15 g), and distilled water (28 g) were homogenized by stirring for 6 h <sup>5</sup>. To this, 4 g of fumed silica (silica precursor) and 11 g of morpholine with water (40 g) were added and the mixture was aged for 24 h to yield a gel. Which was transferred into a teflon-lined stainless steel autoclave. The autoclave was placed in a preheated oven at 200 °C for 24 h and once cooled, the material was washed, filtered (distilled water), dried (12 h at 120 °C), and calcined (5 h, 560°C) to yield SAPO-34.

### 2.2.4 SAPO-11

Synthesis of SAPO-11 was performed by hydrothermal synthesis method in accordance with the reported literature <sup>6</sup>. In a typical preparation procedure, a mixture of pseudoboehmite (15 g), ludox AS-40 (1.6 g), 25.3 g of  $\text{H}_3\text{PO}_4$  (25 g), triethylamine (22 g) in distilled water (95 mL) was stirred. The mixture was homogenized by stirring it for

---

4 h (at room temperature) followed by subjecting it for crystallization by transferring the mixture to a teflon-lined stainless steel autoclave. The autoclave was placed in a pre-heated oven maintained at 200 °C for 24 h. The material was filtered, washed, dried, and calcined (600 °C, 6 h) to yield SAPO-11.

### **2.2.5 Al-SBA-15**

Al-SBA-15 was synthesized by hydrothermal synthesis procedure where SBA-15 was synthesized first and upon the post-synthetic isomorphic substitution method, Al was incorporated in the framework <sup>7</sup>. In a typical preparation procedure of SBA-15, 8 g of structure directing agent [amphiphilic triblock co-polymer poly-(ethylene glycol)-block poly-(propylene glycol)-block poly-(ethylene glycol)], 2M HCl (240 mL), a silicon precursor, tetraethylorthosilicate (16 g) and distilled water (60 mL) were added. The mixture was stirred at 40 °C for 24 h and the gel thus formed was transferred to teflon-lined stainless steel autoclave which then was heated in an oven at 100 °C for 48 h. The material thus obtained was filtered, washed (distilled water), dried, and calcined (550 °C, 6 h). Further, the obtained SBA-15 (10 g) was aged with anhydrous AlCl<sub>3</sub> (4.4 g) and dry ethanol for 10 h at 80 °C to achieve the isomorphic substitution of Al. The modified SBA-15 was filtered, washed (ethanol), dried (at RT), and finally calcined (550 °C, 6 h) to produce Al-SBA-15

### **2.2.6 Sulfated zirconia**

Sulfated zirconia was synthesized by precipitation method in which the zirconium salt was precipitated using a basic solution of aqueous ammonia as per the reported literature <sup>8</sup>. For the synthesis of metal hydroxide, ZrOCl<sub>2</sub>.8H<sub>2</sub>O (25 g) was dissolved in distilled water (200 mL) to which NH<sub>4</sub>OH was added dropwise till pH 8 was attained to yield a precipitate. The material was washed using distilled water till all the chloride ions are removed and the Zr(OH)<sub>4</sub> material was dried for 12 h (at 120 °C). For functionalization that generates Brönsted acidic sites, Zr(OH)<sub>4</sub> (5 g), was sulfated by stirring for 1 h at room temperature using various molar concentrations (1.0, 2.0, 2.5, 3.0, and 4.0M) of aq. H<sub>2</sub>SO<sub>4</sub> (50 mL). The material was filtered, washed (distilled water), dried, and calcined (650 °C for 4 h) to yield sulfated zirconia. The material was washed by refluxing in

distilled water for 6 h to remove the physisorbed sulfate ions and it was filtered, washed, and dried.

### **2.2.7 BUT-8-Cr-SO<sub>3</sub>H**

BUT-8(Cr)-SO<sub>3</sub>H MOF was synthesized by a solvothermal method as per the reported procedure<sup>9</sup>. 30 g of 2,6-naphthalenedicarboxylic acid (NapDC) linker was treated with 100 mL of oleum for 24 h in a three-neck round bottom flask placed in a magnetically stirred oil bath maintained at 140 °C. Once cooled, the unreacted sulfuric acid residues were removed by subjecting the linker to purification steps involving its dissolution by distilled water treatment (40 mL) followed by reprecipitation by HCl treatment (100 mL). This dissolution and precipitation step was repeated thrice in copious amounts of distilled water and HCl treatments in which the linker was dried at 80 °C for 12 h between each purification cycle. Finally, the organic linker was vacuum dried (120 °C, 12 h) to yield the modified linker, 4,8-disulfonyl-2,6-naphthalenedicarboxylic acid linker. 4 g of Cr(NO<sub>3</sub>)<sub>3</sub>·9H<sub>2</sub>O and 3.7 g of the modified linker were homogenized with 60 mL of DMF in an ultrasonic bath for 30 min. To this, hydrofluoric acid (1.1 mL) was added and the solution was transferred to teflon-lined stainless steel autoclave and placed in a preheated oven maintained at 190 °C for 24 h. The green powder collected from the suspension was washed thoroughly by DMF and soaked in DMF (80 °C) and distilled water (RT) for 24 h respectively. The material was finally washed with methanol and dried under a vacuum at 60 °C for 12 h before soaking in 2M H<sub>2</sub>SO<sub>4</sub> solution for 24 h. Then, the material was washed, soaked (distilled water and methanol) to remove the physisorbed H<sub>2</sub>SO<sub>4</sub> species, and was activated under vacuum for 24 h at 60 °C to yield BUT-8(Cr)-SO<sub>3</sub>H.

## **2.3 Catalyst characterization–Theory and experimental procedure**

### **2.3.1 Powder X-ray diffraction**

Powder X-ray diffraction is a non-destructive experimental technique used to determine the crystal structure of solids, the dimension of unit cells, the phase of the materials, the purity of the sample, the orientation of the single crystal, defects in the materials, lattice constants, and geometry<sup>10</sup>. The diffraction is based on constructive interference of a crystalline material with the monochromatic X-rays. An XRD instrument is made up of

---

three major components *viz.* an X-ray tube, a specimen holder, and a detector. X-rays are produced from the cathode ray tube. X-rays of a wavelength of  $\lambda$  ranging from 0.7 to 2Å are generated from a cathode ray tube where the heating of the filament occurs resulting in the production of electrons. These electrons are converted to monochromatic radiation and are collimated. These electrons are bombarded on the specimen and the energy extricates the inner shell electrons of sample <sup>11</sup>. These released electrons are the characteristic X-rays.

The rays get diffracted by the crystalline phases present on the specimen when Bragg's Law is satisfied as presented in equation (1). This law correlates  $\lambda$  (the wavelength of monochromatic X-ray) with the diffraction angle ( $\theta$ ) and the lattice spacing in a crystalline sample ( $d$ )

$$n \lambda = 2d \sin \theta \quad \text{Eq (1)}$$

Where  $n$  is an integer. When the specimen is scanned through a given  $2\theta$  range, a lattice diffraction pattern detected from all the random orientations is obtained.

The measure of the crystallite size of the materials can be done using a Scherrer equation that correlates the mean crystallite size ( $D$ ) with a full width half maximum (FWHM,  $\beta$ ) and the Bragg's angle ( $\theta$ ) with a constant ( $k=0.94$ ) as presented in equation (2)

$$D = \frac{k\lambda}{\beta \cos \theta} \quad \text{Eq (2)}$$

PXRD data of the synthesized catalysts were recorded for a particular  $2\theta$  range using Bruker D2 Phaser X-ray diffractometer. The Cu  $K\alpha$  radiation with  $\lambda = 1.5418 \text{ \AA}$  was the source and the detector was high-resolution Lynxeye detector.

### 2.3.2 X-Ray fluorescence spectroscopy

X-Ray Fluorescence (XRF) is a non-destructive spectroscopic technique that produces fluorescent X-rays emitted from the material helps in the qualitative and quantitative analysis of the elemental composition of catalysts. The fluorescent X-ray is emitted when a transition of an electron from a higher energy state occurs to the vacancy created by the knocking (by X-ray) the inner shell electrons off <sup>12</sup>. The energy of the emitted secondary ray is equal to the energy difference between the two specific quantum states



of the electron. XRF is also used for the identification of alloys, analyze precious metals, obtaining the thickness of coating or plating, etc.

The silica to alumina ratio (SAR) of zeolites (ZSM-5 in specific) was quantitatively determined using Bruker model S4 Pioneer sequential wavelength-dispersive X-ray spectrometer.

### **2.3.3 Inductively coupled plasma optical emission spectroscopy**

Inductively coupled plasma optical emission spectroscopy (ICP-OES) is a quantitative technique that estimates the concentration of elements present in a material with the aid of plasma and a spectrometer<sup>13</sup>. The atoms in the targeted specimen get excited when it is exposed to plasma energy supplied externally. The excited atoms when returned to a lower energy position emit radiation that corresponds to the wavelength of the photon is measured. The element and its concentration are determined by analyzing the position and intensity of the rays of the photon.

The sulfur content in the catalyst was estimated using optima 7000, dual view ICP-OES instrument (Perkin Elmer, USA).

### **2.3.4 Fourier transform infrared spectroscopy**

FTIR spectroscopy is an analytical technique that confirms the type of functional groups/bonds present in the catalyst. The technique uses an IR region of  $400\text{ cm}^{-1}$ – $4000\text{ cm}^{-1}$  to analyze the properties of the synthesized catalyst. When a ray of IR is incident on the material, the functional moieties absorb energy corresponding to a specific wavelength and by using the spectra obtained functional groups and the nature of bonds present can be identified<sup>14</sup>. When IR radiation is made to incident on the target material, the molecules in the material absorb and undergo vibrational transition and witness a shift towards a higher vibrational level. Upon exposure to IR radiation, the molecules experiencing with change in dipole moment are IR active. The molecules with more bond polarity tend to absorb more IR radiation. Different types of molecular vibrations (stretching, wagging, bending rocking, twisting) are known to correspond to specific vibrational energy (wavelength or wavenumber). FTIR instrument is built using several major parts such as an IR source, monochromator, slit, static and moving mirrors, sample holder, and detector. The FTIR spectral data of the functionalized catalysts such as MOF,

---

and sulfated zirconia was acquired using Bruker Alpha-T instrument, scanned over the range from 400 to 4000  $\text{cm}^{-1}$ .

### 2.3.5 Nitrogen sorption measurement

Physisorption of nitrogen is an important technique employed to get information on the porous properties of catalysts. Physisorption is a phenomenon where there is a van der Waals force between the adsorbed gas (nitrogen) with the surface of the catalyst of interest. Brunauer, Emmett, and Teller developed a theory considering the multilayer adsorption concept and delivered a formula called BET equation that yields the surface area, and pore size distribution of catalysts as presented in equation 3<sup>15</sup>. The BET equation correlates, adsorption equilibrium pressure ( $P$ ), the volume of gas adsorbed under pressure ( $v$ ), the saturation vapor pressure of the adsorbate ( $P_0$ ), with the volume of adsorbate required for monolayer coverage ( $v_m$ ), and a constant that is related to the heat of adsorption and liquefaction ( $c$ ).

$$\frac{P}{v(P_0 - P)} = \frac{1}{v_m c} + \left(\frac{c - 1}{v_m c}\right) \left(\frac{P}{P_0}\right) \quad \text{Eq (3)}$$

The  $\text{N}_2$  sorption measurements of various catalysts were performed at liquid  $\text{N}_2$  temperature ( $-196^\circ\text{C}$ ) using Belsorp-mini II instrument (Bel, Japan). BET method with relative pressure ( $P/P_0$ ) range of 0.05 to 0.3 gives the specific surface area of the catalyst corresponding to the monolayer adsorption of the gas. The pore size distribution of the catalysts was obtained using BJH method (derived by Barrett, Joyner, and Halenda), and the total pore volume of the catalysts was obtained at  $P/P_0 = 0.99$ .

### 2.3.6 Acid–base titration for acidity measurement

The amount of Brönsted acidic sites present in the solid acid catalyst with low or moderate thermal stability (e.g., metal organic framework, macro reticular cation exchange resin) can be obtained using the acid–base titration method. From a known concentration of salt ( $\text{NaCl}$ ), the cations ( $\text{Na}^+$ ) are ion exchange with the  $\text{H}^+$  (Brönsted acidic site) of the catalyst. The  $\text{HCl}$  thus formed in the solution, is titrated against a known concentration of a base solution in the presence of an indicator that yields the amount of acidity present in the catalyst.

In a typical acid–base titration method, initially, a solid acid catalyst (0.1 g) and 2 M NaCl (10 mL) were stirred for 8 h to achieve ion exchange. The catalyst was discarded by centrifugation and the ion–exchanged solution containing HCl is titrated against 0.01 M NaOH with phenolphthalein as an indicator.

### **2.3.7 NH<sub>3</sub>–Temperature programmed desorption**

To acquire the strength and amount of acidity and basicity of heterogeneous catalyst, temperature programmed desorption (TPD) analysis is used in which an acid–base interaction (chemisorption) between the probe molecule and the active site occurs. The amount of active sites is estimated by the quantity of probe molecules desorbed with an increase in temperature and time<sup>16,17</sup>. For acidity estimation, NH<sub>3</sub> is used as a probe molecule as it is basic in nature, whereas for basicity estimation, CO<sub>2</sub> an acidic molecule is used as a probe. The TPD analysis can be employed for materials with good thermal stability. The strength (weak, moderate, and strong) of active sites is obtained by integrating the TPD profile with respect to a set of temperatures. The NH<sub>3</sub> species desorbing at higher temperature ranges correspond to strong active site species and the species desorbing at lower temperature ranges correspond to weak active sites.

The estimation of strength and the total amount of acidity (mmol g<sup>-1</sup>) of the solid acid catalyst was performed using Belcat–II (BEL, Japan) instrument. The analysis would start with the pre–treatment of the solid acid catalyst (100 mg) placed in a quartz U–tube under the flow of He gas for an hour at the calcination temperature. Then the temperature was reduced (50 °C) and the probe molecule, here 10% of NH<sub>3</sub> in He was allowed to flow towards the activated catalyst for 30 minutes. To retain the chemisorbed NH<sub>3</sub> species in the sample, the physisorbed NH<sub>3</sub> species were eliminated by purging He for 15 min over the catalyst. Finally, for the measurement, the catalyst was heated up to the calcination temperature with a heating rate of 10 °C min<sup>-1</sup> in the presence of He analyzed using a thermal conductivity detector.

### **2.3.8 Pyridine–FTIR**

IR spectroscopy can be used to identify and differentiate types of acid sites present in the solid acid catalyst<sup>18,19</sup>. The Brønsted and Lewis acidic sites can be characterized by the

---

aid of pyridine as a probe molecule and the study is termed Pyridine–FTIR. During the analysis, pyridine a basic molecule gets chemisorbed differently on Brönsted and Lewis acidic sites of the catalyst. This results in the production of distinguishable IR bands differing in their positions *viz.*  $\sim 1540$  and  $1450\text{ cm}^{-1}$  due to the pyridinium ion interacting with the Brönsted acidic sites and pyridine coordinated to Lewis acid sites respectively. The FTIR spectral data of the pyridine adsorbed pelletized self–supported wafers of solid acid catalysts were acquired using Bruker Alpha–T instrument, scanned over the range from  $1400$  to  $1600\text{ cm}^{-1}$

### **2.3.9 Thermogravimetric analysis**

Thermogravimetric analysis (TGA) is an analytical technique employed to investigate the thermal stability and change in the composition of the sample in a closed system under the influence of a change in temperature<sup>20</sup>. A TGA profile or thermogravimetric curve is obtained by plotting mass (% mass) *v/s* temperature.

The thermal analysis of the solid acid catalyst was tested using Perkin Elmer STA–6000 instrument. The thermal stability of the solid acid catalyst (MOF) was determined by heating the material to  $700\text{ }^{\circ}\text{C}$  (heating rate  $10\text{ }^{\circ}\text{C min}^{-1}$ ) under a nitrogen flow.

### **2.3.10 Scanning electron microscopy (SEM)**

The morphology, particle size, and surface structure of solid acid catalysts can be determined using the electron microscopic technique<sup>21</sup>. The textural properties of catalysts can be obtained when electrons with high energy interact with the material. This interaction generates secondary electron signals from the knocked electrons with reference to the position of the primary beam and gives morphological information via largely magnified micrographs in SEM. SEM instrument comprises an electric gun that generates a beam of electrons, a magnetic lens, scanning coils, apertures (to converge the electron beam), a stage to mount the specimen, and a detector. SEM measurements for various solid acid catalysts were conducted using Hitachi SU, Ultra–55, and Tescan–Mira 3 instruments.

### 3.11 Transmission electron microscopy (TEM)

Transmission electron microscopy is one of the important microscopic techniques that produce high-resolution (to the atomic level) micrographs of specimen<sup>22</sup>. The TEM images of the solid acid catalyst are obtained when the beam of electrons is transmitted through the specimen via various sets of lenses and apertures. The transmitted rays obtained by scattered (elastic, inelastic) or unscattered rays are passed through the lens and are projected on a fluorescent screen to obtain an image. High-resolution images can be obtained from this technique due to the smaller de-Broglie wavelengths offered by electrons.

The TEM micrograph of MOF was obtained using Talos F200S instrument.

## 2.3 Bibliography

- (1) Jia, C.-J.; Liu, Y.; Schmidt, W.; Lu, A.-H.; Schüth, F. Small-sized HZSM-5 zeolite as highly active catalyst for gas phase dehydration of glycerol to acrolein. *Journal of Catalysis* **2010**, *269* (1), 71-79.
- (2) Gil, B.; Mokrzycki, Ł.; Sulikowski, B.; Olejniczak, Z.; Walas, S. Desilication of ZSM-5 and ZSM-12 zeolites: Impact on textural, acidic and catalytic properties. *Catalysis Today* **2010**, *152* (1-4), 24-32.
- (3) Manjunathan, P.; Maradur, S. P.; Halgeri, A.; Shanbhag, G. V. Room temperature synthesis of solketal from acetalization of glycerol with acetone: Effect of crystallite size and the role of acidity of beta zeolite. *Journal of Molecular Catalysis A: Chemical* **2015**, *396*, 47-54.
- (4) Janardhan, H.; Shanbhag, G.; Halgeri, A. Shape-selective catalysis by phosphate modified ZSM-5: Generation of new acid sites with pore narrowing. *Applied Catalysis A: General* **2014**, *471*, 12-18.
- (5) Prakash, A.; Unnikrishnan, S. Synthesis of SAPO-34: high silicon incorporation in the presence of morpholine as template. *Journal of the Chemical Society, Faraday Transactions* **1994**, *90* (15), 2291-2296.
- (6) Meriaudeau, P.; Tuan, V.; Nghiem, V. T.; Lai, S.; Hung, L.; Naccache, C. SAPO-11, SAPO-31, and SAPO-41 molecular sieves: synthesis, characterization, and catalytic properties in octane hydroisomerization. *Journal of catalysis* **1997**, *169* (1), 55-66.

- (7) Shanbhag, G. V.; Kumbar, S.; Halligudi, S. Chemoselective synthesis of  $\beta$ -amino acid derivatives by hydroamination of activated olefins using AISBA-15 catalyst prepared by post-synthetic treatment. *Journal of Molecular Catalysis A: Chemical* **2008**, *284* (1-2), 16-23.
- (8) Marakatti, V. S.; Shanbhag, G. V.; Halgeri, A. Sulfated zirconia; an efficient and reusable acid catalyst for the selective synthesis of 4-phenyl-1, 3-dioxane by Prins cyclization of styrene. *Applied Catalysis A: General* **2013**, *451*, 71-78.
- (9) Yang, F.; Xu, G.; Dou, Y.; Wang, B.; Zhang, H.; Wu, H.; Zhou, W.; Li, J.-R.; Chen, B. A flexible metal–organic framework with a high density of sulfonic acid sites for proton conduction. *Nature Energy* **2017**, *2* (11), 877-883.
- (10) Brock, S. L. *Nanostructures and Nanomaterials: Synthesis, Properties and Applications* By Guozhang Cao (University of Washington). Imperial College Press (distributed by World Scientific): London. 2004. xiv+ 434 pp. \$78.00. ISBN 1-86094-415-9. ACS Publications: 2004.
- (11) Holder, C. F.; Schaak, R. E. Tutorial on powder X-ray diffraction for characterizing nanoscale materials. ACS Publications: 2019; Vol. 13, pp 7359-7365.
- (12) Potts, P. J.; Webb, P. C. X-ray fluorescence spectrometry. *Journal of Geochemical Exploration* **1992**, *44* (1-3), 251-296.
- (13) Ghosh, S.; Prasanna, V. L.; Sowjanya, B.; Srivani, P.; Alagaraja, M.; Banji, D. Inductively coupled plasma–optical emission spectroscopy: a review. *Asian J. Pharm. Ana* **2013**, *3* (1), 24-33.
- (14) Günzler, H.; Gremlich, H.-U. IR spectroscopy. An introduction. **2002**.
- (15) Condon, J. B. *Surface area and porosity determinations by physisorption: measurement, classical theories and quantum theory*; Elsevier, 2019.
- (16) Barrie, P. J. Analysis of temperature programmed desorption (TPD) data for the characterisation of catalysts containing a distribution of adsorption sites. *Physical Chemistry Chemical Physics* **2008**, *10* (12), 1688-1696.
- (17) Védrine, J. C. Acid–base characterization of heterogeneous catalysts: an up-to-date overview. *Research on Chemical Intermediates* **2015**, *41* (12), 9387-9423.
- (18) Viswanathan, B.; Sivasanker, S.; Ramaswamy, A. *Catalysis: principles and applications*; Alpha Science Int'l Ltd., 2002.
-

(19) Concepción, P. Application of infrared spectroscopy in catalysis: impacts on catalysts' selectivity. *Infrared Spectroscopy: Principles, Advances, and Applications* **2018**.

(20) Gabbott, P. *Principles and applications of thermal analysis*; John Wiley & Sons, 2008.

(21) Niemantsverdriet, J. W. *Spectroscopy in catalysis: an introduction*; John Wiley & Sons, 2007.

(22) Maaz, K. *The Transmission Electron Microscope*; BoD–Books on Demand, 2012.





# **Chapter 3**

## **Butanolysis of furfuryl alcohol to produce butyl levulinate**



### 3.1 Introduction

The present era of globalization is leading to the exhaustion of conventional fossil fuels which would diminish the chance of meeting the energy demands for the future. The impact of oil on mankind and its disastrous effects such as an increase in oil price, carbon footprint, foreign oil dependency, and disturbing world peace is evident. Despite its applications in daily life, extraction by mining and drilling itself has a lot of detrimental effects on our ecosystem such as landslides, flash floods, water pollution, and greenhouse gas emissions. Due to the decrease in the reserves of these non-renewable resources, there is a serious necessity to switch to renewable resources which are abundant, carbon-neutral, and environmentally friendly. Apparently, as the oil well drains up, not only the production of transportation fuels is affected, but also the petrochemicals manufactured from crude oil and its derivatives. There are excellent alternatives for fuels and energy production which can replace fossil fuels, for instance, solar energy, wind energy, nuclear energy, biomass, etc. However, these resources chosen should also effectively compete with the existing technology to produce chemicals. Apart from fossil fuels, the only two sustainable, renewable carbon sources are biomass and CO<sub>2</sub>. Therefore, exploiting biomass for manufacturing commodity chemicals, fuels, and fuel additives has gained a lot of consideration in recent years. Among the various chemicals obtained from lignocellulosic biomass, such as., glycerol, lactic acid, serine, aspartic acid, threonine, sorbitol, levoglucosan, xylitol, arabinitol, etc., furfural is projected as one of the 30 potential candidates as building blocks that would transform into multiple functionality chemicals<sup>1</sup>.

Furfuryl alcohol produced by chemoselective hydrogenation of furfural is abundant, C-5 platform chemical used for the synthesis of high-value products like lysine, methyl furan, ascorbic acid, levulinate esters, angelica lactones,  $\gamma$ -valerolactone, lubricants, resins, plasticizers, fragrances and adhesives<sup>2,3</sup>. Annually 62% of the globally produced furfural (approximately 200 000 tonnes) is consumed for the synthesis of furfuryl alcohol due to its expanding application profile and increasing market value. Alcoholysis of furfuryl alcohol yields alkyl levulinate (Scheme 3.1) that has potential applications as biofuels and, additives in flavor and fragrance products<sup>4</sup>. As alkyl levulinates are traditionally produced by the esterification of levulinic acid, an expensive chemical, alcoholysis of

---

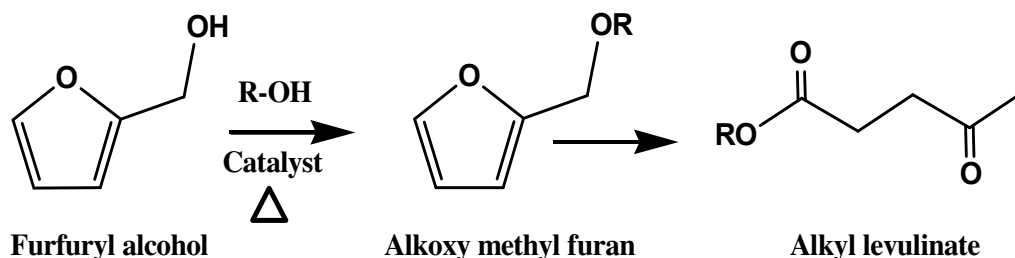
furfuryl alcohol serves as an inexpensive route which also promotes the bio-based economy. This reaction utilizing furfuryl alcohol is challenging as the intermediate 2-(alkoxy methyl) furan (AMF), an ether, formed is to be successfully converted into alkyl levulinate (keto ester) which is difficult compared to carboxylic acid route (levulinic acid). Hence alcoholysis of furfuryl alcohol is a greener approach to yield alkyl levulinate which helps to understand and explore the reaction.

For the liquid phase butanolysis of furfuryl alcohol to butyl levulinate, various solid acid catalysts have been reported which include, graphite oxide (GO) and reduced graphite oxide (rGO) catalysts<sup>5</sup>, lignin-based carbonaceous acid<sup>6</sup>, modified SBA-15<sup>7,8</sup>, titanium exchanged mesoporous silica<sup>9</sup>, modified ionic liquids<sup>10,11</sup>, ionic liquids<sup>12</sup>, zinc exchanged heteropolytungstate supported on niobia,<sup>13</sup> hematite,<sup>14</sup> functionalized fibrous silica<sup>15</sup>, sulfonic acid functionalized TiO<sub>2</sub> nanotubes<sup>16</sup>, tin exchanged tungstophosphoric acid and tin phosphate<sup>17,18</sup>. From these reports, it is understood that the Brønsted acid site plays a major role in the selective synthesis of alkyl levulinate. However, many of these reported catalysts have not been studied for reusability or failed to retain their catalytic activity upon recycling.<sup>5,8,11,12,14,16</sup> The catalyst deactivation is mainly because of the accumulation of oligomeric products formed due to the polymerization of furfuryl alcohol on the active sites of the catalyst. Hence, high thermal stability should be one of the important virtues of the desired catalyst for this reaction as the catalyst regeneration at high temperatures is easily achievable. Some catalysts also reportedly gave good catalytic performance only in the presence of excessive usage of catalyst or reactants<sup>7,9,10,11,13,14,16,17,18</sup>. One promising catalyst that can overcome all these drawbacks is zeolite owing to its high surface area, strong Brønsted acidity, ordered microporosity, high thermal stability, and better recyclability.

There are a few reports, where zeolite-based catalysts have been investigated for this transformation. Lange et al. explored a range of acid catalysts such as H<sub>2</sub>SO<sub>4</sub>, ion-exchanged resins, and zeolites in a semi-batch semi-continuous mode at varying temperatures (125 and 225 °C) for the ethanolysis of furfuryl alcohol. The ZSM-5 (SAR30) was reported 65mol% ethyl levulinate yield which is the best among the other zeolites tested (ZSM-5, ZSM-12, ZSM-23, H-Beta, mordenite). However, zeolites as such were ranked low among the other catalysts<sup>19</sup>. In another study by Yao-Bing Huang

---

et al., HZSM-5 and H-Beta catalysts were compared with various metal salt catalysts under microwave irradiation. The metal salt  $\text{Al}_2(\text{SO}_4)_3$ , showed 80% yield for methyl levulinate, whereas HZSM-5 and H-Beta showed 4.9 and 1% yield respectively<sup>20</sup>. A study on zeolite-based material was reported over H-ZSM-5, hierarchical zeolite, H-Beta and USY for ethanolysis of furfuryl alcohol by Nandiwale et al<sup>21</sup>. The trend for ethyl levulinate yield was 5%, 8%, 13%, and 19% for USY, H-Beta, HZSM-5, and hierarchical zeolite respectively. Under optimized reaction conditions, hierarchical zeolite was found to be the most active catalyst with ethyl levulinate yield of 73%. Additionally, other literatures are focusing on various catalysts by comparing their catalytic performance with zeolites<sup>7,8,22,23,24,25,15,26</sup>. From the careful literature survey, we found that zeolite, in general, can be a potential catalyst for the alcoholysis of furfuryl alcohol, but a detailed study over the zeolite to explore its properties to achieve enhanced performance has not been conducted so far. Moreover, a thorough study on the zeolite catalyst for this reaction is important to understand the intricacies of how the structural and textural properties of the catalyst influence the catalytic reaction. Hence, in this work, a series of conventional solid acid catalysts were tested that included ordered mesoporous aluminosilicate, silicoaluminophosphate, medium and large pore zeolites, and ion-exchange resin. Zeolite ZSM-5 was studied in detail to understand the relation between its physicochemical properties and the alcoholysis reaction. To discover the desired type of acid site for this reaction, post-modification of ZSM-5 was performed by desilication, dealumination, phosphate modification and metal ion exchange. The physicochemical properties of all the catalysts were investigated using various characterizations such as XRF, PXRD, nitrogen adsorption-desorption isotherms,  $\text{NH}_3$ -TPD and SEM. Reaction parameters such as catalyst concentration, reactant mole ratio and temperature were studied using the catalyst with the best performance. To evaluate the reusability of the potential catalyst, the material was screened for multiple cycles at the optimized reaction conditions



**Scheme 3.1.** Conversion of furfuryl alcohol to alkyl levulinate.

### 3.2 Chemicals and reagents

ZSM-5 with different SiO<sub>2</sub> to Al<sub>2</sub>O<sub>3</sub> ratio (SAR), mordenite (SAR20), H-Beta (SAR25), were obtained from Nankai University Catalyst Co. China and Zeolyst International (SAR22) and Y-zeolite (SAR5.1). Furfuryl alcohol, ammonium dihydrogen phosphate (NH<sub>4</sub>H<sub>2</sub>PO<sub>4</sub>), copper nitrate trihydrate, zinc nitrate hexahydrate, tetraethyl orthosilicate, concentrated HCl, concentrated H<sub>2</sub>SO<sub>4</sub>, concentrated H<sub>3</sub>PO<sub>4</sub>, ammonium acetate, aqueous ammonium hydroxide, Al(NO<sub>3</sub>)<sub>3</sub>, NaOH, 1-butanol, 1-propanol, and methanol were purchased from Merck India Pvt. Ltd. Amphiphilic triblock co-polymer poly-(ethylene glycol)-block poly-(propylene glycol)-block poly-(ethylene glycol), ludox, fumed silica and morpholine were purchased from Sigma-Aldrich. Tetrapropyl ammonium bromide and zirconium oxychloride octahydrate were purchased from Loba Chemie. Citric acid and ethanol were procured from Otto biochemical reagents and CSS respectively. Amberlyst-15 was obtained from Alfa-Aesar. Plural SB (pseudoboehmite) was procured from Sasol.

### 3.3 Catalyst synthesis

HZSM-5 catalyst was synthesized from a procedure similar to the reported one<sup>27</sup>. In a typical synthesis, the required quantity of NaOH, Al(NO<sub>3</sub>)<sub>3</sub> (aluminium source), ludox (silicon source) were added to the distilled water and stirred well. To this, a template tetrapropyl ammonium bromide was added. The solution was transferred to a teflon lined autoclave and placed in an oven for 24 h at 180 °C. The material is washed filtered, dried, and calcined at 550 °C. To obtain the ammonium form of the synthesized and commercially obtained ZSM-5, the material was subjected to three-fold ammonium exchange using 0.5M ammonium acetate for 4 h at 80°C. The material was finally

calcined at 550 °C for 5h at a heating rate of 5 °C min<sup>-1</sup> to yield the protonic form of the catalyst<sup>28</sup>. The obtained materials were labeled as HZSM-5.

Desilication was performed by stirring HZSM-5 (SAR95) with 0.1M and 0.2M NaOH at 85 °C for an hour<sup>29</sup>. The materials were filtered, washed with distilled water, and dried at 120 °C for 12 h. They were calcined at 550 °C for 5 h at a heating rate of 5 °C min<sup>-1</sup>. The catalysts were transformed into ammonium form by treating it with 0.5M ammonium acetate solution for 4 h at 80 °C. The solution was filtered and dried. Ammonium exchange was carried out thrice followed by calcination at 550 °C for 5 h resulting in the protonated form of the material. The catalysts thus obtained were labeled as DS (0.1M NaOH) and DS (0.2M NaOH).

Dealumination was performed by treating 0.2M HCl and citric acid with HZSM-5 (SAR95) for 24 h at 80 °C<sup>30</sup>. The materials were filtered, washed with distilled water, and dried at 120 °C for 12 h. They were calcined at 550 °C for 5 h at a heating rate of 5 °C min<sup>-1</sup>. The catalysts thus obtained were labeled as DA (HCl) and DA (Citric acid).

A known amount of ammonium dihydrogen phosphate with varied concentrations was dissolved in distilled water and heated at 65 °C. To this solution, HZSM-5 (SAR95) was added and subjected to evaporation. The material was dried and stepwise calcined at 330 °C for 3 h and 560 °C for 10 h. Finally, to remove the physisorbed phosphate, the catalyst was stirred with distilled water at 80 °C for 12 h, filtered, and dried<sup>28</sup>. The catalysts thus obtained were labelled as 1% P-ZSM-5, 3 % P-ZSM-5 and 5% P-ZSM-5.

HZSM-5 (SAR95) was refluxed with 0.1M aqueous copper nitrate trihydrate solution and 0.1M aqueous zinc nitrate hexahydrate solution at 80 °C for 12 h to obtain Cu-ZSM-5 (SAR95) and Zn-ZSM-5 (SAR95) respectively. The material was washed, filtered, and dried at 120 °C for 12 h. This procedure was repeated twice before calcining at 550 °C for 5 h<sup>30</sup>. The catalysts thus obtained were labeled as Cu-ZSM-5 (SAR95) and Zn-ZSM-5 (SAR95).

Other catalysts such as sulfated zirconia, SAPO-34 and Al-SBA-15 were synthesized from the reported literature<sup>31,32,33</sup>.

For the recyclability study, the spent catalyst was washed with methanol, filtered, dried, and finally calcined at 550 °C for 5 h after each catalyst recycle.

### 3.4 Catalytic activity study

In a typical procedure, the alcoholysis of furfuryl alcohol was performed in a liquid phase batch reaction under magnetic stirring at the desired temperature. The required molar composition of furfuryl alcohol and butanol, and the catalyst (with respect to the total reactants) were taken in a 25 ml round bottom flask connected to a condenser. The reaction of furfuryl alcohol was also conducted with other alcohols with a similar procedure under reflux conditions. The samples of the reaction mixture were periodically collected and quantitatively analyzed by gas chromatography (GC) (Agilent Technologies 7820A) equipped with HP-5 capillary column (0.25 mm I.D., 30 m length) coupled with the flame ionization detector. The identity of the products was confirmed by Gas chromatography mass spectrometry (GCMS). The furfuryl alcohol conversion and butyl levulinate selectivity were determined using the external standard method in the GC.

$$X_{FA}(\%) = \frac{C_{FA(i)} - C_{FA(f)}}{C_{FA(i)}} \times 100$$
$$S_{BL}(\%) = \frac{C_{BL}}{C_{FA(i)} - C_{FA(f)}} \times 100$$

Where  $X_{FA}$  and  $S_{BL}$  are furfuryl alcohol conversion and butyl levulinate selectivity respectively.  $C_{FA(i)}$  and  $C_{FA(f)}$  correspond to initial and final molar concentrations of furfuryl alcohol respectively.  $C_{BL}$  is the molar concentration of butyl levulinate formed in the reaction.

### 3.5 Catalyst characterization

#### 3.5.1 X-ray fluorescence analysis

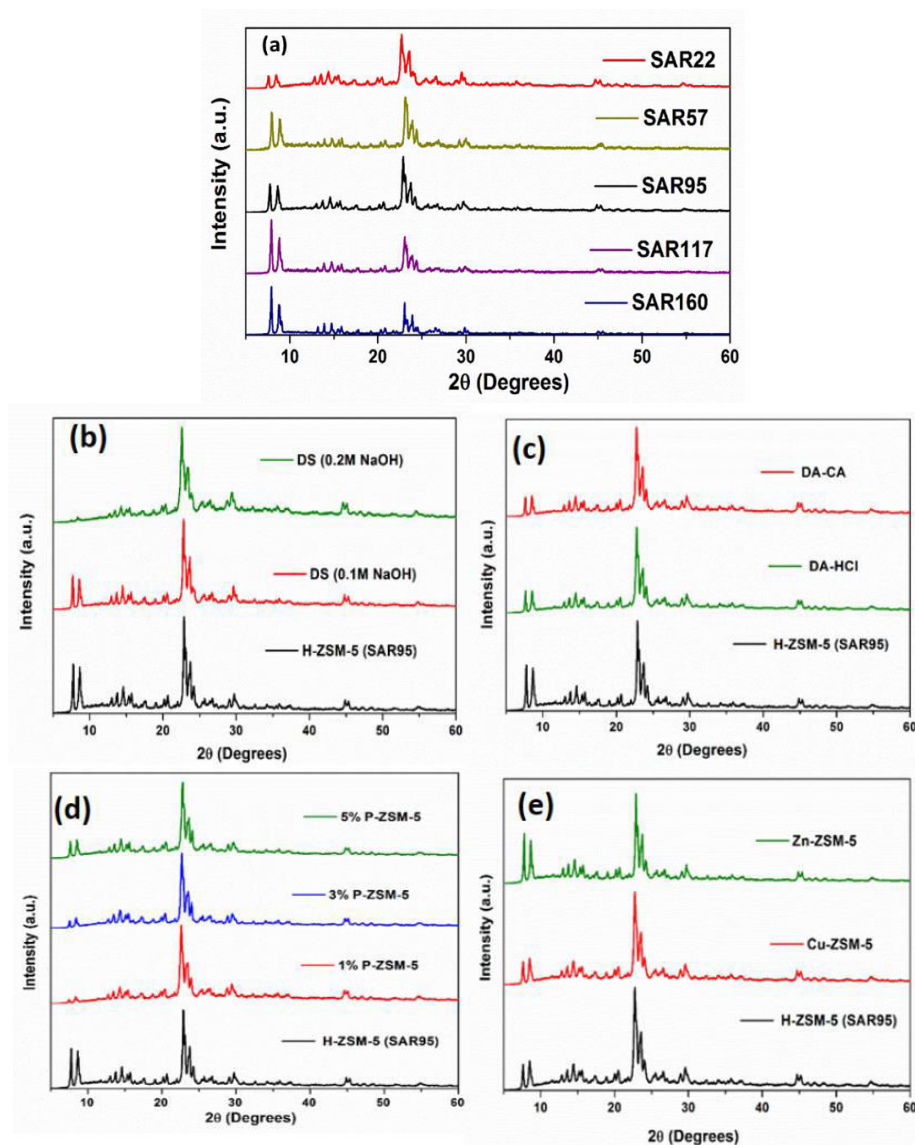
XRF analysis provided the silica to alumina ratio (SAR) of all the commercial and synthesized zeolite catalysts tested for this transformation. The ZSM-5 zeolites with a wide range of SAR from 22 to 160 were chosen for this study.

#### 3.5.2 Powder X-ray diffraction

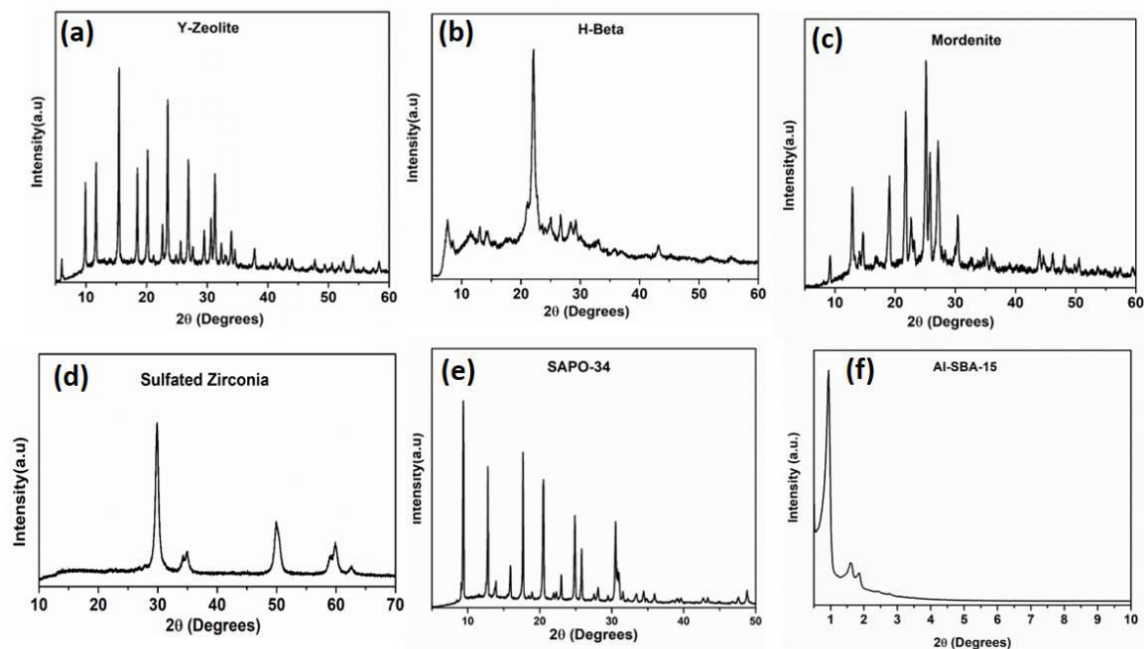
All the diffractograms of HZSM-5 with varied SARs reflect the characteristic pattern of MFI topology with main peaks at  $2\theta$  13°, 23° and 45° [figure 3.1 (a)]<sup>34</sup>. XRD patterns



after the modifications such as desilication, dealumination, phosphate modification, and metal ion exchange showed no change in the structure [figure 3.1 (b–e)]. Also, the XRD patterns of SAPO–34, sulfated zirconia, Al–SBA–15, mordenite, H–Beta, Y–zeolite matched well with the literature [figure 3.2 (a–f)].



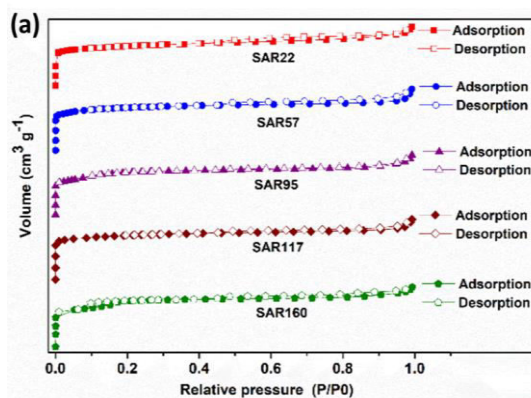
**Figure 1.1.** XRD diffractograms of (a) HZSM–5 with varied SAR (b) desilicated ZSM–5 (c) dealuminated ZSM–5 (d) phosphate modified ZSM–5 (e) metal ion–exchanged ZSM–5

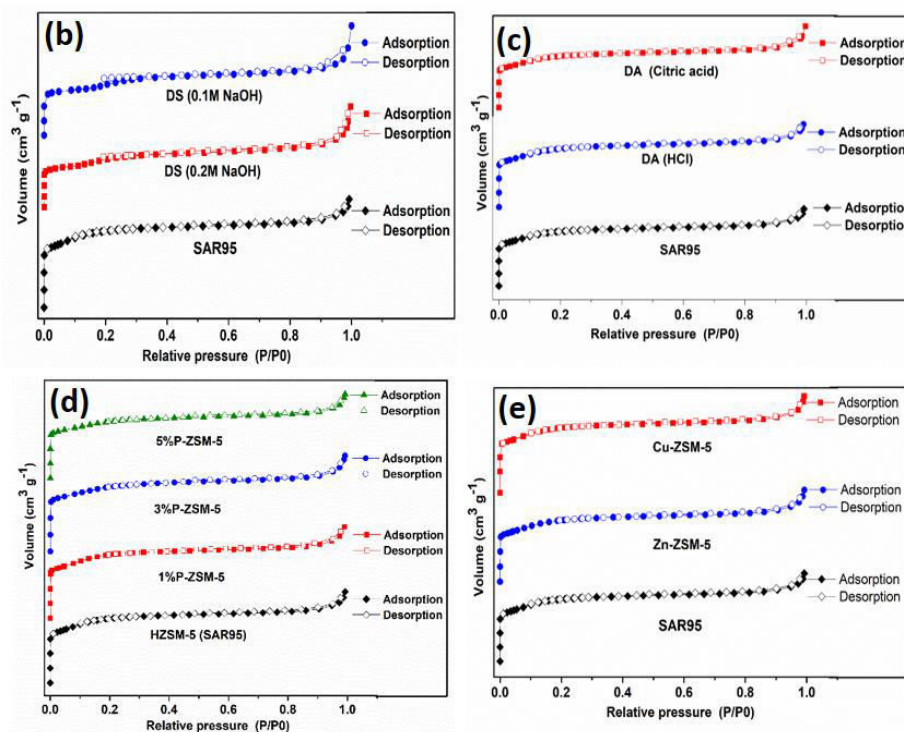


**Figure 3.2.** XRD patterns of (a) Y-zeolite (b) H-Beta (c) Mordenite (d) Sulfated Zirconia (e) SAPO-34 (f) Al-SBA-15

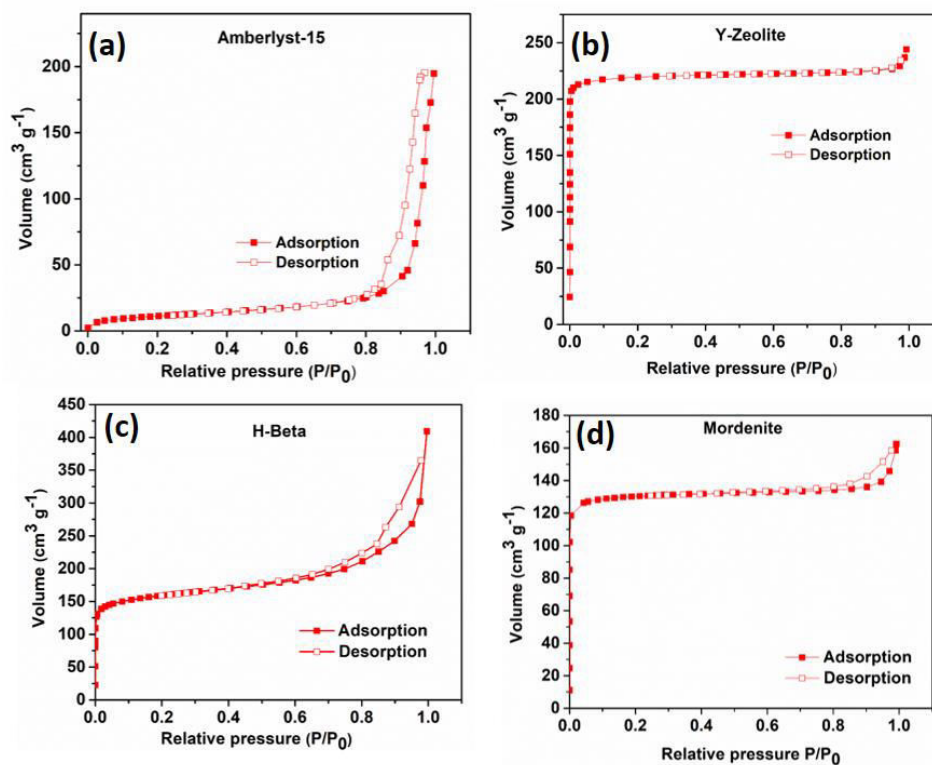
### 3.5.3 Nitrogen sorption studies

The BET surface area of unmodified HZSM-5 with varied SARs was around  $400 \text{ m}^2 \text{ g}^{-1}$  which confirms its high surface area (Table 3.1). The post-modification, by desilication, metal ion exchange, phosphate modification, led to the decrease in surface area as shown in the Table 3.1. But in the case of dealumination, there was a negligible increase in surface area. Also, there was a marginal difference in pore volume among the catalysts. Sorption studies were performed for all the catalysts tested which showed comparable results with the literature (figure 3.3 and figure 3.4)<sup>31,32,33</sup>.





**Figure 3.3.**  $N_2$  sorption isotherms of (a) HZSM-5 with varied SAR (b) desilicated ZSM-5 (c) dealuminated ZSM-5 (d) phosphate modified ZSM-5 (e) metal ion exchanged ZSM-5.



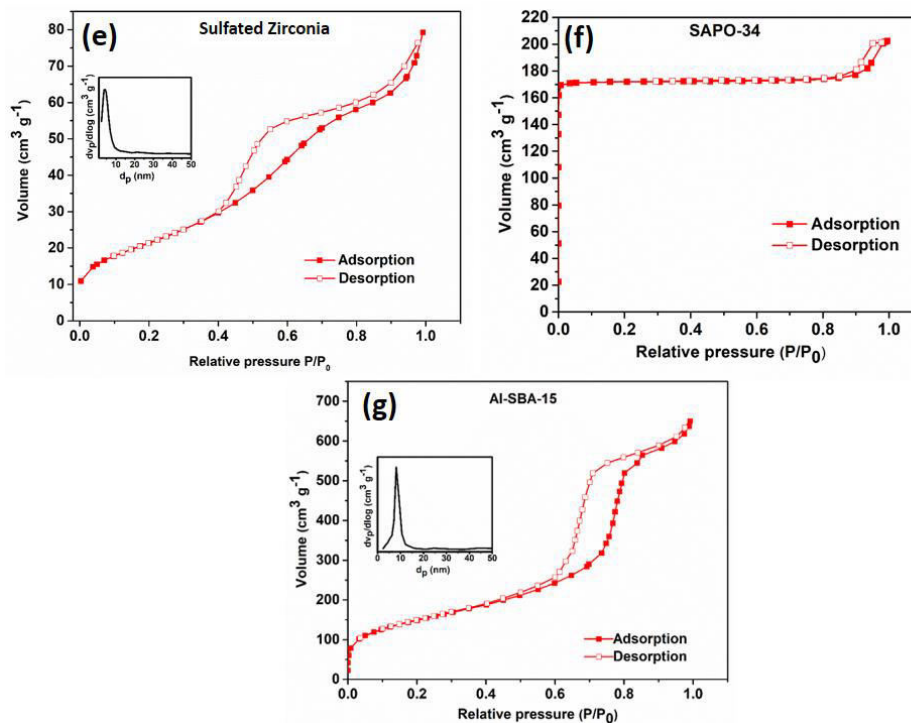


**Figure 3.4.** N<sub>2</sub> sorption isotherms of (a) Amberlyst–15 (b) Y–zeolite (c) H–Beta (d) Mordenite (e) Sulfated Zirconia (f) SAPO–34 (g) Al–SBA–15

### 3.5.4 Temperature programmed desorption and Pyridine–FTIR

The total acidity of HZSM–5 from NH<sub>3</sub>–TPD decreased from 1.06 to 0.28 mmol g<sup>-1</sup> with an increase in SAR from 22 to 160 as expected [figure 3.5 (a), Table 3.1]. The strengths of acidity of all the unmodified HZSM–5 catalysts were dominated by weak and moderate acidic sites. Among them, SAR 57 and 95 possessed a good number of strong acidic sites. Sulfated zirconia and Al–SBA–15 possessed acid strength in the broad range of 50 –550 °C. Y–zeolite contained a similar number of weak and moderate acid sites, whereas H–Beta possessed predominantly strong acid sites. SAPO–34 and Y–zeolite contained mainly weak and moderate acid sites [Table 3.1, figure 3.6 (a–f)].

The treatment of HZSM–5 with 0.1M NaOH decreased the acidity drastically from 0.59 to 0.29 mmol/g which might be due to the removal of extra framework aluminium along with desired silicon atoms. For 0.2M NaOH treatment, the acidity of the catalyst decreased to 0.38mmol/g but it was still higher than 0.1M NaOH treated catalyst. It is because the efficiency of desilication increased with an increase in molar concentration of NaOH to 0.2M, thereby increasing the acidity by removing more silicon atoms compared

to the 0.1M NaOH. However, a subsequent increase in the concentration of NaOH treatment might remove more number of silicon atoms but at the expense of the framework stability.<sup>29</sup> Hence, the NaOH treatment was stopped at 0.2M concentration. In both the treatments of NaOH, the structural integrity of HZSM-5 was found to be retained by PXRD indicating that the zeolite framework was still stable after the removal of silicon atoms. Upon desilication, the B/L ratio of HZSM-5 decreased from 3.9 to 2.1 and 2.0 for 0.1M NaOH and 0.2M NaOH treatment respectively (Table 3.1, figure 3.7). This is due to the generation of extra framework aluminium and also the reincorporation of leached Al species resulting in an increase in Lewis acidity.

Dealumination was performed using HCl and citric acid as these agents act differently in the matrix. The HCl, being a strong acid and small molecule, caused a decrease in acidity to a higher extent than the mild citric acid. The acidity drastically decreased from 0.59 to 0.24 mmolg<sup>-1</sup> for HCl due to its access towards more aluminium sites throughout the matrix. The B/L ratio decreased from 3.9 to 1.9 due to the removal of framework aluminium mainly decreasing the Brönsted acidity. In the case of citric acid, due to its mild acidity, extra framework aluminium (Lewis acid site) could be predominantly dealuminated. The total acidity decreased marginally from 0.59 to 0.53 mmolg<sup>-1</sup>, whereas B/L ratio increased from 3.9 to 4.6 (Table 3.1, figure 3.7)<sup>35,36</sup>.

Phosphate treatment resulted in a decrease in total acidity affecting primarily the strong Brönsted acid sites (>350°C). Upon an increase in the concentration of phosphate treatment from 1 to 5%, the acidity marginally decreased from 0.42 to 0.37 mmolg<sup>-1</sup> (Table 3.1) due to the generation of weaker phosphate type of acid sites<sup>28</sup>. The strong Brönsted acidity decreased from 0.22 to 0.08 mmolg<sup>-1</sup> for HZSM-5 upon an increase in the phosphate treatment from 0 to 5%. The phosphate treatment creates low-strength P-O-H acidic sites by different types of interactions with framework Al sites. Certain interactions can cause the replacement of two Al acid sites by one P-O-H Brönsted acid site leading to a decrease in total acidity. For ZSM-5 with higher SAR, the total acidity might increase due to the enhanced acid site spacing, thus creating more than one P-OH site per Al site. This type of interaction of the phosphate group is more predominant for zeolite with closely positioned acid sites (lower SAR)<sup>37,38,39,40</sup>. The B/L ratio increased from 3.9 (HZSM-5) to 4.3 and 6.8 upon treatment with 1% and 3%P respectively. This

shows that Al acid sites are converted into weaker  $-P-OH$  type acid sites. Further increase in phosphate to 5% decreased the B/L ratio which could be attributed to pore narrowing of the zeolite leading to blocking of accessibility to the pyridine probe molecule (Table 3.1, figure 3.7)<sup>41,28</sup>. Metal ion was exchanged with  $H^+$  of HZSM-5 to induce Lewis acidity in the zeolite matrix. When copper and zinc ions were exchanged with the Brönsted acidic protons of ZSM-5, the Lewis acidity is expected to increase<sup>30</sup>. But the total acidity of HZSM-5 (0.59 mmol/g) was found to decrease to 0.48 and 0.45 mmol g<sup>-1</sup> upon modification with  $Zn^{2+}$  and  $Cu^{2+}$  respectively due to the lowering of Brönsted acidity [figure 3.5 (e)]. The B/L ratio decreased from 3.9 (HZSM-5) to 1.2 and 0.8 for Zn-ZSM-5 and Cu-ZSM-5 respectively as expected due to the incorporation of Lewis acidic metal centers (Table 3.1, figure 3.7). In the case of all the modifications on HZSM-5 (SAR95), it is observed that the strong acid sites were affected the most as there is a shift in the desorption peak towards lower temperature which is evident from the TPD profiles and acidity values (Table 3.1).

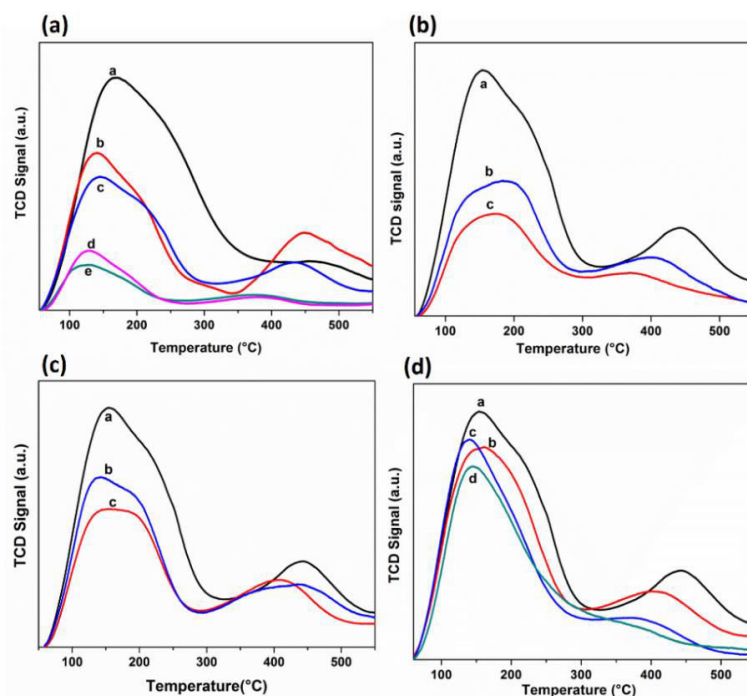


**Figure 3.5.** Temperature programmed desorption profiles of (a) HZSM-5 with varied SAR [a-SAR22, b-SAR57, c-SAR95, d-SAR117, e-SAR160], (b) Desilicated ZSM-5 [a-HZSM-5(SAR95) b-DS (0.2M NaOH) c-DS (0.1M NaOH)] (c) Dealuminated ZSM-5 [a-HZSM-5(SAR95), b-DA (Citric acid), c-DA (HCl)] (d) Phosphate modified ZSM-5 [a-HZSM-5(SAR95), b-1%P-ZSM-5, c-3%P-ZSM-5, d-5%P-ZSM-5].

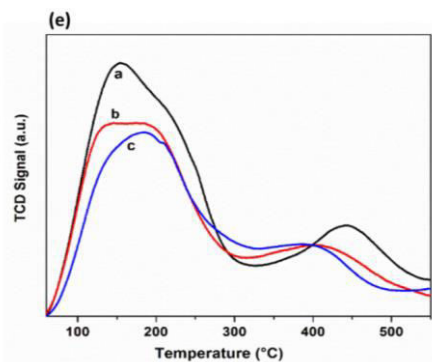


**Figure 3.5.** Temperature programmed desorption profiles of (e) Metal ion exchanged ZSM-5: a-ZSM-5(SAR95), b-Zn-ZSM-5, c-Cu-ZSM-5

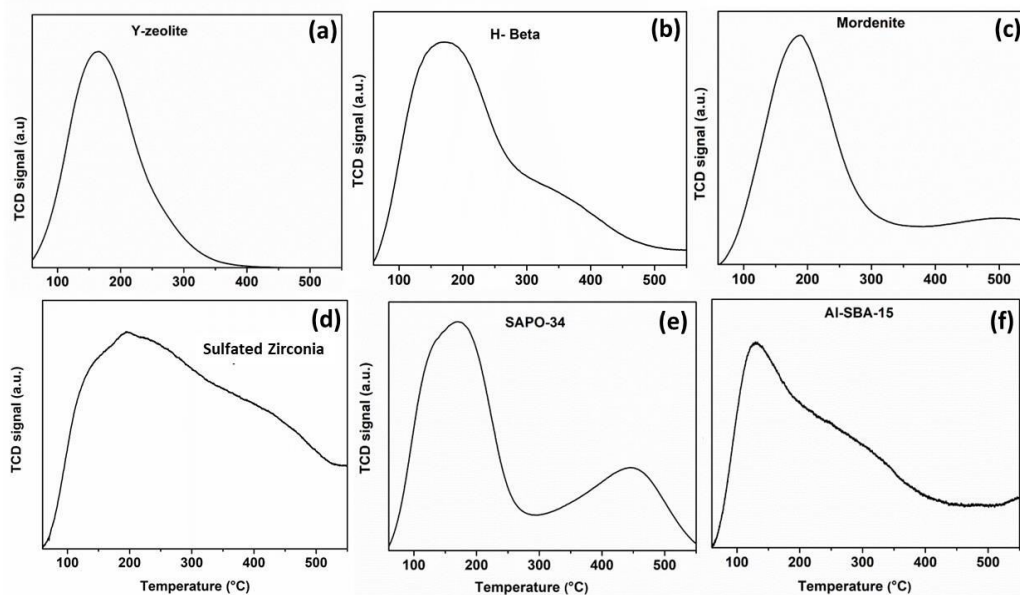


**Figure 3.6.** Temperature programmed desorption profiles of (a) Y-zeolite (b) H-Beta (c) Mordenite (d) Sulfated Zirconia (e) SAPO-34 (f) Al-SBA-15

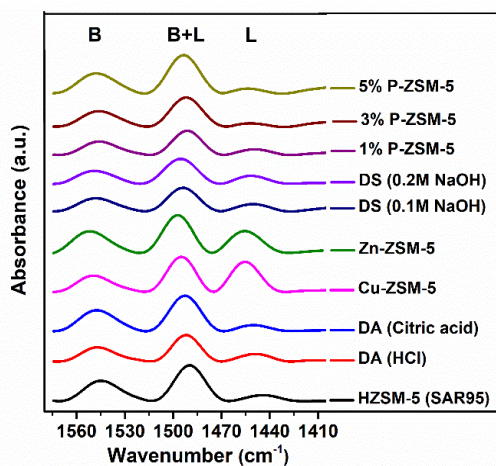


**Figure 3.7.** Pyridine-FTIR spectra of modified and unmodified HZSM-5

**Table 3.1.** Physicochemical properties of the catalysts

Catalyst	Surface area (m <sup>2</sup> g <sup>-1</sup> ) [a]	Pore Volume (cm <sup>3</sup> g <sup>-1</sup> )	Acidity (mmol g <sup>-1</sup> ) [b]				B/L [d]
			Weak	Moderate	Strong	Total	
Sulfated Zirconia	78.2	0.12	0.03	0.10	0.11	0.25	–
SAPO–34	666.6	0.28	0.89	0.55	0.24	1.69	–
Amberlyst–15	40.3	0.27	–	–	–	4.7 <sup>[c]</sup>	–
Al–SBA–15 (SAR35)	677.4	0.88	0.07	0.05	0.06	0.19	–
Y–Zeolite (SAR5.1)	809.5	0.36	0.67	0.66	0.26	1.6	–
H–Beta (SAR25)	592.1	0.16	0.20	0.28	0.43	0.92	–
Mordenite (SAR20)	498.0	0.21	0.63	0.22	0.48	1.34	–
HZSM–5 (SAR22)	403.7	0.17	0.53	0.13	0.39	1.06	–
HZSM–5 (SAR57)	422.1	0.18	0.29	0.10	0.42	0.82	–
HZSM–5 (SAR95)	418.9	0.19	0.19	0.18	0.21	0.59	3.9
HZSM–5 (SAR117)	404.6	0.18	0.20	0.08	0.16	0.45	–
HZSM–5 (SAR160)	426.9	0.19	0.10	0.03	0.14	0.28	–
DS (0.1M NaOH)	364.6	0.18	0.12	0.07	0.09	0.29	2.1
DS (0.2M NaOH)	404.8	0.18	0.16	0.10	0.12	0.38	2.0
DA (HCl)	423.5	0.19	0.05	0.10	0.07	0.24	1.9
DA (Citric acid)	421.8	0.19	0.18	0.17	0.18	0.53	4.6
1% P–ZSM–5	403.1	0.18	0.17	0.14	0.11	0.42	4.3
3% P–ZSM–5	373.4	0.17	0.18	0.12	0.10	0.40	6.8
5% P–ZSM–5	323.7	0.15	0.16	0.13	0.08	0.37	5.3
Cu–ZSM–5	411.6	0.18	0.11	0.18	0.16	0.45	0.8
Zn–ZSM–5	417.1	0.19	0.14	0.17	0.17	0.48	1.2

[a] BET surface area, [b] NH<sub>3</sub>–TPD [c] Acid–base titration [d] Pyridine–FTIR

### 3.5.5 Scanning electron microscopy

SEM analysis of HZSM–5 (SAR95) was performed to investigate the morphology and the particle size. The micrographs disclosed that the material contained spherical morphology with an average particle size of 0.5 μm (figure 3.8).



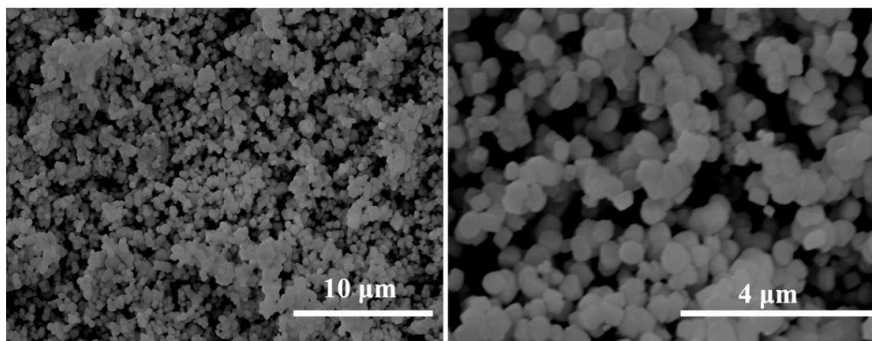


**Figure 3.8.** SEM images of HZSM-5 (SAR95)

## 3.6 Catalytic activity studies

### 3.6.1 Catalyst screening and comparison

From the prior knowledge on the alcoholysis reaction, it is understood to be purely an acid-catalyzed reaction and the Brønsted acid sites specifically play a major role in the selective synthesis of alkyl levulinate. Hence, various conventional solid acid catalysts like zeolites, mesoporous aluminosilicates, silicoaluminophosphate, cation exchange resin and sulfated zirconia were screened for this reaction. To know the essential qualities that are required in a catalyst to get maximum activity, the catalytic conversion and selectivity were correlated with their physicochemical properties.

Butanolysis of furfuryl alcohol to yield butyl levulinate was carried over various solid acid catalysts such as HZSM-5, Y-zeolite, H-Beta, mordenite, amberlyst-15, sulfated zirconia, SAPO-34 and Al-SBA-15. Prior to this study, a blank reaction was performed in the absence of the catalyst which gave a trace level conversion. Amberlyst-15, a pure Brønsted acidic catalyst, gave the highest selectivity (92%) for butyl levulinate followed by HZSM-5 (66%) with conversions for both the catalysts near to completion. The better catalytic performance of amberlyst-15 catalyst can be ascribed to the high number of Brønsted acidity present in it compared to any other catalyst taken in this study. The HZSM-5 with its unique uniform medium-sized micropore structure as well as its strong Brønsted acid character might have helped in getting good performance for this reaction. The rest of the catalysts exhibited lower catalytic activity (< 20 %) as shown in figure 3.9. Mordenite having two channels (channel dimension: 0.70×0.65 and 0.57×0.26) behaves as a one-dimensional pore system as one of the pores restricts the movement of

molecules, lowering its catalytic performance<sup>42</sup>. The low performances of the H-Beta and Y-zeolite show that the large pore structure may not be suitable for this reaction. H-Beta gave  $\geq 99\%$  furfuryl alcohol conversion, but the intermediate butoxy methyl furan (hereafter BMF) conversion into butyl levulinate was low. The presence of strong acidity in H-beta helped to achieve high conversion but resulted in high selectivity towards side products; BMF and 5,5-dibutoxy-2-pentanone. On the other hand, Y-zeolite exhibited poor conversion of furfuryl alcohol itself which may be attributable to the dominated presence of weak and moderate number of acid sites. Though SAPO-34 contained mainly weak and moderate acid sites with good surface area, the presence of weaker phosphate type groups could be the reason for its low furfuryl alcohol conversion (12% at 6 h). Al-SBA-15 possessing mesoporosity, acidity in the broad range of 50–550°C and high surface area gave  $\geq 99\%$  furfuryl alcohol conversion but its low selectivity towards butyl levulinate could be because of the low conversion of the intermediate BMF due to the weaker Al acid sites. Though sulfated zirconia possessed acid strength in the broad range of 50–550°C, conversion of furfuryl alcohol was low (13% at 6 h) which could be due to its smaller surface area and lower number of acidity compared to HZSM-5 (Table 3.1). Both Al-SBA-15 and sulfated zirconia gave a considerably high amount of 5,5-dibutoxy-2-pentanone side product with 11 and 5% selectivity respectively. Hence, we can conclude, in general, that pore size, strength and number of acid sites are largely responsible for the efficiency of the catalyst for this two-step tandem reaction. Amberlyst-15 gave almost complete conversion and high selectivity for butyl levulinate. However, being an organic cation-exchange resin, it is always suspected about its performance in successive catalyst cycles. Due to its low thermal stability (120 °C), the calcination cannot be employed for the removal of the adsorbed substrate/product species which block the active sites. Therefore, recycling by repeated methanol washing and drying at 110 °C for 12 h was employed which, however, did not help in retaining its activity. It is found that there was a drastic decrease in selectivity for butyl levulinate from 92 to 22% during the recyclability as presented in figure 3.10. The selectivity of intermediate side product, butoxy methyl furan increased with every recycle in case of amberlyst-15. Hence, HZSM-5 with high thermal stability

was opted for further studies which gave almost complete conversion and fairly high selectivity of 66% for butyl levulinate.

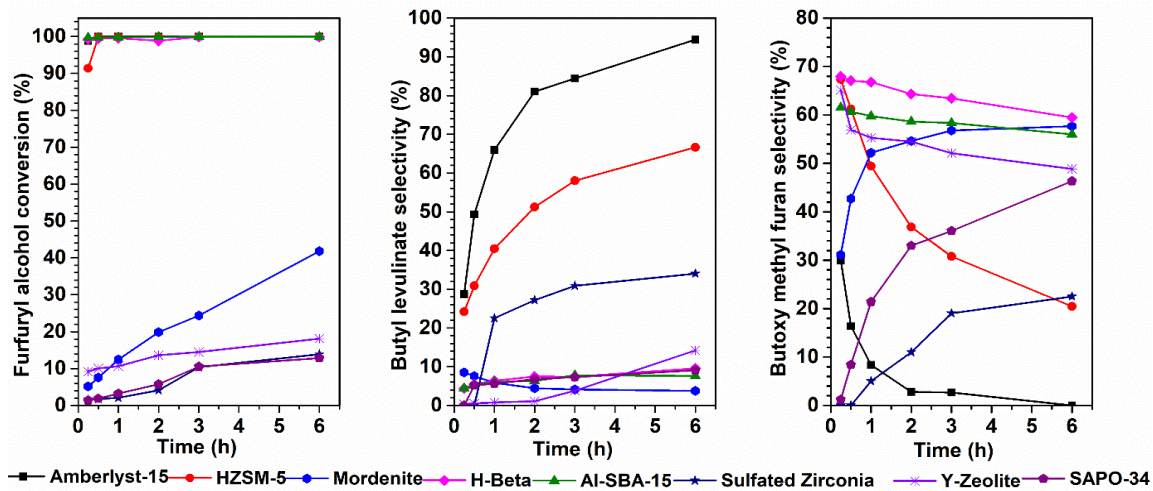


**Figure 3.9.** Catalyst screening. Reaction conditions: catalyst concentration–3wt%, temperature–110 °C, mole ratio– 1:10 (furfuryl alcohol: butanol), reaction time– 6 h

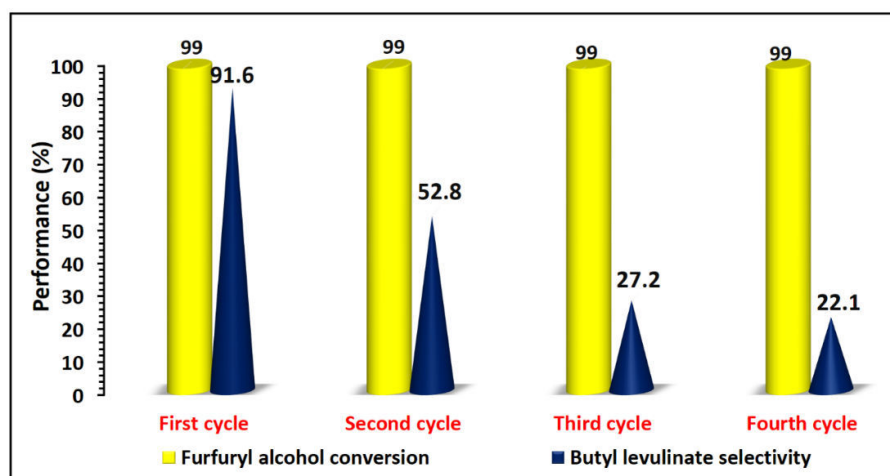


**Figure 3.10.** Catalyst recyclability study of amberlyst–15. Reaction Conditions: temperature: 110 °C, catalyst concentration– 3wt%, mole ratio– 1:10 (furfuryl Alcohol: butanol), reaction time– 6 h

### 3.6.2 Effect of SAR

As the change in SAR in zeolites results in the variation of number and strength of acidity, HZSM–5 with different SAR was investigated for the alcoholysis of furfuryl alcohol with butanol. The conversion of all the HZSM–5 catalysts with the SAR ranging from 22 to 160, was above 95% at 110 °C [figure 3.11 (a)]. Interestingly, the selectivity towards butyl levulinate did not show any linearity with respect to the SARs. However, it

should be marked that the high amount of acidity had less impact on the selectivity though the trend of the catalytic performance was a volcanic peak [figure 3.11 (b)]. The order of the catalytic performance of the SARs in HZSM-5 with respect to selectivity (%) is SAR95 > SAR117 > SAR160 > SAR57 > SAR22. This trend may be due to the competing reactions leading to pore/ active site blockage making the reaction slower with time for HZSM-5 with lower SAR.

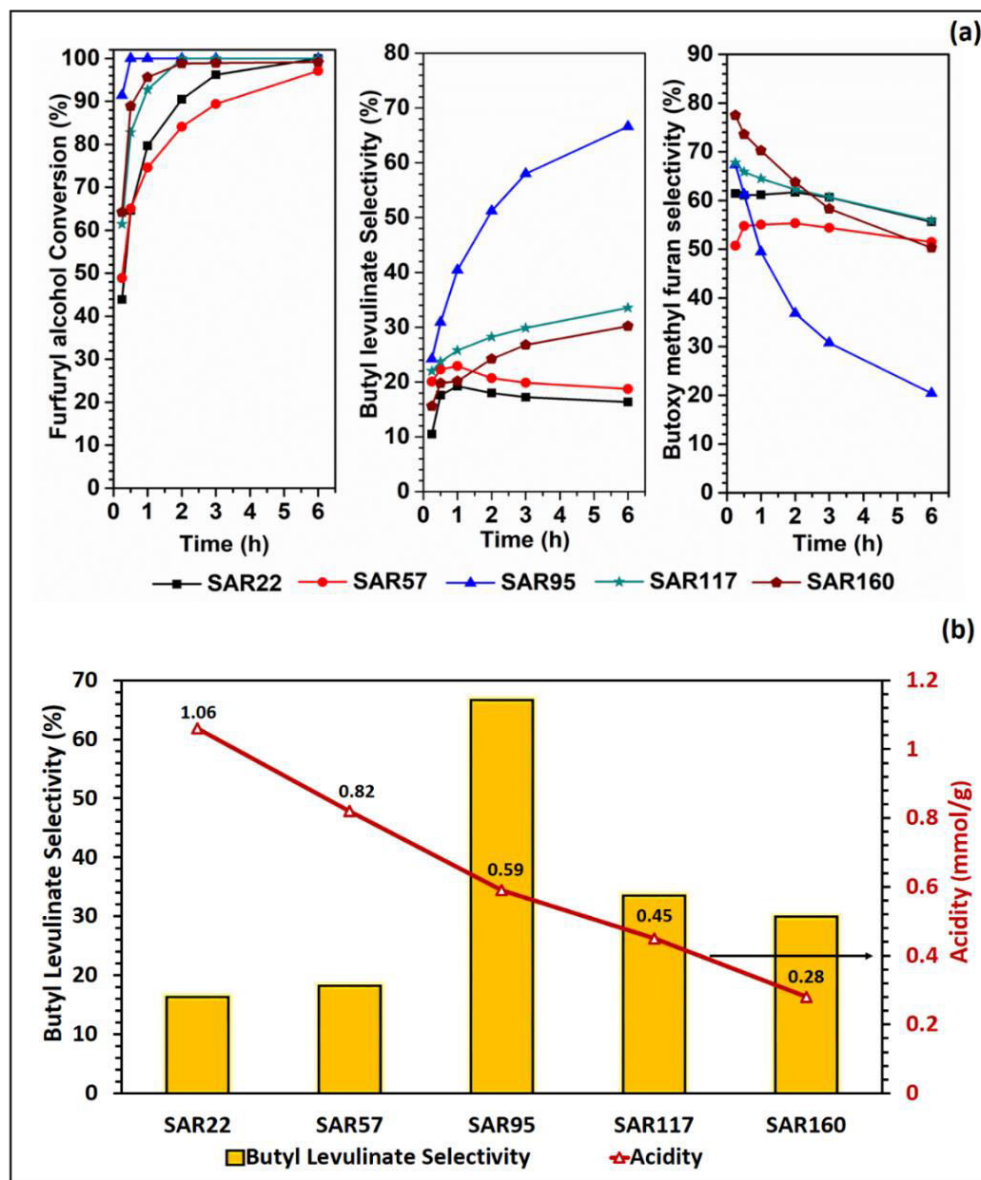


**Figure 3.11.** (a) Effect of silica to alumina ratio (SAR) of HZSM-5 (b) Correlation of butyl levulinate selectivity with acidity. Reaction conditions: Catalyst concentration– 3wt%, temperature– 110 °C, mole ratio– 1:10 (furfuryl alcohol: butanol), reaction time– 6 h. For all the catalysts, furfuryl alcohol conversion  $\geq 99\%$ .

Oligomerization is more prone in lower SAR catalysts due to the higher Brönsted acidity. In the case of higher SARs, low acid site density leads to low catalytic activity. A similar trend was reported for the different acid-catalyzed reactions using HZSM-5<sup>43</sup>. Therefore, SAR95 seems to be the optimal catalyst that favors the efficient production of butyl levulinate compared to the rest. To explore the nature and to understand the active sites responsible for the transformation, the catalyst with the highest catalytic selectivity of 66%, HZSM-5 (SAR95) was post modified by desilication, dealumination, metal-ion exchange and phosphate modification were screened for this reaction.

### 3.6.3 Catalytic activity studies for post synthetically modified HZSM-5

The butanolysis reaction of furfuryl alcohol with butanol was conducted using post synthetically modified HZSM-5 (SAR95) by desilication and dealumination using 0.1M, 0.2M NaOH, and citric acid/ HCl respectively. The alkali treatment was restricted to 0.2M NaOH concentration as it lowers the crystallinity of the material upon an increase in the concentration  $\geq 0.5$ M which would lead to the destruction of the framework resulting in the partial/complete collapse of the zeolite structure<sup>29</sup>. These modifications resulted in a decline in the butyl levulinate selectivity (in the range of 55–42 %) compared with parent HZSM-5 (SAR95) (66.6%) which could be due to the lowering of the number and strength of acidity [figure 3.12 (a,c)]. As the conversion level after modifications were almost similar (>99%), it implies that the conversion of intermediate BMF to butyl levulinate is mainly affected by these modifications [figure 3.12 (b, d)].

Upon treatment with varied concentrations of phosphate, the catalysts were tested to explore the role of weaker acid sites on the reaction. It was found that with an increase in the phosphate treatment the selectivity towards butyl levulinate drastically decreased from 53.2 to 30.9 % [figure 3.13 (a)]. This is due to the decrease in the concentration of strong Brönsted acidity which was replaced by weaker acid sites upon phosphate treatment as expressed in the TPD profile<sup>28</sup>. In the TPD profile of the highest phosphate modification (5% P-ZSM-5), strong Brönsted acid sites diminished after the treatment which explains its poor performance [figure 3.5 (d)]. This proves the necessity of a sufficient number of strong Brönsted acidity for this transformation.

The  $\text{Zn}^{2+}$  and  $\text{Cu}^{2+}$  ions were exchanged with HZSM-5 (SAR95) to understand the role of Lewis acidity on the reaction. While the two modified catalysts retained almost complete conversion, butyl levulinate selectivity decreased with respect to the parent HZSM-5. The initial formation of butyl levulinate of Cu-ZSM-5 and Zn-ZSM-5 till 2 h was close to that of parent HZSM-5 after which the gap between them increased indicating the poorer conversion of BMF intermediate to the product at higher reaction time compared to parent HZSM-5 [figure 3.13 (d)]. The overall decrease in the selectivity of parent HZSM-5 from 66.6 to 50.6 % (Zn-ZSM-5) and 49.1% (Cu-ZSM-5) could be due to a decrease in the number and strength of acid sites [Table 3.1, figure 3.13 (c)].

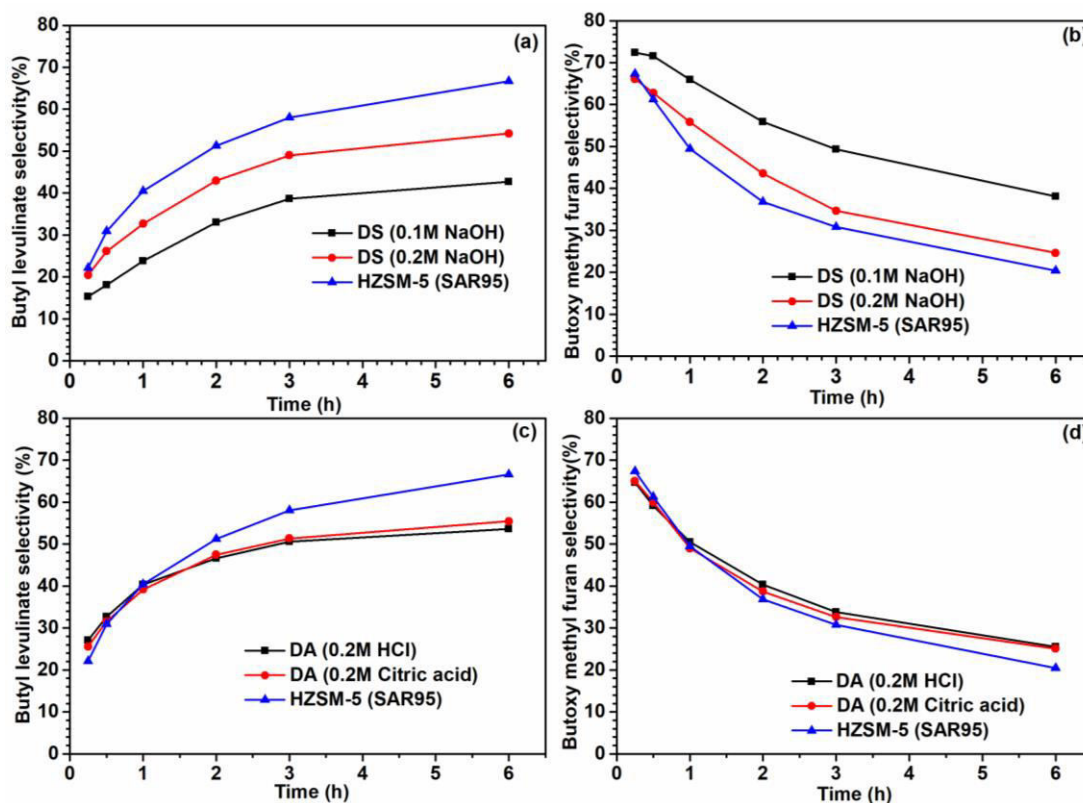


**Figure 3.12.** Catalyst performance of HZSM-5 (SAR 95) upon post modification. Desilication towards the selectivity of (a) BL (b) BMF, dealumination towards the selectivity of (c) BL (d) BMF. Reaction conditions: Catalyst concentration- 3wt%, temperature- 110 °C, mole ratio- 1:10 (furfuryl alcohol: butanol), reaction time- 6 h. Furfuryl alcohol conversions for all the reactions  $\geq 99\%$ .

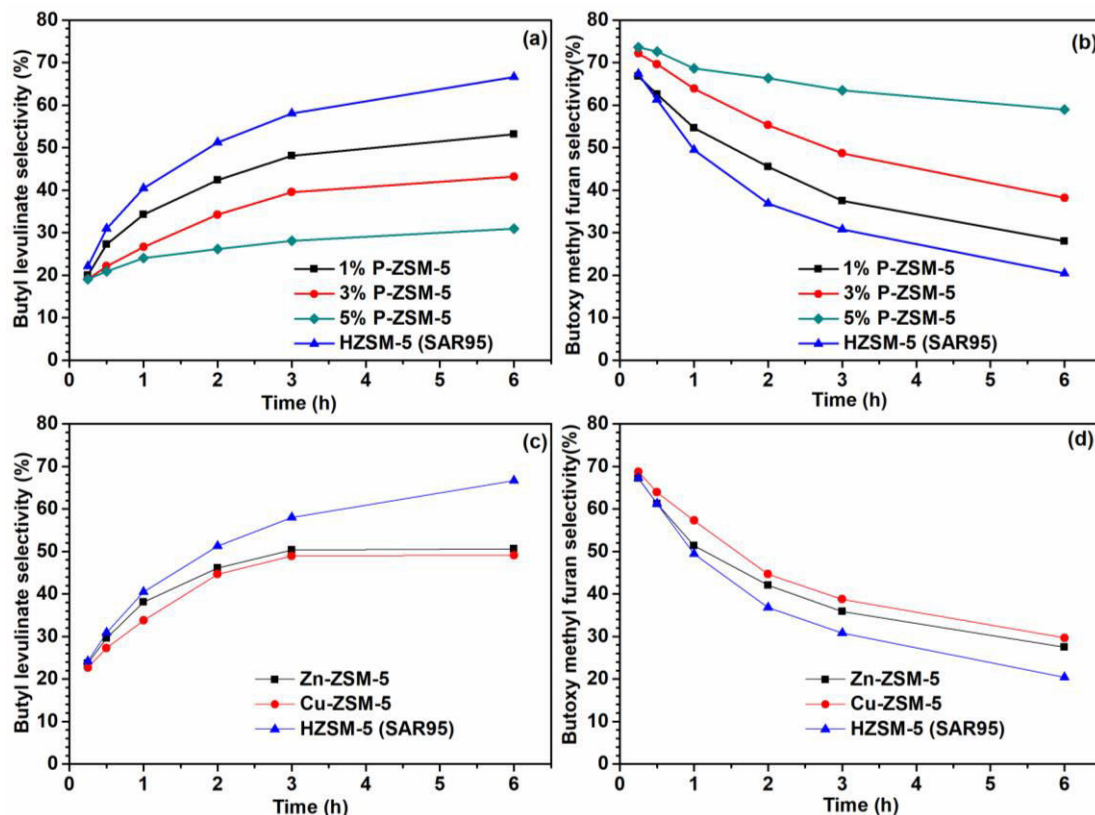


**Figure 3.13.** Catalyst performance of HZSM–5 (SAR 95) upon post modification, phosphate modification towards the selectivity of (a) BL (b) BMF, metal ion exchange towards the selectivity of (c) BL (d) BMF. Reaction conditions: Catalyst concentration–3wt%, temperature– 110 °C, mole ratio– 1:10 (furfuryl alcohol: butanol), reaction time– 6 h. For all catalysts, furfuryl alcohol conversion  $\geq 99\%$ .

### 3.6.4 Influence of reaction conditions

Among all the well-known solid acids and acidity–structure modified ZSM–5 catalysts, HZSM–5 (SAR95) that showed the highest efficiency was selected to study the influence reaction parameters such as catalyst concentration, reactant mole ratio, and temperature.

#### Effect of catalyst concentration

The effect of the catalyst loading ranging from 0.75 to 3.75 wt% (with respect to total reactants) was studied with HZSM–5 (SAR95) as shown in figure 3.14 (a). It is observed that the variation in catalyst loading had a pronounced effect on the butyl levulinate selectivity. The selectivity increased substantially from 25.3 to 66.6 % with an increase in the catalyst loading from 0.75 to 3wt%. At a lower catalyst loading, though the conversion of furfuryl alcohol was not affected ( $\geq 99\%$  at 6 h), it is observed that the

BMF (intermediate) conversion was lower, thereby affecting the butyl levulinate selectivity. Hence, the first transformation of furfuryl alcohol to intermediate BMF occurs easily with a low amount of the catalyst, whereas the second transformation of the intermediate to butyl levulinate requires a higher catalyst amount [figure 3.14 (c)]. With a further increase in the catalyst loading to 3.75 wt%, the selectivity of butyl levulinate decreased as the product concentration was distributed mainly over BMF and other side product, 5,5-dibutoxy-2-pentanone. As the reaction demands a minimum of 3 wt% catalyst loading, which is less compared with that used in most of the previous reports. The catalyst concentration of HZSM-5 (SAR95) was fixed to 3 wt% for further studies.

### **Effect of reactant mole ratio**

Since this reaction involves substrate, furfuryl alcohol which is prone to polymerization, the other substrate concentration (butanol) becomes important. Butanol not only takes part in the alcoholysis but, at the same time, also reduces the formation of polymeric side products by acting as a solvent or a diluent. Thus, the optimized mole ratio (furfuryl alcohol: butanol) helps in reducing the furfuryl alcohol side reactions thereby effectively avoiding catalyst poisoning. Though the conversion of furfuryl alcohol was not altered ( $\geq 99\%$ ) by varying the mole ratio, butyl levulinate selectivity was mainly influenced by it. At lower molar ratios from furfuryl alcohol: butanol, 1:2.5 to 1:7.5, the butyl levulinate selectivity was not much changed (45–47%) [figure 3.14 (b)]. However, upon increasing the mole ratio from 1:7.5 to 1:10, the selectivity of butyl levulinate was enhanced by 20% (66.6%). Further increase in the mole ratio to 1:12.5 and 1:15, the selectivity considerably decreased (51–48 %) which might be due to the partial blockage of active sites for the intermediate BMF to react further by excess butanol that predominantly resides on the active sites being more polar compared to the ether (BMF) [figure 3.14 (e)]. Hence this study confirms that the furfuryl alcohol to butanol ratio of 1:10 is the optimal stoichiometric mole ratio for this reaction.



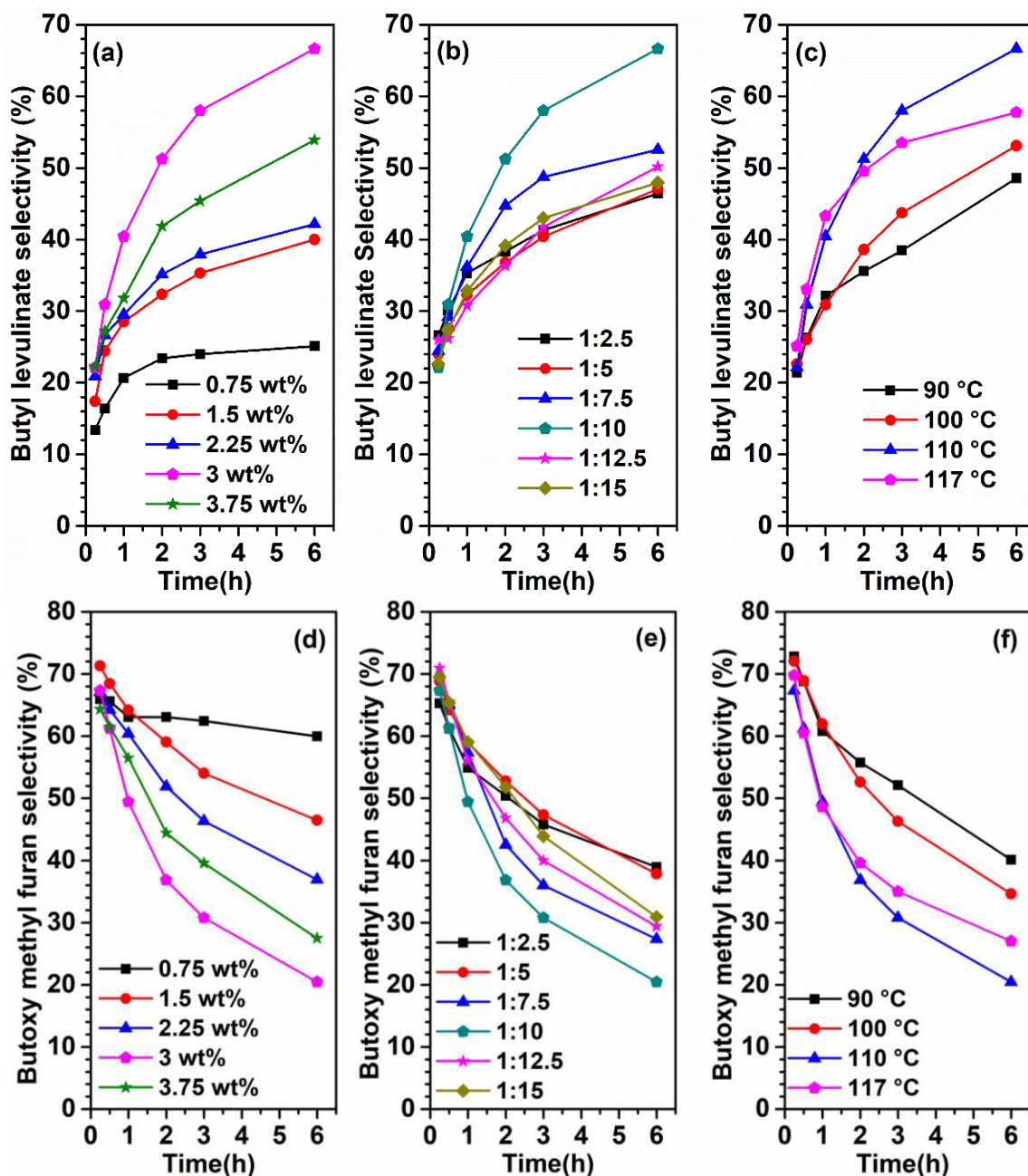


**Figure 3.14.** Influence of reaction conditions towards the selectivities of BL and BMF. (a,d) Effect of catalyst loading : Reaction conditions: Temperature– 110 °C, mole ratio– 1:10 (furfuryl alcohol: butanol), reaction time– 6 h. (b,e) Effect of reactant mole ratio: Reaction conditions: Catalyst concentration– 200mg, temperature– 110 °C, reaction time– 6 h. (c,f) Effect of reaction temperature: Reaction conditions: Catalyst concentration– 3wt%, mole ratio– 1:10 (furfuryl alcohol: butanol), reaction time– 6h. Furfuryl alcohol conversions for all the reactions  $\geq 99\%$ .

### Effect of reaction temperature

The effect of temperature on the alcoholysis of furfuryl alcohol was investigated in the temperature range of 90–117 °C in the batch mode while keeping other parameters constant [figure 3.14 (c)]. Though the temperature change did not affect the furfuryl alcohol conversion ( $\geq 99\%$  at all temperatures), there was a visible impact on the selectivity of butyl levulinate. In the case of temperatures 90 and 100 °C, though the intermediate BMF formed was considerably high in concentration (73%) compared to 110 °C (67%), the conversion of BMF to butyl levulinate over the reaction time was slower (48% for 90 °C and 53% for 100 °C). At a temperature of 110 °C, the selectivity towards butyl levulinate improved to 66.6% due to an appreciable decrease in BMF concentration from 67 to 20% [figure 3.14 (f)]. Further increase in temperature to 117 °C, decreased the butyl levulinate selectivity by 8.9% (to 57.7%). Hence at 110°C, the reaction was suitable for higher butyl levulinate selectivity. Therefore, after the complete investigation of the reaction parameters, the optimized temperature, the mole ratio of furfuryl alcohol to butanol, and catalyst concentration are 110 °C, 1:10, and 3wt% respectively.

### 3.6.5 Catalyst recyclability study

To investigate the catalyst stability towards multiple cycles, experiments were conducted by regenerating the catalyst in between the four cycles under the optimized reaction conditions (figure 3.15). During each cycle, the catalyst demonstrated almost the same catalytic activity as that of the fresh catalyst. This implies that there was no loss of any active sites during the reaction or in the regeneration process which was reflected in the spent catalyst characterization. This proves HZSM-5 (SAR95) to be a highly potential catalyst for alcoholysis reaction as it addresses all the drawbacks of the reported catalysts such as poor recyclability, the need of high catalyst loading and butanol requirement, high cost of the catalyst and difficult synthesis procedures.

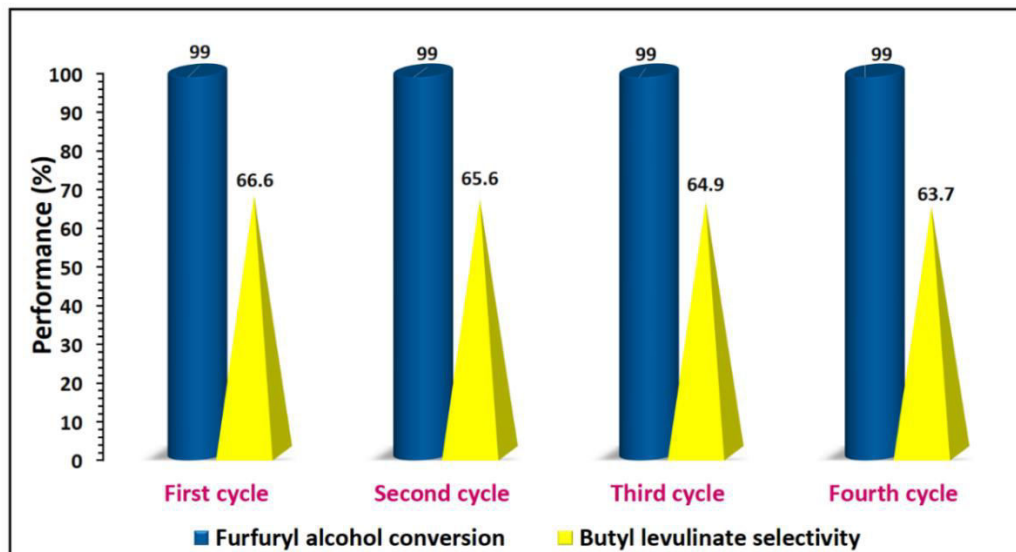


**Figure 3.15.** Catalyst recyclability study. Reaction Conditions: temperature: 110 °C, catalyst concentration– 3wt%, mole ratio– 1:10 (furfuryl Alcohol: butanol), reaction time– 6 h

### 3.6.6 Time resolved study

Time resolved study was carried out for the alcoholysis of furfuryl alcohol for 24 h using HZSM–5 (SAR95) catalyst under the optimized conditions. The catalyst showed  $\geq 99\%$  furfuryl alcohol conversion within an hour and the selectivity towards the intermediate BMF decreased from 67 (15 min) to 1.9% with an increase in time to 24 h. During the reaction, the butyl levulinate selectivity reached 24% in 15 min and then increased rapidly to 66 % in 6 h, but then took more time to finally attain 85% in 24 h (figure 3.16).

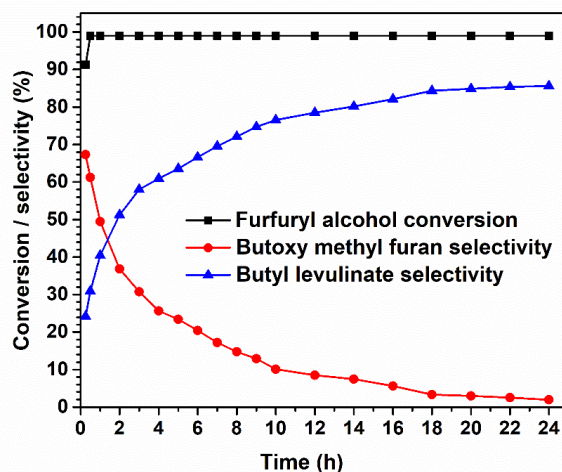
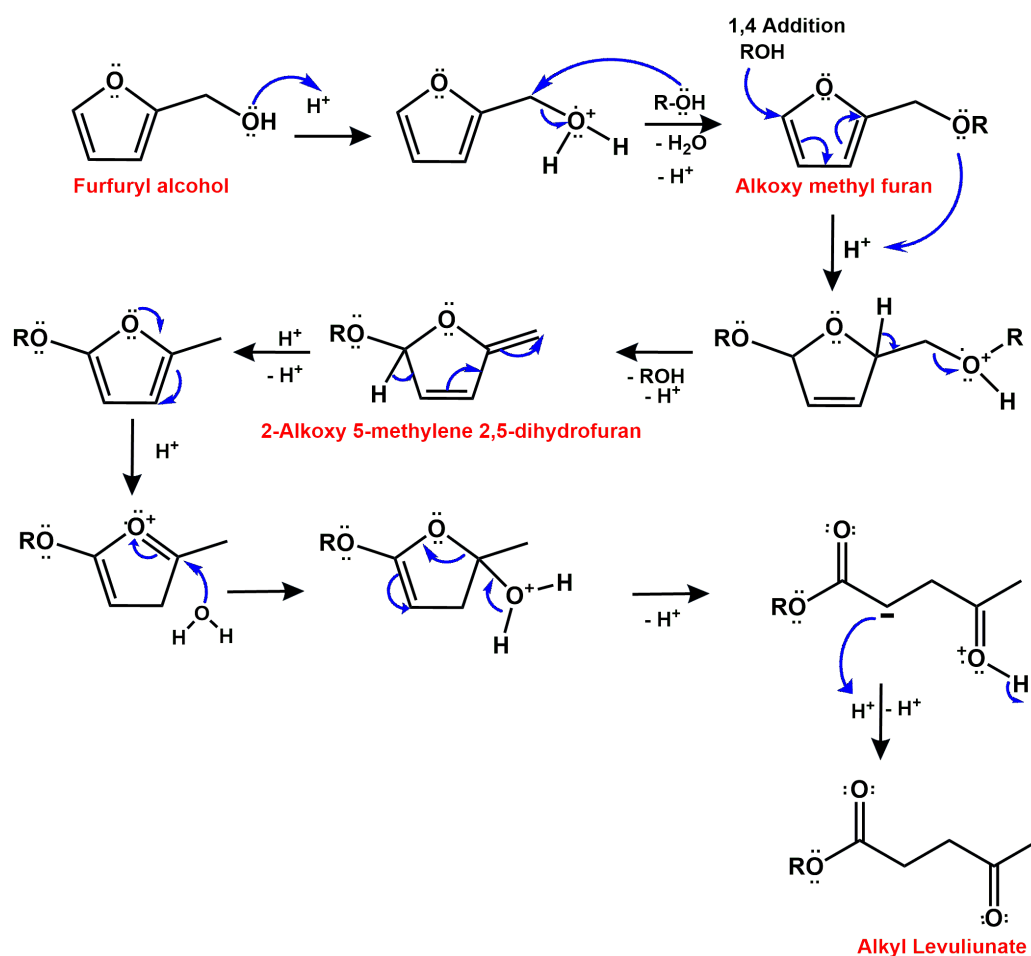


**Figure 3.16.** Time resolved study. Reaction conditions: Catalyst concentration– 3wt%, temperature– 110°C, mole ratio– 1:10 (furfuryl alcohol: butanol), reaction time– 24h

This suggests that there was a slow intermediate (BMF) conversion to butyl levulinate after 6 h that may be attributed to the active site saturation with products in the course of time. The increase in the butyl levulinate selectivity with time also demonstrates the progressive performance of the catalyst with time by efficiently converting the intermediate BMF to the desired product which proves that this is a consecutive reaction.

### 3.7 Plausible reaction mechanism

The plausible mechanistic pathway of alcoholysis of furfuryl alcohol to form alkyl levulinate is proposed in Scheme 3.2. The reaction proceeds by the formation of an intermediate alkoxy methyl furan which then gets transformed to 2-alkoxy-5-methylene-2,5-dihydrofuran by 1,4 addition of alcohol. Ring-opening occurs by subsequent production of alkyl levulinate<sup>44</sup>.



**Scheme 3.2.** Plausible mechanistic pathway for the alcoholysis of furfuryl alcohol to yield alkyl levulinate.

### 3.8 Substrate scope study

Due to the vast applications of various alkyl levulinates, it is interesting to explore the catalytic performance of HZSM-5 (SAR95) catalyst using various alkyl alcohols. Hence, the effect of the substrate was assessed for alcoholysis of furfuryl alcohol to yield methyl levulinate, ethyl levulinate, propyl levulinate and butyl levulinate at reflux temperature. Under optimized conditions, the conversion of furfuryl alcohol, irrespective of the alcohols used, was >95% and the selectivity towards the product increased with an increase in the alkyl chain of the alcohol in the following order methanol < ethanol < propanol < butanol [figure 3.17 (a)].

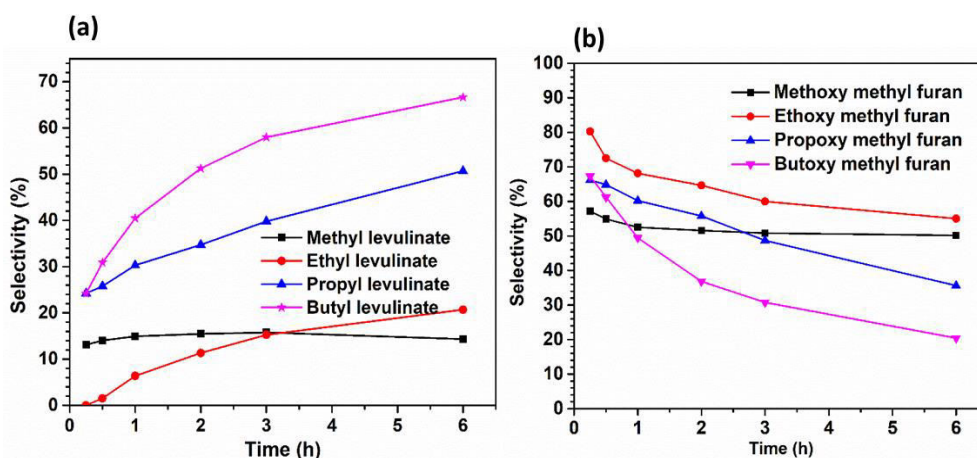


**Figure 3.17.** Effect of alkyl chain on alcoholysis on (a) Selectivity towards alkyl levulinate (b) Selectivity towards the intermediate alkoxy methyl furan. Reaction Conditions: Catalyst– HZSM-5 (SAR95), temperature: Reflux condition, catalyst concentration– 200mg, mole ratio– 1:10 (furfuryl alcohol: alcohol), reaction time– 6h. The furfuryl alcohol conversion of all the substrates >95%

At its reflux temperature, when methanol was employed, the selectivity towards the intermediate methoxy methyl furan (MMF) and other side products were 50.2 and 35.5% respectively. This clearly explains the low selectivity of methyl levulinate (14.3 %) during the reaction. In the case of ethanolysis of furfuryl alcohol, the ethyl levulinate selectivity was 20.7% for a 6 h reaction. The ethoxy methyl furan (EMF) and the other side products were formed with a selectivity of 55.6 and 23.7% respectively. Reactions for propyl levulinate and butyl levulinate synthesis resulted in 50.3 and 66.6 % selectivities for these products respectively under reflux temperature. This trend could be due to the +I effect of the alkyl group guiding the conversion of the intermediate (alkoxy

methyl furan) to its respective products [figure 3.17 (b)]. Therefore, as the alkyl chain in the alcohol is increased, the conversion of the intermediate is enhanced, thereby increasing the selectivity towards the alkyl levulinate.

### 3.9 Comparison with literature results

There are several solid catalysts such as zeolites, mesoporous materials, functionalized metal oxides, ionic liquids, heteropolycompounds, etc reported for the butanolysis of FA to produce BL, and a thorough literature survey with the reaction conditions, recyclability data is presented in table 3.2 in comparison with the HZSM-5 (SAR95) catalyst.

**Table 3.2.** Comparison of catalytic activity of HZSM-5 (SAR 95) with various reported catalysts in the literature for butanolysis of furfuryl alcohol to produce butyl levulinate

SN	Catalysts	Catalyst (wt. %) wrt FA	T (°C)	Mole ratio	BL Yield (%)	Reusability	Ref
1.	Reduced graphite oxide	4	110	1:25	99	NR	5
2.	Sn <sub>1</sub> TPA/K-10	160	120	1:10	98	3 C	17
3.	TPA/SBA-16	300	110	1:65	97	84%-4 C	45
4.	Sulfated SBA-15	25	110	1:35	96	NR	8
5.	Lignin-based carbonaceous acid	75	110	1:53	95	84%-3C	46
6.	Ti-KIT-6	300	110	1:60	94	4 C	9
7.	Al-SBA-15	400	110	1:65	94	82%-4C	47
8.	HPAs and POM-based IL- H <sub>5</sub> AlW <sub>12</sub> O <sub>40</sub> & [MIMBS] <sub>5</sub> [AlW <sub>12</sub> O <sub>40</sub> ]	5% mmol	120	1:55	94	80%-4C	10
9.	Zn <sub>x</sub> TPA/Nb <sub>2</sub> O <sub>5</sub>	300	110	1:65	94	4 C	13
10.	SnPO-P123	100	160	1:10	94	3 C	48
11.	[(HSO <sub>3</sub> -p) <sub>2</sub> im] [HSO <sub>4</sub> ]	13	120	1:22	93	8 C	12
12.	[BmimSO <sub>3</sub> H] <sub>3</sub> PW <sub>12</sub> O <sub>40</sub>	180	120	1:48	93	1 C	11
13.	α- Fe <sub>2</sub> O <sub>3</sub>	5200	250	1:500	86	38%-1C	14
14.	KCC-1/Pr-SO <sub>3</sub> H	98	120	1:10	81	70%-4C	15
15.	TNTs-SO <sub>3</sub> H	300	120	1:55	80	67%-4C	16
16.	HZSM-5 (SAR95)	25	110	1:10	85	3 C	PW <sup>a</sup>

<sup>a</sup> Present work

From table 3.2, it is evident that the mole ratio and catalyst concentration employed for FA butanolysis to produce BL in the presence of HZSM-5 (SAR95) catalyst is relatively low. Also, ZSM-5 is an eco-friendly catalyst with high thermal stability which makes it easy regeneration and recycle processes. Thermal stability of the material for this reaction is important as organic deposits responsible for blocking the active sites can be removed by simple calcination procedure.

### 3.10 Conclusions

Zeolites being one of the classic materials are still startling scientists with its flexible material properties and promising catalytic activities in many important and challenging transformations. In alcoholysis of furfuryl alcohol which was efficiently converted into butyl levulinate with the aid of HZSM-5 (SAR95) in a batch regime proved the exclusive requirement of the uniform medium size micropore structure, high surface area, strong Brønsted acidity, optimal number of acid sites and good thermal stability for this reaction. The combination of the properties inherited by the HZSM-5 with the tuning of acidity makes it different from the other catalysts. Considering the green chemistry principles such as moderate experimental conditions, excellent reusability, low reactants mole ratio and catalyst concentration, HZSM-5 (SAR95) proves to be the best candidate for this transformation as it addresses all the drawbacks of the reported catalysts.

### 3.11 Bibliography

- (1) Werpy, T.; Petersen, G. *Top value added chemicals from biomass: volume I--results of screening for potential candidates from sugars and synthesis gas*; National Renewable Energy Lab., Golden, CO (US), 2004.
- (2) Taylor, M. J.; Durndell, L. J.; Isaacs, M. A.; Parlett, C. M.; Wilson, K.; Lee, A. F.; Kyriakou, G. Highly selective hydrogenation of furfural over supported Pt nanoparticles under mild conditions. *Applied Catalysis B: Environmental* **2016**, *180*, 580-585.
- (3) Tukacs, J. M.; Bohus, M.; Dibó, G.; Mika, L. T. Ruthenium-catalyzed solvent-free conversion of furfural to furfuryl alcohol. *RSC advances* **2017**, *7* (6), 3331-3335.
- (4) Démolis, A.; Essayem, N.; Rataboul, F. Synthesis and applications of alkyl levulinates. *ACS Sustainable Chemistry & Engineering* **2014**, *2* (6), 1338-1352.

- (5) Gitis, V.; Chung, S.-H.; Shiju, N. R. Conversion of furfuryl alcohol into butyl levulinate with graphite oxide and reduced graphite oxide. *FlatChem* **2018**, *10*, 39-44.
- (6) Yu, X.; Peng, L.; Pu, Q.; Tao, R.; Gao, X.; He, L.; Zhang, J. Efficient valorization of biomass-derived furfuryl alcohol to butyl levulinate using a facile lignin-based carbonaceous acid. *Research on Chemical Intermediates* **2020**, *46* (2), 1469-1485.
- (7) Enumula, S. S.; Gurram, V. R. B.; Chada, R. R.; Burri, D. R.; Kamaraju, S. R. R. Clean synthesis of alkyl levulinates from levulinic acid over one pot synthesized WO<sub>3</sub>-SBA-16 catalyst. *Journal of Molecular Catalysis A: Chemical* **2017**, *426*, 30-38.
- (8) Demma Carà, P.; Ciriminna, R.; Shiju, N.; Rothenberg, G.; Pagliaro, M. Enhanced heterogeneous catalytic conversion of furfuryl alcohol into butyl levulinate. *ChemSusChem* **2014**, *7* (3), 835-840.
- (9) Appaturi, J. N.; Johan, M. R.; Ramalingam, R. J.; Al-Lohedan, H. A.; Vijaya, J. J. Efficient synthesis of butyl levulinate from furfuryl alcohol over ordered mesoporous Ti-KIT-6 catalysts for green chemistry applications. *RSC advances* **2017**, *7* (87), 55206-55214.
- (10) Hao, R.; He, J.; Zhao, L.; Zhang, Y. HPAs and POM-based ILs Catalyzed Effective Conversion of Furfuryl Alcohol to Alkyl Levulinate. *ChemistrySelect* **2017**, *2* (26), 7918-7924.
- (11) Zhang, Z.; Dong, K.; Zhao, Z. K. Efficient conversion of furfuryl alcohol into alkyl levulinates catalyzed by an organic-inorganic hybrid solid acid catalyst. *ChemSusChem* **2011**, *4* (1), 112-118.
- (12) Wang, G.; Zhang, Z.; Song, L. Efficient and selective alcoholysis of furfuryl alcohol to alkyl levulinates catalyzed by double SO<sub>3</sub>H-functionalized ionic liquids. *Green Chemistry* **2014**, *16* (3), 1436-1443.
- (13) Rao, B. S.; Kumari, P. K.; Dhanalakshmi, D.; Lingaiah, N. Selective conversion of furfuryl alcohol into butyl levulinate over zinc exchanged heteropoly tungstate supported on niobia catalysts. *Molecular Catalysis* **2017**, *427*, 80-86.
- (14) Ren, D.; Fu, J.; Li, L.; Liu, Y.; Jin, F.; Huo, Z. Efficient conversion of biomass-derived furfuryl alcohol to levulinate esters over commercial  $\alpha$ -Fe<sub>2</sub>O<sub>3</sub>. *RSC advances* **2016**, *6* (26), 22174-22178.



- (15) Mohammadbagheri, Z.; Chermahini, A. N. KCC-1/Pr-SO<sub>3</sub>H as an efficient heterogeneous catalyst for production of n-butyl levulinate from furfuryl alcohol. *Journal of industrial and engineering chemistry* **2018**, *62*, 401-408.
- (16) Zhou, S.; Lai, J.; Liu, X.; Huang, G.; You, G.; Xu, Q.; Yin, D. J. G. E.; Environment. Selective conversion of biomass-derived furfuryl alcohol into n-butyl levulinate over sulfonic acid functionalized TiO<sub>2</sub> nanotubes. **2020**.
- (17) Tiwari, M. S.; Dicks, J. S.; Keogh, J.; Ranade, V. V.; Manyar, H. G. J. M. C. Direct conversion of furfuryl alcohol to butyl levulinate using tin exchanged tungstophosphoric acid catalysts. **2020**, *488*, 110918.
- (18) Manjunathan, P.; Shanbhag, D. Y.; Vinu, A.; Shanbhag, G. V. Recognizing soft templates as stimulators in multivariate modulation of tin phosphate and its application in catalysis for alkyl levulinate synthesis. *Catalysis Science & Technology* **2020**.
- (19) Lange, J. P.; van de Graaf, W. D.; Haan, R. J. Conversion of furfuryl alcohol into ethyl levulinate using solid acid catalysts. *ChemSusChem: Chemistry & Sustainability Energy & Materials* **2009**, *2* (5), 437-441.
- (20) Huang, Y.-B.; Yang, T.; Zhou, M.-C.; Pan, H.; Fu, Y. Microwave-assisted alcoholysis of furfural alcohol into alkyl levulinates catalyzed by metal salts. *Green Chemistry* **2016**, *18* (6), 1516-1523.
- (21) Nandiwale, K. Y.; Pande, A. M.; Bokade, V. V. One step synthesis of ethyl levulinate biofuel by ethanolysis of renewable furfuryl alcohol over hierarchical zeolite catalyst. *RSC advances* **2015**, *5* (97), 79224-79231.
- (22) Appaturi, J. N.; Andas, J.; Ma, Y.-K.; Phoon, B. L.; Batagarawa, S. M.; Khoerunnisa, F.; Hussin, M. H.; Ng, E.-P. Recent advances in heterogeneous catalysts for the synthesis of alkyl levulinate biofuel additives from renewable levulinic acid: A comprehensive review. *Fuel* **2022**, *323*, 124362.
- (23) Zhang, Z.; Dong, K.; Zhao, Z. Efficient conversion of furfuryl alcohol into alkyl levulinates catalyzed by an organic–inorganic hybrid solid acid catalyst. *ChemSusChem* **2011**, *4* (1), 112-118.
- (24) An, S.; Song, D.; Lu, B.; Yang, X.; Guo, Y. H. Morphology Tailoring of Sulfonic Acid Functionalized Organosilica Nanohybrids for the Synthesis of Biomass-Derived Alkyl Levulinates. *Chemistry–A European Journal* **2015**, *21* (30), 10786-10798.

- (25) Lima, T. M.; Lima, C. G.; Rathi, A. K.; Gawande, M. B.; Tucek, J.; Urquieta-González, E. A.; Zbořil, R.; Paixão, M. W.; Varma, R. S. Magnetic ZSM-5 zeolite: a selective catalyst for the valorization of furfuryl alcohol to  $\gamma$ -valerolactone, alkyl levulinates or levulinic acid. *Green Chemistry* **2016**, *18* (20), 5586-5593.
- (26) Paniagua, M.; Melero, J.; Iglesias, J.; Morales, G.; Hernández, B.; López-Aguado, C. Catalytic upgrading of furfuryl alcohol to bio-products: Catalysts screening and kinetic analysis. *Applied Catalysis A: General* **2017**, *537*, 74-82.
- (27) Jia, C.-J.; Liu, Y.; Schmidt, W.; Lu, A.-H.; Schüth, F. Small-sized HZSM-5 zeolite as highly active catalyst for gas phase dehydration of glycerol to acrolein. *Journal of Catalysis* **2010**, *269* (1), 71-79.
- (28) Janardhan, H.; Shanbhag, G.; Halgeri, A. Shape-selective catalysis by phosphate modified ZSM-5: Generation of new acid sites with pore narrowing. *Applied Catalysis A: General* **2014**, *471*, 12-18.
- (29) Gil, B.; Mokrzycki, Ł.; Sulikowski, B.; Olejniczak, Z.; Walas, S. Desilication of ZSM-5 and ZSM-12 zeolites: Impact on textural, acidic and catalytic properties. *Catalysis Today* **2010**, *152* (1-4), 24-32.
- (30) Manjunathan, P.; Maradur, S. P.; Halgeri, A.; Shanbhag, G. V. Room temperature synthesis of solketal from acetalization of glycerol with acetone: Effect of crystallite size and the role of acidity of beta zeolite. *Journal of Molecular Catalysis A: Chemical* **2015**, *396*, 47-54.
- (31) Marakatti, V. S.; Shanbhag, G. V.; Halgeri, A. Sulfated zirconia; an efficient and reusable acid catalyst for the selective synthesis of 4-phenyl-1, 3-dioxane by Prins cyclization of styrene. *Applied Catalysis A: General* **2013**, *451*, 71-78.
- (32) Prakash, A.; Unnikrishnan, S. Synthesis of SAPO-34: high silicon incorporation in the presence of morpholine as template. *Journal of the Chemical Society, Faraday Transactions* **1994**, *90* (15), 2291-2296.
- (33) Shanbhag, G. V.; Kumbar, S.; Halligudi, S. Chemoselective synthesis of  $\beta$ -amino acid derivatives by hydroamination of activated olefins using AISBA-15 catalyst prepared by post-synthetic treatment. *Journal of Molecular Catalysis A: Chemical* **2008**, *284* (1-2), 16-23.

- (34) Widayat, W.; Annisa, A. Synthesis and characterization of ZSM-5 catalyst at different temperatures. In *IOP Conference Series: Materials Science and Engineering*, 2017; Vol. 214.
- (35) Feng, R.; Yan, X.; Hu, X.; Wang, Y.; Li, Z.; Hou, K.; Lin, J. Hierarchical ZSM-5 zeolite designed by combining desilication and dealumination with related study of n-heptane cracking performance. *Journal of Porous Materials* **2018**, 25 (6), 1743-1756.
- (36) Fan, Y.; Bao, X.; Lin, X.; Shi, G.; Liu, H. Acidity adjustment of HZSM-5 zeolites by dealumination and realumination with steaming and citric acid treatments. *The Journal of Physical Chemistry B* **2006**, 110 (31), 15411-15416.
- (37) Van Der Bij, H. E.; Aramburo, L. R.; Arstad, B.; Dynes, J. J.; Wang, J.; Weckhuysen, B. M. Phosphatation of Zeolite H-ZSM-5: A Combined Microscopy and Spectroscopy Study. *ChemPhysChem* **2014**, 15 (2), 283-292.
- (38) Xue, N.; Olindo, R.; Lercher, J. A. Impact of forming and modification with phosphoric acid on the acid sites of HZSM-5. *The Journal of Physical Chemistry C* **2010**, 114 (37), 15763-15770.
- (39) Blasco, T.; Corma, A.; Martínez-Triguero, J. Hydrothermal stabilization of ZSM-5 catalytic-cracking additives by phosphorus addition. *Journal of catalysis* **2006**, 237 (2), 267-277.
- (40) Hodala, J. L.; Halgeri, A. B.; Shanbhag, G. V. Phosphate modified ZSM-5 for the shape-selective synthesis of para-diethylbenzene: Role of crystal size and acidity. *Applied Catalysis A: General* **2014**, 484, 8-16.
- (41) Lyu, J.; Hu, H.; Tait, C.; Rui, J.; Lou, C.; Wang, Q.; Han, W.; Zhang, Q.; Pan, Z.; Li, X. J. C. j. o. c. e. Benzene alkylation with methanol over phosphate modified hierarchical porous ZSM-5 with tailored acidity. **2017**, 25 (9), 1187-1194.
- (42) Hattori, H.; Ono, Y. *Solid acid catalysis: from fundamentals to applications*; CRC Press, 2015.
- (43) Vasiliadou, E. S.; Gould, N. S.; Lobo, R. F. Zeolite-Catalyzed Formaldehyde-Propylene Prins Condensation. *ChemCatChem* **2017**, 9 (23).
- (44) Peng, L.; Li, H.; Xi, L.; Chen, K.; Chen, H. Facile and efficient conversion of furfuryl alcohol into n-butyl levulinate catalyzed by extremely low acid concentration. *BioResources* **2014**, 9 (3), 3825-3834.

- (45) Sankar, E. S.; Reddy, K. S.; Jyothi, Y.; Raju, B. D.; Rao, K. S. R. Alcoholysis of furfuryl alcohol into n-butyl levulinate over SBA-16 supported heteropoly acid catalyst. *Catalysis Letters* **2017**, *147* (11), 2807-2816.
- (46) Yu, X.; Peng, L.; Pu, Q.; Tao, R.; Gao, X.; He, L.; Zhang, J. J. R. o. C. I. Efficient valorization of biomass-derived furfuryl alcohol to butyl levulinate using a facile lignin-based carbonaceous acid. **2020**, *46* (2), 1469-1485.
- (47) Enumula, S. S.; Koppadi, K. S.; Gurrām, V. R. B.; Burri, D. R.; Kamaraju, S. R. R. Conversion of furfuryl alcohol to alkyl levulinate fuel additives over Al<sub>2</sub>O<sub>3</sub>/SBA-15 catalyst. *Sustainable Energy & Fuels* **2017**, *1* (3), 644-651.
- (48) Manjunathan, P.; Shanbhag, D. Y.; Vinu, A.; Shanbhag, G. V. Recognizing soft templates as stimulators in multivariate modulation of tin phosphate and its application in catalysis for alkyl levulinate synthesis. *Catalysis Science & Technology* **2021**, *11* (1), 272-282.

# **Chapter 4**

## **Esterification of furfuryl alcohol to produce furfuryl acetate**



## 4.1 Introduction

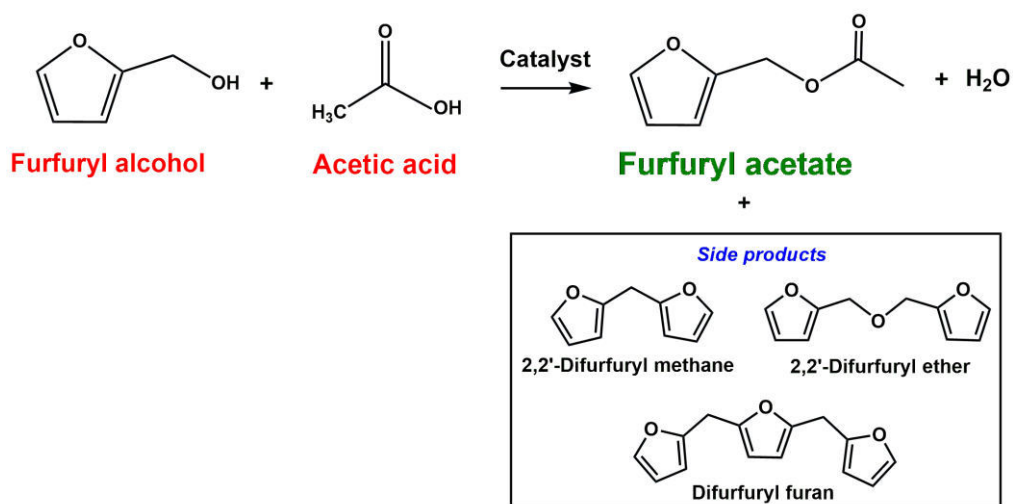
Research towards obtaining fine chemicals and fuel-based materials is evidently shifting from fossil-based materials to renewable sources since yesteryears. This is due to globalization which led many scientists, architects, and economists in planning to build greener, sustainable cities with a balanced carbon footprint. Hoping to end this fossil-dependent era, one can use solar energy, tidal energy, nuclear energy, or waste biomass materials. Biomass is one such growing field where the production of fine chemicals, as well as fuels or fuel additives, can be efficiently done. Therefore, exploring the field of biomass paves the way for a lot of opportunities to build healthier life in the coming years. Furfural and furfuryl alcohol are biomass-derived platform chemicals which can be used to produce various biofuels and biofuel additives such as alkyl levulinate,  $\gamma$ -valerolactone, levulinic acid, furfuryl acetate, ethyl furfuryl ether and bicyclopentane etc <sup>1</sup>. Furfuryl alcohol (FA) is obtained from furfural by chemoselective hydrogenation using various catalysts in both liquid and vapor phase modes. FA can be used to target the production of furfuryl acetate (FAC) (Scheme 4.1) that has applications in the fragrance, flavor industry, and also as a potential biofuel and/or additive <sup>2,3</sup>. The reaction occurs through the acid-catalyzed route where the major challenge is the polymerization of FA at the acidic sites of the catalyst. This leads to the production of undesired polymerized products called humins resulting in low selectivity towards the desired product. Humin blocks the active sites acting as a poison for the catalyst and can be removed by burning them off at higher temperatures. Another strategy can be the addition of a solvent or the usage of a higher amount of the other substrate to achieve less humin formation.

The study on esterification of FA to FAC is limited to very few reports, where a metal ion-exchanged heteropoly acid encapsulated in MOF is reported <sup>4</sup>. In this study, Fe-DTP@ZIF-8 showed a superior catalytic activity of 76% FAC yield. There are few reports on the one-pot synthesis of FAC from furfural, where the reaction occurs via the hydrogenation-esterification route <sup>5,6,7</sup>. As 62% of the furfural is converted into FA, employing FA directly as a starting material seems to be economically viable <sup>8</sup>. Hence, in our study, we chose the less expensive esterification route over the one-pot synthesis

---

route aiming to design a catalyst that can be operated in mild reaction conditions as per the green chemistry principles. In our study, various solid acid catalysts with different active sites were screened for the esterification of FA to FAc. Various characterizations such as PXRD,  $\text{NH}_3$ -TPD, nitrogen sorption studies, FTIR spectroscopy, ICP-OES, and SEM were performed to understand the physicochemical properties of the catalysts. The potential catalyst was used in the study of the effect of variation of the parameters in the reaction such as reactants mole ratio, temperature and catalyst concentration. The reusability of the catalyst was inspected by investigating its catalytic performance at the optimized reaction conditions over multiple cycles. As it is always interesting to know why a certain type of active site performs better than the other among the well-known solid acid catalysts, DFT calculations were performed to find the mechanistic reason for the same.

Scheme 4.1



Scheme 4.1 Esterification of FA to Fac

## 4.2 Chemicals and reagents

Y-Zeolite (SAR 5.1) and H-Beta (SAR25) were supplied by Zeolyst International and Nankai University Catalyst Co. China respectively. Amberlyst-15 and ferrierite (SAR 20) were obtained from Alfa-Aesar. Furfuryl alcohol, tetraethyl orthosilicate, ammonium acetate, aqueous ammonium hydroxide, anhydrous  $\text{AlCl}_3$ , acetone, concentrated acids ( $\text{HCl}$ ,  $\text{H}_3\text{PO}_4$ ,  $\text{H}_2\text{SO}_4$ , acetic acid) were purchased from Merck India Pvt. Ltd.



Amphiphilic triblock co-polymer poly-(ethylene glycol)-block poly-(propylene glycol)-block poly-(ethylene glycol) and Ludox AS-40 were procured from Sigma-Aldrich. Zirconium oxychloride octahydrate was purchased from Loba Chemie. Plural SB (pseudoboehmite) and ethanol were provided by Sasol and CSS respectively.

### 4.3 Catalyst synthesis

Sulfated zirconia catalyst was prepared by precipitating zirconium salt with aqueous ammonia as reported in the literature <sup>9</sup>. In a typical synthesis procedure, to 200 mL distilled water, 25 g of  $ZrOCl_2 \cdot 8H_2O$  was added under stirring at room temperature for which ammonium hydroxide was added dropwise to attain pH 8. The precipitate obtained was washed thoroughly using distilled water to remove the chloride ions present in the material and dried at 120 °C for 12 h. The 5 g of  $Zr(OH)_4$ , was sulfated using 50 mL of aq.  $H_2SO_4$  at various concentrations (1.0, 2.0, 2.5, 3.0, and 4.0M) by stirring for 1 h. The material was filtered, washed, dried, and finally calcined at 650 °C for 4 h. The physisorbed sulfate ions were removed post calcination by refluxing the sulfated zirconia in distilled water for 6 h. The final material was filtered, washed, and dried. The catalysts thus obtained were named SZr(x M-w), where x and w stand for the concentration of  $H_2SO_4$  treatment and washing post calcination respectively.

SAPO-11 was synthesized as per the reported synthesis procedure <sup>10</sup>. Typically, 15 g of pseudo-boehmite and 25.3 g of orthophosphoric acid were stirred with 95 mL of distilled water to which 22.3 g of triethylamine and 1.6 g of ludox AS-40 were added. The mixture was stirred for 4 h at room temperature and then was transferred to a teflon-lined stainless-steel autoclave and heated in an oven at 200 °C for 24 h. The material was filtered, washed, dried, and calcined (600 °C for 6 h) to yield SAPO-11.

Al-SBA-15 was synthesized as per the reported procedure <sup>11</sup>. In a typical synthesis, 4 g of amphiphilic triblock co-polymer poly-(ethylene glycol)-block poly-(propylene glycol)-block poly-(ethylene glycol) and 120 g of 2M HCl were homogenized in 30 g of distilled water. To this solution, 8 g of tetraethyl orthosilicate was added dropwise and stirred for 24 h at 40 °C. The gel formed was transferred to teflon lined stainless steel autoclave and placed in a preheated oven (100 °C) for 48 h. The material was filtered, washed with distilled water, dried, and calcined at 550 °C for 24 h to yield SBA-15.

---

SBA-15 (2 g) was subjected to post-synthetic modification by isomorphically substituting Si with Al (0.88 g of anhydrous AlCl<sub>3</sub>). The precursors were suspended in ethanol and aged for 10 h at 80 °C and further filtered, washed with ethanol, and dried at RT. The final material was calcined at 550 °C for 5 h to yield Al-SBA-15.

#### 4.4 Catalytic activity study

In a typical procedure, the esterification of FA was performed at the desired temperature in a liquid phase batch reaction under magnetic stirring. The required molar composition of FA and acetic acid with the catalyst (weight% with respect to the total weight of reactants) were taken in a 25 mL round bottom flask connected to a condenser. The reaction mixture was collected periodically and quantitatively analyzed by gas chromatography (Agilent Technologies 7820A) equipped with DB-Wax capillary column (30 m x 0.25 mm x 2.5µm) coupled with the flame ionization detector. The identification of the products was confirmed by Gas chromatography Mass Spectrometry (GCMS). The FA conversion and FAc selectivity were determined by gas chromatography.

$$C_{FA}(\%) = \frac{X_{FA(i)} - X_{FA(f)}}{X_{FA(i)}} \times 100$$

$$S_{FAc}(\%) = \frac{X_{FAc}}{X_{FA(i)} - X_{FA(f)}} \times 100$$

$$Y_{FAc}(\%) = \frac{X_{FAc}}{X_{FA(i)}} \times 100$$

$$\text{Turn over number (TON)} = \frac{\text{Moles FA reacted}}{\text{Moles of acid sites}}$$

Where  $C_{FA}$  and  $S_{FAc}$  are FA conversion and FAc selectivity respectively.  $X_{FA(i)}$  and  $X_{FA(f)}$  correspond to the initial and final moles of FA respectively.  $X_{FAc}$  and  $Y_{FAc}$  are the moles of FAc formed and FAc yield respectively.

#### 4.5 DFT Method

Density Functional Theory (DFT) calculations were performed using the ORCA *ab initio* quantum chemistry Program package<sup>12</sup>. We have calculated stationary geometry clusters representing the active sites on the solid acid catalysts. The intention is to keep the

realistic structure for the active site of the catalyst by avoiding geometry optimization. To make the computations feasible for many possible active site structures of different catalysts as well as for the structures with the molecules adsorbed over them, we used the LANL2DZ basis set<sup>13,14,15,16</sup>. Usage of a single basis set for all the elements to avoid the need to make the basis set superposition error corrections was done. Calculations were performed using Density Functional Theory (DFT) coupled with the hybrid, three-parameter functional B3LYP<sup>17</sup>.

## 4.6 Characterization of the catalysts—Results and discussion

### 4.6.1 Powder X-ray diffraction

All the X-ray diffractograms of the screened catalysts matched well with the reported literature. A well-defined low-angle PXRD pattern with peaks at  $2\theta$  of 0.9, 1.6, and 1.8° for the Al-SBA-15 catalyst is obtained matching the standard pattern<sup>11</sup>. The XRD patterns of the commercially procured zeolites *viz.* ferrierite, H-Beta, Y-zeolite, and synthesized SAPO-11 have matched with the standard patterns as presented in figure 4.1. The XRD patterns of sulfated zirconia (SZr) with different sulfation are presented in figure 4.1. In general, the unmodified zirconia calcined at 650 °C is expected to predominantly contain the monoclinic phase at  $2\theta$  of 28.3, 31.5, and 34.3°. However, upon sulfation, peaks were dominated by the tetragonal phase for most of the SZr materials as the sulfation leads to the transformation of the monoclinic phase to the tetragonal phase. (i.e., sulfation activates the tetragonal phase)<sup>9</sup>. As expected, at lower sulfate treatment, the SZr(1M) and SZr(1M-w) materials showed peaks exclusively dominated by the tetragonal phase ( $2\theta$  at 29.9, 34.6, 49.6, 59.6, 62.3°). Interestingly, the presence of the monoclinic phase along with the tetragonal peaks was witnessed in SZr(2M-w), SZr(2.5M-w), SZr(3M-w) due to the loss of the leachable physisorbed sulfur upon washing. For SZr(2.5M-w), stable monoclinic peaks were found to be dominating the tetragonal peaks. The difference in such crystal structure of all the materials with the same calcination temperature of 650 °C could be due to the difference in concentration of H<sub>2</sub>SO<sub>4</sub> taken for sulfate treatment.

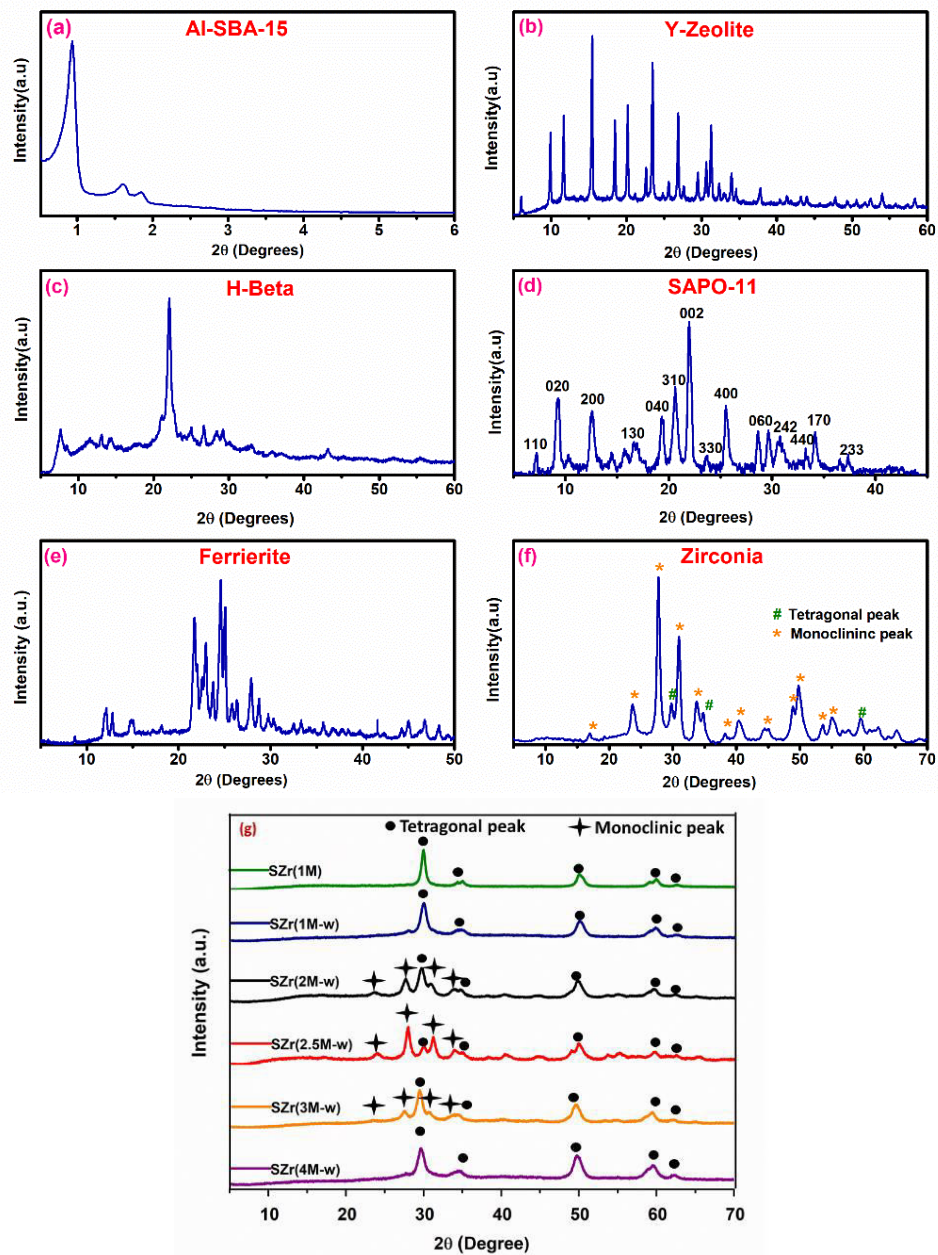


**Figure 4.1.** XRD patterns of (a) Al–SBA–15 (b) Y–Zeolite (c) H–Beta (d) SAPO–11 (e) Ferrierite (f) zirconia (g) sulfated zirconia with varied sulfation

#### 4.6.2 Nitrogen sorption studies

The BET surface areas were determined for all the screened catalysts such as zeolites, ion–exchange resin, silicoaluminophosphates, and mesoporous materials (Table 1). Some of the screened catalysts such as Al–SBA–15, Y–Zeolite, and H–Beta possessed a high surface area of 677, 809, and 592  $\text{m}^2 \text{g}^{-1}$  respectively, whereas SAPO–11 and ferrierite showed a good surface area of 507 and 341  $\text{m}^2 \text{g}^{-1}$  respectively. Amberlyst–15,

a macroporous polymeric catalyst had a low surface area of  $40 \text{ m}^2 \text{ g}^{-1}$ . Al-SBA-15 showed type-IV isotherm with H1 hysteresis loop, whereas SAPO-11, ferrierite, H-Beta, and Y-zeolite exhibited type-1 isotherm typical of microporous material as presented in figure 4.2(A).

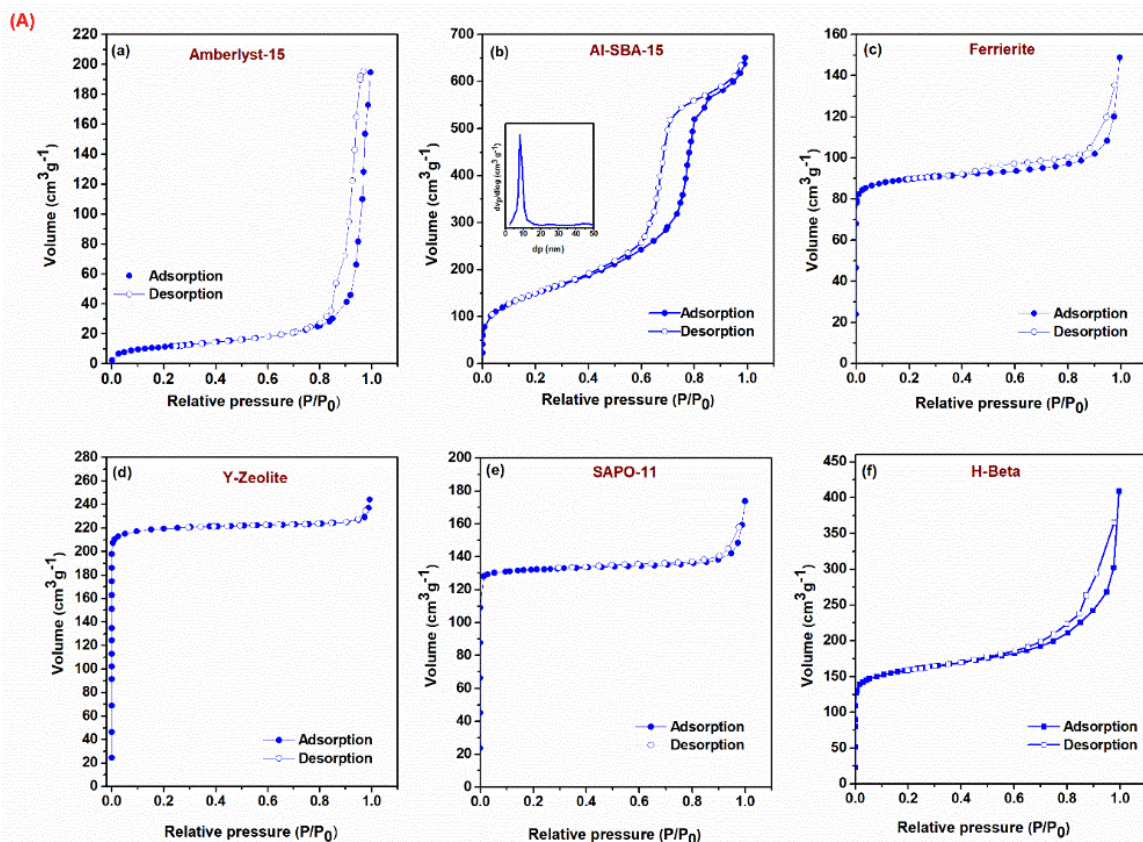


**Figure 4.2 (A)** N<sub>2</sub> sorption isotherms of all the screened catalysts (a) amberlyst-15, (b) Al-SBA-15, (c) ferrierite, (d) Y-Zeolite, (e) SAPO-11, (f) H-Beta

In the case of SZr (washed) catalysts, the surface area was found to increase with an increase in sulfation up to 2.5M from  $78$  to  $117 \text{ m}^2 \text{ g}^{-1}$  (Table 2). Above 2.5M i.e., at 3M and 4M aq. H<sub>2</sub>SO<sub>4</sub> treatment, the surface area decreased to 112 and  $87 \text{ m}^2 \text{ g}^{-1}$  respectively which might be due to the material saturation by sulfate ions and the migration of the excess sulfate ions to the bulk. The N<sub>2</sub> adsorption-desorption isotherms of all the SZr catalysts with varied sulfation calcined at  $650 \text{ }^\circ\text{C}$  displayed type-IV isotherm with hysteresis loop of H2 type confirming mesoporosity of the material [figure 4.2(B)]. Interestingly, even with the higher sulfation ( $>3\text{M}$ ), the mesoporosity of the SZr was intact which proves that the porosity of the material was not affected.

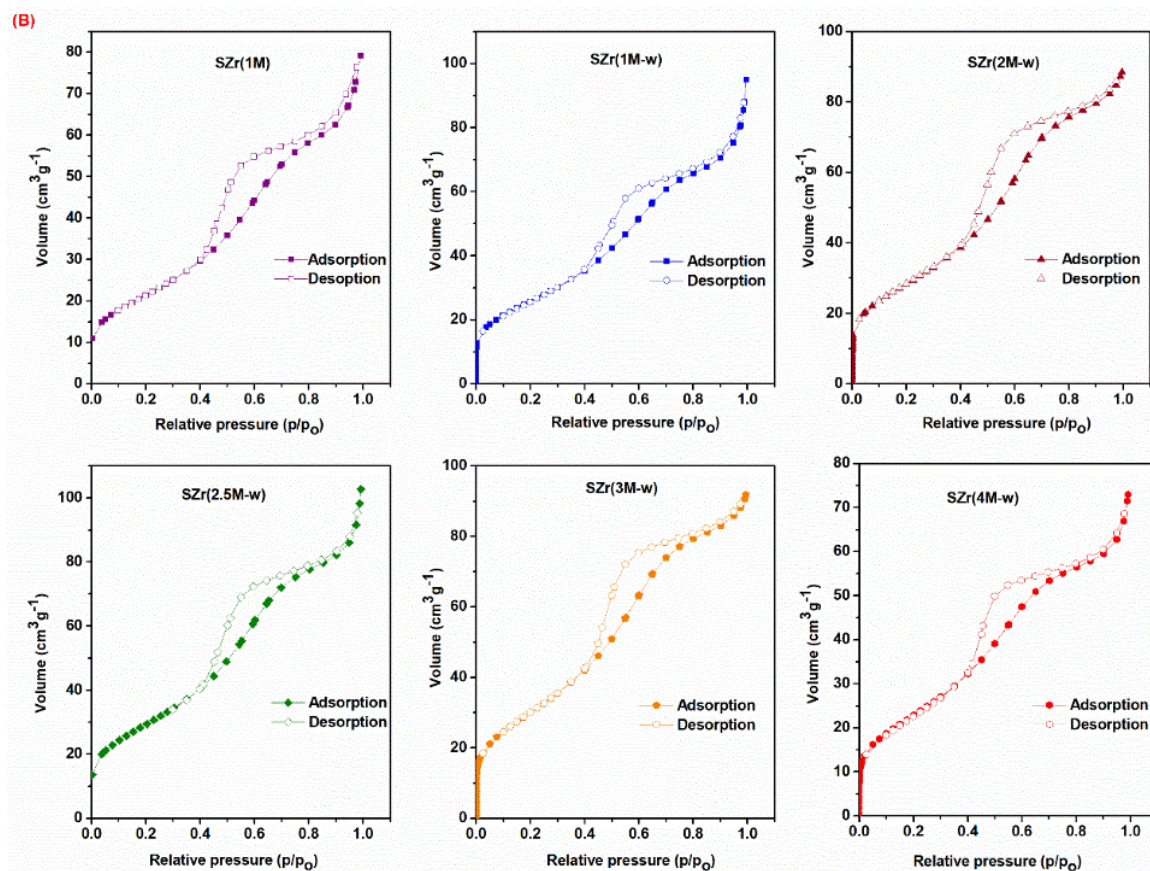


**Figure 4.2 (B).**  $N_2$  sorption isotherms of sulfated zirconia catalysts with varied sulfation

The pore dimension of all the sulfated SZr was almost identical with an average pore size of  $\sim 5$  nm [figure 4.2(C)]. The uniformity in the pore diameter could be due to the removal of the leachable and excess physisorbed sulfate ions.

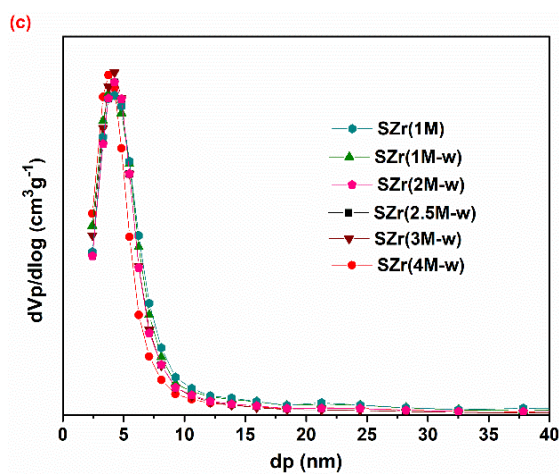


**Figure 4.2. (C)** Mean pore diameter of sulfated zirconia catalysts with varied sulfation

### 4.6.3 Temperature programmed desorption and Pyridine–FTIR

The zeolite catalysts i.e., ferrierite, H–Beta, and Y–Zeolite exhibited high amounts of total acidity in the range of 0.7–1.6 mmol g<sup>-1</sup>. The strength of acidity in these catalysts is dominated by strong acidity compared with that in other non–zeolitic catalysts. SAPO–11 with the acidity of 0.23 mmol g<sup>-1</sup> predominantly contained weak and moderate active sites. The strength of acidity of Al–SBA–15 was distributed over a range of temperatures from 50 to 550 °C with a total amount of acidity of 0.19 mmol g<sup>-1</sup>. The SZr similar to Al–SBA–15 showed a mild amount of acidity around 0.2 mmol g<sup>-1</sup> dispersed as weak, moderate, and strong over a temperature range from 50 to 650°C [Table 4.2, figure 4.3(A)]. The SZr(1M) and post synthetically washed SZr(1M–w) catalysts exhibited 0.25 and 0.20 mmol g<sup>-1</sup> of acidity respectively which evidently shows the lowering in the total acidity of the later catalyst due to the removal of the leachable physisorbed sulfate species [Table 4.2, figure 4.3 (B)]. Further, upon post synthetically washing all the SZr catalysts with varied sulfation, there was a marginal increment in the total acidity from 0.2 to 0.26 mmol g<sup>-1</sup> (for 1–3M sulfation). With an increase in sulfation, the SZr(4M–w) material displayed a decrease in the acidity (0.24 mmol g<sup>-1</sup>) which could be due to the saturation of sulfate species and the formation of sulfate species that are in isolated/polysulfate form as well. The distribution pattern of strengths of acidity for different SZr catalysts was similar (Table 2).

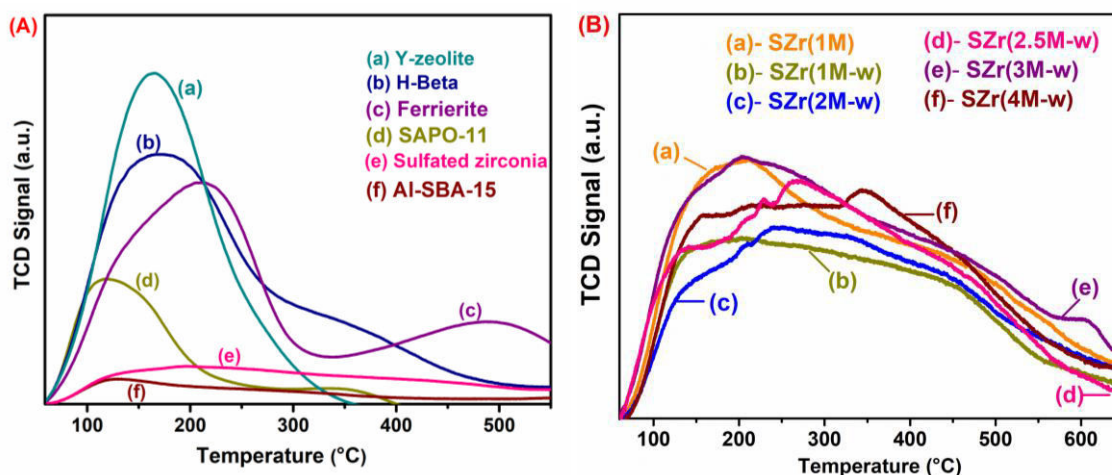


**Figure 4. 3.** NH<sub>3</sub>–Temperature programmed desorption profiles of (A) various solid acid catalysts, (B) sulfated zirconia catalysts with varied sulfation

The pyridine–FTIR of various catalysts screened showed a decrease in B/L ratio in the order; ferrierite>sulfated zirconia>Y–zeolite>SAPO–11>Al–SBA–15> H–Beta (Table 4.1, figure 4.4). The results of the sulfur content estimated by ICP–OES analysis were in agreement with the trend of acidity of SZr catalysts with varied sulfation (Table 4.2).

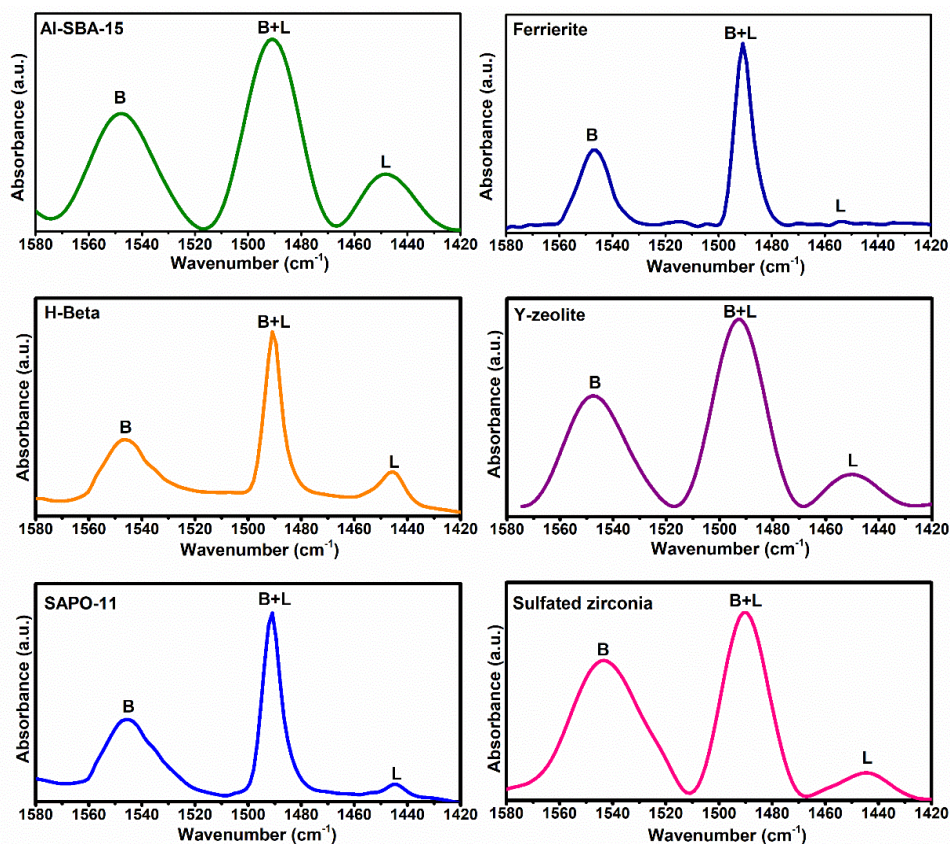


**Figure 4.4.** Pyridine–FTIR spectra of screened catalysts

**Table 4.1.** Physicochemical properties of the various solid acid catalysts

Catalyst	Surface area (m <sup>2</sup> g <sup>-1</sup> ) <sup>[a]</sup>	Pore Volume (cm <sup>3</sup> g <sup>-1</sup> )	Acidity (mmol g <sup>-1</sup> ) <sup>[b]</sup>				B/L <sup>[d]</sup>
			Weak	Moderate	Strong	Total	
SAPO–11	507	0.21	0.04	0.15	0.05	0.23	2.8
Amberlyst–15	40.3	0.27	–	–	–	4.7 <sup>[c]</sup>	–
Al–SBA–15 (SAR35)	677.4	0.88	0.07	0.05	0.06	0.19	2.7
Y–Zeolite (SAR5.1)	809.5	0.36	0.67	0.66	0.26	1.6	3.4
H–Beta (SAR25)	592.1	0.16	0.20	0.28	0.43	0.92	1.6
Ferrierite (SAR 20)	341	0.14	0.27	0.24	0.21	0.72	25.5
SZr(2.5M–w)	117.2	0.13	0.01	0.088	0.13	0.23	5.3

[a] BET surface area, [b] NH<sub>3</sub>–TPD, [c] Acid–base titration, [d] Pyridine–FTIR



**Table 4.2.** Physicochemical properties of the sulfated zirconia catalysts with varied sulfation.

Catalyst	Surface area (m <sup>2</sup> g <sup>-1</sup> ) [a]	Pore Volume (cm <sup>3</sup> g <sup>-1</sup> )	Acidity (mmol g <sup>-1</sup> ) [b]				Sulfur content (mmol g <sup>-1</sup> ) [c]
			Weak	Moderate	Strong	Total	
SZr(1M)	78.2	0.12	0.02	0.09	0.14	0.25	0.70
SZr(1M-w)	94.6	0.13	0.01	0.08	0.11	0.20	0.48
SZr(2M-w)	106.2	0.13	0.01	0.09	0.12	0.22	0.67
SZr(2.5M-w)	117.2	0.13	0.01	0.09	0.13	0.23	0.65
SZr(3M-w)	112.8	0.15	0.02	0.09	0.15	0.26	0.76
SZr(4M-w)	87.7	0.10	0.02	0.09	0.14	0.25	0.68

[a] BET surface area, [b] NH<sub>3</sub>-TPD, [c] ICP-OES

#### 4.6.4. FTIR spectroscopy

FTIR spectra of SZr with varied sulfation are presented in figure 4.5. The sulfate species in the catalyst appear in the region of 1250–1000 cm<sup>-1</sup> which includes symmetric, asymmetric stretching of sulfone and sulfoxide groups. The peaks appearing at 1219, 1153, 1067, and 1010 cm<sup>-1</sup> support the presence of sulfate species in the catalyst<sup>18</sup>.

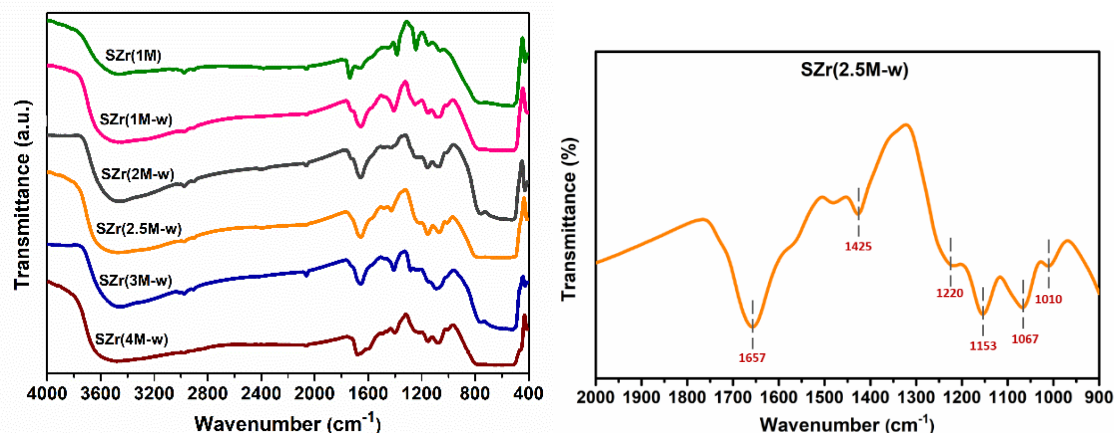


**Figure 4.5.** FTIR spectra of sulfated zirconia catalysts with varied sulfation

#### 4.6.5. Scanning electron microscopy

SEM micrographs of SZr catalysts disclosed the presence of particles with varied sizes that have irregular morphology. The morphologies of SZr(1M) and after the water treatment [SZr(1M-w)] were found to be similar. Sulfuric acid treatment of SZr with 1 to 4 M concentrations did not make a noticeable impact on the morphology of the particles (figure 4.6).

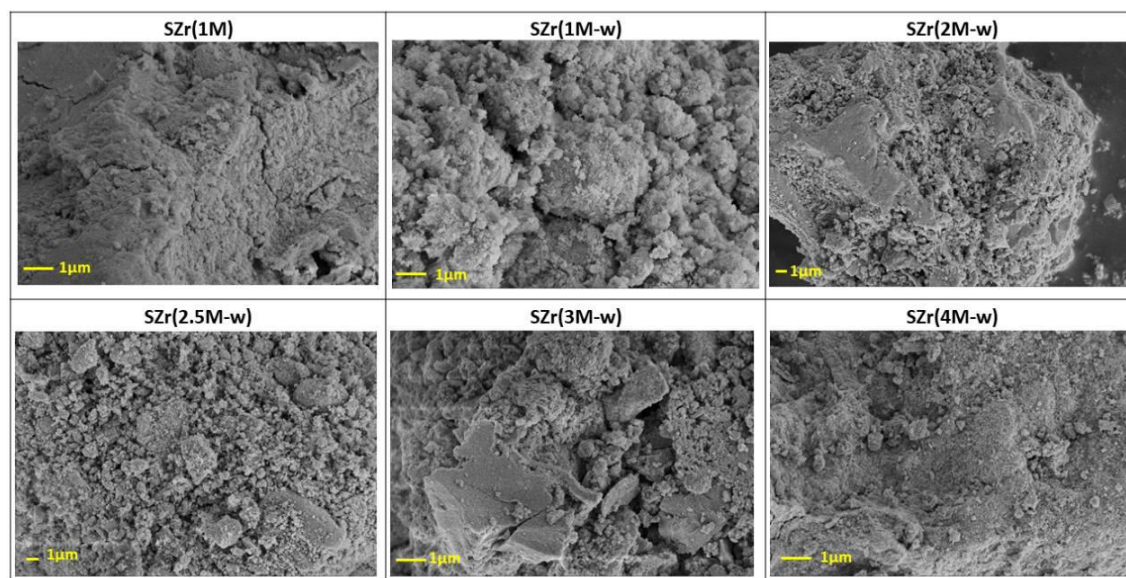


**Figure 4.6.** SEM micrographs of sulfated zirconia catalysts with different sulfation

## 4.7 Catalytic activity study

### 4.7.1 Catalyst screening and comparison

It is known that the esterification reaction is an acid-catalyzed reaction and the Brønsted acid sites play a major role in the esterification of FA to FAc. Hence, the behavior of various solid acid catalysts differing in properties such as the pure solid Brønsted acid catalyst (ion-exchanged resin amberlyst-15), zeolites (H-Beta, Y-Zeolite, ferrierite), silicoalumino phosphates (SAPO-11), ordered mesoporous materials (Al-SBA-15), and superacid catalyst (sulfated zirconia) were screened at 70 °C for this transformation. The physicochemical properties were correlated with TON (or catalytic conversion and selectivity) to identify the nature of the active sites required to achieve the competing activity. Prior to this study, a blank reaction was performed at 70 °C in the absence of the catalyst which gave a trace level (3%) FAc yield. Figure 4.7 presents the catalytic performance of various catalysts for FAc production from FA and acetic acid with a mole ratio of 1:10 at 70 °C for 4 h. The catalytic performance with respect to TON is obtained for these catalysts in the order; sulfated zirconia > Al-SBA-15 > SAPO-11 > ferrierite > H-Beta > amberlyst-15 > Y-zeolite as presented in figure 4.7.

Zeolites such as ferrierite, H-Beta, and Y-zeolite inheriting high Brønsted acidity relatively showed lower yield for FAc. Ferrierite, though owned the highest B/L ratio of 25.5 with a trace amount of Lewis acid sites (figure 4.4) performed poorly (6% FAc

yield) due to pore size restriction owing to its medium pore size with dimensions (4.2 x 5.4 Å; 3.5 x 4.8 Å)<sup>19</sup>. For H-Beta and Y-zeolite, a higher amount and strength of Brönsted acidity led to lower product yield due to the formation of side products in high concentration (difurfuryl ether, and difurfuryl furan). Owing to its one-dimensional medium pore system and mild acidic strength, SAPO-11 was reported to be a good catalyst in several reactions mainly isomerization of hydrocarbons but seldom employed in furfural and FA related transformations<sup>19</sup>. Though TON was higher (75) for SAPO-11, the FAc yield was low (~5%) probably due to its topological steric constraints<sup>19</sup>. Al-SBA-15 being an ordered mesoporous aluminosilicate with a high surface area, B/L ratio of 2.7 and moderate acidity showed a good TON of 49 with FA conversion of 17% and FAc selectivity of 36% along with side products such as 2,2'-difurfurylmethane and difurfuryl ether. A highly acidic cation exchanged resin, amberlyst-15 with its remarkably high Brönsted acidity of 4 mmol g<sup>-1</sup> due to polystyrene sulfonic acid matrix displayed a low TON of 10. Though it gave 42.5% FA conversion and 42.7% FAc selectivity, the catalyst failed to regain the catalytic performance over the successive cycles due to regeneration issues. FA polymerizes at the strong acidic sites and the removal of such organic species by calcination cannot be performed for amberlyst-15 as its thermal stability is very low. SZr catalyst, though contained a lower surface area compared to most of the catalysts tested, had the combination of high Brönsted acidic sulfate moieties with B/L = 5.4, and the moderate number of total acidity that synergistically helped to get high FA conversion and FAc selectivity of 28 and 47% respectively. The side products were formed with ~10 to 12 % selectivity each (difurfurylfuran, difurfuryl ether, and 2,2'-difurfurylmethane) under the applied reaction condition in this study. Hence, considering the FAc yield, SZr stands second best after amberlyst-15 which is preferred for further studies due to the highest TON of 126 and the aforementioned disadvantages of amberlyst-15.

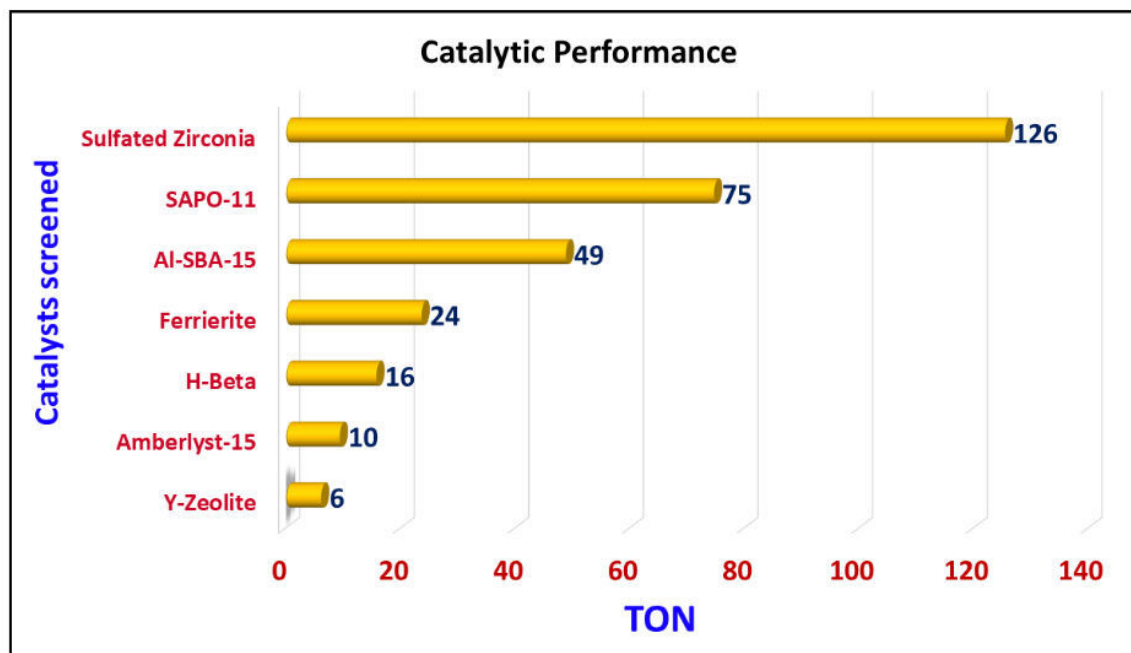
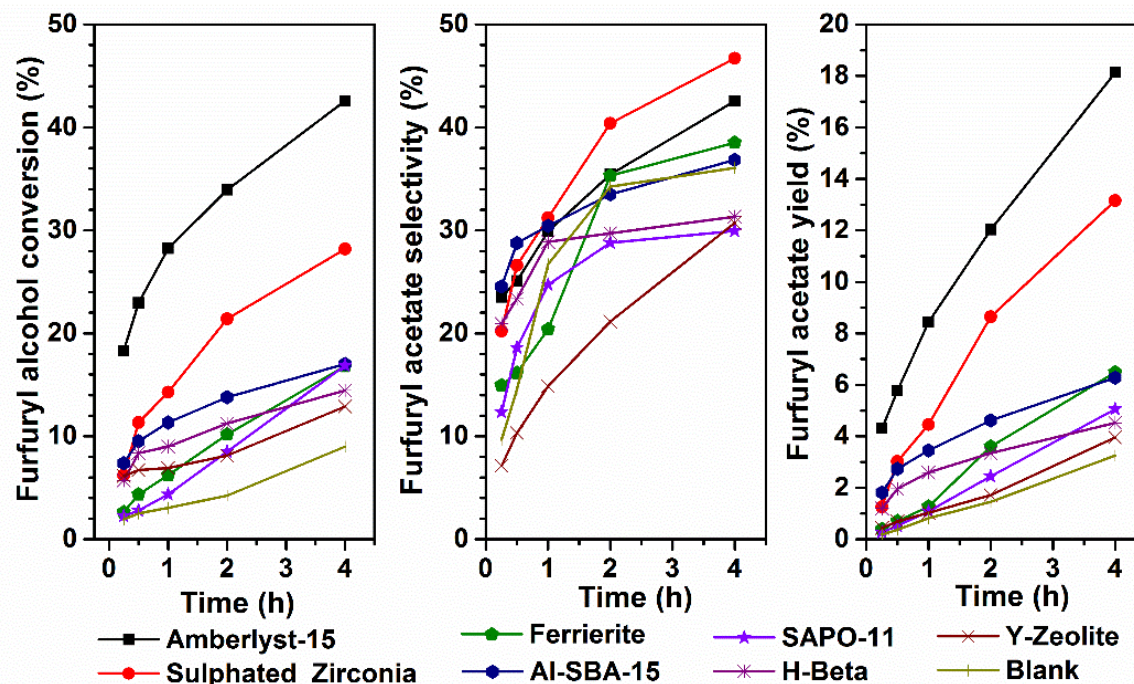


**Figure 4.7.** Catalyst screening. Reaction conditions: catalyst concentration– 1.5wt%, temperature– 70 °C, reaction time– 4 h, mole ratio– 1:10 (FA: acetic acid).

#### 4.7.2 Optimization of sulfation on zirconia support

The catalytic activity of the SZr catalyst was examined for different concentrations of sulfation from 1 to 4M. Initially, though SZr(1M) catalyst showed the highest catalytic performance, the sulfate ions were found to leach during the reaction. Hence to avoid

leaching, all the materials synthesized with different sulfate concentrations were refluxed at 80 °C for 6 h post calcination to remove the physisorbed sulfate species. The results of the catalytic activity of the water-treated SZr catalysts were compared with the SZr (without post water treatment) as presented in figure 4.8. The catalyst performance for SZr(1M) after water treatment retained high conversion and selectivity which shows that there were sufficient chemisorbed sulfate species that existed on SZr which was not washed away after water treatment. This could be attributed to the acidity created on the zirconia phases through sulfate ion interaction which is irreversibly bound to the support matrix. The washed SZr showed no leaching of sulfate ions during the esterification reaction. With an increase in sulfation, the FA conversion and FAc selectivity were found to increase up to 2.5M sulfate treatment. Further increase in the sulfation decreased the conversion marginally. The SZr(2.5M-w) catalyst showed the best catalytic performance with 83% FA conversion and 85% FAc selectivity which was used to study the effect of reaction parameters.

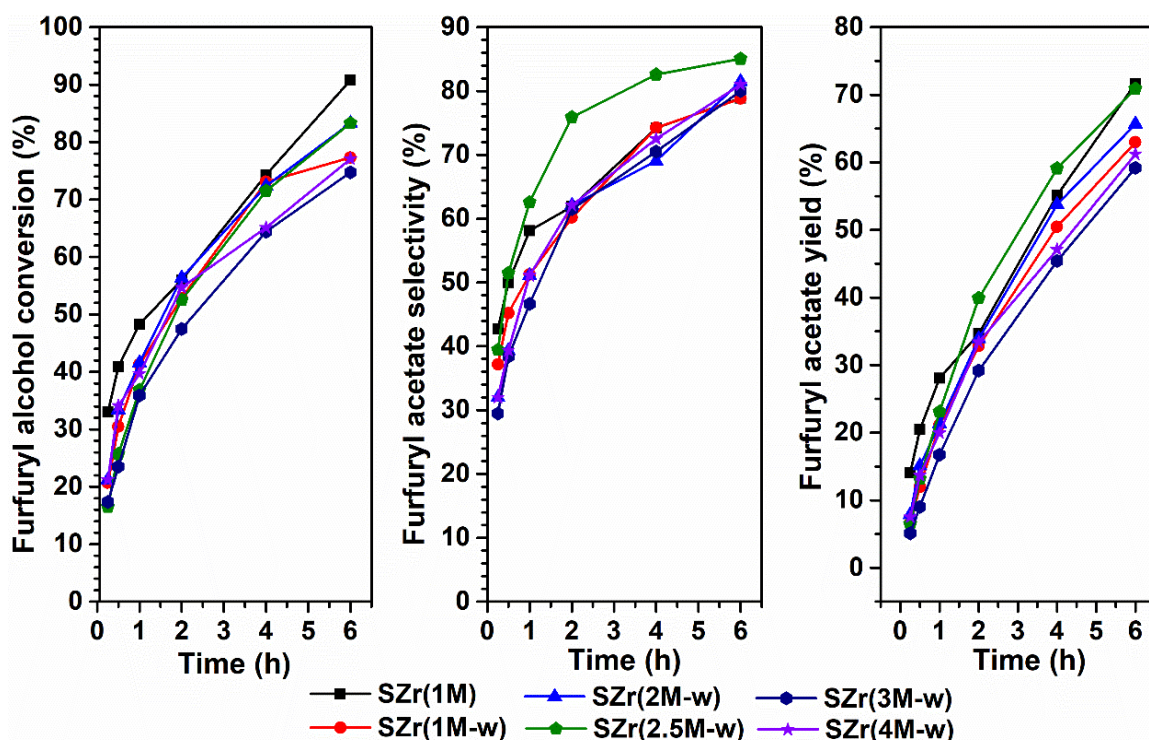


**Figure 4.8.** Optimization of sulfation on zirconia support. Reaction conditions: Catalyst–SZr, catalyst concentration– 1.5wt%, temperature– 100 °C, reactants mole ratio– 1:10 (FA: acetic acid), reaction time– 6 h.

### 4.7.3 Influence of reaction conditions

#### Effect of temperature

The influence of the reaction temperature was studied with SZr(2.5M-w) over a range of temperatures from 70 to 110 °C (figure 4.9). As the temperature increased from 70 to 90 °C, there was an increase in the FA conversion from 29 to 43% in 6 h. At 70 °C, the FAc selectivity was 54% at 6 h with ~10 to 12 % selectivity for each side products (2,2'-difurfurylmethane, difurfuryl ether, difurfuryl furan). The selectivity for FAc at 80 and 90 °C were almost the same (73–74%) in 6 h reaction time with side products majorly being 2,2'-difurfurylmethane and difurfuryl ether. Upon increasing to 100 °C resulted in 83% FA conversion and 85% FAc selectivity with 2,2'-difurfurylmethane, difurfuryl ether as major side products. Further raising to 110 °C, FA conversion increased marginally to 89% but the selectivity towards FAc decreased to 75% due to the increase in the side products, difurfuryl ether, and furfuryl furan. Hence, temperature 100 °C was found to be the optimum temperature for this transformation aided by SZr(2.5M-w) catalyst.

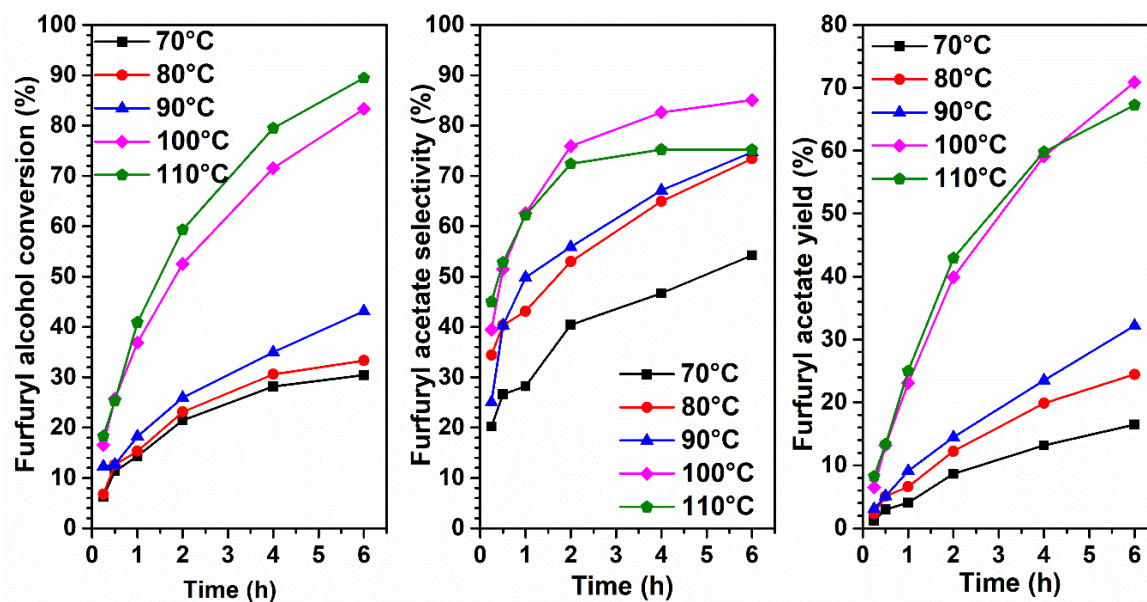


**Figure 4.9.** Effect of temperature: Reaction conditions: Catalyst– SZr(2.5M-w), catalyst concentration– 1.5wt%, reactants mole ratio– 1:10 (FA: acetic acid), reaction time– 6 h.

### Effect of reactants mole ratio

The optimization of the reactants mole ratio (FA: acetic acid) is important as a lower ratio might lead to the enhanced polymerization of FA, whereas the dilution at higher ratios might lower the catalytic activity. Usually, solvents or the reactant (used in excess), prevent polymerization thereby reducing the risk of catalyst poisoning and lower product yield. The effect of reactant mole ratio by varying acetic acid concentration from 1:4 to 1:14 was studied. At lower ratios like 1:4 and 1:6, the FA conversion was 70 and 73% respectively (figure 4.10). With an increase in acetic acid concentration up to 1:10, there was an increase in FA conversion to 83%. Above, 1:10 mole ratio, i.e. 1:12 and 1:14, the FA conversion marginally dropped which can be attributed to the dilution effect. The FAc selectivity had similar results ranging from 80 to 86% for all the mole ratios tested which proves that the variation in the concentration of the reactants has less impact on the product selectivity. Hence, the optimum reactants mole ratio was found to be 1:10 with the highest FA conversion of 83% with 85% FAc selectivity.

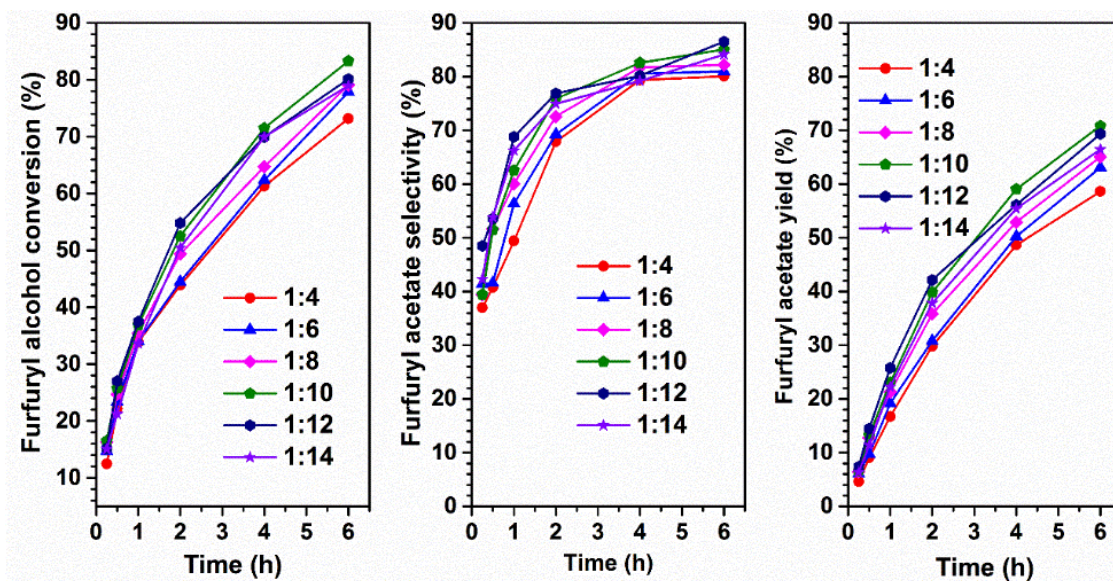


**Figure 4.10.** Effect of reactants mole ratio. Reaction conditions: Catalyst–SZr(2.5M–w), catalyst concentration– 1.5wt%, temperature– 100 °C, reaction time– 6 h.

### Effect of catalyst loading

The variation in the catalyst loading with SZr(2.5M–w) was investigated over a range of concentrations from 0.15 to 2.25wt% (with respect to the concentration of the total reactants). The studies revealed that with an increase in catalyst loading from 0.15 to

1.15wt%, the FA conversion increased from 62 to 71%, above which the FA conversion decreased to 68% (figure 4.11). The FAc selectivity remained around 85 to 88% irrespective of the catalyst concentration with the major side product being difurfuryl ether. Though the increase in catalyst loading increased the conversion, it was not proportional to the increase in weight of the catalyst. It may be due to the formation of side products at a higher proportion at the beginning of the reaction that might have slowed down the conversion of the FA. The FAc yields for 0.37 and 1.15wt% catalyst loading were similar (69 and 70% respectively). Hence, the lower catalyst concentration of 0.37wt% was chosen as the optimized catalyst concentration.

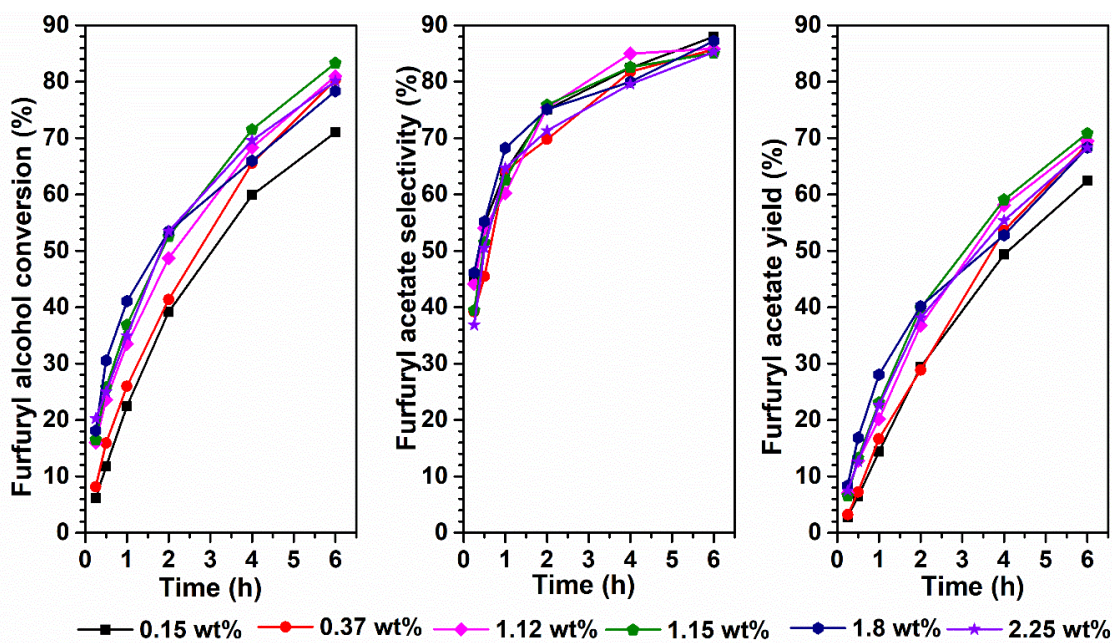


**Figure 4.11.** Effect of catalyst loading. Reaction conditions: Catalyst– SZr(2.5M–w), temperature– 100 °C, reactants mole ratio– 1:10 (FA: acetic acid), reaction time– 6 h.

#### 4.7.4 Catalyst recyclability study

The potential catalyst, SZr (2.5M–w) was examined for its stability by employing the catalyst over successive cycles of the experiment under the optimized reaction conditions of 0.37wt% catalyst loading, 1: 10 (FA: acetic acid) reactants mole ratio for 6 h at 100 °C reaction temperature. The catalyst was regenerated prior to each cycle by washing the spent catalyst with acetone followed by calcination at 650 °C. During the first recycle, there was a marginal decrease in both FA conversion from 80 to 79% and FAc selectivity from 86 to 85% (figure 4.12) at the end of 6 h time. For the next successive recycles,



there was a small decrease in the FA conversion from 79 to 76% and the FAc selectivity also decreased to 81%. Overall, there was a 7% decrease in conversion and a 5% decrease in selectivity after the 3 recycles in 6 h. There was a marginal decrease in acidity from 0.23 to 0.20 mmol g<sup>-1</sup> which may be due to the deactivation of some active sites which could not be regenerated (Table 4.3). Therefore, the recyclability of SZr up to 3 recycles was found to be good.

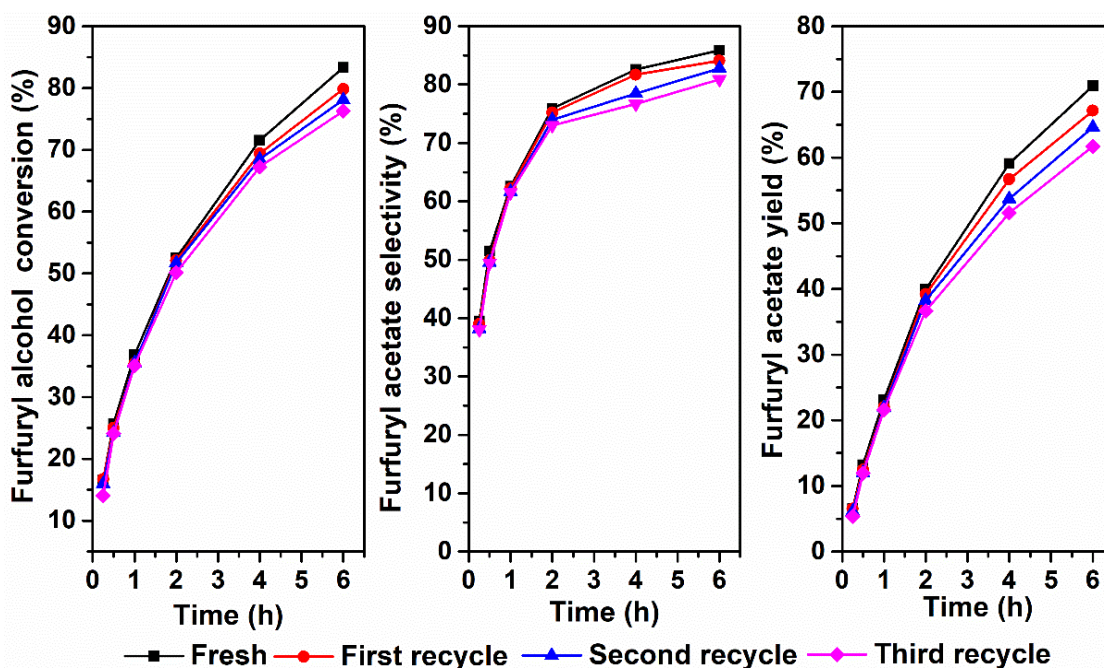


**Figure 4.12.** Catalyst recyclability study. Reaction conditions: Catalyst– SZr(2.5M–w), catalyst concentration– 0.37wt%, temperature–100 °C, reaction time– 6 h.

**Table 4.3** Acidity of the fresh and spent SZr(2.5M–w) catalyst for comparison

Catalyst	Acidity (mmol g <sup>-1</sup> ) from NH <sub>3</sub> -TPD			
	Weak	Moderate	Strong	Total
SZr(2.5M–w)	0.01	0.09	0.13	0.23
SZr(2.5M–w) –Used	0.01	0.06	0.13	0.20

#### 4.7.5 Time resolved study

The effect of time over a period of 24 h was examined for the best catalyst, SZr(2.5M–w) under the optimized reaction conditions. The catalytic performance was found to increase progressively with an increase in time (figure 4.13). The catalyst showed 95% furfuryl alcohol conversion and 98% FAc selectivity at 24 h.

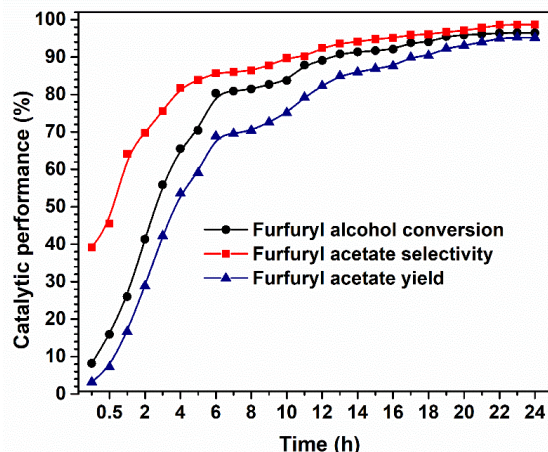
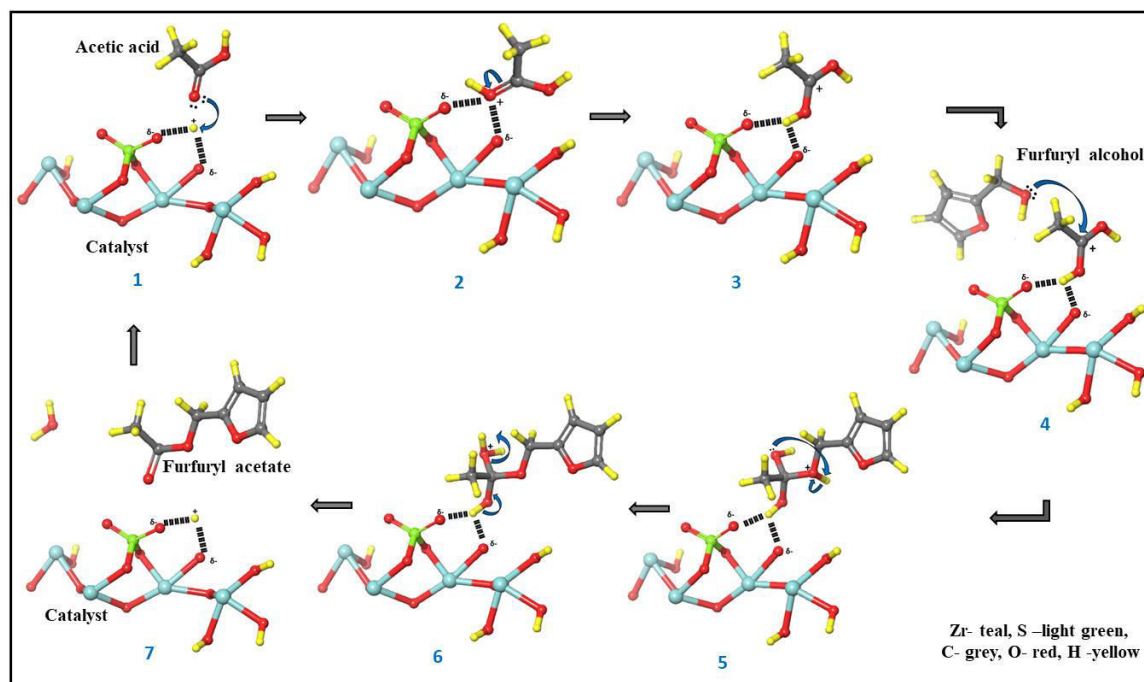


**Figure 4.13.** Time resolved study. Reaction conditions: Catalyst– SZr(2.5M–w), catalyst concentration– 0.37wt%, temperature– 100 °C, reactants mole ratio– 1:10 (FA: acetic acid), reaction time– 24 h

#### 4.8 Plausible reaction mechanism

The plausible mechanistic pathway of the esterification of furfuryl alcohol to yield furfuryl acetate using acetic acid is proposed in Scheme 4.2. The reaction proceeds via Eley–Rideal mechanism as the solid acid catalysts used in this study contain stronger acidic strength than reactant acetic acid.



**Scheme 4.2.** Plausible mechanistic pathway for the esterification of furfuryl alcohol to yield furfuryl acetate

The mechanism starts with the protonation of acetic acid by the acidic site of the catalyst<sup>20</sup>. The resulting carbocation is attacked by nucleophilic oxygen of another reactant, furfuryl alcohol. Proton transfer from the oxonium ion of the attached furfuryl alcohol to the hydroxyl group of the acid occurs resulting in the elimination of water and subsequent desorption of the product, furfuryl acetate from the catalyst system.

## 4.9. DFT approach

### 4.9.1. Model

Based on the testing of solid acid catalysts described above, we chose to study three top-performing solid acid catalysts. We studied sulfated zirconia<sup>17,21,22</sup> and a couple of other solid acid catalysts namely SAPO-11<sup>23,24,25</sup> and Al-SBA-15<sup>26,27</sup> in order to understand the critical features of these catalysts that control their performance so that some guidelines can be derived for designing high-performance catalysts in the future. The cluster models of active sites for three catalyst systems shown in figure 4.14 were built using Avogadro software<sup>28</sup>.

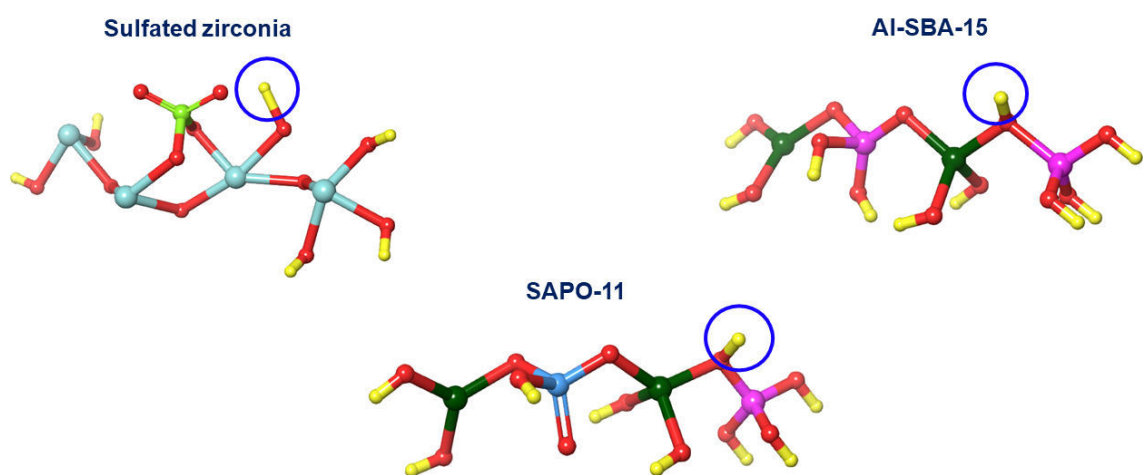


**Figure 4.14.** Cluster models used to represent the active sites in three top-performing catalysts. Zr, S, Si, Al, P, O, and H atoms are represented by teal, light green, pink, dark green, dark blue, red, and yellow color respectively. The Brønsted acidic sites which are the site of activation of molecules are encircled with blue color

Since we are employing a single-point energy calculation, the O–H bond distances for different catalysts are chosen based on the earlier ab initio calculations for such systems<sup>29,30,31,32</sup>. The experimentally determined O–H distances for H-bonded solid systems and solid Brønsted acid sites are manually set based on the studies of the active sites of the

catalysts<sup>33</sup>. To define the proton donor site (encircled with blue color) in SAPO-11 and Al-SBA-15, the O-H bond distance is set to 1.10 Å. In the case of sulfated zirconia catalyst, the acidity is due to the polarization induced by the oxygen of the sulfate species with hydrogen. To represent the proton donor site, the O-H bond distance is set to 1.4 Å<sup>34,35,36,37</sup> and the distance between the oxygen of the sulfate species with the Brønsted acidic hydrogen is set to 2 Å indicating the presence of a hydrogen bond.

#### 4.9.2. Calculation of adsorption energy for the molecules and intermediates on the catalyst surface

Experimental results acquired for this reaction proved that sulfated zirconia, SAPO-11, and Al-SBA-15 as the top-performing catalysts in terms of TON among the other screened catalysts (figure 4.7). Therefore, DFT calculations were performed to obtain adsorption energy for the various substrate molecules adsorbed over the catalyst surface. The potential energy curve along with the reaction coordinate and all the substrates in the reaction mixture (reactants, intermediates, and products) were calculated. The energy of the catalyst cluster and the adsorbates can be termed  $E_{\text{cat}}$  and  $E_{\text{sub}}$  respectively. The energy after the adsorption of the substrates on the catalyst active site was calculated and is termed as  $E_{(\text{Cat+Sub})}$ . The adsorption energy was calculated using the following formula.

$$\text{Adsorption Energy} = [E_{\text{cat}} + E_{\text{sub}}] - [E_{(\text{Cat+Sub})}]$$

This study reveals the preferred reaction pathway leading to a high yield of furfuryl acetate from furfuryl alcohol. The adsorption energy of all the molecules over the top-performing catalysts, namely sulfated zirconia, Al-SBA-15, and SAPO-11 are plotted against all the steps of the reaction as per the plausible mechanism (figure 4.15). The adsorption energy profile reveals that the sulfated zirconia catalyst has the least activation energy barrier followed by Al-SBA-15 and SAPO-11 catalysts. These results correlate well with the experimentally observed catalytic performance of sulfated zirconia. The reasons can be assigned to the presence of the H-bonded -S-O-H-O-Zr type of active site compared to the conventional Brønsted acid sites in Al-SBA-15 and SAPO-11, with -Si-O-Al-O-H, and -P-O-Al-O-H active species, respectively. Thus, the models and methods gain more trust based on the above discussions.

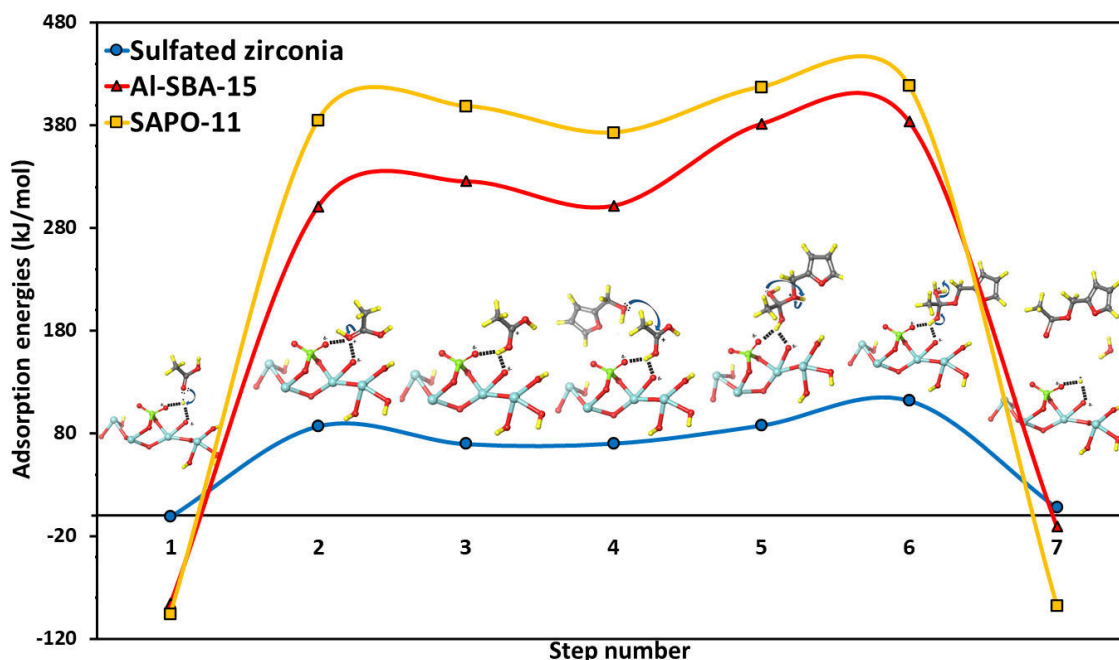


**Figure 4.15.** The adsorption energy profile diagrams of reactant, product, and five intermediates for sulfated zirconia, Al-SBA-15, and SAPO-11 catalysts.

By analyzing the energy profiles more carefully, we found the results as given in Table 3. The difference between the adsorption energy values of reactant (step-1) and product (step-7) are almost the same for sulfated zirconia and SAPO-11, whereas it is maximum for Al-SBA-15. The informal barrier to be crossed (difference between 1 and 6) is minimal for sulfated zirconia. After step-6, the reaction is taking the ‘down-the-hill’ path for all three catalysts. Thus, the results in figure 4.15 and Table 4.4 are affirming the experimental findings.

**Table 4.4.** Comparison of adsorption energy for reactant, intermediate, and product over the three top-performing catalysts

Catalysts	Difference in adsorption energy (kJ/mol)		
	1 and 7	1 and 6	6 and 7
Sulfated zirconia	8.773	113.078	-104.305
Al-SBA-15	74.993	469.907	-394.915
SAPO-11	8.099	514.642	-506.543

#### 4.9.3. Hydrogen removal energy

Hydrogen removal energy is an indication of the proton donor capability of solid acid catalysts. Since the esterification is an acid-catalyzed reaction and the screened catalysts

are Brønsted acidic in nature. The H removal energy was computed for the three top-performing catalysts and the results are shown in Table 4.5.

**Table 4.5.** Energy to remove one H from the catalysts

Catalyst	Energy before H removal (Ha)	Energy after H removal (Ha)	Energy to remove one H (Ha)	Energy to remove one H (kJ/mol)
Sulfated zirconia	256.952	256.506	0.446	1170.54
SAPO-11	2.027	1.579	0.448	1176.98
Al-SBA-15	0*	-0.474	0.474	1244.27

\*Energy before H removal for Al-SBA-15 ( -920.12 Ha) is taken as the reference

The trend of the hydrogen removal energy for the three top-performing catalysts was in agreement with the TON. The order of the amount of energy required to remove H<sup>+</sup> is Al-SBA-15 > SAPO-11 > Sulfated zirconia which reveals that this is a salient parameter to predict the performance of solid acid catalysts. These results strongly suggest that the TON of the catalyst can be enhanced by designing catalysts with lower values of hydrogen removal energy (figure 4.16).

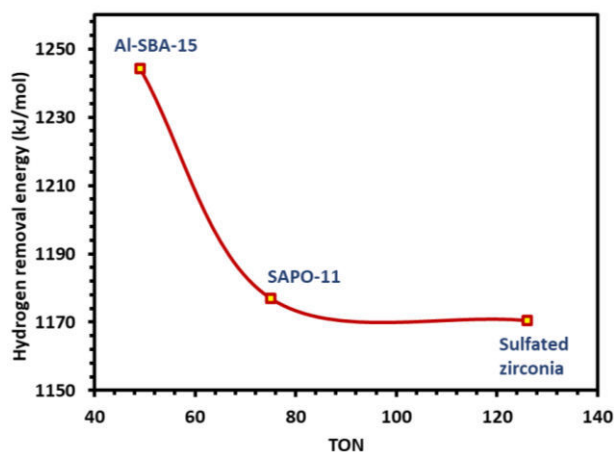


**Figure 4.16.** Hydrogen removal energy profile versus TON for sulfated zirconia, SAPO-11, and Al-SBA-15

#### 4.10 Comparison with literature results

The FAc yield of the only other reported catalyst with the reaction conditions and recyclability are presented in Table 4.6. Sulfated zirconia could achieve a higher yield of

95% at a longer duration of 24 h compared to the MOF based catalyst. Moreover, sulfated zirconia has better thermal stability and a simple preparation procedure compared to the other catalyst.

**Table 4.6.** The Literature survey of furfuryl alcohol esterification to produce furfuryl acetate

<b>Sn</b>	<b>Catalyst</b>	<b>Reaction conditions</b>	<b>FAc Yield (%)</b>	<b>Reusability</b>	<b>Ref</b>
1.	Fe-DTP@ZIF-8 MOF	T=100 °C, time =6h, mole ratio = 1:6	78	73%–5 runs	4
2	Sulfated zirconia (2.5M-w)	T=100 °C, time =24h, mole ratio = 1:10	95	69 % to 62 % in 4 runs (time: 6 h)	PW <sup>a</sup>

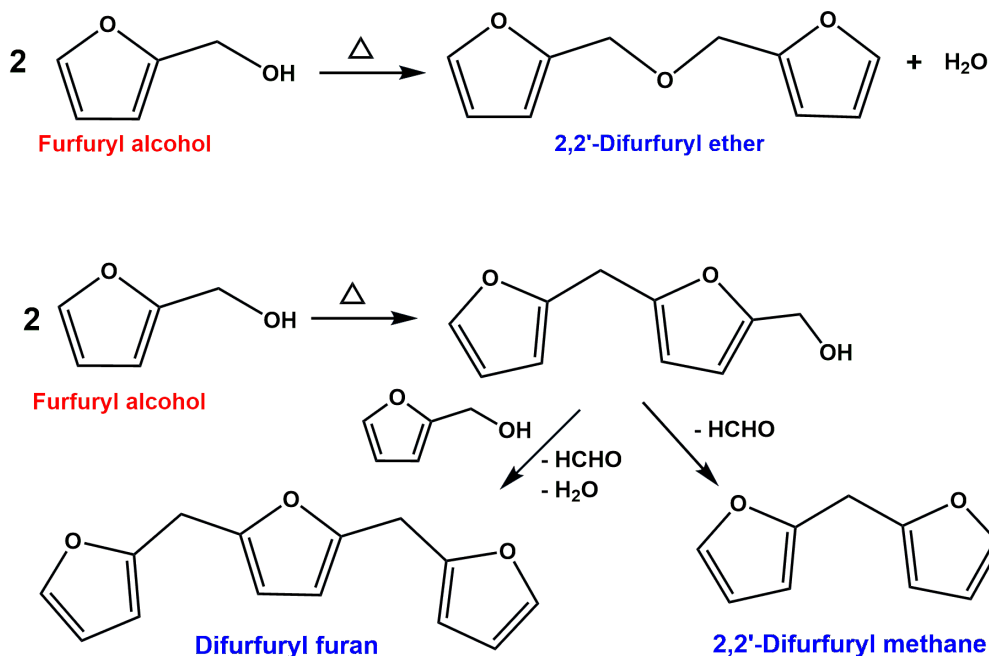
<sup>a</sup>Present work

## 4.11. Conclusions

Various solid acid catalysts such as zeolites, silicoalumino phosphates, ionic resins, mesoporous materials with diverse physicochemical properties were studied to understand the nature of active sites required to efficiently convert FA to FAc. It is found that the moderate number and strength of acidity, high thermal stability, and mesoporosity are the optimum qualities required for the catalyst to obtain a high yield towards FAc. These properties are inherently present in sulfated zirconia as it demonstrated excellent catalytic activity of 96% FA conversion and 98% FAc selectivity at the optimized reaction conditions. SZr after washing addressed leaching issues and showed very good recyclability up to 3 recycles. DFT calculations were performed to study the adsorption of reactants, intermediates, and product molecules based on the mechanism over the three top-performing catalysts. The method and models used in the DFT approach are validated using the adsorption energy profiles. The concept of using hydrogen removal energy as the parameter to design and optimize the efficiency of the catalysts was established in this study. Thus, this integrated experimental and computational study shows that sulfated zirconia is a potential catalyst with the best catalytic performance at the most desirable reaction conditions for esterification of furfuryl alcohol. This specific integrated approach using DFT and experimental data could be useful for other solid acid catalyzed organic transformations in the future.

## Annexure

The scheme for side product formation



## 4.11. Bibliography

- (1) Mariscal López, R.; Maireles-Torres, P.; Ojeda Pineda, M.; Sádaba Zubiri, I.; López Granados, M. Furfural: A renewable and versatile platform molecule for the synthesis of chemicals and fuels. **2016**.
- (2) Modelska, M.; Binczarski, M. J.; Dziugan, P.; Nowak, S.; Romanowska-Duda, Z.; Sadowski, A.; Witońska, I. A. Potential of Waste Biomass from the Sugar Industry as a Source of Furfural and Its Derivatives for Use as Fuel Additives in Poland. *Energies* **2020**, *13* (24), 6684.
- (3) Yan, K.; Wu, G.; Lafleur, T.; Jarvis, C. Production, properties and catalytic hydrogenation of furfural to fuel additives and value-added chemicals. *Renewable and sustainable energy reviews* **2014**, *38*, 663-676.
- (4) Malkar, R. S.; Daly, H.; Hardacre, C.; Yadav, G. D. Novelty of iron-exchanged heteropolyacid encapsulated inside ZIF-8 as an active and superior catalyst in the esterification of furfuryl alcohol and acetic acid. *Reaction Chemistry & Engineering* **2019**, *4* (10), 1790-1802.



- (5) Yu, W.; Tang, Y.; Mo, L.; Chen, P.; Lou, H.; Zheng, X. One-step hydrogenation–esterification of furfural and acetic acid over bifunctional Pd catalysts for bio-oil upgrading. *Bioresource technology* **2011**, *102* (17), 8241-8246.
- (6) Yu, W.; Tang, Y.; Mo, L.; Chen, P.; Lou, H.; Zheng, X. Bifunctional Pd/Al-SBA-15 catalyzed one-step hydrogenation–esterification of furfural and acetic acid: A model reaction for catalytic upgrading of bio-oil. *Catalysis Communications* **2011**, *13* (1), 35-39.
- (7) Hashim, L. H.; Halilu, A.; Sudarsanam, P.; Umar, Y. B.; Johan, M. R. B.; Bhargava, S. K. Bifunctional rice husk-derived SiO<sub>2</sub>-Cu-Al-Mg nanohybrid catalyst for one-pot conversion of biomass-derived furfural to furfuryl acetate. *Fuel* **2020**, *275*, 117953.
- (8) Vaishnavi, B.; Sujith, S.; Kulal, N.; Manjunathan, P.; Shanbhag, G. V. Utilization of renewable resources: Investigation on role of active sites in zeolite catalyst for transformation of furfuryl alcohol into alkyl levulinate. *Molecular Catalysis* **2021**, *502*, 111361.
- (9) Marakatti, V. S.; Shanbhag, G. V.; Halgeri, A. Sulfated zirconia; an efficient and reusable acid catalyst for the selective synthesis of 4-phenyl-1, 3-dioxane by Prins cyclization of styrene. *Applied Catalysis A: General* **2013**, *451*, 71-78.
- (10) Meriaudeau, P.; Tuan, V.; Nghiem, V. T.; Lai, S.; Hung, L.; Naccache, C. SAPO-11, SAPO-31, and SAPO-41 molecular sieves: synthesis, characterization, and catalytic properties in octane hydroisomerization. *Journal of catalysis* **1997**, *169* (1), 55-66.
- (11) Shanbhag, G. V.; Kumbar, S.; Halligudi, S. Chemoselective synthesis of  $\beta$ -amino acid derivatives by hydroamination of activated olefins using AlSBA-15 catalyst prepared by post-synthetic treatment. *Journal of Molecular Catalysis A: Chemical* **2008**, *284* (1-2), 16-23.
- (12) Neese, F.; Wennmohs, F.; Becker, U.; Riplinger, C. The ORCA quantum chemistry program package. *The Journal of Chemical Physics* **2020**, *152* (22), 224108.
- (13) Hay, P. J.; Wadt, W. R. Ab initio effective core potentials for molecular calculations. Potentials for the transition metal atoms Sc to Hg. *The Journal of chemical physics* **1985**, *82* (1), 270-283.
- (14) Dunning, T. H.; Hay, P. J. Methods of electronic structure theory. *Modern theoretical chemistry* **1977**, *3*, 1-28.

- (15) Wadt, W. R.; Hay, P. J. Ab initio effective core potentials for molecular calculations. Potentials for main group elements Na to Bi. *The Journal of Chemical Physics* **1985**, 82 (1), 284-298.
- (16) Elleuchi, S.; Ortiz de Luzuriaga, I.; Sanchez-Gonzalez, A. n.; Lopez, X.; Jarraya, K.; Calhorda, M. J.; Gil, A. Computational Studies on the Binding Preferences of Molybdenum (II) Phenanthroline Complexes with Duplex DNA. The Important Role of the Ancillary Ligands. *Inorganic Chemistry* **2020**, 59 (17), 12711-12721.
- (17) Beck, A. D. Density-functional thermochemistry. III. The role of exact exchange. *J. Chem. Phys* **1993**, 98 (7), 5648-5646.
- (18) Aboul-Gheit, A.; El-Desouki, D.; Abdel-Hamid, S.; Ghoneim, S.; Ibrahim, A.; Gad, F. Sulfated zirconia catalysts for low temperature isomerization of n-pentane. *Egypt. J. Chem* **2012**, 55 (5), 509-527.
- (19) Hattori, H.; Ono, Y. *Solid acid catalysis: from fundamentals to applications*; CRC Press, 2015.
- (20) Kirumakki, S. R.; Nagaraju, N.; Narayanan, S. A comparative esterification of benzyl alcohol with acetic acid over zeolites H $\beta$ , HY and HZSM5. *Applied Catalysis A: General* **2004**, 273 (1-2), 1-9.
- (21) Grecea, M. L.; Dimian, A. C.; Tanase, S.; Subbiah, V.; Rothenberg, G. Sulfated zirconia as a robust superacid catalyst for multiproduct fatty acid esterification. *Catalysis Science & Technology* **2012**, 2 (7), 1500-1506.
- (22) Saravanan, K.; Tyagi, B.; Bajaj, H. Esterification of caprylic acid with alcohol over nano-crystalline sulfated zirconia. *Journal of sol-gel science and technology* **2012**, 62 (1), 13-17.
- (23) Yu, G.; Qiu, M.; Wang, T.; Ge, L.; Chen, X.; Wei, W. Optimization of the pore structure and acidity of SAPO-11 for highly efficient hydroisomerization on the long-chain alkane. *Microporous and Mesoporous Materials* **2021**, 320, 111076.
- (24) Griffe, B.; Sierraalta, A.; Brito, J. L. Theoretical study of the water effect on CO adsorbed over Au/SAPO-11 catalysts. *Journal of Computational Methods in Sciences and Engineering* **2009**, 9 (4-6), 281-287.

- (25) Griffe, B.; Sierralta, A.; Brito, J. L. Theoretical study of the CO catalytic oxidation on Au/SAPO-11 zeolite. *International Journal of Quantum Chemistry* **2010**, *110* (13), 2573-2582.
- (26) Liu, B.; Wang, D.; Wang, Z.; Zhao, Z.; Chen, Y.; Lan, J. The structure and activity of potassium supported on SBA-15 molecular sieve: Density functional theory study. *Journal of Theoretical and Computational Chemistry* **2014**, *13* (01), 1350076.
- (27) Szczodrowski, K.; Prélôt, B.; Lantenois, S.; Douillard, J.-M.; Zajac, J. Effect of heteroatom doping on surface acidity and hydrophilicity of Al, Ti, Zr-doped mesoporous SBA-15. *Microporous and mesoporous materials* **2009**, *124* (1-3), 84-93.
- (28) Hanwell, M. D.; Curtis, D. E.; Lonie, D. C.; Vandermeersch, T.; Zurek, E.; Hutchison, G. R. Avogadro: an advanced semantic chemical editor, visualization, and analysis platform. *Journal of cheminformatics* **2012**, *4* (1), 1-17.
- (29) Hofmann, A.; Sauer, J. Surface structure of hydroxylated and sulfated zirconia. A periodic density-functional study. *The Journal of Physical Chemistry B* **2004**, *108* (38), 14652-14662.
- (30) Hong, Z.; Fogash, K.; Watwe, R.; Kim, B.; Masqueda-Jimenez, B.; Natal-Santiago, M.; Hill, J.; Dumesic, J. Experimental and DFT studies of initiation processes for butane isomerization over sulfated-zirconia catalysts. *Journal of Catalysis* **1998**, *178* (2), 489-498.
- (31) Haase, F.; Sauer, J. The surface structure of sulfated zirconia: periodic ab initio study of sulfuric acid adsorbed on ZrO<sub>2</sub> (101) and ZrO<sub>2</sub> (001). *Journal of the American Chemical Society* **1998**, *120* (51), 13503-13512.
- (32) Wang, Z.; Wang, D.; Zhao, Z.; Chen, Y.; Lan, J. A DFT study of the structural units in SBA-15 mesoporous molecular sieve. *Computational and Theoretical Chemistry* **2011**, *963* (2-3), 403-411.
- (33) Huo, H.; Peng, L.; Grey, C. P. Measuring Brønsted Acid Site O–H Distances in Zeolites HY and HZSM-5 with Low-Temperature 17O–1H Double Resonance MAS NMR Spectroscopy. *The Journal of Physical Chemistry C* **2011**, *115* (5), 2030-2037.
- (34) Kanougi, T.; Atoguchi, T.; Yao, S. Periodic density functional study of superacidity of sulfated zirconia. *Journal of Molecular Catalysis A: Chemical* **2002**, *177* (2), 289-298.

- (35) Hino, M.; Kurashige, M.; Matsubishi, H.; Arata, K. The surface structure of sulfated zirconia: Studies of XPS and thermal analysis. *Thermochimica acta* **2006**, *441* (1), 35-41.
- (36) Li, X.; Nagaoka, K.; Simon, L. J.; Olindo, R.; Lercher, J. A.; Hofmann, A.; Sauer, J. Oxidative activation of n-butane on sulfated zirconia. *Journal of the American Chemical Society* **2005**, *127* (46), 16159-16166.
- (37) Wang, P.; Wang, S.; Yang, C.; Li, C.; Bao, X. Effect of aluminum addition and surface moisture content on the catalytic activity of sulfated zirconia in n-butane isomerization. *Industrial & Engineering Chemistry Research* **2019**, *58* (32), 14638-14645.

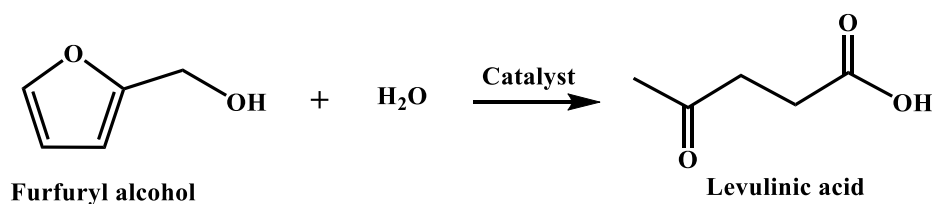
# **Chapter 5**

## **Hydrolysis of furfuryl alcohol to produce levulinic acid**



## 5.1 Introduction

The economic recovery post-pandemic has increased the level of energy consumption and on the bright side, the global demand for biofuels is set to elevate by 28% from 2021 to 2026 as reported by the International Energy Agency (IAE) <sup>1</sup>. Importantly, employing biobased speciality chemicals, fuels, and fuel additives for any required sector would reduce the burden on fossil-based fuels. Additionally, government policies are revised due to the rise in environmental concerns as well as the necessity of self-reliance in energy sectors. The scientific community is contributing immensely towards the goal of achieving renewable carbon-neutral technology by utilizing biobased feedstocks to get hydrogen, fuels/fuel additives, platform/intermediate chemicals alternative to petrochemicals. Lignocellulosic biomass offers different platform chemicals that can be transformed into various multifunctional intermediates and value-added chemicals that would promote the biorefinery industry <sup>2,3</sup>. Furfuryl alcohol (FA) is one such intermediate obtained from the hydrogenation of furfural, which has enormous application in the synthesis of chemicals used as solvents, biofuel, plasticizers, thermostatic resins, pharmaceuticals, polymers, flavoring, and fragrancng agents, etc <sup>4 5</sup>. Hydrolyzing FA with the aid of a solid acid catalyst yields levulinic acid (LA) (Scheme 5.1) which itself is one of the most important platform chemicals.



**Scheme 5.1** Hydrolysis of furfuryl alcohol to produce levulinic acid

LA (also called  $\gamma$ -ketovaleric acid) can be obtained from two routes *viz.* cellulose route via hydroxymethylfurfural (HMF) and hemicellulose route via furfuryl alcohol <sup>6</sup>. LA is used in the synthesis of chemicals such as alkyl levulinate, angelica lactone, tetrahydrofuran,  $\gamma$ -valerolactone, 5-bromolevulinic acid, 1,4-pentanediol, methyl butanediol, 2-methyltetrahydrofuran, and pyrrolidinones <sup>7,8</sup>. These chemicals have applications as solvents, detergents, plasticizers, pharmaceuticals, fuel additives, polymers, resins, etc. Owing to its vast applications, the choice of the synthesis route

becomes important during commercial production. The cellulose route mainly used to produce bioethanol and HMF. LA can be produced from cellulose route via HMF. However, presently HMF is more expensive than LA. Hence, we chose the economically viable pathway, where FA is used as a starting material (hemicellulose route). FA hydrolysis is a Brönsted acid-catalyzed reaction, but FA is prone to polymerization in an acidic reaction medium or at elevated temperatures. To avoid this process that curbs the catalyst performance, several strategies (to reduce the degree of polymerization) such as burning off the adsorbed species by calcination, lowering the reaction temperature, reducing the FA concentration, or the addition of the second reactant (or substrate) in excess can be employed<sup>9</sup>. These approaches can be used if the material has a good thermal stability, the reaction is feasible at a lower operating temperature, or the active site availability is huge which would reduce the impact of the effect of dilution. Importantly, it is recommended to use a solvent for this transformation to achieve homogeneity in the reaction as well as to address the polymerization issue as FA and water are immiscible. Also, in the absence of a solvent, due to the lack of homogeneity, the polymerization of FA occurs to such a high degree that the reaction mixture solidifies within a few minutes of the reaction (<15 mins). Hence, the choice of the solvent, catalyst system, reactor setup, and operating conditions become crucial to tackle this major challenge, and therefore this reaction is reported in a very few literatures. M. A. Mellmer et al. studied various catalyst systems such as zeolites (H-ZSM-5, H-mordenite, H-ferrierite, H-Beta), ion-exchange resins (amberlyst-70, nafion SAC-13), mineral acid (sulfuric acid), silica-alumina, sulfonated carbon with different physicochemical properties<sup>6</sup>. HZSM-5 showed >70% LA yield, however, they reported a high rate of polymerization in the first recycle which was solved by calcining the spent catalyst. I. Guzman et al. have also screened a series of solid acid catalysts *viz.* HZSM-5, hydrated phosphotungstic acid, sulfated zirconia, and amberlyst-35, etc among which HZSM-5 showed 58% LA yield under optimized reaction conditions<sup>10</sup>. In another report, ArSO<sub>3</sub>H-Et-HNS (alkyl-bridged organosilica nanosphere) catalyst is reported to yield 80% of LA<sup>11</sup>. Another catalyst, SO<sub>3</sub>H-functionalized silica nanoflowers (SiNFeSO<sub>3</sub>H) showed 90% LA yield in 2.5 h under pressurized reaction conditions, but the catalytic activity was found to decrease upon recyclability<sup>12</sup>. Also, modified zeolites



(dealuminated ZSM-5, CoZSM-5) catalysts are reported for this transformation with moderate yields<sup>13</sup>. Various solvents such as acetone, tetrahydrofuran, dioxane, methyl ethyl ketone, cyclopentylmethyl ether,  $\gamma$ -valerolactone, acetonitrile, dimethyl sulfoxide, etc were employed for the studies in the aforementioned literatures.

The reported studies performed for this transformation, employ a high amount of catalyst<sup>6,12</sup>, and also some catalysts have failed to retain their catalytic activity upon recycling<sup>10,11,12,13</sup>. A few literatures reported the operation of the reaction in high-pressure autoclave reactor set up<sup>10,11,12</sup>. Some of the reported solvents are mostly lower boiling compounds which might compromise the homogeneity in the reaction mixture and additionally cause the polymerization of furfuryl alcohol<sup>6,11,13</sup>. A proper investigation of a suitable solvent system is necessary that would help in the reduction of the humin formation thereby increasing the selectivity towards LA.

As hydrolysis involves water as a substrate, we aim to design a high-performance Brønsted acid catalyst, that is water-stable and can be operated in a simple reactor system to obtain a high LA yield. Sulfonic acid moieties as active site species have shown competitive LA yield suggesting that employing such types of active sites would be beneficial<sup>11,12</sup>. Hence, in this work, we choose a scarcely studied flexible metal-organic framework (MOF) called BUT-8(Cr)-SO<sub>3</sub>H which is post-synthetically functionalized by sulfonic acid moiety for the efficient conversion of FA to LA. MOFs are porous, crystalline synthetic materials formed by the aggregation of organic linkers and metal clusters yielding an ordered framework<sup>14</sup>. MOFs find applications in various fields such as heterogeneous catalysis<sup>15,16</sup>, bioremediation<sup>17</sup>, chemical sensors<sup>18</sup>, proton conductivity<sup>19</sup>, hydrogen economy<sup>20</sup>, gas storage, and separation<sup>21</sup>. The physicochemical properties of BUT-8(Cr)-SO<sub>3</sub>H MOF along with other conventional catalysts were studied and correlated with their respective catalytic activities. The catalyst was well characterized by powder XRD, FTIR, NH<sub>3</sub>-TPD, Acid-base titration measurements, SEM, TEM, and TGA.

## 5.2 Chemicals and reagents

HZSM-5 (SAR 23) and amberlyst-15 were supplied by Zeolyst International and Alfa-Aesar respectively. Furfuryl alcohol, levulinic acid, H<sub>2</sub>SO<sub>4</sub>, HF, and HCl were purchased from Merck India Pvt. Ltd. DMF and diglyme were purchased from Avra Synthesis Pvt Ltd. 2,6-naphthalenedicarboxylic acid and chromium (III) nitrate were obtained from TCI and SRL respectively. Oleum was provided by Sd Fine-chem Limited.

## 5.3 Catalyst preparation

2,6-naphthalenedicarboxylic acid (NapDC) linker (30 g) was treated with oleum (100 mL) and the mixture of the solution was magnetically stirred for 24 h in an oil bath maintained at 140 °C as per the reported procedure<sup>22</sup>. After cooling, the oleum-treated linker was washed thoroughly by subjecting it to repeated dissolution and precipitation processes using distilled water and HCl respectively to remove the residues of the oleum. The modified linker thus obtained was dried overnight at 120 °C to produce modified linker (4,8-disulfonyl-2,6-naphthalenedicarboxylic acid). Further, the modified linker (3.76 g), Cr(NO<sub>3</sub>)<sub>3</sub>·9H<sub>2</sub>O (4 g), with DMF (60 mL) as solvent were homogenized for 30 mins in a sonication bath. The solution was transferred to a teflon-lined stainless steel autoclave and a modulator, HF (1.1 mL) was added to it. The autoclave was then placed in an oven for 24 h maintained at 190 °C for the solvothermal synthesis of MOF. Once cooled, DMF was added to the material and the MOF (green powder) was collected using a glass pipette from the suspension of the solution thus formed. The unwanted bright green crystals settled at the bottom were discarded. For the purification of the material, the MOF was soaked in DMF and placed in an oven maintained at 80°C for 24 h and then in distilled water at room temperature for 24 h. The material thus obtained was washed using methanol and dried at 60 °C for 12 h under a vacuum. The MOF was further soaked in 2M H<sub>2</sub>SO<sub>4</sub> for 24 h and washed with methanol and finally activated at 60 °C for 24 h under vacuum to produce BUT-8(Cr)-SO<sub>3</sub>H.

## 5.4 Catalytic activity study

In a typical procedure, the hydrolysis of FA was performed in a sealed tube glass reactor where a calculated amount of molar composition of FA, H<sub>2</sub>O, and solvent was added. To this mixture of reactants, the catalyst (in weight % with respect to the FA and H<sub>2</sub>O) was added and the reactor is placed in an oil bath maintained at a certain temperature, and for desired time the reaction mixture is magnetically stirred. The reaction mixture was quantitatively analyzed employing gas chromatography (Shimadzu GC–2014, Shimadzu 00411–Serial number: C121652). It was equipped with DB–Wax as a capillary column (30 m x 0.25 mm x 2.5 μm) and a flame ionization detector. The products were confirmed by Gas chromatography Mass Spectrometry (GCMS). The FA conversion and LA selectivity were determined by the GC.

$$C_{FA}(\%) = \frac{X_{(i)} - X_{(f)}}{X_{(i)}} \times 100$$

$$S_{LA}(\%) = \frac{P_{LA}}{X_{(i)} - X_{(f)}} \times 100$$

$$Y_{LA}(\%) = \frac{P_{LA}}{X_{(i)}} \times 100$$

where  $C_{FA}$  and  $S_{LA}$  are FA conversion and LA selectivity respectively.  $X_{(i)}$  and  $X_{(f)}$  correspond to the initial and final moles of the FA respectively.  $P_{LA}$  and  $Y_{LA}$  are moles of the LA formed and LA yield respectively.

## 5.5 Catalyst characterization–Results and discussion

### 5.5.1 Powder X–ray diffraction

The X–ray diffractograms of HZSM–5 (SAR23) and BUT–8(Cr)–SO<sub>3</sub>H MOF matched well with their respective standard patterns as per the reported literature<sup>23,24</sup>. The characteristic peaks appearing at  $2\theta$  of 7.0, 11.2, 13.2, 18.2, and 20.3° in the PXRD pattern of BUT–8(Cr)–SO<sub>3</sub>H, correspond to the pattern of the reported MOF [figure 5.1 (a)]. Upon post–synthetic modification by H<sub>2</sub>SO<sub>4</sub> treatment, there were no new peaks detected suggesting that the structural integrity of the material was preserved without any loss in the crystallinity. In the case of HZSM–5, the XRD diffractogram with major peaks

of  $2\theta$  present at 13, 23, and  $45^\circ$  matched well with the characteristic pattern of the MFI framework [figure 5.1 (b)].

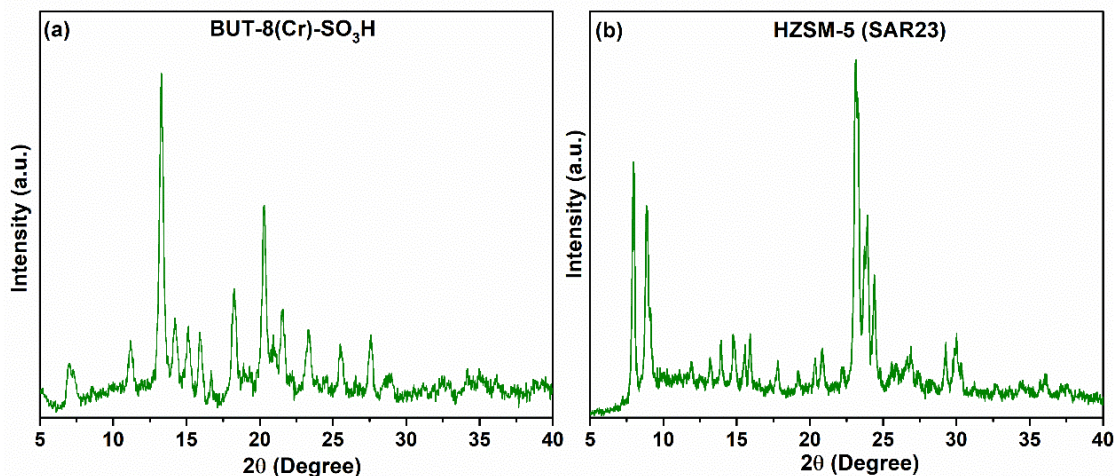


**Figure 5.1.** XRD patterns of (a) BUT-8(Cr)-SO<sub>3</sub>H, (b) HZSM-5 (SAR23)

### 5.5.2 FTIR spectroscopy

The characteristic peaks of the -SO<sub>3</sub>H moiety of BUT-8(Cr)-SO<sub>3</sub>H lie in the range of 1000 to 1250 cm<sup>-1</sup> in the FTIR spectrum as depicted in figure 5.2. The peaks of symmetric and asymmetric stretching modes of O=S=O species reflect at 1196 cm<sup>-1</sup> and 1242 cm<sup>-1</sup> respectively. The peak present at 1038 cm<sup>-1</sup> corresponds to the S-O species. The peaks at 618 and 667 cm<sup>-1</sup> correspond to the C-S and Cr-O bonds respectively. The C=O bond of carboxylate and C=C bond of the naphthalene correspondingly appear at 1633 and 1419 cm<sup>-1</sup>. A broad peak existing around 3500 cm<sup>-1</sup> in the spectrum is ascribed to the -OH group.

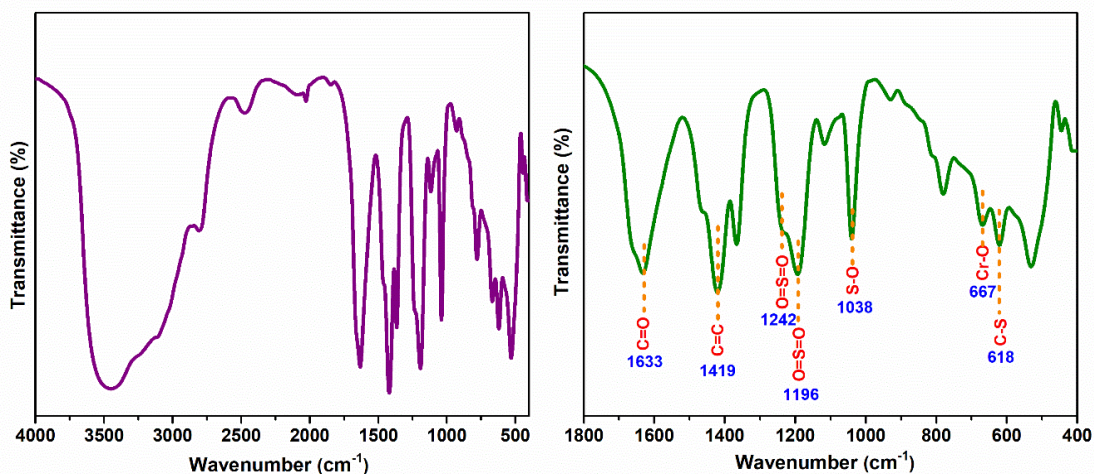


**Figure 5.2.** FTIR spectrum of BUT-8(Cr)-SO<sub>3</sub>H

### 5.5.3 Thermogravimetric analysis

Thermogravimetric analysis profile of BUT-8(Cr)-SO<sub>3</sub>H as provided in figure 5.3 reveals that the maximum thermal stability of the MOF is ~300 °C. The weight loss at the first decomposition step (30 to 320 °C) is due to the removal of moisture. Above 320 °C, the second decomposition step occurs with a weight loss of 40% indicating the disintegration of the linker thereby collapsing the framework of MOF. Additionally, the DTA (differential thermal analysis) curve suggests that the initial weight loss step below 300 °C can be attributed to the removal of one particular type of species (moisture) from the hydrophilic pores of the catalyst.

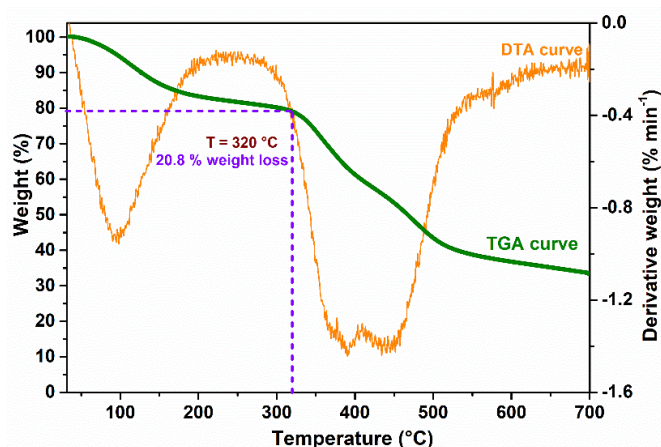


**Figure 5.3.** TGA profile of BUT-8(Cr)-SO<sub>3</sub>H MOF

### 5.5.4 Temperature programmed desorption

The acidity of BUT-8(Cr)-SO<sub>3</sub>H was obtained using NH<sub>3</sub>-TPD by employing a new methodology developed for the materials with moderate thermal stability. When the sample is subjected to analysis with and without NH<sub>3</sub> (probe molecule), the resulting difference in the value yields the amount of acidity obtained exclusively due to NH<sub>3</sub> chemisorption meanwhile eliminating the thermal decomposition peaks. The amount of acidity of BUT-8(Cr)-SO<sub>3</sub>H MOF with moderate thermal stability (~ 300 °C) was 1.65 mmol g<sup>-1</sup> [Table 5.1 and figure 5.4 (a)]. This was confirmed using the acid-base titration method which revealed the acidity of the MOF to be 1.8 mmol g<sup>-1</sup>. The amount of acidity of HZSM-5 (SAR23) was 1.06 mmol g<sup>-1</sup> and exhibited a typical NH<sub>3</sub>-TPD profile of HZSM-5 zeolite [Table 5.1 and figure 5.4 (b)].

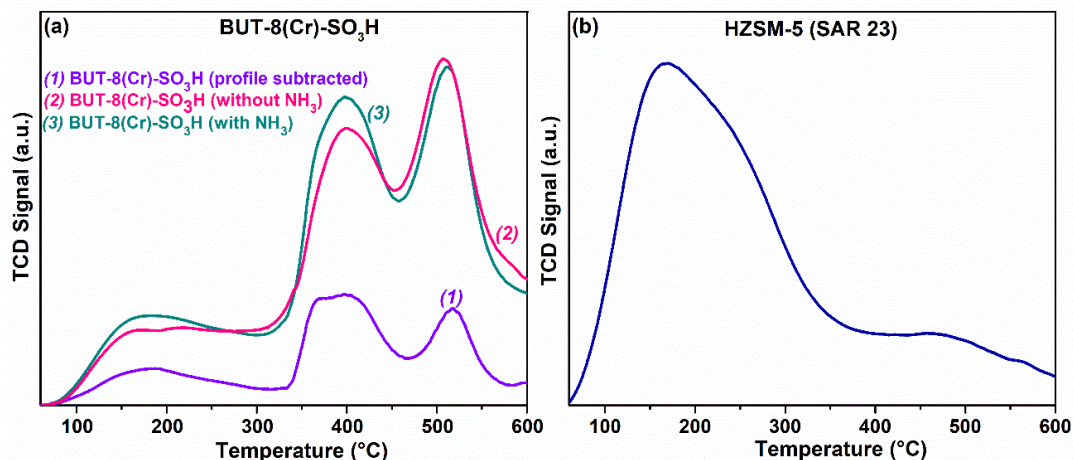


**Figure 5.4.** NH<sub>3</sub>-TPD profiles of (a) BUT-8(Cr)-SO<sub>3</sub>H and (b) HZSM-5 (SAR23)

### 5.5.5. Microscopic techniques

SEM analysis of BUT-8(Cr)-SO<sub>3</sub>H was performed to obtain the morphological and particle size. The micrographs disclosed the presence of numerous nanofibres with an average fiber length of 85 nm [figure 5.5(a)]. TEM image exhibited nanofibres with an average fiber width of 28 nm as presented in figure 5.5(b).

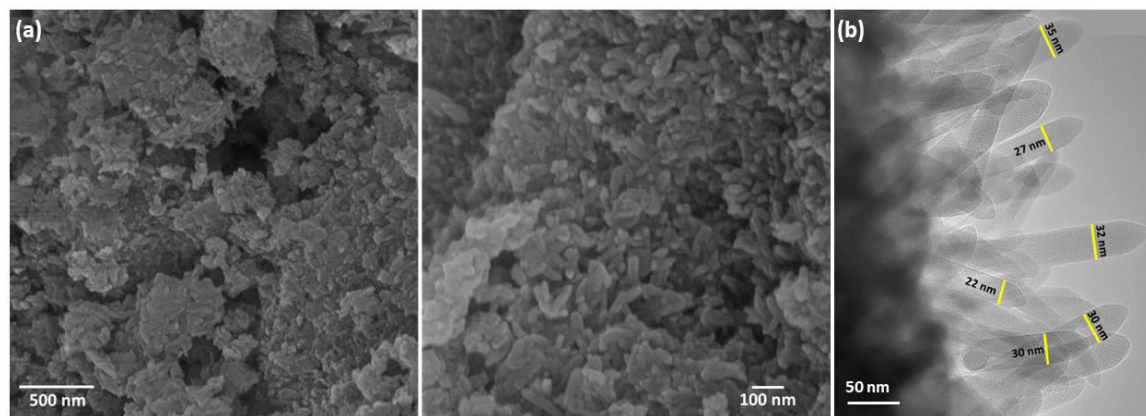


**Figure 5.5.** (a) SEM and (b) TEM images of BUT-8(Cr)-SO<sub>3</sub>H

## 5.6 Catalytic activity study

### 5.6.1 Catalyst screening and comparison

Selective synthesis of LA from FA via hydrolysis was evaluated using acid catalysts as there is a requirement of strong acid sites specifically, Brønsted acid sites for the efficient conversion of FA. Therefore, conventional solid acid catalysts such as ZSM-5 and amberlyst-15 along with a Brønsted acidic MOF, BUT-8(Cr)-SO<sub>3</sub>H were initially screened in order to discover the type and nature of acid sites required to get high LA

yield and to correlate their catalytic performance with the physicochemical properties of the material. A blank reaction was performed to check the influence of temperature (at 100 °C) in the absence of a catalyst. The study revealed that the reaction is a catalytically driven one and the transformation of FA to LA is negligible in the absence of a catalyst. Figure 5.6 presents the catalytic performance of ZSM-5, amberlyst-15, and BUT-8(Cr)-SO<sub>3</sub>H on FA hydrolysis to produce LA at 100 °C for 1h with 6 wt% catalyst with respect to total reactant weight. As FA and H<sub>2</sub>O are immiscible in nature, a polar aprotic solvent, diglyme with a high boiling point of 162 °C is chosen with the mole ratio FA: H<sub>2</sub>O: diglyme of 1:20:20. Polar protic solvents such as alkyl alcohols, mild acids would let FA undergo different reaction route to produce different products such as alkyl levulinates, furfuryl acetate, etc. Hence, polar aprotic solvent diglyme is used to avoid polymerization of FA. The FA conversion in the case of amberlyst-15 and BUT-8(Cr)-SO<sub>3</sub>H was high with 99 and 97 % respectively. The selectivity towards LA was high for amberlyst-15 (92%) and the MOF (80%) along with 4,5,5-trihydroxypentan-2-one as side product (8 to 15%). HZSM-5 (SAR23) performed poorly and demonstrated very low FA conversion (~1.3%) though the LA selectivity (>99%) was high.

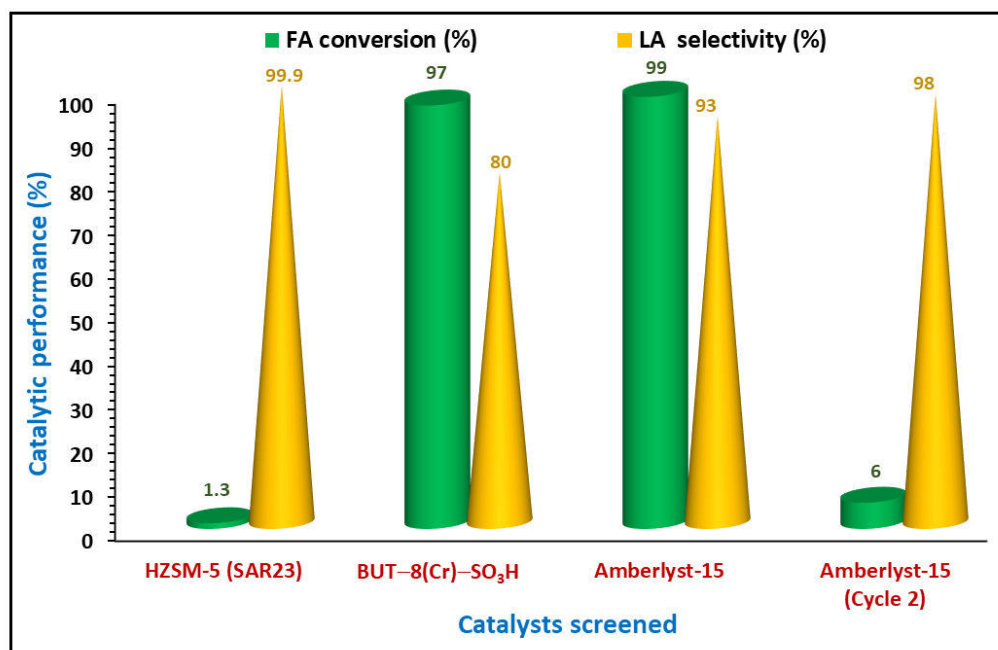


**Figure 5.6.** Catalyst screening. Reaction conditions: temperature-100 °C, cat conc-6wt%, FA: H<sub>2</sub>O: diglyme-1:20:20, time-1 h

The trend in terms of decreasing LA yield is in the order of amberlyst-15 > BUT-8(Cr)-SO<sub>3</sub>H > HZSM-5 (SAR23) indicating that the sulfonic acid moieties as active sites are responsible for better catalytic activity over the Al-Brönsted acid sites of the zeolites (Table 5.1). Importantly, the total amount of acidity has played a vital role in enhancing the yield towards LA as both amberlyst-15 and BUT-8(Cr)-SO<sub>3</sub>H owned 4.7 and 1.8 mmol g<sup>-1</sup> of acidity respectively which is quite higher than the acidity (1.01 mmol g<sup>-1</sup>) of HZSM-5 (SAR23). The better catalytic performance of amberlyst-15 catalyst can be ascribed to the higher number of Brönsted acidity present in it and yet could not be regenerated appreciably resulting in a drop of conversion level to 6% upon one recycle itself (figure 5.6). Hence, the best potential catalyst among the three, a flexible Brönsted acidic BUT-8(Cr)-SO<sub>3</sub>H was chosen to further explore the effect of reaction conditions.

**Table 5.1.** Acidity and catalytic performance of the solid acid catalysts

Catalyst	Acidity (mmol g <sup>-1</sup> )	Catalytic activity (%) <sup>[c]</sup>		
		FA conversion	LA selectivity	LA yield
BUT-8(Cr)-SO <sub>3</sub> H	1.65 <sup>[a]</sup> 1.8 <sup>[b]</sup>	97.5	80.6	78.6
Amberlyst-15	4.7 <sup>[b]</sup>	99.9	92.8	92.8
HZSM-5 (SAR23)	1.06 <sup>[a]</sup>	1.3	99.9	1.2

[a] NH<sub>3</sub>-TPD, [b] Acid-base titration, [c] Catalyst screening-reaction conditions: temperature-100 °C, catalyst wt-6 wt%, reactants mole ratio (FA: H<sub>2</sub>O: diglyme)-1:20:20, time-1 h

## 5.6.2 Influence of reaction conditions

### Effect of reaction temperature

As the operating temperature has significant control over the polymerization of FA, an appropriate temperature is needed to inhibit humin formation and also to get a better catalytic activity. A temperature study was carried out with temperatures ranging from 80 to 120°C as depicted in figure 5.7 (a). For every 10° C increment from 80°C to 100 °C, the FA conversion increased by ~8 %. With further increase in temperature to 110 and 120°C, there was a minor increase in FA conversion (1% per 10 °C). The temperature change had a similar effect on LA selectivity which increased from 65 to 80 % with an increase in temperature from 80 to 100 °C. Further increase to 110 °C decreased the selectivity to 75% and remained the same thereafter. This study revealed that 100 °C was



the optimized reaction temperature to get high conversion of 97.5% with selectivity of 80.6% for LA.

### **Effect of reactants mole ratio**

Optimization of the reactant mole ratio of FA and H<sub>2</sub>O from 1:10 to 1:35 was performed at 100°C and 6 wt% catalyst loading without change in the concentration of solvent diglyme. Initially at 1:10 mole ratio, the FA conversion was 85% which subsequently increased to 91% and 97% for 1:15 and 1:20 mole ratios respectively. Further increase in H<sub>2</sub>O concentration to 1:25 (94.7%), 1:30 (89.4%), and 1:35 (78.5%) decreased the FA conversion gradually probably due to enhanced dilution of the reaction mixture with H<sub>2</sub>O. In the case of LA selectivity, the change in the mole ratio did not have any drastic impact and the overall difference in the LA selectivity was ~6%. Therefore, the best LA yield of 78% was for the reactant mole ratio of 1:20:20 for FA: H<sub>2</sub>O: diglyme as presented in figure 5.7 (b).

### **Effect of catalyst loading**

The effect of catalyst concentration towards the LA production from FA was investigated by loading different amounts of BUT-8(Cr)-SO<sub>3</sub>H catalyst from 2 to 8 wt% (with respect to concentration of total reactants) as shown in figure 5.7 (c). With an increase in catalyst loading from 2 to 3 wt% and later to 4 wt%, there was a proportional increase in both the FA conversion and LA selectivity. There was a dramatic increase in FA conversion (60 to 76 %) and LA selectivity (56 to 70%) with an increase in catalyst loading from 2 to 3 wt%. The major side product in the reaction was found to be 4,5,5-trihydroxypentan-2-one. Further increase in the catalyst loading to 4 wt%, the FA conversion and LA selectivity increased to 83 and 80 % respectively. At 6 wt% catalyst loading, the FA conversion increased to 97 %, while the LA selectivity remained the same. Above 6 wt%, there was a slow increase in FA conversion (~0.6%) with the LA selectivity remaining constant (80.7 %). Hence, the lower catalyst loading of 6 wt% which gave a 78% LA yield was chosen for further studies. The optimized reaction conditions obtained by the investigation done on the influence of reaction conditions over BUT-8(Cr)-SO<sub>3</sub>H MOF is 1:20 reactant mole ratio (FA: H<sub>2</sub>O), 100°C temperature, and 6 wt% catalyst loading.

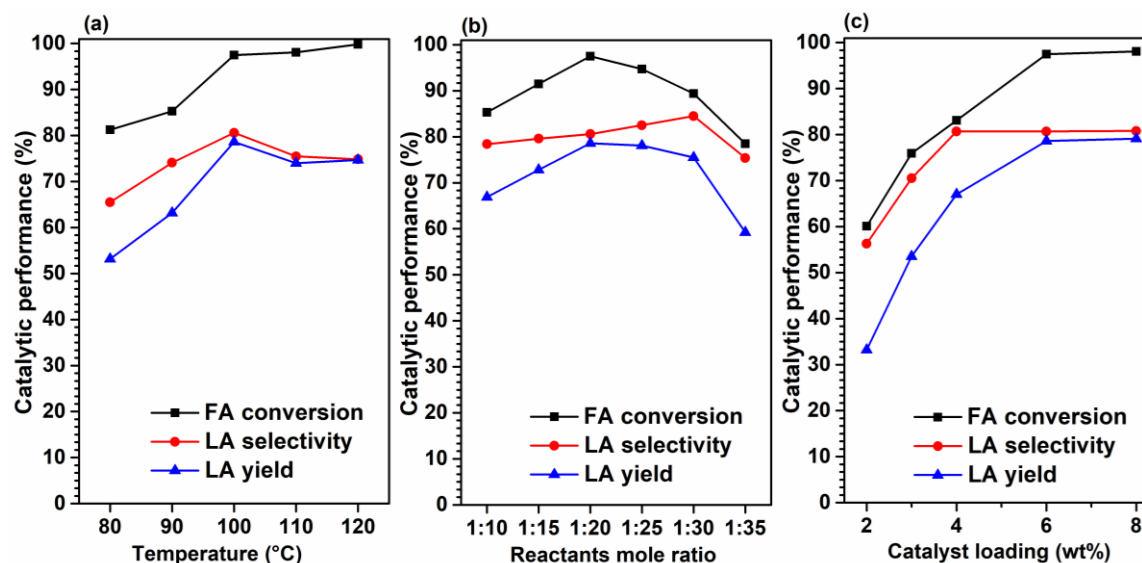


**Figure 5.7.** Influence of reaction conditions. **(a)** Effect of reaction temperature: catalyst concentration–6wt%, FA:H<sub>2</sub>O:diglyme–1:20:20, time–1 h. **(b)** Effect of reactants mole ratio (FA: H<sub>2</sub>O): Catalyst concentration–6wt%, temperature–100 °C, time–1 h. **(c)** Effect of catalyst loading: Reaction conditions: FA:H<sub>2</sub>O: diglyme–1:20:20, temperature–100 °C, time–1 h.

### Effect of solvent and solvent concentration

The reactants (FA and H<sub>2</sub>O) are immiscible with each other and this lack of homogeneity would hinder the selectivity towards LA and cause the polymerization of FA as well. Therefore, an investigation on the addition of appropriate polar aprotic solvents was performed as most polar protic solvents like alkyl alcohols or carboxylic acids are not inert in this reaction. Different polar aprotic solvents such as DMF, DMSO, diglyme, dioxane, THF, and acetone were screened at optimized reaction conditions that offer miscibility for reaction mixtures. With the use of DMF and DMSO solvents, the catalyst showed no activity at all probably due to their basic nature which might have poisoned the acid sites of the catalyst. The order of the increase in the levulinic acid yield with respect to solvents is THF (31%) < acetone (42 %) < dioxane (67 %) < and diglyme (78 %) as presented in figure 5.8 (a). The LA selectivity for diglyme, dioxane, and acetone was 80, 68, and 41 % respectively with > 97 % FA conversion. When THF was employed as a solvent, the FA conversion (82 %) and LA selectivity (38 %) were low. Overall, the solvents with a lower boiling point [acetone (56 °C) and THF (66 °C)] performed poorly than the solvent with higher boiling points [dioxane (101 °C) and

diglyme (162 °C)]. The Lower LA yield for low boiling solvents (< 100 °C) could be because of the vaporization of solvent in the sealed pressure tube reaction at 100 °C reaction with high boiling reactants thereby decreasing the miscibility of FA and water. This phenomenon could be subsided for the solvents with a higher boiling point (diglyme and dioxane), thereby achieving better catalytic yield. With FA: H<sub>2</sub>O mole ratio of 1:20, the diglyme concentration was varied from 10 to 30 moles with reference to FA. When the mole composition of FA: H<sub>2</sub>O: Diglyme was 1:20:10, the FA conversion and LA selectivity were 98 and 85 % respectively, which increased by ~1% (FA conversion) and ~2% (LA selectivity) with an increase in diglyme concentration by 5 moles. Above, 1:20:15, there was a marginal decrease in overall LA yield from 87 % to 78 –76 % (1:20:20, 1:20:30) which could be due to the dilution effect. The highest LA selectivity of 86.6% with 99% FA conversion at FA: H<sub>2</sub>O: diglyme mole ratio of 1:20:15 was chosen as the optimized composition for further studies.

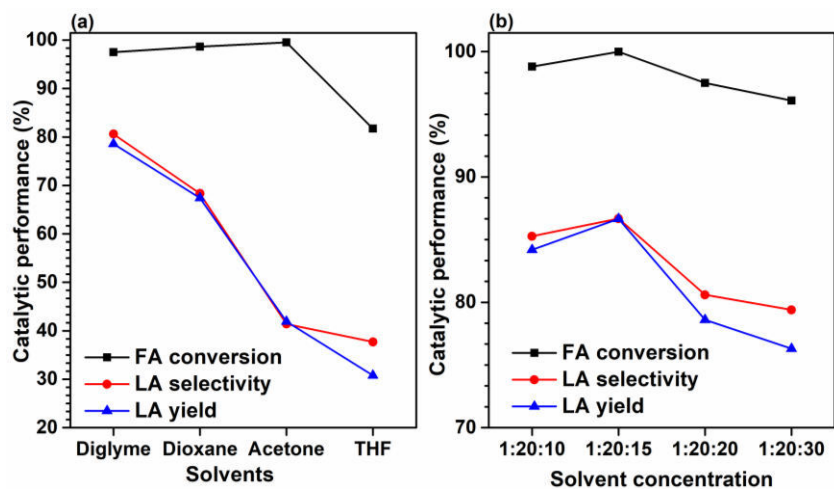


**Figure 5.8.** (a) Effect of solvent. Reaction condition: temperature–100°C, cat conc–6wt%, FA:H<sub>2</sub>O:solvent–1:20:20, time–1 h. (b) Effect of solvent concentration. Reaction condition: temperature–100°C, cat conc–6wt%, FA:H<sub>2</sub>O–1:20, time–1 h

### 5.6.3 Catalyst recyclability study

The reusability capability of the catalyst that validates the material stability was assessed over four successive cycles at the optimized reaction condition (temperature–100°C, cat conc– 6wt%, FA: H<sub>2</sub>O: diglyme–1:20:15, time–1 h). The spent catalyst was recovered by centrifugation and was further subjected to thorough washing using acetone before its activation under a vacuum (60°C for 12 h). During each recycle, there was a negligible

decrease in LA selectivity (~1 %) with no effect on the FA conversion (>99 %) as summarized in figure 5.9. Overall, at the end of the fourth cycle, there was a marginal decrease of ~3.4% in LA selectivity. The catalyst BUT-8(Cr)-SO<sub>3</sub>H proved to perform well over successive cycles which might be due to the suitable selection of solvent as well as the chemical stability of the material offered against humins. The usage of solvent diglyme assisted in restraining the polymerization of FA thereby protecting the active sites from saturation by humins. Moreover, the sulfonic acid functionalization of the linker was performed prior to the synthesis of MOF which would essentially generate a strong bond between the carbon of the linker with the sulfur moiety. Also, the MOF was subjected to thorough washing using methanol which would remove all the physisorbed active site species thus avoiding the leaching phenomena.

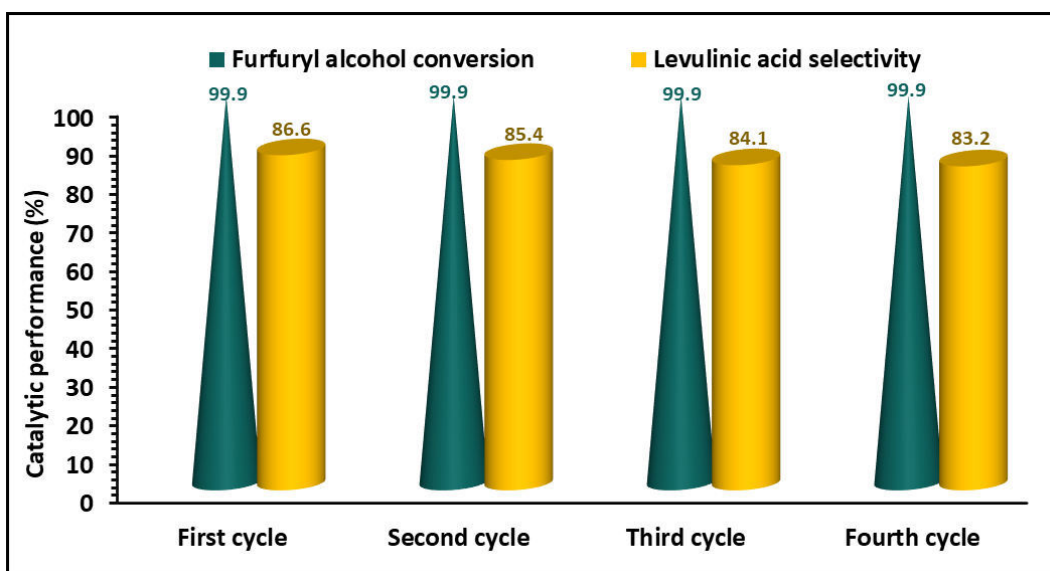


**Figure 5.9.** Catalyst recyclability study. Reaction conditions: temperature–100°C, cat conc–6wt%, FA:H<sub>2</sub>O:diglyme–1:20:15, time–1 h

#### 5.6.4 Time-resolved study

The impact of reaction time over a period of 3 h was evaluated using BUT-8(Cr)-SO<sub>3</sub>H under optimized reaction conditions. Initially, at 1 h, the FA conversion was >99% with 86% selectivity for LA. There was a slow progress in the LA selectivity with an increase in reaction time and at 2 h, the LA selectivity reached 92%. Further, increase in the time to 3 h, the LA selectivity increased to 98% and thereafter remained the same as presented in figure 5.10.

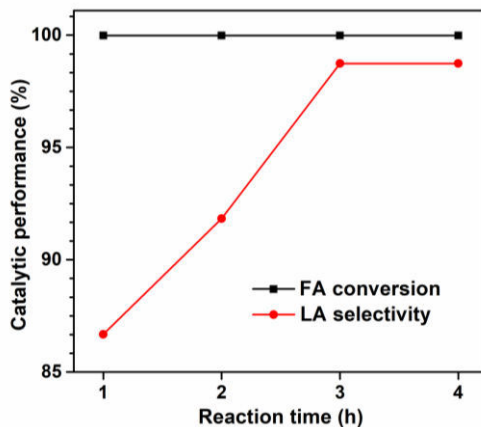
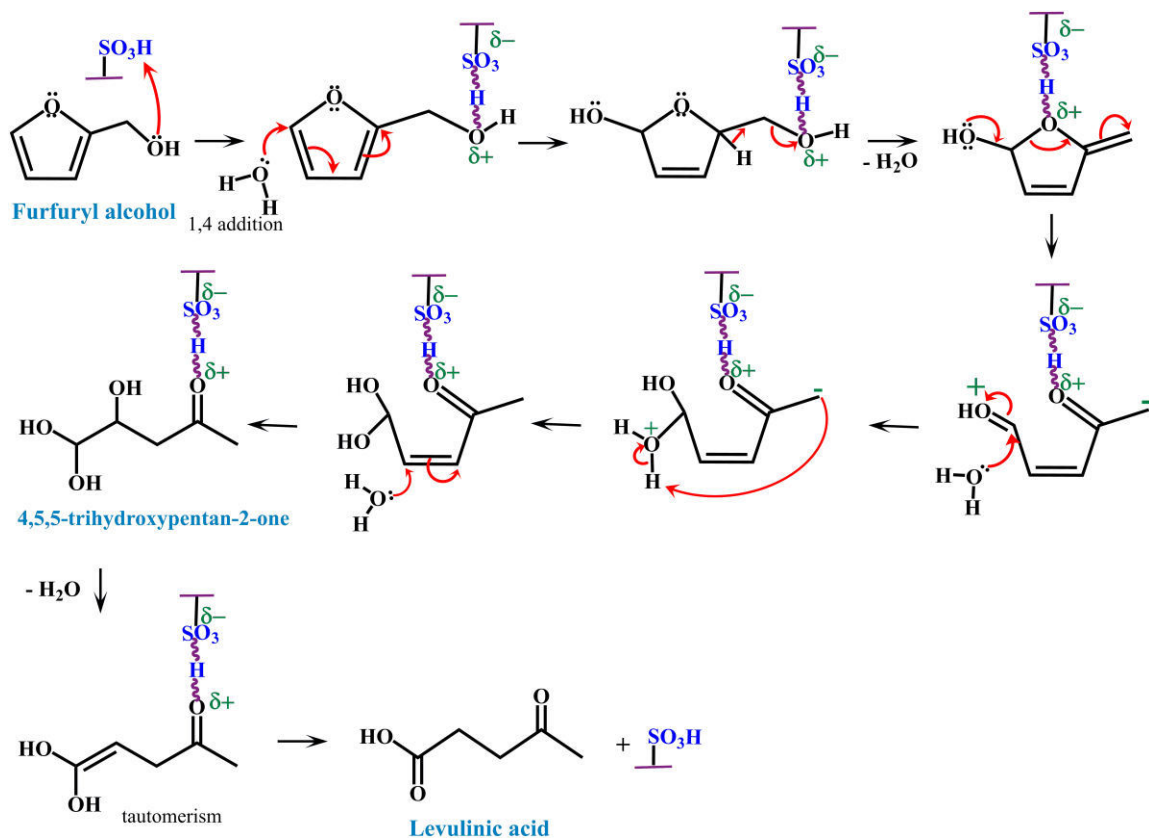


**Figure 5.10.** Time-resolved study. Reaction conditions: temperature=100 °C, cat conc=6wt%, FA:H<sub>2</sub>O:diglyme=1: 20: 15, time=3 h

### 5.7 Plausible reaction mechanism

The furfuryl alcohol hydrolysis to yield levulinic acid proceeds through an acid-catalyzed reaction with sulfonic acid moiety as an active site as depicted in the proposed pathway in Scheme 5.2.



**Scheme 5.2.** Plausible reaction mechanism for the levulinic acid synthesis over BUT-8(Cr)-SO<sub>3</sub>H MOF

Initially, protonation of FA by the Brönsted acidic site of MOF occurs followed by 1,4 addition of the secondary reactant H<sub>2</sub>O. Further, intramolecular rearrangement followed by the addition and removal of water occurs to produce an intermediate 4,5,5-trihydropentane-2-one. The intermediate undergoes keto-enol tautomerism upon removal of H<sub>2</sub>O to produce levulinic acid.

## 5.8 Comparison with literature results

The LA yields of various solid catalysts reported so far were compared with BUT-8(Cr)-SO<sub>3</sub>H catalyst and the reaction conditions along with the details of the recyclability study are presented in Table 5.2.

**Table 5.2.** Comparison of catalytic activity of BUT-8(Cr)-SO<sub>3</sub>H with various reported catalysts in the literature for hydrolysis of furfuryl alcohol to produce levulinic acid

Sn	Catalyst	Temp, catalyst conc, time	FA: H <sub>2</sub> O: solvent mole ratio	Reactor system	LA Yield (%)	Reusability cycles	Ref
1.	SiNFeSO <sub>3</sub> H	120 °C, 99wt %, 2.5h,	1: 55: 95 (GVL)	30 bar N <sub>2</sub> in HPA <sup>a</sup>	90	3C (decreased)	12
2.	ArSO <sub>3</sub> H-Et-HNS	120°C, 2h	1: 15: 15 (Acetone)	HPA <sup>a</sup>	83	3C (decreased)	11
3.	Dealuminate d HZSM-5 (SAR 23)	120 °C, 39 wt %, 0.5h	1: 18: 40 (Acetone)	Seal tube	76	3 C (decreased)	13
4.	HZSM-5 (SAR 23)	120 °C, 62 wt %, 0.5h	1: 9.3: 9.3 (THF)	Seal tube	74	2 C (Good)	6
5.	HZSM-5 (SAR 50)	140 °C, 9.8 wt %, 23 h	1: 5.6: 4.2 (MEK)	10 bar H <sub>2</sub> in HPA <sup>a</sup>	77	2 C (decreased)	10
6.	BUT-8(Cr)-SO <sub>3</sub> H	100 °C, 6 wt %, 3h	1: 20: 15 (Diglyme)	Seal tube	98	4C (good)	PW <sup>b</sup>

<sup>a</sup>high pressure autoclave, <sup>b</sup>present work

Catalyst BUT-8(Cr)-SO<sub>3</sub>H showed a remarkable performance by producing the highest LA yield among these reported catalysts. From the point of view of green chemistry principle, BUT-8(Cr)-SO<sub>3</sub>H catalyst performed exceptionally at the lower reaction

temperature, with a lower amount of catalyst and solvent, good recyclability, and also omitting the usage of a high-pressure reactor system. The catalyst has addressed all the drawbacks with reference to the reported literature and is the first metal-organic framework to show competitive results for the production of LA from FA.

## 5.9 Conclusions

MOFs being a new generation of materials are still startling scientists with their flexible material properties and promising catalytic activities in many important and challenging transformations. BUT-8(Cr)-SO<sub>3</sub>H is found to be an efficient heterogeneous catalyst in the hydrolysis of furfuryl alcohol to produce levulinic acid. It proved the exclusive requirement of the densely populated acidic sites (1.8 mmol/g) in its pores with good chemical and thermal stability for this reaction. There was no leaching of the active species and the material showed very good recyclability up to 4 cycles. From the approach of the green chemistry principles such as the usage of green solvent (diglyme), good reusability, lower catalyst concentration, and the reactants mole ratio, this flexible MOF, BUT-8(Cr)-SO<sub>3</sub>H, presents excellent catalytic performance for any -SO<sub>3</sub>H acid-driven catalytic reaction.

## 5.10 Bibliography

- (1) *International Energy Agency : Renewables* 2021. <https://www.iea.org/reports/renewables-2021> (accessed).
- (2) Šivec, R.; Grilc, M.; Huš, M.; Likozar, B. Multiscale modeling of (hemi) cellulose hydrolysis and cascade hydrotreatment of 5-hydroxymethylfurfural, furfural, and levulinic acid. *Industrial & Engineering Chemistry Research* **2019**, 58 (35), 16018-16032.
- (3) Wang, F.; Ouyang, D.; Zhou, Z.; Page, S. J.; Liu, D.; Zhao, X. Lignocellulosic biomass as sustainable feedstock and materials for power generation and energy storage. *Journal of Energy Chemistry* **2021**, 57, 247-280.
- (4) Iroegbu, A. O.; Hlangothi, S. P. Furfuryl alcohol a versatile, eco-sustainable compound in perspective. *Chemistry Africa* **2019**, 2 (2), 223-239.

- (5) Vaishnavi, B.; Sujith, S.; Kulal, N.; Manjunathan, P.; Shanbhag, G. V. Utilization of renewable resources: Investigation on role of active sites in zeolite catalyst for transformation of furfuryl alcohol into alkyl levulinate. *Molecular Catalysis* **2021**, *502*, 111361.
- (6) Mellmer, M. A.; Gallo, J. M. R.; Martin Alonso, D.; Dumesic, J. A. Selective production of levulinic acid from furfuryl alcohol in THF solvent systems over H-ZSM-5. *ACS Catalysis* **2015**, *5* (6), 3354-3359.
- (7) Hayes, G. C.; Becer, C. R. Levulinic acid: A sustainable platform chemical for novel polymer architectures. *Polymer Chemistry* **2020**, *11* (25), 4068-4077.
- (8) Signoretto, M.; Taghavi, S.; Ghedini, E.; Menegazzo, F. Catalytic production of levulinic acid (LA) from actual biomass. *Molecules* **2019**, *24* (15), 2760.
- (9) Vaishnavi, B.; Sujith, S.; Vaibhava, K. R.; Bhat, P. J.; Vetrivel, R.; Shanbhag, G. V. Selective synthesis of furfuryl acetate over solid acid catalysts and active site exploration using density functional theory. *Catalysis Science & Technology* **2022**.
- (10) Guzmán, I.; Heras, A.; Guemez, M.; Iriondo, A.; Cambra, J. F.; Requies, J. s. Levulinic acid production using solid-acid catalysis. *Industrial & Engineering Chemistry Research* **2016**, *55* (18), 5139-5144.
- (11) An, S.; Song, D.; Sun, Y.; Zhang, Q.; Zhang, P.; Guo, Y. Conversion of furfuryl alcohol to levulinic acid in aqueous solution catalyzed by shell thickness-controlled arenesulfonic acid-functionalized ethyl-bridged organosilica hollow nanospheres. *ACS Sustainable Chemistry & Engineering* **2018**, *6* (3), 3113-3123.
- (12) Wang, R.; Shen, F.; Tang, Y.; Guo, H.; Smith Jr, R. L.; Qi, X. Selective conversion of furfuryl alcohol to levulinic acid by SO<sub>3</sub>H-containing silica nanoflower in GVL/H<sub>2</sub>O system. *Renewable Energy* **2021**, *171*, 124-132.
- (13) Yan, P.; Wang, H.; Liao, Y.; Sun, P.; Wang, C. Introducing mesopore and regulating Al distribution for improving catalytic performances of ZSM-5 in furfuryl alcohol to levulinic acid. *Fuel* **2022**, *329*, 125213.
- (14) Zhou, H.-C.; Long, J. R.; Yaghi, O. M. Introduction to metal-organic frameworks. ACS Publications: 2012; Vol. 112, pp 673-674.
- (15) Yang, D.; Gates, B. C. Catalysis by metal organic frameworks: perspective and suggestions for future research. *Acs Catalysis* **2019**, *9* (3), 1779-1798.



- (16) Gong, W.; Liu, Y.; Li, H.; Cui, Y. Metal-organic frameworks as solid Brønsted acid catalysts for advanced organic transformations. *Coordination Chemistry Reviews* **2020**, *420*, 213400.
- (17) Ladole, M. R.; Pokale, P. B.; Patil, S. S.; Belokar, P. G.; Pandit, A. B. Laccase immobilized peroxidase mimicking magnetic metal organic frameworks for industrial dye degradation. *Bioresource Technology* **2020**, *317*, 124035.
- (18) DMello, M. E.; Sundaram, N. G.; Singh, A.; Singh, A. K.; Kalidindi, S. B. An amine functionalized zirconium metal–organic framework as an effective chemiresistive sensor for acidic gases. *Chemical communications* **2019**, *55* (3), 349-352.
- (19) Jiao, L.; Seow, J. Y. R.; Skinner, W. S.; Wang, Z. U.; Jiang, H.-L. Metal–organic frameworks: Structures and functional applications. *Materials Today* **2019**, *27*, 43-68.
- (20) Bakuru, V. R.; DMello, M. E.; Kalidindi, S. B. Metal-organic frameworks for hydrogen energy applications: advances and challenges. *ChemPhysChem* **2019**, *20* (10), 1177-1215.
- (21) Li, H.; Wang, K.; Sun, Y.; Lollar, C. T.; Li, J.; Zhou, H.-C. Recent advances in gas storage and separation using metal–organic frameworks. *Materials Today* **2018**, *21* (2), 108-121.
- (22) Yang, F.; Xu, G.; Dou, Y.; Wang, B.; Zhang, H.; Wu, H.; Zhou, W.; Li, J.-R.; Chen, B. A flexible metal–organic framework with a high density of sulfonic acid sites for proton conduction. *Nature Energy* **2017**, *2* (11), 877-883.
- (23) Jia, C.-J.; Liu, Y.; Schmidt, W.; Lu, A.-H.; Schüth, F. Small-sized HZSM-5 zeolite as highly active catalyst for gas phase dehydration of glycerol to acrolein. *Journal of Catalysis* **2010**, *269* (1), 71-79.
- (24) Dou, Y.; Zhang, H.; Zhou, A.; Yang, F.; Shu, L.; She, Y.; Li, J.-R. Highly efficient catalytic esterification in an– SO<sub>3</sub>H-functionalized Cr (III)-MOF. *Industrial & Engineering Chemistry Research* **2018**, *57* (25), 8388-8395.



# **Chapter 6**

## **Ethyl levulinate synthesis from furfuryl alcohol/ levulinic acid and ethanol**



## 6.1 Introduction

Climate change is one of the rising global issues apart from poverty, malnourishment, hunger, war, pollution, health care, etc. The Intergovernmental Panel on Climate Change (IPCC), a body of the United Nations reported that there are evidences of some irreversible damages done to the earth due to anthropogenic activities where some are burning of fossil fuels resulting in emissions of greenhouse gases, deforestation, livestock farming, etc. Among major contributors such as energy and transport sectors has a fair share of contaminating the environment. The various alternatives that help in mitigating climate change and improving environmental health are hydrogen, nuclear power, solar Energy, wind energy, hydroelectric energy, biomass, and geothermal energy. The renewable, non-fossil fuel resource which can be used as an energy source as well as for the synthesis of fuel, fuel additives, and chemicals is biomass. Valorization of biomass or biomass-derived platform chemicals improves the CO<sub>2</sub> balance by 30%<sup>1</sup>. Lignocellulosic biomass (LCB) can yield various building block chemicals/ intermediates that find applications in industries, transportation, textiles, safe food supply, environmental health, health and hygiene, housing, communication, etc<sup>2</sup>. Important platform chemicals derived from LCB are H<sub>2</sub>, glycerol, lactic acid, succinic acid, fumaric acid, furfural, levulinic acid, lysine, citric acid, gluconic acid, sorbitol, glucaric acid, ferulic acid, etc<sup>2</sup>. Among all these potential building blocks available from biomass, furfuryl alcohol and levulinic acid (LA) are projected as important feedstocks for biofuel synthesis.

Hemicellulose and cellulose are the basic constituents of the LCB that constitute 25–35 wt% and 40–50 wt% respectively in the total composition of LCB. Furfuryl alcohol, a major hemicellulose derivative is obtained by a series of transformations *viz.* hydrolysis, dehydration, and chemoselective hydrogenation via acid-catalyzed reactions. FA can be valorized to synthesize various intermediate or speciality chemicals such as  $\gamma$ -valero lactone, alkyl furfuryl ether, levulinic acid, tetrahydrofurfuryl alcohol, furfuryl acetate, pentanediols, etc<sup>3,4</sup>. These chemicals including furfuryl alcohol have applications as biofuels/biofuel additives, solvents, resins, plasticizers, foundry binders, pharmaceuticals, wood adhesives, flavors, fragrances, etc<sup>5,6</sup>. Cellulose upon hydrolysis, dehydration, and ring-opening reaction with the aid of various acid catalysts yields LA.

Similar to FA and glycerol, LA also acts as a versatile biomass-derived feedstock to produce a wide range of chemicals applied in/as fuels, resins, food and flavoring industries, solvents, polymers, herbicides, and pharmaceuticals <sup>7,8</sup>. From both these feedstocks *viz.* FA and LA, a keto-ester, alkyl levulinate (AL) can be produced by alcoholysis and esterification respectively <sup>9,10,11</sup>. AL has a wide range of applications in commercial sectors such as fuels/fuel additives, bio-lubricants, plasticizing agents, polymer precursors, chemical synthesis, green solvents, and in industries such as cosmetics, herbicide, food flavoring, and pharmaceuticals <sup>9,10,12,13</sup>. Ethyl levulinate (EL) and butyl levulinate (BL) in specific have proven to be used as oxygenating additives because when blended, they enhance the conductivity, combustion emission, and lubricity of the fuel <sup>14</sup>.

For the synthesis of EL from FA in a liquid phase batch mode, various solid acid catalysts have been explored which include, zeolites and modified zeolites (ZSM-5 <sup>15</sup>, H-Beta <sup>15</sup>, mordenite <sup>15</sup>, SBA-15/H-ZSM-5 <sup>16</sup>, SnO<sub>2</sub>/H-Mordenite <sup>17</sup>, nano H-ZSM-5 <sup>18</sup>), metal organic frameworks (MIL-101(Cr)-SO<sub>3</sub>H <sup>19</sup>, meso-MIL-101(Cr) <sup>20</sup>, UiO-66(Hf)-SO<sub>3</sub>H <sup>21</sup>), modified/supported heteropolyacids (modified zirconium phosphate <sup>22</sup>, ZrTPA/ $\beta$ -zeolite <sup>23</sup>, phosphomolybdic acid/ activated charcoal <sup>24</sup>, p-TSA-PFD <sup>25</sup>, organo-silica nanotube (ArSO<sub>3</sub>H-Si(Et)Si-Ph-NTs) <sup>26</sup>, Si(Et)Si-Pr/ArSO<sub>3</sub>H-hollow nanospheres <sup>27</sup>, PW<sub>12</sub>/ZrO<sub>2</sub>-Si(Et)Si nanotubes <sup>28</sup>, Al-TUD-1 <sup>29</sup>,  $\alpha$ -Fe<sub>2</sub>O<sub>3</sub> <sup>30</sup>, Zr-DBS <sup>31</sup>), carbonaceous catalysts (sulfonic acid polystyrene microspheres PS-SO<sub>3</sub>H <sup>32</sup>, P doped metal-free carbon <sup>33</sup>, ArSO<sub>3</sub>H-HMCS <sup>34</sup>), and ionic liquid ([H(SO<sub>3</sub>-p)<sub>2</sub>im][HSO<sub>4</sub>]) <sup>35</sup>, etc. Some catalysts have been reported to give a high ethyl levulinate yield of >95% (modified zirconium phosphate <sup>22</sup>, ZrTPA/ $\beta$ -zeolite <sup>23</sup>, Zr-DBS <sup>31</sup>, [H(SO<sub>3</sub>-p)<sub>2</sub>im][HSO<sub>4</sub>]) <sup>35</sup>).

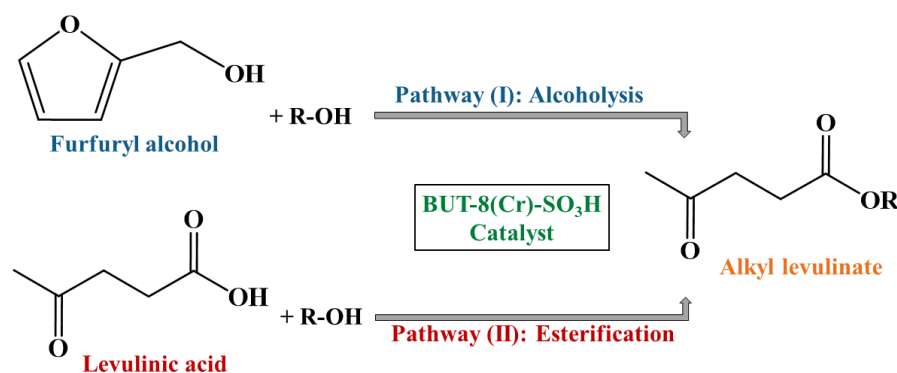
Similarly for the LA esterification to yield EL, the reported catalysts are zeolites/modified zeolites (micro/Meso-HZSM-5 <sup>36</sup>, micro-mesoporous H/BEA zeolite <sup>37</sup>, desilicated HZSM-5 <sup>38</sup>, hierarchical ZSM-12 nanolayers <sup>39</sup>), metal organic frameworks (UiO-66(Hf)-SO<sub>3</sub>H <sup>21</sup>, UiO-66-(COOH)<sub>2</sub> <sup>40</sup> UiO66-SO<sub>3</sub>H <sup>41</sup>, MOF supported polyoxometalates [Cu-BTC][HPM] <sup>42</sup>), resin (amberlyst-15 <sup>43</sup>), silica based catalysts (organo-silica nanotube(ArSO<sub>3</sub>H-Si(Et)Si-Ph-NTs) <sup>26</sup>, HClO<sub>4</sub>/SiO<sub>2</sub> <sup>44</sup>, silica supported

sulfonic acid <sup>45</sup>, sulfated ZrSBA-15 <sup>46</sup>), modified/ supported heteropolyacids (TPA/ 3D graphene aerogel <sup>47</sup>, dodecaTPA/desilicated H-ZSM-5 <sup>48</sup>, PWA/ZrO<sub>2</sub> <sup>49</sup>, phosphomolybdic acid /activated charcoal <sup>24</sup>, EPTN (phosphotungstic acid/TiO<sub>2</sub>)<sup>50</sup>, mesoporous H<sub>3</sub>PW<sub>12</sub>O<sub>40</sub>/ZrO<sub>2</sub>-Si(Ph)Si <sup>51</sup>, silicotungstic acid/ AISBA-15 <sup>52</sup>), metal oxides/modified metal oxide (sulphated TiO<sub>2</sub>/ZrO<sub>2</sub> nano-composites <sup>53</sup>, sulfated TiO<sub>2</sub> nano-rods <sup>53</sup>, nanosized tin oxide <sup>54</sup>, sulphated zirconia nano particles <sup>55</sup>, sulphated Si-doped ZrO<sub>2</sub> <sup>56</sup>, mesoporous zirconia UDCaT-5 <sup>57</sup>, sulfated SnO<sub>2</sub> <sup>58</sup>, sulfated TiO<sub>2</sub> <sup>58</sup>, sulfated Nb<sub>2</sub>O<sub>5</sub> <sup>58</sup>, sulfated ZrO<sub>2</sub> <sup>58</sup>), carbonaceous catalysts (ArSO<sub>3</sub>H-HMCS <sup>34</sup>, sulphonated carbon nano tubes <sup>59</sup>, sulfonated hydrothermal carbon <sup>60</sup>, loofah sponge-derived carbon <sup>61</sup>, carboncryogel crystal <sup>62</sup>) and ionic liquid (-SO<sub>3</sub>H functionalized benzimidazolium-poly IL <sup>63</sup>).

Catalytic syntheses of alkyl levulinates from FA and LA have been rigorously explored despite having a few serious drawbacks. Most of the reported literature for both the transformations has drawbacks such as an issue with the recyclability/ no information on reusability of the catalyst <sup>21,36,51,53,57,58,59,60,61,62,64</sup>, usage of excess amount of reactants <sup>19,20,21,23,22,24,29,28,31,34,35,42,44</sup>, higher operating temperatures <sup>17,20,22,30,31,57,62,64</sup>, more reaction time <sup>39,40,46,56,64,61,65,62,63</sup>.

Among the different reported catalysts, we found that MOF-based catalysts have the potential to be better catalysts if designed suitably as per the requirement of the concerned reactions. Moreover, a few catalysts are reported that suitably convert both FA and LA separately to EL <sup>21,24,26,34</sup>. MOFs are a class of synthetic materials comprising organic linkers with metal clusters interacting with the organic linkers leading to the formation of networks <sup>66</sup>. Studies on MOFs in various applications such as catalysis <sup>67,68</sup>, hydrogen economy <sup>69</sup>, bioremediation <sup>70</sup>, gas storage and separation <sup>71</sup>, sensing <sup>72</sup>, etc have been exclusively done. Owing to all these drawbacks of reported catalysts, we looked into a rarely studied Brønsted acidic metal organic framework (MOF), BUT-8(Cr)-SO<sub>3</sub>H with prime advantages such as structural flexibility, chemical stability over a wide range, and the presence of high-density active sites in the channel enhancing the catalytic performance. This MOF is made of Cr (III) metal clusters which is less toxic compared to Cr (VI) ions as reported in literature <sup>73</sup>. In this work, we aim to investigate

the catalytic application of a MOF, BUT-8(Cr)-SO<sub>3</sub>H and compare with conventional catalysts having distinct nature of active sites, morphology, topology, chemical, and thermal stability to obtain a high ethyl levulinate yield operating under milder reaction conditions thereby overcoming the aforementioned drawbacks (Scheme 6.1). To unravel the intricacies of the catalyst screened, the material was well characterized by various techniques. The catalyst with the best catalytic performance was used to study the influence of the factors such as catalyst amount, reactant mole ratio, reaction temperature, and time. The catalyst reusability and substrate scope study were also performed to evaluate the catalyst potential.



**Scheme 6.1** Alcoholsis of FA and esterification of LA with alkyl alcohols to produce alkyl levulinate

## 6.2 Chemicals and reagents

H-Beta (SAR30) and HZSM-5 (SAR 23) were supplied by Nankai University Catalyst Co. China and Zeolyst International respectively. Amberlyst-15 was procured from Alfa-Aesar. Furfuryl alcohol, levulinic acid, methanol, 1-butanol, 1-propanol, HF, H<sub>2</sub>SO<sub>4</sub>, and HCl were purchased from Merck Life Science Pvt. Ltd. 2,6-Naphthalenedicarboxylic acid was obtained from TCI. Oleum and chromium (III) nitrate were provided from Sd Fine-chem Limited and SRL respectively. Ethanol and DMF were purchased from CSS and Avra Synthesis Pvt Ltd respectively.

## 6.3 Catalyst synthesis

BUT-8(Cr)-SO<sub>3</sub>H catalyst was synthesized from a procedure similar to the reported one<sup>73</sup>. For linker pre-modification, 30 g of 2,6-naphthalenedicarboxylic acid (NapDC)



linker was treated with 100 mL of oleum for 24 h in a three-neck round bottom flask placed in a magnetically stirred oil bath maintained at 140 °C. Once cooled, the unreacted sulfuric acid residues were removed by subjecting the linker to purification steps involving its dissolution by distilled water treatment (40 mL) followed by linker precipitation by HCl treatment (100 mL). This dissolution and precipitation step was repeated thrice in copious amounts of distilled water and HCl treatments in which the linker was dried at 80 °C for 12 h between each purification cycle. The 4,8-disulfonyl-2,6-naphthalenedicarboxylic acid (modified linker) was vacuum dried for 12 h at 120 °C.

The MOF, BUT-8(Cr)-SO<sub>3</sub>H was solvothermally synthesized using Cr(NO<sub>3</sub>)<sub>3</sub>·9H<sub>2</sub>O and 4,8-disulfonyl-2,6-naphthalenedicarboxylic acid as the metal cluster and linker respectively. In a typical synthesis, 4 g of chromium precursor and 3.76 g of the modified linker were homogenized with 60 mL of DMF in an ultrasonic bath for 30 min. 1.1 mL of hydrofluoric acid was added to the mixture and the solution was transferred to autoclave (teflon-lined stainless steel) and placed in a preheated oven (24 h, 190 °C). The material thus obtained was stirred in DMF where the green powder present in the suspension was collected immediately (within 1 minute) with the aid of a glass pipette and the larger bright green particles settled at the bottom were discarded. Further, the material was washed thrice and soaked in DMF (80 °C) and distilled water (RT) for 24 h respectively. The material was finally washed with methanol and dried under a vacuum at 60 °C for 12 h before soaking in 2M H<sub>2</sub>SO<sub>4</sub> solution for 24 h. Then, the material was washed and soaked in distilled water and methanol to remove the physisorbed H<sub>2</sub>SO<sub>4</sub> species and was activated under vacuum for 24 h at 60 °C to yield BUT-8(Cr)-SO<sub>3</sub>H.

#### 6.4 Catalytic activity study

In a typical reaction procedure, the alcoholysis and esterification of FA and LA respectively to yield EL were performed using a 50 mL sealed tube glass reactor in a liquid phase batch regime. A calculated amount of molar composition of reactants (FA/LA and alkyl alcohol) along with catalyst (in weight % with respect to total reactants) was magnetically stirred at the desired temperature. The quantitative analyses of the reaction mixtures for alcoholysis and esterification reactions were evaluated using gas

chromatography with DB–Wax (0.25 mm I.D., 30 m length) capillary column mounted in Shimadzu GC–2014 and HP–5 (0.25 mm I.D., 30 m length) capillary column installed in Agilent Technologies 7820A respectively. The products were validated by Gas chromatography Mass Spectrometry (GCMS). The FA/LA conversion and EL selectivity were determined by the GC.

$$C_R(\%) = \frac{R_{(i)} - R_{(f)}}{R_{(i)}} \times 100$$

$$S_{EMF}(\%) = \frac{P_{EMF}}{R_{(i)} - R_{(f)}} \times 100$$

$$S_{EL}(\%) = \frac{P_{EL}}{R_{(i)} - R_{(f)}} \times 100$$

$$Y_{EL}(\%) = \frac{P_{EL}}{R_{(i)}} \times 100$$

where  $C_R$  is the conversion of the reactant FA or LA for two pathways alcoholysis and esterification, respectively.  $R_{(i)}$  and  $R_{(f)}$  correspond to the initial and final moles of the reactant (FA or LA) respectively.  $S_{EMF}$  and  $S_{EL}$  are the selectivities of EMF (intermediate of pathway (I) alcoholysis reaction) and EL respectively.  $P_{EMF}$  and  $P_{EL}$  are the moles of the intermediate EMF and EL respectively.  $Y_{EL}$  is attributed to the EL yield.

## 6.5 Characterization of the catalysts: Results and discussion

### 6.5.1 Powder X–ray diffraction

All the X–ray diffractograms of the commercially procured catalysts [H–Beta (SAR25) and H–ZSM–5 (SAR23)] and BUT–8(Cr)–SO<sub>3</sub>H have matched well with the standard patterns as per the reported literature as presented in figure 6.1<sup>74,75</sup>. The sulfonic acid functionalized MOF, BUT–8(Cr)–SO<sub>3</sub>H exhibited five characteristic diffraction peaks at  $2\theta = 7.06, 11.24, 13.28, 18.21, \text{ and } 20.34^\circ$  whose reflection peaks matched with the pattern of the post–synthetically modified MOF as reported. Importantly, after the H<sub>2</sub>SO<sub>4</sub> treatment, there was no loss in the crystallinity of the material.

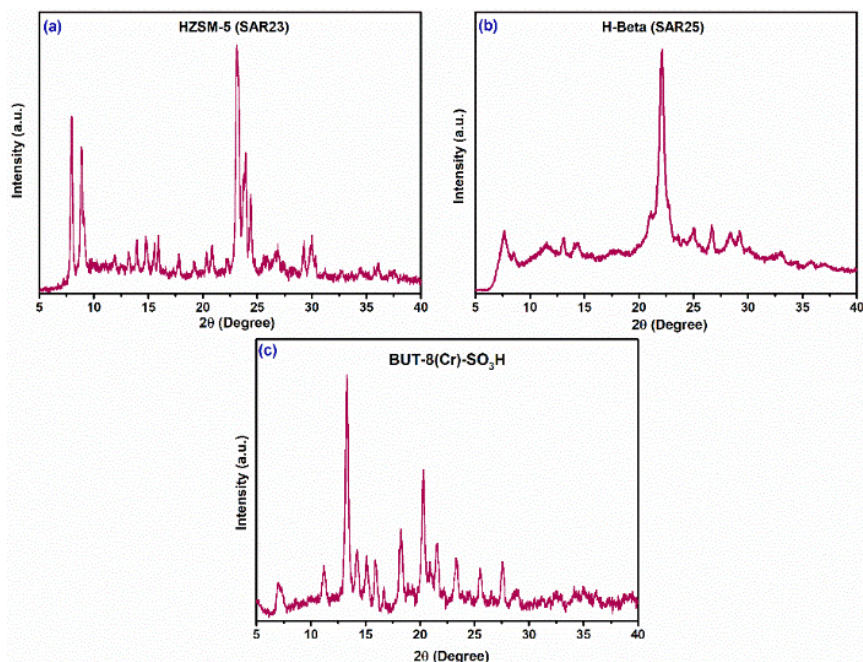


**Figure 6.1.** PXRD diffractograms of (a) HZSM-5 (SAR23), (b) H-Beta (SAR25), (c) BUT-8(Cr)-SO<sub>3</sub>H

### 6.5.2 FTIR spectroscopy

FTIR spectrum of BUT-8(Cr)-SO<sub>3</sub>H MOF is presented in figure 6.2. The broad peak around 3500 cm<sup>-1</sup> was attributed to -OH groups present in the material. The peaks at 1633 and 1419 cm<sup>-1</sup> are ascribed to C=O of carboxylate and C=C of naphthalene ring respectively. The peak at 667 cm<sup>-1</sup> corresponds to the Cr-O bond and the peak at 618 cm<sup>-1</sup> referred to the C-S bond. The characteristic peaks of the -SO<sub>3</sub>H group lie in the range of 1000 to 1250 cm<sup>-1</sup>. The peaks 1196 cm<sup>-1</sup> and 1242 cm<sup>-1</sup> can be assigned to symmetric stretching and asymmetric stretching modes of O=S=O moieties. The S-O moiety appears at 1038 cm<sup>-1</sup> in the spectrum.

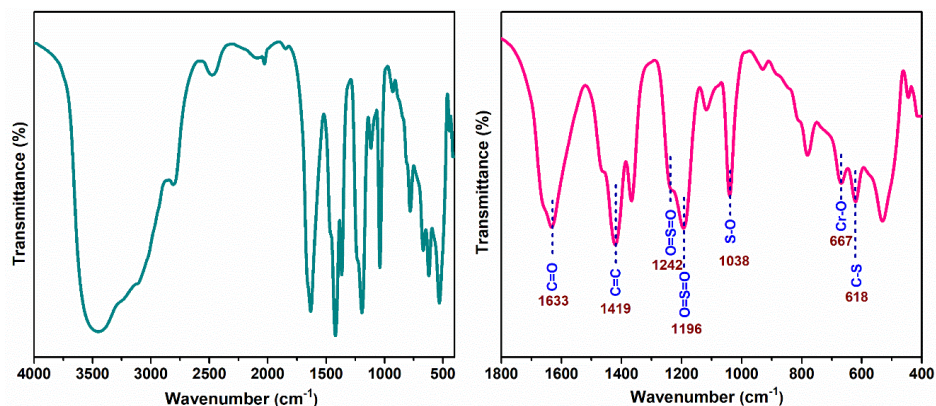


**Figure 6.2.** FTIR spectrum of BUT-8(Cr)-SO<sub>3</sub>H

### 6.5.3 Thermogravimetric analysis

The weight loss profile of BUT-8(Cr)-SO<sub>3</sub>H MOF was obtained by thermogravimetric analysis and is depicted in figure 6.3. There was an initial weight loss from 30 to 320 °C that can be ascribed to the removal of moisture. From the differential thermal analysis, this weight loss can be attributed to the removal of moisture as this water-stable catalyst has hydrophilic pores. After 320 °C, the disintegration of the framework occurred suggesting the maximum thermal stability of the MOF is ~300 °C. The second decomposition peak was observed between 320 to 550 °C with weight loss of ~ 40 wt% corresponding to the degradation of the linker.

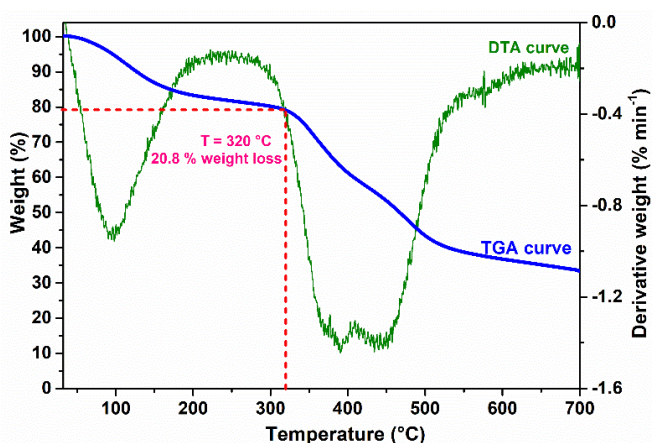


**Figure 6.3.** Thermogravimetric analysis profile of BUT-8(Cr)-SO<sub>3</sub>H MOF

### 6.5.4 Temperature programmed desorption

The zeolite catalysts HZSM-5 (SAR 23) and H-Beta (SAR 25) exhibited a high amount of total acidity of 0.92 and 1.06 mmol g<sup>-1</sup> respectively and the NH<sub>3</sub>-TPD profile was typical of these specific zeolites [Table 6.1 and figure 6.4 (a, b)]. For the MOFs with moderate thermal stability (~300°C), a new methodology was developed to estimate the amount of acidity using NH<sub>3</sub>-TPD. The actual acidity of the MOF was obtained by excluding the thermal decomposition peaks due to heating the sample above its thermal stability. Hence, a difference in the value obtained with and without the probe molecule (NH<sub>3</sub>) gave the amount of acidity due to NH<sub>3</sub> chemisorption on the acid sites and the profile is presented in figure 6.4 (c). From this method, the amount of acidity of BUT-8(Cr)-SO<sub>3</sub>H was found to be 1.65 mmol g<sup>-1</sup> and was confirmed by acid-base titration (1.8 mmol g<sup>-1</sup>).

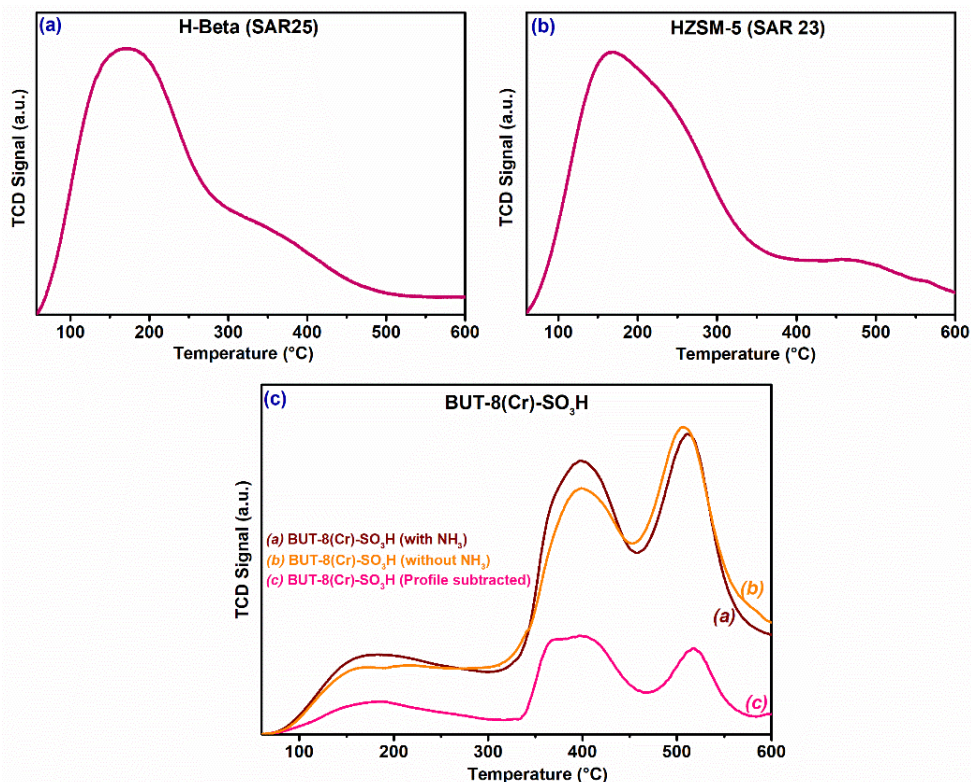


**Figure 6.4.**  $\text{NH}_3$ -Temperature programmed desorption profiles of (a) HZSM-5 (SAR23), (b) H-Beta (SAR25), (c) BUT-8(Cr)- $\text{SO}_3\text{H}$

### 6.5.5 Microscopic techniques

The morphological details of BUT-8(Cr)- $\text{SO}_3\text{H}$  were obtained by the SEM which revealed the presence of numerous nanofibres with an average length of 85 nm (figure 6.5). TEM analysis confirms the presence of nanofibres with an average width of 28 nm as presented in figure 6.6.

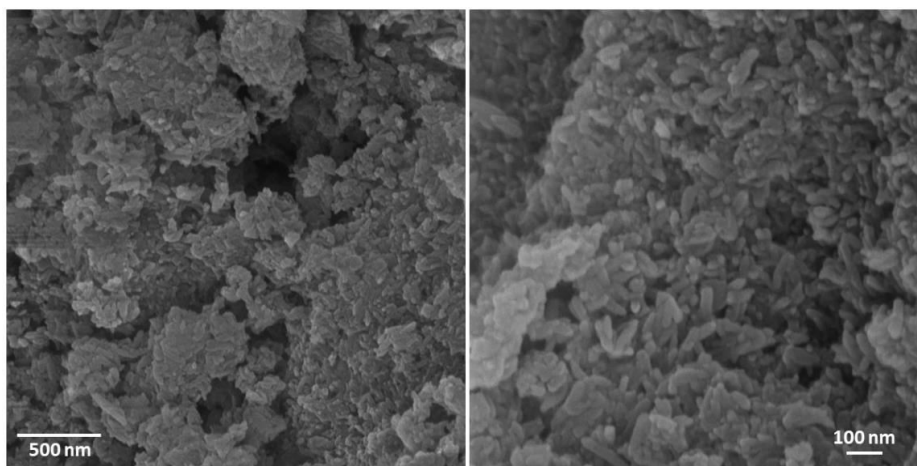


**Figure 6.5.** SEM micrographs of BUT-8(Cr)- $\text{SO}_3\text{H}$  MOF

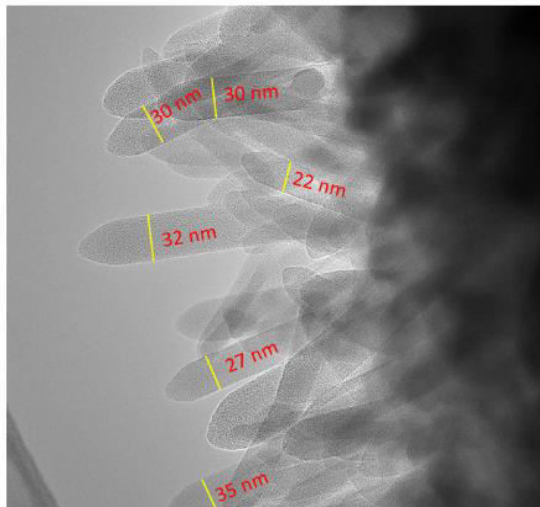


**Figure 6.6.** TEM image of BUT-8(Cr)-SO<sub>3</sub>H MOF

## 6.6 Catalytic activity study

### 6.6.1 Catalyst screening and comparison

From the prior understanding of the ethanolysis and esterification reactions, it is known that Brønsted acidic sites would be the ideal active sites to achieve high alkyl levulinate yield. Therefore, conventional Brønsted acid catalysts (zeolite, acidic resin) were screened along with a sulfonic acid functionalized MOF, BUT-8(Cr)-SO<sub>3</sub>H for furfuryl alcohol ethanolysis and levulinic acid esterification to yield ethyl levulinate in a sealed tube stirred reactor under autogenous pressure. There was quite a difference in the values of the total amount of acidity of the catalysts. Amberlyst-15 and BUT-8(Cr)-SO<sub>3</sub>H contained 4.7 and 1.65 mmol g<sup>-1</sup> of acidity respectively which is higher than the acidity of HZSM-5 (SAR23); 1.06 mmol g<sup>-1</sup> and H-Beta (SAR25); 0.9 mmol g<sup>-1</sup>. Therefore, we investigated the initial screening of various catalysts to identify the best catalyst by maintaining uniformity in keeping the same number of acid sites. Prior to this study, a blank reaction in the absence of a catalyst was performed which revealed that both transformations would occur only with the aid of a catalyst. Furfuryl alcohol alcoholysis showed 21% FA conversion and 12% EL selectivity (at 120 °C, 1:20 reactant mole ratio, 6 h) whereas, in the case of LA esterification, there was a low LA conversion of 9% with 93% EL selectivity (at 90 °C, 1:5 reactant mole ratio, 6 h).

In pathway (I), for FA alcoholysis, the FA conversion for BUT-8(Cr)-SO<sub>3</sub>H was >99% and EMF intermediate selectivity was 30% which decreased to 0.6 % upon increasing

time (up to 6h) (figure 6.7). The EL selectivity increased from 54 to 99.4 % with an increase in reaction time from 30 min to 6 h. Amberlyst-15 showed a very good FA conversion of 82% with EMF and EL selectivities of 30 and 40 % respectively. HZSM-5 (SAR23) and H-Beta (SAR25) showed similar results with respect to EL selectivity of (30 to 36%) at 6 h though there was a difference in FA conversion. The EMF selectivities for H-Beta and HZSM-5 were 32 and 55 % respectively and HZSM-5 had fewer side products (< 10%) compared to H-Beta and amberlyst-15.

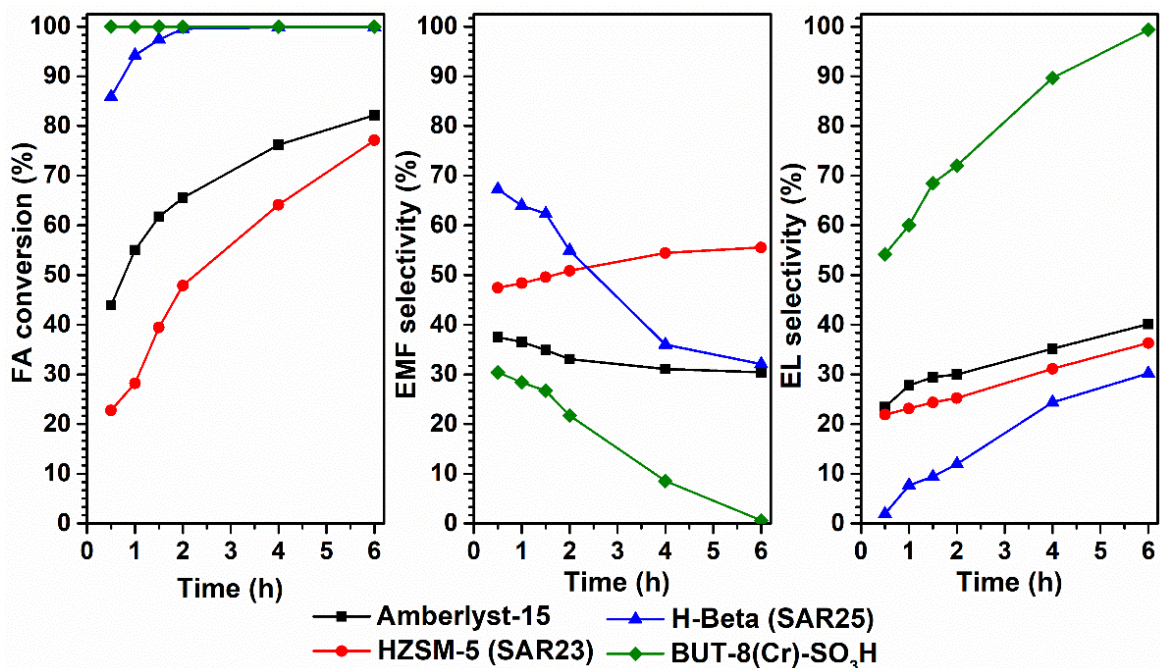


**Figure 6.7.** Pathway (I) Alcoholysis of FA. Catalyst screening Reaction conditions: Temperature- 120 °C, FA- 1.52 mmol, EtOH- 30.58 mmol, catalyst wt- 0.065 mmol acid sites, time- 6 h

In the case of pathway (II), for the esterification of LA, the selectivity towards EL remained the same throughout the reaction time when BUT-8(Cr)-SO<sub>3</sub>H is used (figure 6.8). However, the LA conversion for BUT-8(Cr)-SO<sub>3</sub>H and amberlyst-15 increased substantially over time to 96 and 60 % respectively at 6 h whereas, the zeolites (HZSM-5 and H-Beta) performed poorly (LA conversion of ~18 to 19 %). The EL selectivity for amberlyst-15 and zeolites were 97 % and ~73 to 74 % respectively.

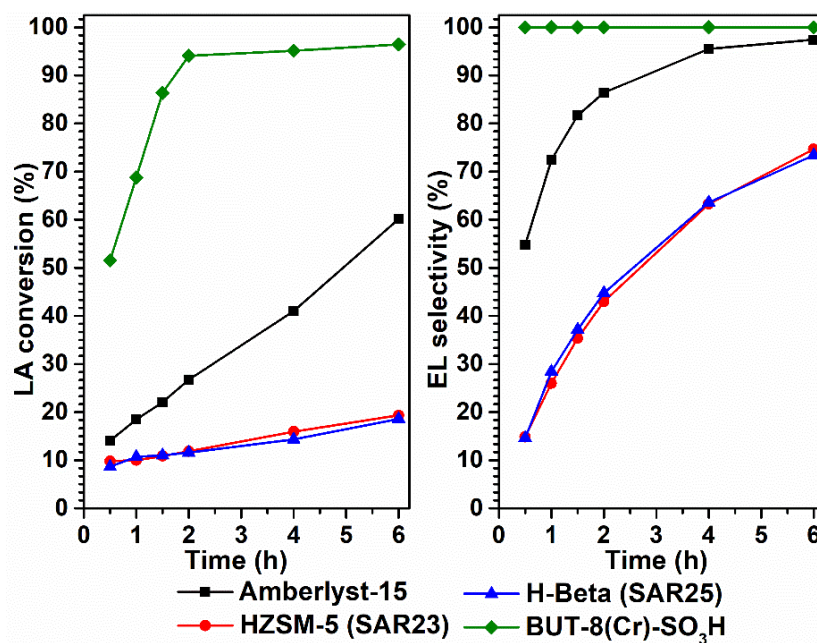


**Figure 6.8.** Pathway (II) Esterification of LA. Catalyst screening. Reaction conditions: Temperature– 90 °C, LA– 5.16 mmol, EtOH– 25.83 mmol, catalyst wt– 0.075 mmol acid sites, time– 6 h

For both the pathways, the trend in terms of decreased EL yield (Table 6.1) is in the order of BUT–8(Cr)–SO<sub>3</sub>H > amberlyst–15 > [HZSM–5 (SAR 23) ~ H–Beta (SAR25)] which indicates that –SO<sub>3</sub>H groups (present in BUT–8(Cr)–SO<sub>3</sub>H and amberlyst–15) had a significant influence in the catalytic performance over the Al–Brönsted acid sites of the zeolites. The aromatic naphthalene structure with the sulfonic moieties of BUT–8(Cr)–SO<sub>3</sub>H MOF had a much stronger influence on the catalytic performance than the sulfonic acid moieties present in the styrene framework of the amberlyst–15. The MOF–based catalyst, BUT–8(Cr)–SO<sub>3</sub>H with very good chemical stability similar to zeolites, and a fairly high amount of acidic sites similar to amberlyst–15 showed the best catalytic activity for both pathways. The poor performance of conventional zeolites can be due to the limitation in the diffusion of the reactive species offered by the microporous channels. Amberlyst–15, owing to its very low thermal stability (120 °C) and swelling effect of the material caused due to the permanent absorption of the reactants fails to reproduce its catalytic activity over multiple cycles. The highest catalytic efficiency of BUT–8(Cr)–SO<sub>3</sub>H can be attributed to the presence of a specific type of nature of active site *viz.* –SO<sub>3</sub>H, a high number of acidic sites and their higher strength which enhance the



accessibility of the reactive species to the active sites, and fairly high chemical and thermal stability.

**Table 6.1.** Physicochemical properties and catalytic performance of the various solid acid catalysts

Catalyst	Acidity (mmol g <sup>-1</sup> )	EL yield (%)	
		FA alcoholysis <sup>[c]</sup>	LA esterification <sup>[d]</sup>
BUT-8(Cr)-SO <sub>3</sub> H	1.65 <sup>[a]</sup> , 1.8 <sup>[b]</sup>	99	96
Amberlyst-15	4.7 <sup>[b]</sup>	31	54
H-Beta (SAR25)	0.92 <sup>[a]</sup>	30	14
HZSM-5 (SAR23)	1.06 <sup>[a]</sup>	28	12

[a] NH<sub>3</sub>-TPD, [b] Acid-base titration, [c] Alcoholysis of FA: Catalyst screening Reaction conditions: Temperature- 120 °C, FA- 1.52 mmol, EtOH- 30.58 mmol, catalyst wt- 0.065 mmol acid sites, time- 6 h. [d] Esterification of LA Catalyst screening. Reaction conditions: Temperature- 90 °C, LA- 5.16 mmol, EtOH- 25.83 mmol, catalyst wt- 0.075 mmol acid sites, time- 6 h

### 6.6.2 Influence of reaction conditions

Among all the conventional Brønsted acid catalysts screened with different nature of active sites, amount of acidity, topology, morphology, and chemical stability, BUT-8(Cr)-SO<sub>3</sub>H MOF, the best performing catalyst was selected to investigate its influence on reaction parameters such as reactants mole ratio, catalyst loading and temperature for both the pathways to yield EL.

#### 6.6.2.1 Pathway (I) Alcoholysis of furfuryl alcohol

##### Effect of temperature

As the reaction is performed in a sealed tube, the effect of variation in temperature can be generously studied above the boiling point of the reactants. The temperature variation from (30 to 130 °C) had a pronounced influence on the EL and EMF selectivities [figure 6.10 (c)]. At a lower reaction temperature of 30 °C, the FA conversion was 6% with no selectivity towards EMF or EL. At 60 °C, the conversion of FA increased to 62% with the selectivities towards EMF and EL of 43 and 7 % respectively. Further, at 80 °C, the EMF and EL selectivities were 55 and 12% respectively, but with an increase in temperature to 120 °C the EL selectivity increased six folds (72%). Further increase in

temperature to 130°C the EL selectivity came down to 51% generating a higher amount (34%) of side products.

### **Effect of reactants mole ratio**

The concentration of the reactants (FA and EtOH) has a significant impact on this reaction system as it affects the selectivity of the EL. As the operating reaction temperature is 120 °C, the concentration of EtOH (low boiling reactant) in the mixture dictates the possibility of resinification of the furanic species on the active sites. Therefore, the concentration of the second reactant which acts as a solvent as well should be carefully chosen to reduce the side product formation and to avoid resinification as the catalyst used is with a high amount of acidity. Initially, at a lower reactants mole ratio of 1:10 (FA: EtOH), the EMF and EL selectivities were 14 and 79% respectively as presented in figure 6.9 (a). Upon increasing the mole ratio to 1:15, there was an improvement in the EL selectivity (86 %) and a decrease in the concentration of the intermediate EMF (8%). Further increase in the reactant mole ratio to 1:20, 1:25, and 1:30, resulted in the enhanced selectivity towards the intermediate EMF (~ 21 to 25%) and the decreased EL selectivity to 60 % (at 1:30). This might be because of the effect of dilution, where the EtOH reduces the accessibility of the EMF towards the acidic site which is necessary for further converting to EL. The study suggests that the 1:15 reactant mole ratio with the highest EL selectivity is the optimal mole ratio for this reaction which is lower compared with the previous reports.

### **Effect of catalyst concentration**

Influence of concentration of BUT-8(Cr)-SO<sub>3</sub>H catalyst was explored with different catalyst weights ranging from 0.50 to 1.75 wt% (with respect to total reactant weight). Though the conversion of FA was constant (> 99%) in this study, there was a considerable impact on the EL and EMF selectivities with an increase in the amount of catalyst loading from 0.5 to 1.5 wt% as shown in figure 6.9 (b). The EL selectivity increased from 25 to 91%, whereas EMF selectivity decreased from 44 to 5%. However, upon a further increase in the catalyst amount to 1.75 wt%, the EL selectivity decreased to 86 % with EMF selectivity of 4%. The other side product formed was DEP (5,5-diethoxy-2-pentanone).

The investigation on the influence of reaction parameters on FA alcoholysis with the aid of BUT-8(Cr)-SO<sub>3</sub>H as catalyst revealed that 1:15 (reactant mole ratio), 1.5 wt% catalyst loading, and 120 °C reaction temperature as optimum reaction conditions to be operated to achieve highest EL formation.

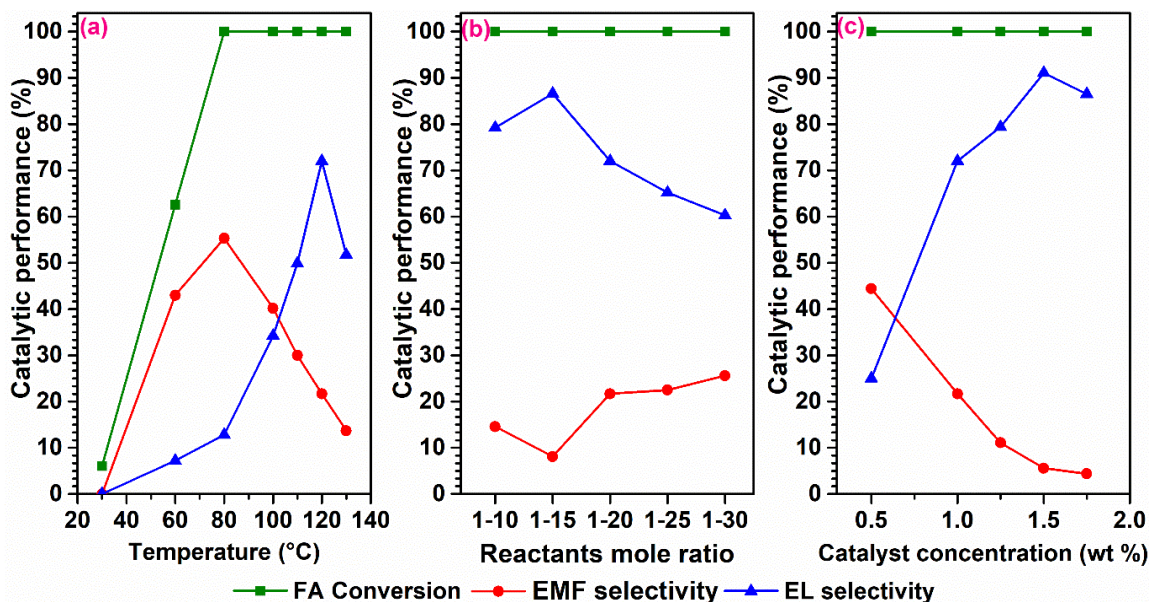


**Figure 6.9.** Influence of reaction conditions: Pathway (I) Alcoholysis of furfuryl alcohol. (a) Effect of reaction temperature: Reaction conditions: Catalyst concentration– 1 wt%, mole ratio– 1:20 (FA: EtOH), time– 2 h. (b) Effect of reactants mole ratio (FA: EtOH): Reaction conditions: Catalyst concentration– 1 wt%, temperature– 120 °C, time– 2 h. (c) Effect of catalyst concentration: Reaction conditions: Temperature– 120 °C, mole ratio– 1:20 (FA: EtOH), time– 2 h

### 6.6.2.2 Pathway (II) Esterification of levulinic acid

#### Effect of temperature

As the reaction is performed in a sealed tube, similar to FA alcoholysis, the influence of the reaction temperature for the LA esterification was studied over a wide range of temperatures *viz.* 30 to 100 °C [figure 6.10 (a)]. At a lower temperature of 30 °C, the LA conversion and EL selectivity was 8 and 92% respectively. As the reaction temperature was increased from 60 to 70 °C, LA conversion increased from 57 to 78%, and the EL selectivity also increased from 94 to 99 %. With further increase in temperature to 80 and 90 °C, the LA conversion increased to 89 and 94% respectively. However, >90 °C, there was only a marginal increase in the catalytic activity and the increment in LA conversion was ~3 %.

### **Effect of reactants mole ratio**

The study was performed by varying the reactant mole ratio (LA:EtOH) from 1:1 to 1:10, where the EL selectivity remained 100% but conversion varied. With an increase in mole ratio up to 1:8, the LA conversion increased from 81 to 96%, whereas at 1:10, the LA conversion decreased to 83% probably due to the dilution effect as depicted in figure 6.10 (b). The overall increment in LA conversion was ~15% and the optimal mole ratio was found to be 1:8 (LA: EtOH). Compared to EL synthesis from FA, the requirement of EtOH was lower for this pathway. Additionally, the issue of resinification did not occur in LA esterification as it is not a furanic compound.

### **Effect of catalyst concentration**

Catalyst loading corresponds to the number of active sites distributed in the reaction medium directly influencing the reactant conversion and product selectivity. Initially, at 0.5 wt% (wrt total reactants weight) catalyst loading, the LA conversion was 79%, but with an increase in the catalyst loading to 1.0, 1.25, and 1.5 wt% there was a huge increment in LA conversion (~ 94 to 96%) as shown in figure 6.10 (c). The LA conversion remained almost similar with a further increase in catalyst loading to 3.5 wt%. The highest LA conversion of 96% was obtained at a lower amount of catalyst loading (1.5 wt%) implying the efficiency of the BUT-8(Cr)-SO<sub>3</sub>H catalyst. Based on the above results, a 1:8 reactant mole ratio (LA: EtOH), 90 °C reaction temperature, and 1.5 wt% catalyst loading were opted as the optimum reaction conditions for further studies.

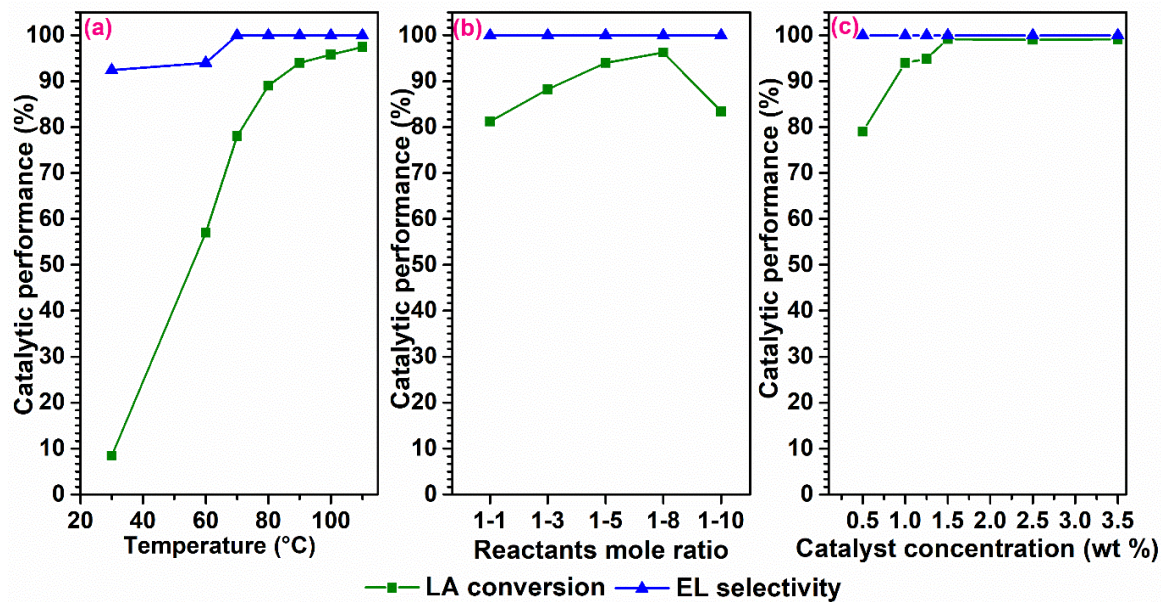


**Figure 6.10.** Influence of reaction conditions: Pathway (II) Esterification of Levulinic acid. (a) Effect of reaction temperature: Reaction conditions: Catalyst concentration– 1 wt%, mole ratio– 1:5 (LA: EtOH), time– 4 h. (b) Effect of reactants mole ratio (LA: EtOH): Reaction conditions: Catalyst concentration– 1 wt%, temperature– 90 °C, time– 4 h. (c) Effect of catalyst concentration: Reaction conditions: Temperature– 90 °C, mole ratio– 1:5 (LA: EtOH), time– 4 h.

### 6.6.3 Catalyst recyclability study

The reusability of BUT–8(Cr)–SO<sub>3</sub>H catalyst was inspected for both the pathways *viz.* alcoholysis of FA and esterification of LA under optimized reaction conditions to confirm the catalyst stability over multiple cycles by utilizing the regenerated catalyst. Though FA is always suspected to undergo resinification at acidic sites of the catalysts and elevated temperatures. However, in our reaction conditions, this phenomenon was found to be curbed due to the presence of EtOH in excess (1:15). Therefore, one of the biggest challenges of FA valorization using an acid–catalyzed reaction was addressed. Compared to zeolites, the catalyst BUT–8(Cr)–SO<sub>3</sub>H has a better tolerance towards side product formation due to resinification. Further, this was proved by using a simple regeneration method by washing the spent catalyst with acetone a few times and vacuum drying it at 60°C for 12 h. During each recycle for both pathways to yield EL [figure 6.11 and figure 6.12], the catalyst exhibited catalytic activity with a negligible decrease (~0.4 to 0.7%) compared to the fresh catalyst.

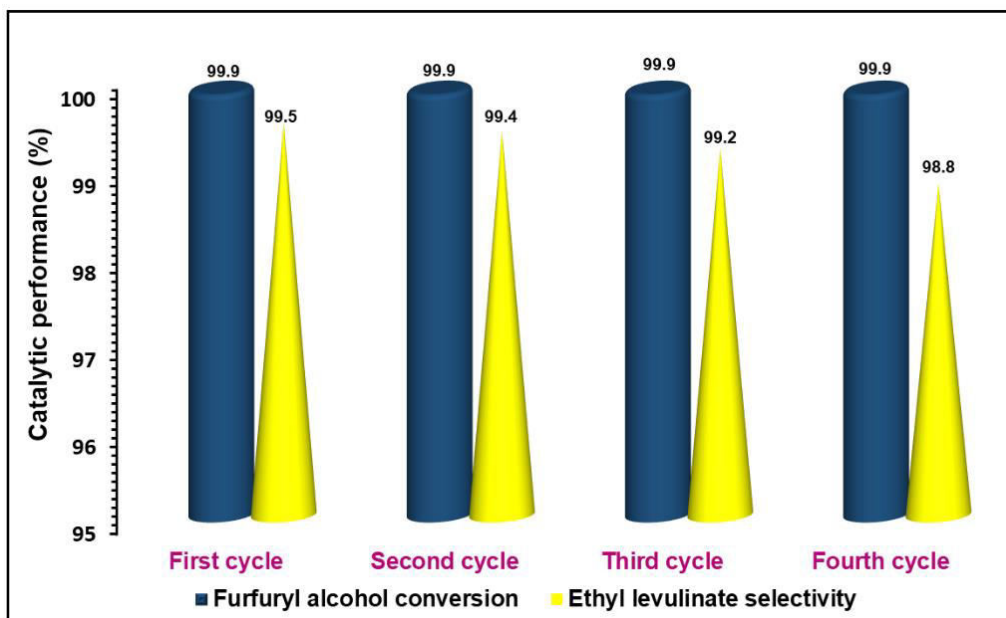


**Figure 6.11.** Catalyst recyclability study: Pathway (I) Alcoholysis of furfuryl alcohol– Reaction conditions: Reactants mole ratio (FA: EtOH)– 1:15, Catalyst concentration– 1.86 wt%, temperature– 120 °C, time– 2 h

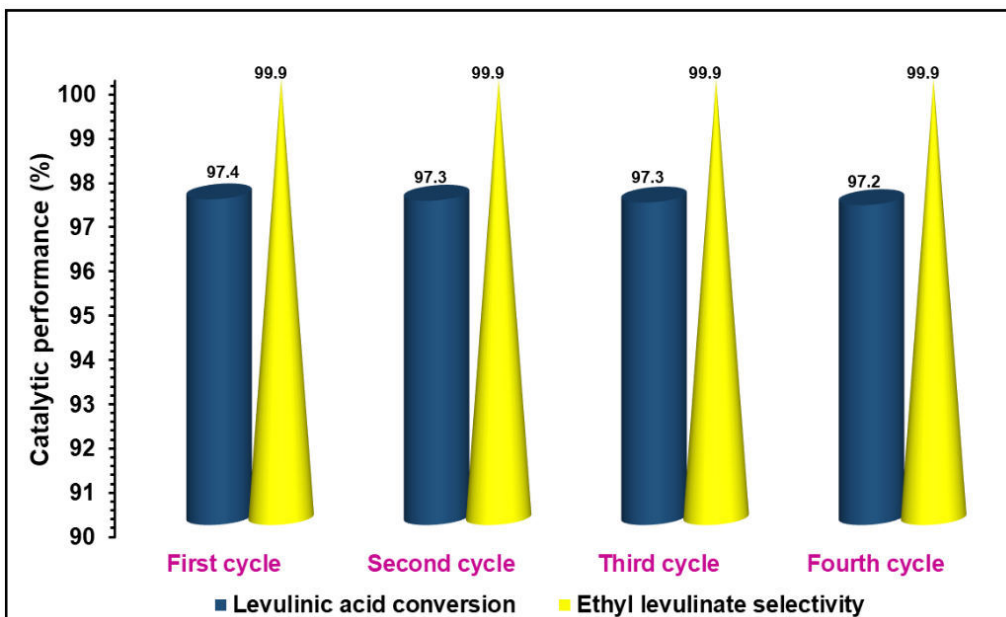


**Figure 6.12.** Catalyst recyclability study: Pathway (II) Esterification of Levulinic acid– Reaction conditions: Reactants mole ratio (LA: EtOH)– 1:8, Catalyst concentration– 1.25wt%, temperature– 90 °C, time– 4 h

The XRD pattern of the spent BUT–8(Cr)–SO<sub>3</sub>H matched well with the characteristic peaks of fresh catalyst which indicates that there was no change in the structure of the catalyst even after four consecutive cycles (figure 6.13).

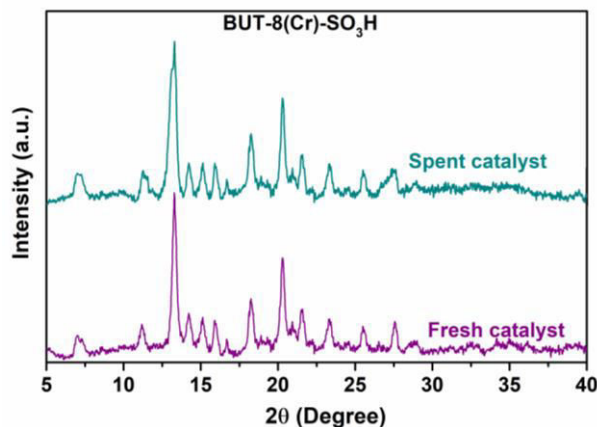


Figure 6.13 PXRD diffractograms of fresh and spent catalysts.

#### 6.6.4 Time resolved study

The influence of reaction time under the optimized reaction conditions was examined using the best catalyst BUT-8(Cr)-SO<sub>3</sub>H for both pathways. The FA alcoholysis showed 99% FA conversion in initial hours, whereas the EL selectivity increased from 63 to 99% with an increase in time from 1 to 3 h as shown in figure 6.14 (a). The intermediate (EMF) with the selectivity of 26% completely converted to EL after 1 h. In the case of LA esterification, there was a negligible increment (~0.8%) in the LA conversion from 96 to 97 % with an increase in reaction time from 2 to 6 h [figure 6.14 (b)].

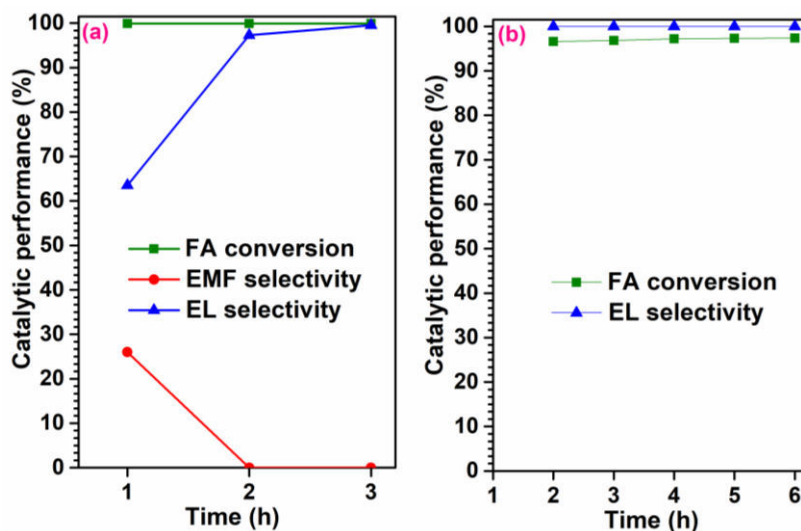
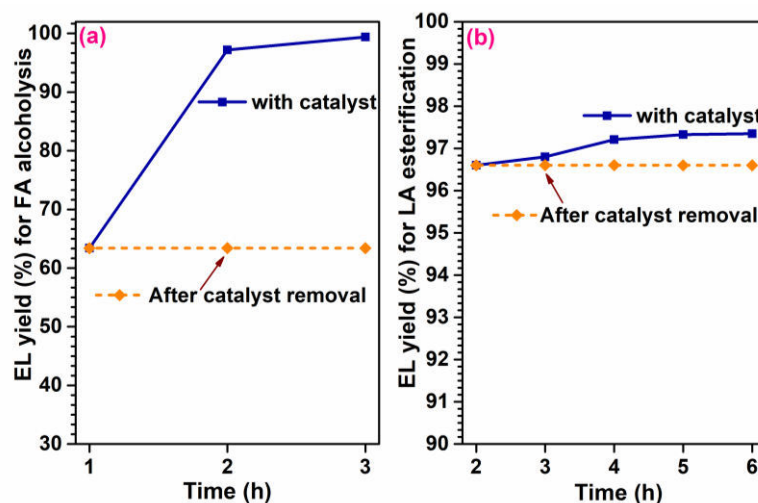


Figure 6.14. Effect of reaction time (a) Pathway (I) Alcoholysis of furfuryl alcohol–Reaction conditions: Reactants mole ratio (FA: EtOH) – 1:15, Catalyst concentration– 1.86 wt%, temperature– 120 °C. (b) Pathway (II) Esterification of Levulinic acid –Reaction conditions: Reactants mole ratio (LA: EtOH)– 1:8, Catalyst concentration– 1.25 wt%, temperature– 90 °C

### 6.6.5 Leaching studies

The leaching study that evaluates the heterogeneity of the catalyst was performed with the active catalyst BUT-8(Cr)-SO<sub>3</sub>H. The reaction was stopped after 1 h for FA alcoholysis and 2 h for LA esterification, and the catalyst was removed from the respective reaction mixture by centrifugation. The supernatant liquid was further employed for reaction at the required temperature in the absence of a catalyst. The EL yield upon the catalyst removal remained the same for both transformations as shown in figure 6.15. It confirms the heterogeneity of the catalyst without any loss of active site species in the reaction. The post-synthetic thorough washing of the linker, as well as the MOF during catalyst preparation could remove all the leachable physisorbed species from the material.



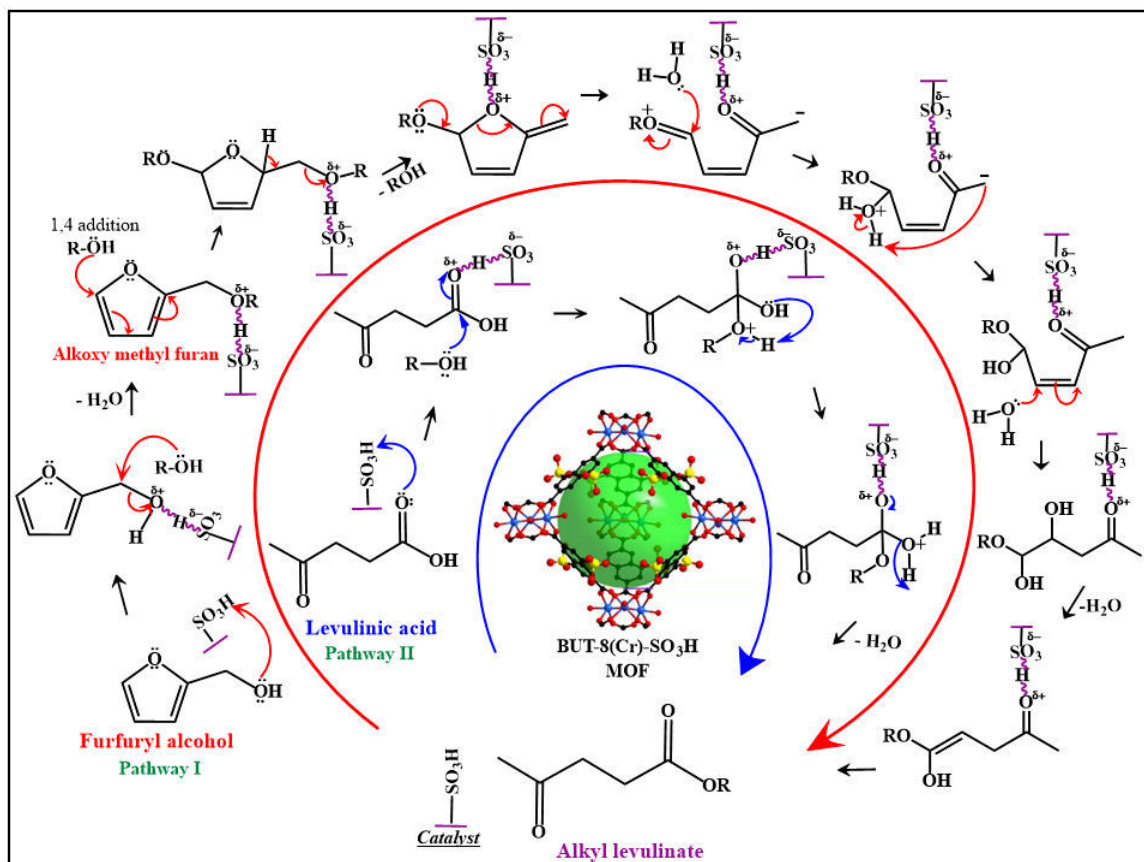
**Figure 6.15.** Leaching studies (a) Pathway (I) Alcoholysis of furfuryl alcohol– Reaction conditions: Reactants mole ratio (FA: EtOH)– 1:15, Catalyst concentration– 1.86 wt%, temperature– 120 °C. (b) Pathway (II) Esterification of Levulinic acid– Reaction conditions: Reactants mole ratio (LA: EtOH)– 1:8, Catalyst concentration– 1.25 wt%, temperature– 90 °C

### 6.7 Plausible reaction mechanism

The plausible mechanistic pathways for the alcoholysis of furfuryl alcohol (Pathway I) and esterification of levulinic acid (Pathway II) to yield alkyl levulinate is proposed in Scheme 6.2. The alcoholysis reaction initiates by the formation of an intermediate alkoxy methyl furan due to the protonation of the furfuryl alcohol by the Brønsted acid sites of the catalyst. The intermediate upon 1,4 addition of the alkyl alcohol converts to



2-alkoxy-5-methylene-2,5-dihydrofuran which on the ring-opening produces alkyl levulinate. The esterification of levulinic acid to obtain alkyl levulinate initiates with the protonation of the levulinic acid by the Brønsted acidic sites of the catalyst followed by nucleophilic attack of the oxygen of alkyl alcohol on the carbocation. Finally, the proton transfer occurs resulting in the removal of a water molecule yielding alkyl levulinate.



**Scheme 6.2** Plausible mechanistic pathway for the furfuryl alcohol alcoholysis and levulinic acid esterification to yield alkyl levulinate

## 6.8 Substrate scope study

The efficiency and applicability of the BUT-8(Cr)-SO<sub>3</sub>H MOF was evaluated under the optimized reaction conditions for the synthesis of different alkyl levulinates which have different applications. The FA and LA transformations to different alkyl levulinates were conducted by varying the alcohols such as methanol (MeOH), propanol (PrOH), isopropanol (i-PrOH), 1-butanol (BuOH), 2-butanol (2-BuOH), and tertiary-butanol (t-BuOH) yielding methyl levulinate (ML), propyl levulinate (PL), isopropyl levulinate (i-PL), butyl levulinate (BL), 2-butyl levulinate (2-BL) and tertiary-butyl levulinate

(t-BL) respectively. In the case of pathway (I), the FA conversion remained >98% with varying amounts of side products *viz.* methoxy methyl furan (MMF), propoxy methyl furan (PMF), butoxy methyl furan (BMF), isopropoxy methyl furan (i-PMF), 2-butoxy methyl furan (2-BMF), and t-butoxy methyl furan (t-BMF) of 4.8, 1.2, 11.8, 27.7, 50.6, and 41.8 % selectivities respectively. The alkyl levulinate selectivity decreased in the following order; PL (98%) > EL (97%) > BL (76%) > ML (73%) > 2-BL (36%) > i-PL (35%) > t-BL (32%) as presented in figure 6.16 (a). In the case of the pathway (II), the FA conversion was > 99% for most of the alcohols (except when MeOH and EtOH were used with FA conversion of 95 and 91 % respectively). The selectivity towards LA remained 100% for ML, EL, PL, and BL, whereas for 2-BL, i-PL, t-BL, the selectivities were 66, 51, and 27 % respectively as shown in figure 6.16 (b).

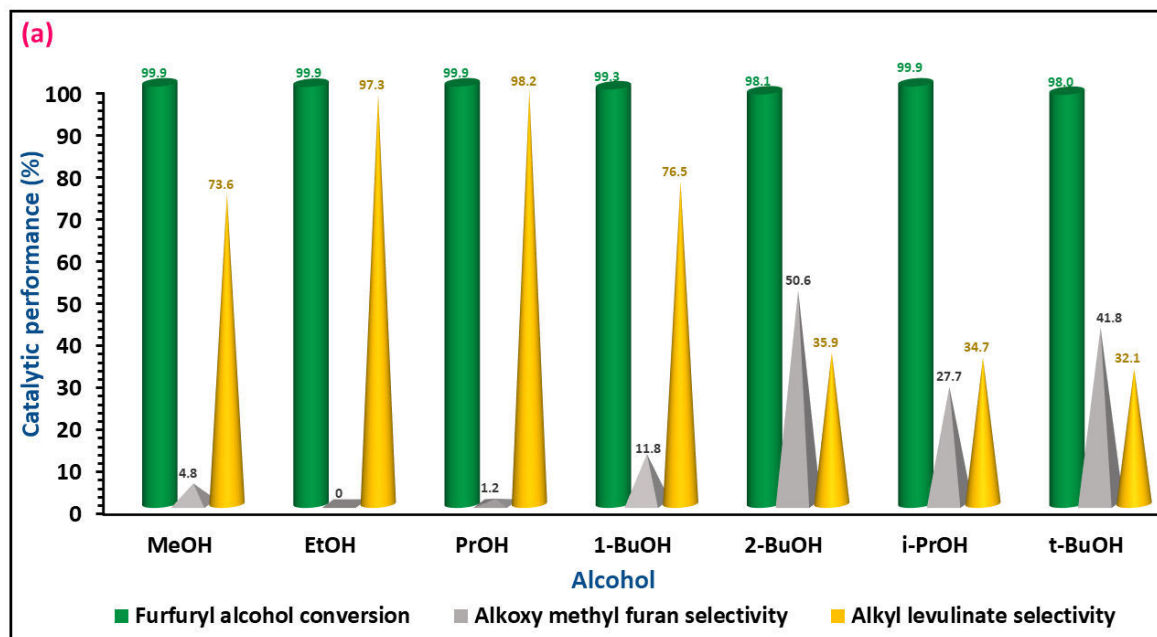


**Figure 6.16 (a)** Effect of the alkyl chain. Pathway (I) Alcoholysis of furfuryl alcohol– Reaction conditions: Reactants mole ratio (FA: alcohol)– 1:15, Catalyst concentration–1.86 wt%, temperature–120 °C, time– 2 h.

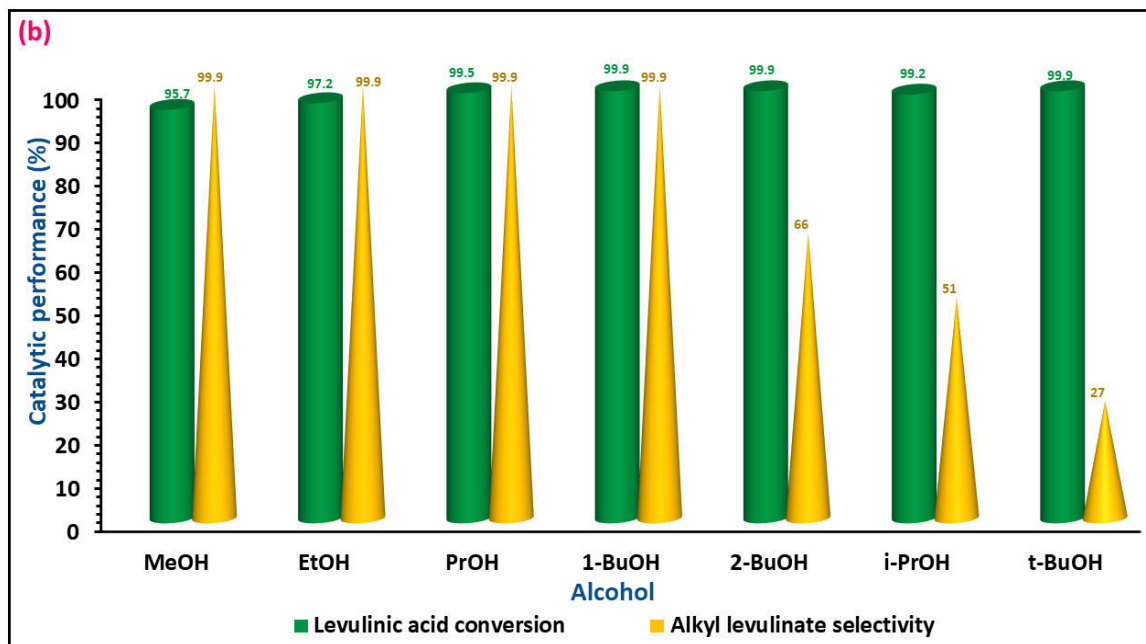


**Figure 6.16 (b)** Effect of the alkyl chain. Pathway (II) Esterification of Levulinic acid: Reaction conditions: Reactants mole ratio (LA: alcohol)–1:8, Catalyst concentration– 1.25 wt%, temperature– 90 °C, time– 4 h.

In general, the alcohols with higher acidic strength gave better selectivity for alkyl levulinate compared to longer chain alcohols as well as branched alcohols which have lower acidic strength. This is in accordance with the mechanism explained in the previous section, where the proton of the alcohol has to depart after the attack on FA or LA. The overall study on substrate scope for both pathways suggests that straight chain alkyl alcohols perform better with FA and LA than the branched chain alkyl alcohols (i-PrOH, BuOH, 2-BuOH) at given reaction conditions. BUT-8(Cr)-SO<sub>3</sub>H showed a competitive catalytic activity to yield different alkyl levulinates for both pathways.

## 6.9 Comparison with literature results

The catalytic performance of BUT-8(Cr)-SO<sub>3</sub>H for both the pathways was compared with the reported solid acid catalysts. Table 6.2 and Table 6.3 summarize the reaction conditions, recyclability, and EL yield.

**Table 6.2.** Comparison of catalytic activity of BUT-8(Cr)-SO<sub>3</sub>H with various reported catalysts in the literature for furfuryl alcohol ethanolsis to produce ethyl levulinate

Sn	Catalysts	T (°C)	Time (h)	Mole ratio	EL yield (%)	Reusability	Ref
1.	BUT-8(Cr)-SO <sub>3</sub> H	120	2.0	1:15	99	4C	PW <sup>a</sup>
2.	Modified zirconium phosphate	200	2	1:50	97	94%-4C	22
3.	TiHTPA	120	0.5	1:43	97	95%-5C	76
4.	ZrTPA/β-zeolite	130	5	1:85	96	4C	23
5.	Zr-DBS	150	2	1:170	95	4C	31
6.	[(HSO <sub>3</sub> -p) <sub>2</sub> im][HSO <sub>4</sub> ]	110	3	1:27	95	4C	35
7.	Polystyrene microspheres PS-SO <sub>3</sub> H	120	1.5	1:170	95	4C	32
8.	p-TSA-PFD	78	6	1:30	94	6C	25
9.	SBA-15/H-ZSM-5	110	5	1:35	89	48%-4C	16
10.	UiO-66 (Hf)-SO <sub>3</sub> H	120	4	1:350	88	73%-4C	21
11.	Meso-MIL-101(Cr)	160	2	1:60	84	66%-5C	20
12.	ArSO <sub>3</sub> H-Si(Et)Si-Ph-NTs	120	2	1:60	83	59%-5C	26
13.	ArSO <sub>3</sub> H-HMCS	120	-	1:69	82	-	34
14.	Al-TUD-1	140	1	1:56	80	-	29
15.	P doped carbon	140	6	1:54	80	56%-6 C	33
16.	MIL-101(Cr)-SO <sub>3</sub> H	140	2	1:60	79	71%-5C	19
17.	α-Fe <sub>2</sub> O <sub>3</sub>	250	1	1:20	73	38%	30
18.	Nano H-ZSM-5	120	6	1:8	69	5C decreased	18
19.	PW <sub>12</sub> /ZrO <sub>2</sub> -Si(Et)Si	120	2	1:60	64	53%-3 C	28
20.	Phosphomolybdic acid/ activated charcoal	140	3	1:168	63	-	24
21.	ZSM-5 (30)	125	-	1:2.7	65		
22.	H-Beta	125	-	1:2.7	15	-	15
23.	Mordenite	225	-	1:2.7	37		
24.	Si(Et)Si-PrSO <sub>3</sub> H-Et-H NS	120	2	1: 60	59	56%-3C	27

<sup>a</sup>PW-present work

**Table 6.3.** Comparison of catalytic activity of BUT-8(Cr)-SO<sub>3</sub>H with various reported catalysts in the literature for levulinic acid esterification to produce ethyl levulinate

Sn	Catalyst	T (°C)	Time (h)	Mole ratio	EL yield (%)	Reusability	Ref
1.	BUT-8(Cr)-SO <sub>3</sub> H	100	2	1:8	97	4C	PW <sup>a</sup>
2.	ArSO <sub>3</sub> H-HMCS	78	4	1:7	100	10C	34
3.	UDCaT-5	160	3	-	100	-	57
4.	MOF supported polyoxometalates Cu BTC	120	4	-	100	3C	42
5.	SO <sub>3</sub> H- benzimidazolium based polyionic liquid	70	9	1:10	99	5-C	63
6.	HClO <sub>4</sub> /SiO <sub>2</sub>	100	5	1:86	99	90%-5C	44
7.	UiO-66- (COOH) <sub>2</sub>	78	24	1:20	97	93%-5C	40
8.	PWA/ZrO <sub>2</sub>	150	3	1:17	97	81%-5C	49
9.	Micro/meso-HZSM-5	120	5	1:8	95	-	36
10.	Desilicated HZSM-5	120	5	1:8	95	6C	38
11.	EPTN (phosphotungstic acid/TiO <sub>2</sub> )	120	2	1:42	95	5C	50
12.	Sulfonated hydrothermal carbon glucose	60	3	1:5	94	-	60
13.	DodecaTPA/desilicated H-ZSM-5	84	4	1:8	94	4C	48
14.	ArSO <sub>3</sub> H-Si(Et)Si-Ph-NTs	78	3	1:7	94	3C	26
15.	Loofah sponge derived carbon	80	10	1:5	91	4C	61
16.	H <sub>3</sub> PW <sub>12</sub> /ZrO <sub>2</sub> -Si(Ph)Si	Reflux	3	1:7	91	75%-3C	51
17.	H <sub>4</sub> SiW <sub>12</sub> O <sub>40</sub>	25	8	1:18	90	-	77
18.	Sulphated TiO <sub>2</sub> /ZrO <sub>2</sub> nano-composites	105	3	-	90	60%-5C	53
19.	Sulfonated carbon	120	9	1:5	88	76%-2C	78
20.	Silicotungstic acid/AlSBA-15	75	5	1:10	87	41%-4C	52
21.	UiO66-SO <sub>3</sub> H	80	6	1:10	87	84%-5C	41
22.	Carboncryogel crystal	150	4	1:15	87	-	62
23.	Sulfated zirconia NP	70	8	1:10	86	81%-3C	55
24.	UiO-66(Hf) -SO <sub>3</sub> H	120	2	1:330	86	82%-5C	21

25.	Phosphomolybdic acid /activated charcoal	80	15	1:100	80	3C–decreased	24
26.	Sulfated ZrSBA–15	70	24	1:10	79	55%–5C	46
27.	Hierarchical ZSM–12 nanolayers	100	24	1:1	77	–	39
28.	Nanosized tin oxide	70	7.5	1:5	77	–	54
29.	Amberlyst–15	78	5	1:20	71	–	43
30.	Sulfated Si–doped ZrO <sub>2</sub>	70	10	1:10	65	5	56
31.	Carboncryogel crystal	78	10	1:19	61	–	62
32.	Sulphonated MWCNT	70	5	1:5	54	–	59
33.	Micro–meso H/BEA zeolite	78	5	1:6	40	4	37
34.	Powder Sulfated zirconia	70	7	1:3	40	39%–5C	62

<sup>a</sup>PW–present work

The BUT–8(Cr)–SO<sub>3</sub>H MOF for FA ethanolysis, showed the best EL yield (>99 %) reported so far with lower FA: EtOH mole ratio and good recyclability. For the LA esterification reaction, BUT–8(Cr)–SO<sub>3</sub>H MOF showed a competitive EL yield (97%) with reference to the reported catalysts with good recyclability. Overall, BUT–8(Cr)–SO<sub>3</sub>H catalyst showed promising results for both the transformations and also proved to be a promising heterogeneous catalyst for acid–catalyzed organic reactions.

## 6.10 Conclusions

Alkyl levulinate synthesis from biomass derivatives is an important area of research due to its variety of applications and designing a suitable solid acid catalyst for this transformation is a matter of great interest. The catalytic application for the BUT–8(Cr)–SO<sub>3</sub>H MOF has not been explored well as it was reported for the first time as a material very recently in 2017. The MOF is made of Cr (III) metal clusters which are less toxic compared to Cr (VI) ions as reported in the literature. In this work, the sulfonic moieties bound to the aromatic naphthalene structure of BUT–8(Cr)–SO<sub>3</sub>H MOF was found to have a much stronger influence on the catalytic performance than the sulfonic acid moieties bound to the styrene framework of amberlyst–15. The MOF outperformed zeolites *viz.* H–Beta (SAR30) and HZSM–5 (SAR 23) proving the superiority of –SO<sub>3</sub>H moieties as active sites over the Al–Brönsted acid sites of zeolites for these reactions.

The catalyst, BUT-8(Cr)-SO<sub>3</sub>H showed no leaching of active sites and good recyclability up to 4 cycles for both pathways. Also, the spent catalyst characterization by PXRD confirmed the material stability upon recycle. The catalyst showed good activity with FA/LA and alkyl alcohols recommending its applications in the synthesis of different alkyl levulinates. BUT-8(Cr)-SO<sub>3</sub>H MOF showed a high yield towards ethyl levulinate of 99 and 98% respectively for both the pathways *viz.* alcoholysis and esterification at lower reactant mole ratio, catalyst loading, and temperature. From the sustainability and renewability perspective, BUT-8(Cr)-SO<sub>3</sub>H catalyst due to its high Brönsted acidity, can be used for various organic transformations for fine chemical synthesis in the future.

## 6.10 Bibliography

- (1) Balat, H.; Kirtay, E. Hydrogen from biomass—present scenario and future prospects. *International journal of hydrogen energy* **2010**, 35 (14), 7416-7426.
- (2) Werpy, T.; Petersen, G. *Top value added chemicals from biomass: volume I--results of screening for potential candidates from sugars and synthesis gas*; National Renewable Energy Lab., Golden, CO (US), 2004.
- (3) Mariscal, R.; Maireles-Torres, P.; Ojeda, M.; Sádaba, I.; Granados, M. L. Furfural: a renewable and versatile platform molecule for the synthesis of chemicals and fuels. *Energy & environmental science* **2016**, 9 (4), 1144-1189.
- (4) Vaishnavi, B.; Sujith, S.; Vaibhava, K. R.; Bhat, P. J.; Vetrivel, R.; Shanbhag, G. V. Selective synthesis of furfuryl acetate over solid acid catalysts and active site exploration using density functional theory. *Catalysis Science & Technology* **2022**.
- (5) Tukacs, J. M.; Bohus, M.; Dibó, G.; Mika, L. T. Ruthenium-catalyzed solvent-free conversion of furfural to furfuryl alcohol. *RSC advances* **2017**, 7 (6), 3331-3335.
- (6) Iroegbu, A. O.; Hlangothi, S. P. Furfuryl alcohol a versatile, eco-sustainable compound in perspective. *Chemistry Africa* **2019**, 2 (2), 223-239.
- (7) Hayes, G. C.; Becer, C. R. Levulinic acid: A sustainable platform chemical for novel polymer architectures. *Polymer Chemistry* **2020**, 11 (25), 4068-4077.
- (8) Signoretto, M.; Taghavi, S.; Ghedini, E.; Menegazzo, F. Catalytic production of levulinic acid (LA) from actual biomass. *Molecules* **2019**, 24 (15), 2760.

- (9) Démolis, A.; Essayem, N.; Rataboul, F. Synthesis and applications of alkyl levulinates. *ACS Sustainable Chemistry & Engineering* **2014**, 2 (6), 1338-1352.
- (10) Badgujar, K. C.; Badgujar, V. C.; Bhanage, B. M. A review on catalytic synthesis of energy rich fuel additive levulinate compounds from biomass derived levulinic acid. *Fuel Processing Technology* **2020**, 197, 106213.
- (11) Appaturi, J. N.; Andas, J.; Ma, Y.-K.; Phoon, B. L.; Batagarawa, S. M.; Khoerunnisa, F.; Hussin, M. H.; Ng, E.-P. Recent advances in heterogeneous catalysts for the synthesis of alkyl levulinate biofuel additives from renewable levulinic acid: A comprehensive review. *Fuel* **2022**, 323, 124362.
- (12) Ahmad, E.; Alam, M. I.; Pant, K.; Haider, M. A. Catalytic and mechanistic insights into the production of ethyl levulinate from biorenewable feedstocks. *Green Chemistry* **2016**, 18 (18), 4804-4823.
- (13) Lomba, L.; Giner, B.; Bandrés, I.; Lafuente, C.; Pino, M. R. Physicochemical properties of green solvents derived from biomass. *Green chemistry* **2011**, 13 (8), 2062-2070.
- (14) Di Bucchianico, D. D. M.; Wang, Y.; Buvat, J.-C.; Pan, Y.; Moreno, V. C.; Leveneur, S. Production of levulinic acid and alkyl levulinates: a process insight. *Green Chemistry* **2022**, 24 (2), 614-646.
- (15) Lange, J. P.; van de Graaf, W. D.; Haan, R. J. Conversion of furfuryl alcohol into ethyl levulinate using solid acid catalysts. *ChemSusChem: Chemistry & Sustainability Energy & Materials* **2009**, 2 (5), 437-441.
- (16) Prajapati, R.; Srivastava, S.; Jadeja, G.; Parikh, J. A Novel SBA-15/H-ZSM-5 Composite Catalyst for Conversion of Furfuryl Alcohol to Ethyl Levulinate. *Waste and Biomass Valorization* **2022**, 1-10.
- (17) SK, H.; Balla, P.; Ponnala, B.; Ginjupalli, S.; Nekkala, N.; Koppadi, K. S.; Komandur, V. Efficient Transformation of Furfuryl Alcohol Into Ethyl Levulinates via Alcoholysis Reaction Catalyzed by SnO<sub>2</sub>/H-Mordenite Catalyst. *Catalysis Surveys from Asia* **2022**, 26 (2), 104-114.
- (18) Li, Y.; Wang, S.; Fan, S.; Ali, B.; Lan, X.; Wang, T. Nano-H-ZSM-5 with Short b-Axis Channels as a Highly Efficient Catalyst for the Synthesis of Ethyl Levulinate from Furfuryl Alcohol. *ACS Sustainable Chemistry & Engineering* **2022**, 10 (12), 3808-3816.



- (19) Liu, X.-F.; Li, H.; Zhang, H.; Pan, H.; Huang, S.; Yang, K.-L.; Yang, S. Efficient conversion of furfuryl alcohol to ethyl levulinate with sulfonic acid-functionalized MIL-101 (Cr). *RSC advances* **2016**, 6 (93), 90232-90238.
- (20) Liu, X.; Pan, H.; Zhang, H.; Li, H.; Yang, S. Efficient catalytic upgradation of bio-based furfuryl alcohol to ethyl levulinate using mesoporous acidic MIL-101 (Cr). *ACS omega* **2019**, 4 (5), 8390-8399.
- (21) Gupta, S. S. R.; Kantam, M. L. Catalytic conversion of furfuryl alcohol or levulinic acid into alkyl levulinates using a sulfonic acid-functionalized hafnium-based MOF. *Catalysis Communications* **2019**, 124, 62-66.
- (22) Zhai, P.; Lv, G.; Cai, Z.; Zhu, Y.; Li, H.; Zhang, X.; Wang, F. Efficient production of ethyl levulinate from furfuryl alcohol catalyzed by modified zirconium phosphate. *ChemistrySelect* **2019**, 4 (13), 3940-3947.
- (23) Rao, B. S.; Subrahmanyam, C.; Lingaiah, N. The selective conversion of furfuryl alcohol to ethyl levulinate over Zr-modified tungstophosphoric acid supported on  $\beta$ -zeolites. *New Journal of Chemistry* **2021**, 45 (6), 3224-3233.
- (24) Chhabra, T.; Rohilla, J.; Krishnan, V. Nanoarchitectonics of phosphomolybdic acid supported on activated charcoal for selective conversion of furfuryl alcohol and levulinic acid to alkyl levulinates. *Molecular Catalysis* **2022**, 519, 112135.
- (25) Patil, C. R.; Kamble, S. P.; Rode, C. V. Single-Pot Alcoholysis of Furfuryl Alcohol to Alkyl Levulinates Using Heterogenized p-TSA Catalyst. *ChemistrySelect* **2021**, 6 (26), 6636-6643.
- (26) Song, D.; An, S.; Sun, Y.; Zhang, P.; Guo, Y.; Zhou, D. Ethane-Bridged Organosilica Nanotubes Functionalized with Arenesulfonic Acid and Phenyl Groups for the Efficient Conversion of Levulinic Acid or Furfuryl Alcohol to Ethyl Levulinate. *ChemCatChem* **2016**, 8 (12), 2037-2048.
- (27) An, S.; Song, D.; Lu, B.; Yang, X.; Guo, Y. H. Morphology Tailoring of Sulfonic Acid Functionalized Organosilica Nanohybrids for the Synthesis of Biomass-Derived Alkyl Levulinates. *Chemistry—A European Journal* **2015**, 21 (30), 10786-10798.
- (28) Song, D.; An, S.; Sun, Y.; Guo, Y. Efficient conversion of levulinic acid or furfuryl alcohol into alkyl levulinates catalyzed by heteropoly acid and ZrO<sub>2</sub> bifunctionalized organosilica nanotubes. *Journal of Catalysis* **2016**, 333, 184-199.

- (29) Neves, P.; Antunes, M. M.; Russo, P. A.; Abrantes, J. P.; Lima, S.; Fernandes, A.; Pillinger, M.; Rocha, S. M.; Ribeiro, M. F.; Valente, A. A. Production of biomass-derived furanic ethers and levulinate esters using heterogeneous acid catalysts. *Green Chemistry* **2013**, *15* (12), 3367-3376.
- (30) Ren, D.; Fu, J.; Li, L.; Liu, Y.; Jin, F.; Huo, Z. Efficient conversion of biomass-derived furfuryl alcohol to levulinate esters over commercial  $\alpha$ -Fe<sub>2</sub>O<sub>3</sub>. *RSC advances* **2016**, *6* (26), 22174-22178.
- (31) Li, X.; Li, Y.; Wang, X.; Peng, Q.; Hui, W.; Wang, H. Zr-DBS with sulfonic group: A green and highly efficient catalyst for alcoholysis of furfuryl alcohol to ethyl levulinate. *Catalysis Letters* **2021**, *151* (9), 2622-2630.
- (32) Hu, A.; Wang, H.; Ding, J. Novel Sulfonic Acid Polystyrene Microspheres for Alcoholysis of Furfuryl Alcohol to Ethyl Levulinate. *Catalysis Letters* **2022**, 1-10.
- (33) Zhang, H.; Wang, S.; Zhang, H.; Cui, L.; Cao, F. P-doped carbon as an efficient metal-free catalyst for alcoholysis of furfural alcohol to ethyl levulinate. *Fuel* **2022**, *324*, 124024.
- (34) Song, D.; An, S.; Lu, B.; Guo, Y.; Leng, J. Arylsulfonic acid functionalized hollow mesoporous carbon spheres for efficient conversion of levulinic acid or furfuryl alcohol to ethyl levulinate. *Applied Catalysis B: Environmental* **2015**, *179*, 445-457.
- (35) Wang, G.; Zhang, Z.; Song, L. Efficient and selective alcoholysis of furfuryl alcohol to alkyl levulinates catalyzed by double SO<sub>3</sub>H-functionalized ionic liquids. *Green Chemistry* **2014**, *16* (3), 1436-1443.
- (36) Nandiwale, K. Y.; Bokade, V. V. Environmentally benign catalytic process for esterification of renewable levulinic acid to various alkyl levulinates biodiesel. *Environmental Progress & Sustainable Energy* **2015**, *34* (3), 795-801.
- (37) Patil, C.; Niphadkar, P.; Bokade, V.; Joshi, P. Esterification of levulinic acid to ethyl levulinate over bimodal micro-mesoporous H/BEA zeolite derivatives. *Catalysis Communications* **2014**, *43*, 188-191.
- (38) Nandiwale, K. Y.; Niphadkar, P. S.; Deshpande, S. S.; Bokade, V. V. Esterification of renewable levulinic acid to ethyl levulinate biodiesel catalyzed by highly active and reusable desilicated H-ZSM-5. *Journal of Chemical Technology & Biotechnology* **2014**, *89* (10), 1507-1515.

- (39) Dugkhuntod, P.; Imyen, T.; Wannapakdee, W.; Yutthalekha, T.; Salakhum, S.; Wattanakit, C. Synthesis of hierarchical ZSM-12 nanolayers for levulinic acid esterification with ethanol to ethyl levulinate. *RSC advances* **2019**, *9* (32), 18087-18097.
- (40) Wang, F.; Chen, Z.; Chen, H.; Goetjen, T. A.; Li, P.; Wang, X.; Alayoglu, S.; Ma, K.; Chen, Y.; Wang, T. Interplay of Lewis and Brønsted acid sites in Zr-based metal-organic frameworks for efficient esterification of biomass-derived levulinic acid. *ACS applied materials & interfaces* **2019**, *11* (35), 32090-32096.
- (41) Desidery, L.; Yusubov, M. S.; Zhuiykov, S.; Verpoort, F. Fully-sulfonated hydrated UiO66 as efficient catalyst for ethyl levulinate production by esterification. *Catalysis Communications* **2018**, *117*, 33-37.
- (42) Guo, T.; Qiu, M.; Qi, X. Selective conversion of biomass-derived levulinic acid to ethyl levulinate catalyzed by metal organic framework (MOF)-supported polyoxometalates. *Applied Catalysis A: General* **2019**, *572*, 168-175.
- (43) Ramli, N. A. S.; Hisham, N. I.; Amin, N. A. S. Esterification of levulinic acid to levulinate esters in the presence of sulfated silica catalyst. *Sains Malaysiana* **2018**, *47* (6), 1131-1138.
- (44) Yang, F.; Tang, J. Catalytic upgrading of renewable levulinic acid to levulinate esters using perchloric acid decorated nanoporous silica gels. *ChemistrySelect* **2019**, *4* (4), 1403-1409.
- (45) Maggi, R.; Shiju, N. R.; Santacroce, V.; Maestri, G.; Bigi, F.; Rothenberg, G. Silica-supported sulfonic acids as recyclable catalyst for esterification of levulinic acid with stoichiometric amounts of alcohols. *Beilstein journal of organic chemistry* **2016**, *12* (1), 2173-2180.
- (46) Kuwahara, Y.; Fujitani, T.; Yamashita, H. Esterification of levulinic acid with ethanol over sulfated mesoporous zirconsilicates: Influences of the preparation conditions on the structural properties and catalytic performances. *Catalysis Today* **2014**, *237*, 18-28.
- (47) Wu, M.; Zhang, X.; Su, X.; Li, X.; Zheng, X.; Guan, X.; Liu, P. 3D graphene aerogel anchored tungstophosphoric acid catalysts: characterization and catalytic performance for levulinic acid esterification with ethanol. *Catalysis Communications* **2016**, *85*, 66-69.

- (48) Nandiwale, K. Y.; Sonar, S. K.; Niphadkar, P. S.; Joshi, P. N.; Deshpande, S. S.; Patil, V. S.; Bokade, V. V. Catalytic upgrading of renewable levulinic acid to ethyl levulinate biodiesel using dodecatungstophosphoric acid supported on desilicated H-ZSM-5 as catalyst. *Applied Catalysis A: General* **2013**, *460*, 90-98.
- (49) Ramli, N. A. S.; Sivasubramaniam, D.; Amin, N. A. S. Esterification of levulinic acid using ZrO<sub>2</sub>-supported phosphotungstic acid catalyst for ethyl levulinate production. *BioEnergy Research* **2017**, *10* (4), 1105-1116.
- (50) Ahmad, E.; Pant, K. K.; Haider, M. A. Synthesis and application of TiO<sub>2</sub>-supported phosphotungstic acid for ethyl levulinate production. *Materials Science for Energy Technologies* **2022**, *5*, 189-196.
- (51) Su, F.; Wu, Q.; Song, D.; Zhang, X.; Wang, M.; Guo, Y. Pore morphology-controlled preparation of ZrO<sub>2</sub>-based hybrid catalysts functionalized by both organosilica moieties and Keggin-type heteropoly acid for the synthesis of levulinate esters. **2013**.
- (52) Lucas, N.; Gurrala, L.; Athawale, A. Heteropolyacids supported on mesoporous AISBA-15 as efficient catalysts for esterification of levulinic acid. *Journal of Porous Materials* **2019**, *26* (5), 1335-1343.
- (53) Li, Z.; Wnetrzak, R.; Kwapinski, W.; Leahy, J. J. Synthesis and characterization of sulfated TiO<sub>2</sub> nanorods and ZrO<sub>2</sub>/TiO<sub>2</sub> nanocomposites for the esterification of biobased organic acid. *ACS applied materials & interfaces* **2012**, *4* (9), 4499-4505.
- (54) Popova, M.; Shestakova, P.; Lazarova, H.; Dimitrov, M.; Kovacheva, D.; Szegedi, A.; Mali, G.; Dasireddy, V.; Likozar, B.; Wilde, N. Efficient solid acid catalysts based on sulfated tin oxides for liquid phase esterification of levulinic acid with ethanol. *Applied Catalysis A: General* **2018**, *560*, 119-131.
- (55) Popova, M.; Szegedi, Á.; Lazarova, H.; Dimitrov, M.; Kalvachev, Y.; Atanasova, G.; Ristić, A.; Wilde, N.; Gläser, R. Influence of the preparation method of sulfated zirconia nanoparticles for levulinic acid esterification. *Reaction Kinetics, Mechanisms and Catalysis* **2017**, *120* (1), 55-67.
- (56) Kuwahara, Y.; Kaburagi, W.; Nemoto, K.; Fujitani, T. Esterification of levulinic acid with ethanol over sulfated Si-doped ZrO<sub>2</sub> solid acid catalyst: study of the structure–activity relationships. *Applied Catalysis A: General* **2014**, *476*, 186-196.

- (57) Yadav, G. D.; Yadav, A. R. Synthesis of ethyl levulinate as fuel additives using heterogeneous solid superacidic catalysts: Efficacy and kinetic modeling. *Chemical Engineering Journal* **2014**, *243*, 556-563.
- (58) Fernandes, D.; Rocha, A.; Mai, E.; Mota, C. J.; Da Silva, V. T. Levulinic acid esterification with ethanol to ethyl levulinate production over solid acid catalysts. *Applied Catalysis A: General* **2012**, *425*, 199-204.
- (59) Oliveira, B. L.; da Silva, V. T. Sulfonated carbon nanotubes as catalysts for the conversion of levulinic acid into ethyl levulinate. *Catalysis Today* **2014**, *234*, 257-263.
- (60) Pileidis, F. D.; Tabassum, M.; Coutts, S.; Titirici, M.-M. Esterification of levulinic acid into ethyl levulinate catalysed by sulfonated hydrothermal carbons. *Chinese Journal of Catalysis* **2014**, *35* (6), 929-936.
- (61) Li, N.; Jiang, S.; Liu, Z.-Y.; Guan, X.-X.; Zheng, X.-C. Preparation and catalytic performance of loofah sponge-derived carbon sulfonic acid for the conversion of levulinic acid to ethyl levulinate. *Catalysis Communications* **2019**, *121*, 11-14.
- (62) Zainol, M. M.; Amin, N. A. S.; Asmadi, M. Effects of thermal treatment on carbon cryogel preparation for catalytic esterification of levulinic acid to ethyl levulinate. *Fuel Processing Technology* **2017**, *167*, 431-441.
- (63) Khiratkar, A. G.; Balinge, K. R.; Krishnamurthy, M.; Cheralathan, K.; Patle, D. S.; Singh, V.; Arora, S.; Bhagat, P. R. Sulphonic acid-functionalized benzimidazolium based poly ionic liquid catalyzed esterification of levulinic acid. *Catalysis Letters* **2018**, *148* (2), 680-690.
- (64) Enumula, S. S.; Gurram, V. R. B.; Chada, R. R.; Burri, D. R.; Kamaraju, S. R. R. Clean synthesis of alkyl levulinates from levulinic acid over one pot synthesized WO<sub>3</sub>-SBA-16 catalyst. *Journal of Molecular Catalysis A: Chemical* **2017**, *426*, 30-38.
- (65) Wu, M.; Zhao, Q.-Q.; Li, J.; Su, X.-L.; Wu, H.-Y.; Guan, X.-X.; Zheng, X.-C. Tungstophosphoric acid-based mesoporous materials anchored to MCM-41: characterization and catalytic performance in esterification of levulinic acid with ethanol. *Journal of Porous Materials* **2016**, *23* (5), 1329-1338.
- (66) Zhou, H.-C.; Long, J. R.; Yaghi, O. M. Introduction to metal-organic frameworks. ACS Publications: 2012; Vol. 112, pp 673-674.

- (67) Yang, D.; Gates, B. C. Catalysis by metal organic frameworks: perspective and suggestions for future research. *Acs Catalysis* **2019**, *9* (3), 1779-1798.
- (68) Gong, W.; Liu, Y.; Li, H.; Cui, Y. Metal-organic frameworks as solid Brønsted acid catalysts for advanced organic transformations. *Coordination Chemistry Reviews* **2020**, *420*, 213400.
- (69) Bakuru, V. R.; DMello, M. E.; Kalidindi, S. B. Metal-organic frameworks for hydrogen energy applications: advances and challenges. *ChemPhysChem* **2019**, *20* (10), 1177-1215.
- (70) Ladole, M. R.; Pokale, P. B.; Patil, S. S.; Belokar, P. G.; Pandit, A. B. Laccase immobilized peroxidase mimicking magnetic metal organic frameworks for industrial dye degradation. *Bioresource Technology* **2020**, *317*, 124035.
- (71) Li, H.; Wang, K.; Sun, Y.; Lollar, C. T.; Li, J.; Zhou, H.-C. Recent advances in gas storage and separation using metal–organic frameworks. *Materials Today* **2018**, *21* (2), 108-121.
- (72) DMello, M. E.; Sundaram, N. G.; Singh, A.; Singh, A. K.; Kalidindi, S. B. An amine functionalized zirconium metal–organic framework as an effective chemiresistive sensor for acidic gases. *Chemical communications* **2019**, *55* (3), 349-352.
- (73) Yang, F.; Xu, G.; Dou, Y.; Wang, B.; Zhang, H.; Wu, H.; Zhou, W.; Li, J.-R.; Chen, B. A flexible metal–organic framework with a high density of sulfonic acid sites for proton conduction. *Nature Energy* **2017**, *2* (11), 877-883.
- (74) Vaishnavi, B.; Sujith, S.; Kulal, N.; Manjunathan, P.; Shanbhag, G. V. Utilization of renewable resources: Investigation on role of active sites in zeolite catalyst for transformation of furfuryl alcohol into alkyl levulinate. *Molecular Catalysis* **2021**, *502*, 111361.
- (75) Dou, Y.; Zhang, H.; Zhou, A.; Yang, F.; Shu, L.; She, Y.; Li, J.-R. Highly efficient catalytic esterification in an– SO<sub>3</sub>H-functionalized Cr (III)-MOF. *Industrial & Engineering Chemistry Research* **2018**, *57* (25), 8388-8395.
- (76) Lingaiah, N. One pot selective transformation of biomass derived chemicals towards alkyl levulinates over titanium exchanged heteropoly tungstate catalysts. *Catalysis Today* **2018**, *309*, 269-275.

(77) Vilanculo, C. B.; de Andrade Leles, L. C.; da Silva, M. J. H<sub>4</sub>SiW<sub>12</sub>O<sub>40</sub>-catalyzed levulinic acid esterification at room temperature for production of fuel bioadditives. *Waste and Biomass Valorization* **2020**, *11* (5), 1895-1904.

(78) Liu, C.; Zhang, K.; Liu, Y.; Wu, S. Esterification of levulinic acid into ethyl levulinate catalyzed by sulfonated bagasse-carbonized solid acid. *BioResources* **2019**, *14* (1), 2186-2196.





# **Chapter 7**

## **Summary and Conclusions**



The summary and conclusions chapter comprises the overall conclusions drawn from each chapter. The thesis work presents the design of solid acid catalysts for the utilization of biomass derivative platform chemicals *viz.* furfuryl alcohol and levulinic acid to obtain speciality chemicals. The furfuryl alcohol was subjected to butanolysis, esterification, hydrolysis, and ethanolysis to produce butyl levulinate, furfuryl acetate, levulinic acid, and ethyl levulinate respectively. Realizing the importance of ethyl levulinate, along with furfuryl alcohol ethanolysis, the esterification of levulinic acid using ethanol was also explored using the same catalyst. Various heterogeneous acid catalysts such as HZSM-5, desilicated HZSM-5, dealuminated HZSM-5, metal ion exchanged ZSM-5, phosphate loaded HZSM-5, H-Beta, Y-Zeolite, mordenite, ferrierite, amberlyst-15, sulfated zirconia, Al-SBA-15, SAPO-34, SAPO-11, BUT-8(Cr)-SO<sub>3</sub>H, etc. were employed for aforementioned transformations. Characterization techniques such as PXRD, XRF, ICP-OES, FTIR spectroscopy, BET, acid-base titration, NH<sub>3</sub>-TPD, pyridine FTIR, SEM, and TEM were employed to understand the physicochemical properties of the solid acid catalysts. The major aspect that has to be always considered during furfuryl alcohol valorization is the resinification of furfuryl alcohol that occurs at high reaction temperatures or due to the presence of an acidic environment. As most of the reactions are acid-catalyzed reactions, the usage of catalysts with acidic sites cannot be omitted. Hence, there are a few strategies such as reducing the operating temperature, employing solvents, or addition of the second reactant in excess that would help in bringing down the resinification phenomena.

The summary and conclusion of the chapters are as follows.

### **Butanolysis of furfuryl alcohol to produce butyl levulinate**

The furfuryl alcohol alcoholysis using butanol produces butyl levulinate which has applications in/as fuel additives, flavor, and fragrance products. The chapter describes the investigation of the nature of acid sites of various catalysts such as HZSM-5, H-Beta, SAPO-34, sulfated zirconia, amberlyst-15, mordenite, etc for butyl levulinate synthesis.

---

Though most of the screened catalysts performed well in terms of FA conversion, they failed to produce butyl levulinate from the intermediate butoxy methyl furan. The catalyst HZSM-5 with better catalytic performance was chosen to further evaluate the effect of the silica to alumina ratio (SAR) and post-synthetic modification studies (desilication, dealumination, metal ion exchange, and phosphate loading). All the screened catalysts were well characterized using various characterization techniques. The unmodified HZSM-5 (SAR95) showed high activity towards butyl levulinate compared to all the other catalysts screened along. Hence, the optimum pore size, strength, and number of acid sites are responsible for the best catalytic activity offered by HZSM-5 (SAR95). Also, a good correlation with respect to the amount of acidity and SAR was obtained. The active catalyst, unmodified HZSM-5 (SAR95) gave 99% furfuryl alcohol conversion with 85 % selectivity to butyl levulinate under the optimized reaction conditions. The catalyst reusability study confirmed the material stability upon recycling upto 4 cycles without any appreciable loss in the catalytic acidity. The catalyst addressed all the drawbacks identified in the reported literatures.

### **Esterification of furfuryl alcohol to produce furfuryl acetate**

Furfuryl acetate is a potential biofuel/additive and is used in the flavor and fragrance industries. There is one reported catalyst for the direct production of furfuryl acetate from furfuryl alcohol via esterification. This pathway is economical as one pot production of furfuryl acetate from furfural occurs via hydrogenation and esterification. The usage of expensive noble metal for the latter can be avoided if furfuryl alcohol is chosen as the starting material. Various solid acid catalysts such as sulfated zirconia, H-Beta, Y-zeolite, H-ferrierite, SAPO-11, Al-SBA-15, amberlyst-15 with diverse physicochemical properties were used for the initial screening. Sulfated zirconia, SAPO-11, and Al-SBA-15 were the top three performing catalysts with respect to the turn over number (TON) which could be attributed to the presence of a moderate amount of total acidity. Density Functional theory (DFT) calculations were performed to integrate

---

the experimental results with the computational study. DFT gave the adsorption energy profiles for the various substrate species adsorbed on the top three performing catalyst surfaces. The profile disclosed that the sulfated zirconia had the least activation energy barrier over the Al-SBA-15 and SAPO-11 catalysts. The better catalytic activity of the sulfated zirconia catalyst could be due to the presence of the H-bond in the sulfate species of the sulfated zirconia. Importantly, a concept of hydrogen removal energy was introduced for the first time which correlated the proton donor capability of the solid acid catalysts *viz.* sulfated zirconia, SAPO-11, and Al-SBA-15 with the catalytic activity (TON). The study revealed that sulfated zirconia is a better acid catalyst as it has better proton donor capability than the rest. Sulfated zirconia was chosen for further studies, and at the optimized reaction conditions, the furfuryl alcohol conversion and furfuryl acetate selectivity were 96 and 98 % respectively. Leaching of the sulfate species was addressed by post-synthetic washing of the material and the catalyst showed very good recyclability by retaining its catalytic performance for 4 cycles. In conclusion, sulfated zirconia (2.5M-w) catalyst is shown to be an efficient catalyst for the esterification of furfuryl alcohol with acetic acid to produce furfuryl acetate in a high yield.

### **Hydrolysis of furfuryl alcohol to produce levulinic acid**

Levulinic acid is a platform chemical whose valorization produces various important chemicals such as  $\gamma$ -valerolactone,  $\alpha$ -angelicalactone, 5-bromolevulinic acid, levulinate esters,  $\delta$ -amino levulinic acid, 5-nonanone, 2-methyl tetrahydrofuran, diphenolic acid. These chemicals find applications as/in fuels, detergents, herbicides, solvents, pharmaceuticals, polymer industries, plasticizers, resins, food, flavoring, and fragrance industries. Hydrolysis of furfuryl alcohol produces levulinic acid when an acid catalyst is employed. Conventional solid acid catalysts such as ZSM-5 and amberlyst-15 along with a Brønsted acidic flexible metal organic framework, BUT-8(Cr)-SO<sub>3</sub>H were initially screened to discover the type and nature of the acid site required to obtain a

better levulinic acid yield. Catalysts with sulfonic acid moieties (BUT-8(Cr)-SO<sub>3</sub>H and amberlyst-15) performed better than the Al-Brönsted acid sites of the zeolites. As the reactants, furfuryl alcohol and water are immiscible, investigation on different polar aprotic solvents *viz.* DMF, DMSO, diglyme, THF, dioxane, and acetone was done with the best performing catalyst, BUT-8(Cr)-SO<sub>3</sub>H. Diglyme due to its higher boiling point performed better than the rest and under the optimized reaction conditions, the sulfonic acid functionalized flexible MOF BUT-8(Cr)-SO<sub>3</sub>H showed 98 % levulinic acid yield with good recyclability for 4 cycles. The best performance is due to the presence of densely populated sulfonic acid groups through the channels of the catalyst resulting in enhanced catalytic performance.

#### **Ethyl levulinate synthesis from furfuryl alcohol/levulinic acid and ethanol**

Ethanolysis of furfuryl alcohol and esterification of levulinic acid both yield ethyl levulinate which has an application as an oxygenating additive for fuels, potential biofuel, food-flavor agents, polymer or resin precursors, green solvents, etc. The investigation on aiming to arrive at one acid catalyst to aid both pathways was performed using HZSM-5, H-Beta, amberlyst-15 and BUT-8(Cr)-SO<sub>3</sub>H. BUT-8(Cr)-SO<sub>3</sub>H is a Brönsted acidic metal organic framework made up of Cr(III) metal clusters and 4,8-disulfonyl-2,6-naphthalenedicarboxylic acid linker with sulfonic acid moieties bound to the linker as the active sites. For both the pathways, the trend in terms of increase in ethyl levulinate yield was in the order of [HZSM-5 (SAR 23)~H-Beta (SAR25)] < amberlyst-15 < BUT-8(Cr)-SO<sub>3</sub>H, indicating the superior efficiency of the sulfonic acid moieties (-SO<sub>3</sub>H) as active sites compared to Al-Brönsted acid sites of the zeolites. The best catalyst, BUT-8(Cr)-SO<sub>3</sub>H was employed for the study on the influence of reaction conditions for both pathways to obtain the best catalytic yield. Substrate scope study by varying the alcohols *viz.* methanol, propanol, isopropanol, 1-butanol, 2-butanol, and tertiary-butanol, for both the pathways to check the potential

of the catalyst. Leaching study and spent catalyst characterization revealed that the catalyst is truly heterogeneous as no leaching of active species was observed. The catalyst was recycled up to 4 times and there was a negligible decrease in activity (<0.7%) after 4 cycles for both transformations. At the optimized reaction conditions, the ethyl levulinate yield for furfuryl alcohol ethanolysis and levulinic acid esterification was 99 and 97% respectively. Thus BUT-8(Cr)-SO<sub>3</sub>H MOF proved to be an efficient solid acid catalyst for the pathways transformation to produce ethyl levulinate.

---



---

# **Annexures**

---

---

## List of publications

1. Selective synthesis of furfuryl acetate over solid acid catalysts and active site exploration using density functional theory, **B. J. Vaishnavi**, S. Sujith, K. M. Rajashekhar Vaibhava, P. Jyothi Bhat, Rajappan Vetrivel, and Ganapati V. Shanbhag *Catalysis Science & Technology* **12** (2022): 4298-4311
2. Utilization of renewable resources: Investigation on role of active sites in zeolite catalyst for transformation of furfuryl alcohol into alkyl levulinate, **B. J. Vaishnavi**, S. Sujith, K. M. Nagendra Kulal, Pandian Manjunathan and Ganapati V. Shanbhag, *Molecular Catalysis* **502** (2021): 111361
3. Identification and tuning of active sites in selected mixed metal oxide catalysts for cyclic carbonate synthesis from epoxides and CO<sub>2</sub>, Nagendra Kulal, **B. J. Vaishnavi**, and Ganapati V. Shanbhag, *Journal of CO<sub>2</sub> Utilization* **33** (2019): 434-444
4. Highly selective aromatization of light naphtha using mesoporous aluminosilicate catalysts and theoretical model for predicting activity, S. Sujith†, **B. J. Vaishnavi** †, Girish Kamath, Ranjith R. Kumar, R. Sudarshan Reddy, G. Valavarasu, Raman Ravishankar, Sanjeev P. Maradur, C. Bennet, and Ganapati V. Shanbhag, *Journal of Porous Materials*, doi: 10.1007/s10934-022-01404-0.
5. Heterogeneous Catalysis for Chemical Fixation Reactions of CO<sub>2</sub> via Carbonylation, Ganapati V. Shanbhag, Nagendra Kulal, and **B. J. Vaishnavi**, *Climate Change and Green Chemistry of CO<sub>2</sub> Sequestration*: Springer Nature, 2021, 141-169 (Book chapter)
6. Catalytic Hydrogen Generation from Biomass and their derivatives, **B. J. Vaishnavi** and Ganapati V. Shanbhag, *Handbook of Emerging Materials for Sustainable Energy*, Elsevier, in press (Book chapter)
7. Selective synthesis of levulinic acid by hydrolysis of furfuryl alcohol using high density sulfonic acid functionalized flexible MOF. **B. J. Vaishnavi**, S. Sujith, K. M. Rajashekhar Vaibhava, Rajappan Vetrivel, and Ganapati V. Shanbhag (**Manuscript under communication**)
8. Transformation of biomass derivative furfuryl alcohol/ levulinic acid into alkyl levulinate, a fuel additive using sulfonated metal organic framework catalyst, **B. J. Vaishnavi**, S. Sujith, Harsha Murudappa, K. M. Rajashekhar Vaibhava, Meghana Kundapura, Rajappan Vetrivel, and Ganapati V. Shanbhag (**Manuscript under communication**)

---

## **Awards and Achievements**

1. Awarded **CSIR-Senior research fellowship-Direct** for a period of two years (November 2020 to October 2022). Sanctioned letter Id : 09/1052(0011)2020-EMR-I
2. Received **Best Research Scholar Award-2023** for outstanding performance during my 5 years of research at Poornaprajna Institute of Scientific Research, Bangalore. The award was given on 2<sup>nd</sup> February 2023
3. Received the **Best oral presentation award** for the paper titled “Transformation of biomass derivative furfuryl alcohol into alkyl levulinates over zeolite catalyst” at an international conference on “Emerging Trends in Catalysis” jointly organized by the School of advanced science, VIT, Vellore; Royal Society of Chemistry, UK on January 6–8, 2020
4. Received the **Best oral presentation award** for the paper titled “Transformation of biomass derivative furfuryl alcohol into alkyl levulinates over zeolite catalyst: Investigation on the role of active sites” in the National Conference on Frontiers of Catalysis Science & Technology and its Applications (FOCSTA-2020). It was organized by St. Joseph's College Bengaluru in association with the Catalysis Society of India, Bengaluru Chapter on 10 and 11th January 2020
5. Received the **Best oral presentation award** for the paper titled “Biomass derivative furfuryl alcohol conversion to furfuryl acetate over solid acid catalysts: Adsorption studies using DFT” in National Webinar on Recent Advances in Solid State Chemistry and Allied Sciences organized by Central University, Kerala during September 16<sup>th</sup>–18<sup>th</sup> 2021
6. Received the **Best oral presentation award** for the paper titled “Synthesis of furfuryl acetate from furfuryl alcohol over solid acid catalysts: Investigation of active sites using DFT Studies” during 2 days (24<sup>th</sup> and 26<sup>th</sup> march 2020) national conference on “Emerging Trends in Chemistry and Material Science-2022” organized by Department of Chemistry, KLS Gogte Institute of Technology, Belagavi, Karnataka
7. My proposal on “Synthesis of fuel additives and speciality chemicals from biomass–derived platform chemicals with the aid of solid acid catalysts” was selected for oral presentation for the category of young scientist award in Rasayanam Paper organized by KV Rao scientific society, research awards on 18<sup>th</sup> June 2022
8. Received the **Best Seminar award** at PPISR weekly seminar for the year 2019 for the topic “Hydrogen production from biomass”



### **Conferences attended**

1. Participated in a “19th Orientation Program in Catalysis” organized by the National Centre for Catalysis Research, Indian Institute of Technology Madras for 15 days from 30<sup>th</sup> November to 17<sup>th</sup> December 2018.
2. Participated in an International Conference on “Emerging Trends in Catalysis” jointly organized by the School of advanced science, VIT, Vellore; Royal Society of Chemistry, UK on January 6–8, 2020. Presented an oral presentation on the topic “Transformation of biomass derivative furfuryl alcohol into alkyl levulinates over zeolite catalyst”
3. Participated in National Conference on Frontiers of Catalysis Science & Technology and its Applications (FOCSTA-2020) on 10 and 11th January 2020 organized by St. Joseph's College Bengaluru in association with Catalysis Society of India, Bengaluru Chapter. The topic of the oral presentation was “Transformation of biomass derivative furfuryl alcohol into alkyl levulinates over zeolite catalyst: Investigation on the role of active sites”
4. Attended the “1st Virtual International Symposium on C–H Activation” from 27 to 30 July 2020.
5. Participated in the Conference of Catalysis Research Scholars Meet (CATSCHOL 2020) on 19 and 20th December 2020
6. Presented an oral presentation at the UK catalysis conference 2021 on 07-01-2021 on the topic “Valorization of bio-derived furfuryl alcohol to make furfuryl acetate over solid acid catalysts: Effect of acidity and porosity on activity”
7. Presented a talk on the topic “Heterogeneous Catalysis and its Applications in Modern Day Research” online at Virtual Research Orientation Workshop 2020–2021 organized by PPC Udupi.
8. Participated in a webinar on the “Synthesis of porous solids” organized by NCCR, IITM on 7<sup>th</sup> May 2021.
9. Attended the webinar “Shimadzu GC-MS Training” organized by Toshvin Analytical Pvt Ltd on 24th May 2021





10. Participated in "National Webinar on Recent Advances in Solid State Chemistry and Allied Sciences" held at Central University of Kerala on 16<sup>th</sup>–17<sup>th</sup> August 2021. The presented topic was “Biomass derivative furfuryl alcohol conversion to furfuryl acetate over solid acid catalysts: Adsorption studies using DFT”
11. Participated in "Emerging Trends in Catalysis for Sustainable Chemical Processes (ETCSCP–2021), an international conference organized jointly by the Indian Institute of Chemical Engineers (IChE) and the Catalysis Society of India from 26<sup>th</sup> to 28<sup>th</sup> August 2021. Presented an oral presentation on “Selective synthesis of furfuryl acetate from biomass derivative furfuryl alcohol over solid acid catalysts: Active site exploration using Density Functional Theory”.
12. Presented my research finding at the second virtual international conference on “Molecules to Materials–2021” organized by the Sardar Vallabhbhai National Institute of Technology (SVNIT), Surat (17<sup>th</sup>–18<sup>th</sup> December 2021). The topic of the presentation was “Biomass derivative furfuryl alcohol conversion over solid acid catalysts to yield furfuryl acetate: Adsorption studies using Density Functional Theory”
13. Participated and presented the research finding in “Emerging Trends in Chemistry and Material Science-2022” organized by the Department of Chemistry, KLS Gogte Institute of Technology, Belagavi, Karnataka from 24<sup>th</sup> to 26<sup>th</sup> March 2022. The topic of the presentation was “Synthesis of furfuryl acetate from furfuryl alcohol over solid acid catalysts: Investigation of active sites using DFT Studies”
14. Presented my research findings for the category of young scientist award in Rasayanam Paper organized by KV Rao scientific society, research awards on 18<sup>th</sup> June 2022. The topic of the presentation was “Synthesis of fuel additives and speciality chemicals from biomass–derived platform chemicals with the aid of solid acid catalysts”